PHARMACOKINETICS OF DOXORUBICIN IN CANCER CHEMOTHERAPY.

FESTUS FAWEHINMI
Bachelors of Science, Federal University of Agriculture, Abeokuta, Ogun State, Nigeria, 2012

A thesis/project submitted
in partial fulfilment of the requirements for the degree of

MASTER OF SCIENCE

in

PHYSICS

Department of Physics and Astronomy
University of Lethbridge
LETHBRIDGE, ALBERTA, CANADA

PHARMACOKINETICS OF DOXORUBICIN IN CANCER CHEMOTHERAPY.

FESTUS FAWEHINMI

Date of Defence: December 19, 2019

Dr. Kenneth Vos Supervisor	Associate Professor	Ph.D.
Dr. Behnam Seyed-Mahmoud Thesis Examination Committee Member	Associate Professor	Ph.D.
Dr. Marc Roussel Thesis Examination Committee Member	Professor	Ph.D.
Dr. Mark Walton Chair, Thesis Examination Committee	Professor	Ph.D.

Dedication

I dedicate this thesis to the almighty God.

The fountain of all knowledge and the lifter of my head.

And to the memory of my parents.

Abstract

The pharmacokinetics (PK) of doxorubicin (DOX) is characterized by a large degree of inter-individual variation, which translates to unpredictability in the drug toxicity and response profiles from one individual to the next. In this work, we introduce a saturable model of DOX PK with fractal exponents using a population PK approach. The initial one-compartment model was expanded to a two-molecule model of DOX and encapsulated DOX, and a four-molecule, three-compartment model of DOX and its toxic metabolite doxorubicinol (DOL). Using this approach, the kinetic parameters of the molecules were developed by minimizing the weighted percentage variance of individual models. Our model provides interesting insights when testing the effects of some covariates on the PK of the molecules. We notice that factors such as patients' gender, race, body weight and liver impairment influence the elimination PK of DOX and DOL.

Acknowledgments

Firstly, I want to acknowledge the almighty God, who is my rock and my strength. By him and through him alone is this thesis possible.

I am also eternally grateful to my supervisor, Dr. Kenneth J.E. Vos for the fantastic opportunity bestowed on me to join his lab and to work on something that I feel so deeply about. I cannot positively emphasize how much I have learnt from working with him, and how much I have been able to grow as a person in the process. His love for teaching Physics and all things science resonates strongly with me and is something that I hope to transmit in my further endeavors.

I would also like to thank the members of my committee, Dr. Marc Roussel and Dr. Benham Seyed Mahmoud, their constructive yet concise criticism and encouragement actively helped in my quest to complete this project. Likewise knowing that I could approach them regarding any of the research-related challenges gave me a sense of confidence that I cannot put in words.

Special thanks go to the School of Graduate Studies, Faculty of Arts and Science, and the Department of Physics and Astronomy for their support with funding and assistantships that have greatly supported me in this journey. I will also like to appreciate friends in the department of Physics for making me feel at home and welcoming me with open arms whenever and wherever.

This research is also possible in part through the support of Compute Canada Calcul Canada (www.computecanada.ca) and WestGrid (www.westgrid.ca) via the computing systems Cedar and Beluga.

It is only fair that I acknowledge my lab mates with whom I had insightful discussions

and shared ideas, here is to a higher and better future.

To everyone else, I say thank you!

Contents

List of Tables

List of Figures

List of Abbreviations

5-FU	5-Fluorouracil
6-OH-PTX	6α-Hydroxyl-Paclitaxel
ADM	Adriamycin
ADME	Absorption, Distribution, Metabolism and Elimination
AIC	Anthracycline Induced Carditoxicity.
AUC	Area Under the Curve
BLM	Bleomycin
BOBYQA	Bound Optimization By Quadratic Approximation
BMI	Body Mass Index
CBR1	Carbonyl Reductase 1
$C_{\mathbf{max}}$	Maximum Drug Concentration
CP	Cyclophosphamide
DOX	Doxorubicin
DOL	Doxorubicinol
EPR	Enhanced Permeability and Retention
FDA	Food and Drug Administration
FdUMP	Fluorodeoxyuridine monophosphate
HBV	Hepatitis B Virus
HCV	Hepatitis C Virus
HPV	Human Papilloma Virus

IBW	Ideal Body Weight
LD	Liposomal Doxorubicin
MTX	Methotrexate
PD	Pharmacodynamics
PEG	Polyethylene glycol
PGP	P-glycoprotein
PK	Pharmacokinetics
PLD	Pegylated Liposomal Doxorubicin
PTX	Paclitaxel
RK	Runge-Kutta
RNA	Ribonucleic acid
ROS	Reactive Oxygen Species
TBW	Total Body Weight
VCR	Vincristine

List of Symbols

k	Rate constant.
$C(t)$	Concentration at time t.
$[E]$	Enzyme concentration.
$[S]$	Substrate concentration.
$[P]$	Product concentration.
v	Reaction velocity.
K_M	Michaelis-Menten's constant.
D	Dose
V_d	Volume of distribution
I_{ij}	Infusion rate of molecule i into physical space j.
$k^{(i)}_{jlm}$	Flow rate of molecule i from physical space j into l during reaction reaction m.
$\Gamma^{(i)}_{jlm}$	Saturable flow rate of molecule i from physical space j into l during reaction reaction m.
C_{d_i,c_i}	Concentration of molecule d_i in physical space c_i.
V_{D,d_i,c_i}	Volume of distribution of molecule d_i in physical space c_i.

Chapter 1

Introduction

Cancer is not just a dividing cell. It's a complex disease:

It invades, it metastasizes, it evades the immune system.

– Siddhartha Mukherjee

1.1 Thesis Structure

This study includes five chapters that have been organized in a chronological sequence. Chapter 1 contains an introduction to the general idea of pharmacokinetics (PK), some of the mathematics of pharmacokinetic modelling and a review of past doxorubicin (DOX) literature. Chapter 2 explores the materials and methods used to achieve the aim of this work and outlines the model equations. The model results and analysis are presented in chapter 3. The applications of the results are described in chapter 4. Chapter 5 outlines the conclusion and suggestions for further studies.

1.2 An Overview Of Cancer

Cancer stands as the leading cause of death in developed countries, and second in underdeveloped ones [1]. Current data from the Canadian Cancer Society supports the fact that cancer continues to be the leading cause of death in Canada, and is responsible for one in every four deaths [2]. An even more significant statistic released by the Canadian Cancer Society shows that one in two Canadians will be diagnosed with cancer during their lifetime [3]. These predictions show the extent to which disease occurrence is increasing,

and the challenge of clinicians to produce an effective plan for treatment of the disease. Cancer occurs when there is a corruption of the information carried in cellular DNA [4], leading to abnormalities in gene expression. Cancerous cells exhibit changes from normal cellular behaviours, which are known as cancer hallmarks [5], such as unregulated division, evasion of programmed cell death, and metastasis to distance sites. There are over 200 distinct types of cancers, each with a name corresponding to the part of the body in which it forms [6]. Currently, the causes of cancers are unclear [7], however, some risk factors for the disease have been suggested including dietary and genetic factors, tobacco use, alcohol use, physical inactivity, exposure to ionizing radiation sources, and some viral infections such as Hepatitis B (HBV), Hepatitis C (HCV) and Human Papilloma Virus (HPV) [8]. One of the most common pathways of oncogenic transformation on the cellular level is the mutation of the tumour suppressor ($P53$) gene, ensuring that cells lose their ability to inhibit cellular division [9, 10]. This loss of $P53$ results in the formation of tumours as damaged cells rapidly divide and aggregate to become cancerous.

Two main classes of cancers exist: benign and malignant. While benign cancers are not life-threatening and do not rapidly grow, malignant cancers can continue their process of division even after invading nearby tissues and organs. They are also able to metastasize to newer sites within the body, culminating in the development of new blood vessels that supplies blood to the tumour, aiding its growth at the secondary site. Cancers are staged based on disease extent and prognosis in a process called cancer-staging [11]. The following parameters allow for accurate staging of tumours [12]:

- Tumour size
- Extent of involvement of the lymph nodes
- Tendency to metastasize

Most cancer types have different staging metric centered around these three considerations in addition to the type of tumour and the part of the body it develops within.

1.3 Cancer Treatment

The best treatment method for solid, localized, and non-metastasizing tumours is surgical removal, although other methods such as radiotherapy and chemotherapy may also be viable treatment alternatives. Generally, the choice of treatment for cancers depends on factors such as

1. Type, histology, and stage of cancer [13].
2. Age, social status, and overall health profile of the patient [14].
3. Societal, cultural attitude towards cancer [15].

The goal of cancer treatment may be short or long term. The short-term goal for patients with incurable cancers usually revolves around more conservative treatment options such as managing the disease symptoms and treatment side effects. In other cases, the long term goal is disease cure; however, for more advanced diseases, the long term goal is disease management, especially to prolong patient survival and maintain the highest possible quality of life. In line with the objective of this work, we will focus on the chemotherapeutic method of cancer treatment, the treatment of tumours with chemical agents.

1.4 Chemotherapy

Anticancer drug development seeks an end-goal of better anti-tumour response and lower toxicity. As a result, chemotherapy treatment may involve one, or more drugs, depending on the type and complexity of the tumour. Chemotherapy may be used in a neoadjuvant fashion, which is to shrink the size of cancer, increasing the success of surgical removal. It can also be used as an adjuvant therapy to kill off residual or metastasized cancer cells or to treat inoperable cancers [16]. One of the main drawbacks of chemotherapy as a treatment method is the non-specific cell targeting nature of chemotherapy drugs. This implies that anticancer drugs cannot readily differentiate between normal and cancerous cells. Further, some of these drugs are developed to interfere with cells at specific cell

cycle stage due to the continuous uncontrolled division of cancer cells [17], as a result, other rapidly dividing body cells such as hair cells also have their cell cycle phase affected by these drugs [18], producing undesirable side effects. In the last decade, many studies into targeted drug delivery in vivo have suggested several protocols for selective delivery of cancer agents [19, 20]. Furthermore, cancer cells have been observed to have defective vasculature and an underdeveloped lymphatic drainage [21]. This means drugs with increased molecular weight can quickly enter through passive diffusion, and tumour cells will retain large concentrations of the drug. The enhanced permeability and retention effect (EPR) [22] describes the accumulation of anticancer drugs at the tumour site. Anticancer drugs can also be taken in combination to increase efficacy or to reduce toxicity; this is known as combination chemotherapy. The primary reason for the improvement in efficacy when using combination chemotherapy is that it reduces the chances of drug resistance. The combined drugs can achieve this by arresting the tumour cells at different cell cycle phases. During the cycle, cells duplicate genetic materials which they pass on to their daughters. Four distinct phases characterize the process of duplication and transfer [23, 24]: The Gap 1 (G1) phase is characterized by an increase in the physical extent of the cell and the synthesis of nutrients necessary for DNA replication. The replication of DNA and a copy of the centrosome for the daughter cells characterizes the Synthesis (S) phase. Synthesis of the protein complements occurs in the Gap 2 (G2) phase, and lastly, cell division occurs in the Mitotic (M) phase. Figure 1.1 shows three anticancer agents and the stage of the cell cycle where cancer cells are most vulnerable to their effect. Anticancer agents that target specific cell cycle stages are referred to as cell cycle phase-specific agents, for example, vincristine is effective in the M-phase, paclitaxel in the G1-phase, bortezomib in the G2-phase and DOX in the S-phase.

The choice of the best combination for any chemotherapy regimen depends on the cell cycle phase activity of the individual drugs. For instance, vincristine (M-phase), a vinca-alkaloid, and DOX (S-phase), an anthracycline, have been reported to be an ideal drug

combination in the treatment of breast cancer [25] as both drugs target the cancer cells at different stages in their life cycle. When drugs are taken in combinations, and cell cycle stages are interrupted, cellular checkpoint proteins, which monitor cell cycle progression are induced [26] delaying the transition into a new phase. This may result in the termination of the cell division process or induce cell death (apoptosis).

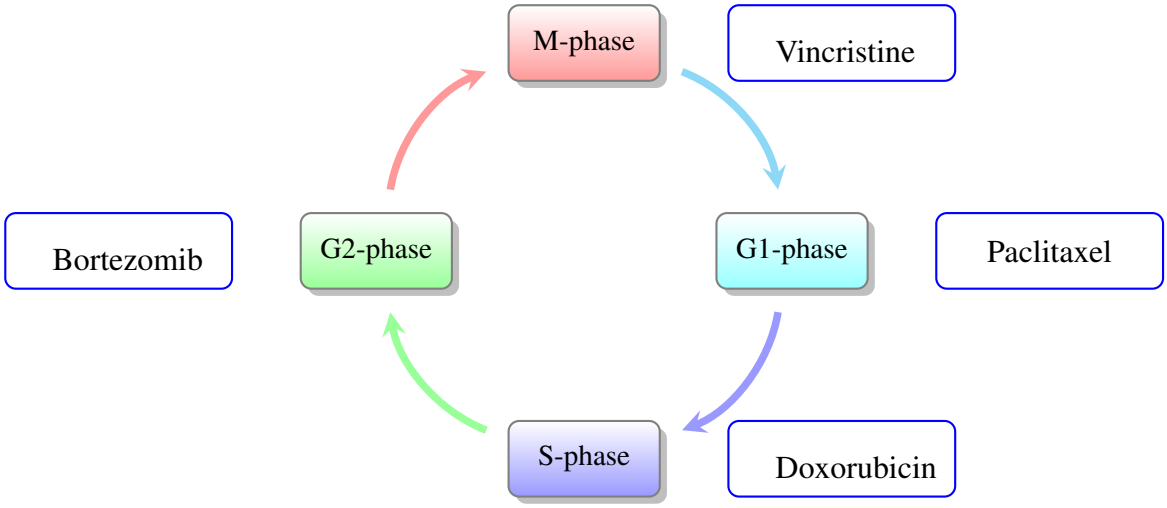

Figure 1.1: Anticancer drugs and cell cycle targets.

1.4.1 Classes of Antineoplastic Drugs

Antineoplastic drugs, which are cancer-destroying, are categorized based on their composition and the cell cycle stage they target. We can further group drugs within each class based on their tumour activity as cytotoxic, which are cancer-killing drugs, and cytostatic, which are drugs that halt cell division. An important concept in cancer therapy is apoptosis, which is programmed cell death through the action of a cytotoxic agent. Apoptosis is a primary consideration in the treatment of tumours. Therefore, cytotoxic agents are developed to induce apoptosis in the tumour cells by expressing the P53 transcription factor [27], which acts on cells at specific cell cycle checkpoints. During the early stages of tumorigenesis, which is the development or formation of tumours, cancer cells are subjected to several types of stress, in response to this, P53 is activated and, depending on the expression levels and the type of stress signal, may suppress the growth or kill off the cell [28]. Table 1.1

shows the general classes of anticancer agents, the type of cancers for which they are most active, and an example agent in each class.

Table 1.1: The different classes of antineoplastic agents and examples of the drugs within the class. The last column shows the type of cancers the drugs are effective against.

Class	Agent Name	Active Metabolite	Target	Indications
Antifolates [29]	Methotrexate	7-OH-Methotrexate	Dihydrofolate reductase, Serum albumin	Breast, head and lung cancer; ostreogenic sarcoma.
Alkalyating agents [30]	Cyclophosphamide	OH-cyclo and Phosphoramide mustard	DNA	Breast, ovary and lung cancer; soft tissue sarcoma, non-Hodgkin's lymphoma.
Anthracyclines [31]	DOX	DOL	Topoisomerase inhibiton; DNA intercalation	Breast, lung, and stomach cancer; soft tissue sarcoma, Hodgkin's and non-Hodgkin's lymphoma.
Taxanes [32]	Paclitaxel	6-OH-Paclitaxel , C3Oh-Paclitaxel	Serum albumin; Apoptosis regulator Bcl2.	Ovarian, lung, bladder and neck cancer.
Vinca Alkaloids [33]	Vincristine	DCVR	Interaction with CYP3A5	Wilm's tumour, Hodgkin's and non-Hodgkin's lymphoma.
Proteasome inhibitors [34]	Bortezomib	Bortezomib Metabolite M1 & M2	Inhibits 26S proteasome activity within the cell	Multiple myeloma
Antibiotics [35]	Bleomycin	desamido-bleomycin	Inhibits synthesis of tumour cell DNA	Malignant neoplasms
Pyrimidine antagonists [36]	5-Fluorouracil	Fluorodeoxyuridine monophosphate	Binding of active metabolite to thymidylate synthase	breast, rectum and cervical carcinomas

1.5 Pharmacokinetics

PK is the study of the effect of the body on the drug. The PK of any drug consists of four major activities: Absorption, Distribution, Metabolism, and Elimination (ADME). All four processes are important in the lifetime of the drug and represent significant considerations

in the goal of drug development: efficacy. PK modelling provides a quantitative basis to characterize the time course of a drug as it undergoes these activities within the body, and can serve as a vital tool in determining optimal dosage, best drug combinations, and scheduling.

1.5.1 Absorption

Absorption is the first step of the ADME process. It characterizes the introduction of a drug to the body via some means. Usually, the drug is rapidly circulated into the body by passive diffusion through the blood vessels, with a dose-dependent absorption rate. The rate of absorption may also depend on the surface area available at the point of infusion. Drug administration may occur in several ways, classified as:

1. Enteral routes, e.g. oral and rectal administration.
2. Parenteral routes, e.g. intravenous and intramuscular routes.

1.5.2 Distribution

Following administration, the drug next undergoes the process of distribution. Distribution refers to the transportation of the drug via regional blood flow. For drugs administered intravenously, absorption is rapid, followed by a concurrently rapid distribution phase. Organic drug concentration depends on the rate of blood flow to the said organ; hence, more drugs are distributed to organs or tissues that are constantly in contact with the blood than to those that are not.

1.5.3 Metabolism

Upon distribution, the drug is metabolized. Metabolism is the process by which the drug undergoes biotransformation via a series of chemical reactions. It is prudent to mention here that most drugs are metabolized in the liver, although biotransformation may occur in other tissues within the body [37]. Metabolism is an enzymatic reaction; that is, it requires the

action of enzymes to speed up the process. The metabolites from most drugs are more soluble than their parent compound and are more readily eliminated by the kidneys. The result of drug metabolism can serve one of two purposes; on one hand, it helps to inactivate the active drug, thereby reducing the toxic effect of the drug on the body by eliminating its metabolite. Alternatively, the administered drug may be a prodrug, which is a non-active drug. In this case, metabolism helps to release the active anti-tumour drug. The cytochrome P450 (CYP450) enzyme class is mostly responsible for drug metabolism, although research is ongoing regarding other enzyme classes that may be active in the process [38, 39].

1.5.4 Elimination

Elimination is the last stage of the PK process. During elimination, the organs responsible for biliary (liver) or renal (kidney) excretion, remove the drugs, and in some cases, the metabolites, from the body via urine or other means such as sweat and saliva. The elimination process allows us to estimate the amount of drug resident in the body at any instant of time. Knowledge of the rate of elimination can help design better dosage plans and is an important consideration in drug choice and treatment procedures.

1.6 Pharmacokinetic Modelling

PK models provide a means of quantitatively measuring the time course of a drug in a biological system. One of the challenges of experimental drug therapeutics is in the comparison of administration protocols [40]. Thus model development is an essential tool in providing a more quantitative measure of in vivo processes and making suggestions based on systematic data. The goal of model building is not to develop an exhaustive model that characterizes all the complexity of the system, but a simplified form relating only to the intended use of the model. In a PK model, the four distinct activities, ADME, are depicted using a set of mathematical equations [41]. One can trace the history of PK modelling to Torsten Teorell, who in 1937 proposed a biological drug kinetics pattern that depended

on an interconnected vascular circuitry system [42, 43]. However, it was not until advancements in numerical simulations that the use of PK models as a supplement of clinical trials became possible. The major parameters in any PK model are the biological species-dependent parameters, which includes the biological characteristics of the species, tissue or organ characteristics, the known rate constants and the enzyme/metabolite type; The drug-dependent parameters, which describes the class and type of the drug, active metabolites, and the protein binding affinity. Other parameters may also be important depending on the intended use of the model, these parameters include the route of infusion of the drug, which may be intravenous, oral, intramuscular, or intraperitoneal, and the composition of the administered drug, which may be a prodrug or a nanoparticle encapsulated drug.

Lin et al. [43] have suggested the following procedure for model development:

i Search for associated literature

ii Specify model structure

iii Build equations and code model

iv Model parameterization

v Model evaluation

vi Determine model applications

1.6.1 Rate Equation

Reaction rates characterize the PK processes. These rates are a measure of the speed of the reaction and may depend on the concentration of the drug or some physiological factors. A reaction may occur following zeroth, first, second or some mixed order rate laws.

Zeroth Order Reaction

This is a reaction most observed in the elimination of alcohol where the rate of elimination is constant after reaching maximum plasma concentration. Generally, zeroth-order

kinetics occurs when there is a saturation of the reaction catalyst. This implies that increasing the substrate concentration will not produce any change to the speed of the reaction. This type of reaction kinetics does not hold when the concentration of the substrate is low relative to the enzyme. The rate equation for this type of reaction is given by

$$\frac{dC}{dt} = -k^{(0)}, \tag{1.1}$$

with the solution

$$C(t) = C(t_0) - k^{(0)}\Delta t. \tag{1.2}$$

In equation 1.2, $C(t)$ is the time-dependent drug concentration, $k^{(0)}$ is the zeroth order rate constant, $\frac{dC}{dt}$ is the rate of change of the drug concentration with time, and $\Delta t = t - t_0$ is the time difference between successive steps.

First Order Reaction

Most drug reactions are first order and they depend on the concentration of the drug over time. In a first order reaction, the rate of elimination of a drug is given by the equation

$$\frac{dC(t)}{dt} = -k^{(1)}C(t), \tag{1.3}$$

where $C(t)$ is the drug concentration, $k^{(1)}$ is the first order rate constant, and $\frac{dC}{dt}$ is the rate of change of the drug concentration with time. The solution for concentration, $C(t)$, from equation 1.3 is written as

$$C(t) = C(t_0)e^{-k^{(1)}\Delta t}. \tag{1.4}$$

Second Order Reaction

Second order reactions are described by the equation

$$\frac{dC(t)}{dt} = -k^{(2)}(C(t))^2, \tag{1.5}$$

where the concentration and time are the same as the first-order reaction and $k^{(2)}$ is the second-order rate constant. Equation 1.5 shows that the rate of elimination is dependent on the square of the concentration value. The solution of the equation above is

$$C(t) = \frac{C_0(t)}{1 + C_0(t)k^{(2)}\Delta t}. \tag{1.6}$$

Multi-Order Reaction

Biological processes usually involve enzyme-catalyzed reactions. In such reactions, a concentration of substrate, $[S]$, reacts with an enzyme, $[E]$, to form a product $[P]$. These reactions can be described by a chemical equation, which takes the form

$$[\mathrm{E}] + [\mathrm{S}] \underset{k_{-1}}{\overset{k_1}{\rightleftharpoons}} [\mathrm{ES}] \xrightarrow{k_2} [\mathrm{E}] + [\mathrm{P}], \tag{1.7}$$

where $[ES]$ represents the concentration of the enzyme-substrate complex formed during an intermediate step in the reaction. k_1, k_{-1} and k_2 are the rate constants of forward reaction, reverse reaction and product formation respectively. In the pre-steady state period, the complex concentration rapidly builds up as the substrate reacts with the available enzyme. However, a steady state is quickly reached where the complex concentration remains approximately constant due to the equilibrium attained between its rate of formation and dissociation. In 1913, Leonor Michaelis and Maud Menten [44, 45], developed the mathematical expression of the velocity (v) of an enzyme-catalyzed reaction. The rate of the final step of the reaction, which results in the formation of a product (P) may be written as

$$v = \frac{d[P]}{dt} = k_2[ES]. \tag{1.8}$$

From the steady state assumption one can write the rate of change of $[ES]$ in terms of all three rate terms as

$$\frac{d[ES]}{dt} = k_1[E][S] - (k_2 + k_{-1})[ES] = 0. \tag{1.9}$$

Therefore,

$$k_1[E][S] = (k_2 + k_{-1})[ES]. \tag{1.10}$$

Rearranging terms we get:

$$\frac{[E][S]}{[ES]} = \frac{k_2 + k_{-1}}{k_1}. \tag{1.11}$$

The term $\frac{k_2+k_{-1}}{k_1}$ is defined as the Michaelis constant, K_M.

$$\begin{aligned} K_M = \frac{[E][S]}{[ES]} &= \frac{k_2 + k_{-1}}{k_1} \\ &\Rightarrow [ES] = \frac{[E][S]}{K_M}. \end{aligned} \tag{1.12}$$

Since the total amount of enzyme present in the reaction is conserved, it follows that at any time during the reaction, the total concentration of enzyme, $[E]_T$, is equal to the sum of the bound and unbound enzyme concentrations

$$\begin{aligned} [E]_T &= [ES] + [E] \\ &\Rightarrow [E] = [E]_T - [ES]. \end{aligned} \tag{1.13}$$

Substituting the value of $[E]$ from equation 1.13 into 1.12, a new expression for the complex concentration can be obtained as

$$[ES] = \frac{[E]_T[S]}{K_M + [S]}. \tag{1.14}$$

Substituting equation 1.14 into 1.8, the rate of product formation can be written as

$$\begin{aligned} v &= k_2 \frac{[E]_T[S]}{K_M + [S]} \\ &= V_{max} \frac{[S]}{K_M + [S]}. \end{aligned} \tag{1.15}$$

Equation 1.15 is the Michaelis-Menten equation, and is a quantitative representation of the rate of reaction for enzyme-mediated processes. The V_{max} term represents the maximum

rate of the reaction, and is obtained when the binding sites on the enzyme molecules are fully saturated with substrates. K_m is a measure of the concentration of substrate necessary to achieve half the maximum rate of reaction. The rate of reaction from equation 1.15 has 3 distinct possibilities:

1. When $K_M >> [S]$, the reaction is a first order process and the rate is directly proportional to the available substrate concentration.

2. When $K_M << [S]$, the reaction proceeds at a constant rate which is equal to the maximum rate V_{max}.

3. When $K_M \approx [S]$, the rate of reaction is approximately half V_{max}.

1.6.2 Compartmental Models

The most common model used in PK is the compartmental model. In the compartmental model, we resolve the body into a series of compartments wherein the ADME processes occur. The compartmental models represent the most efficient method of categorizing the body into smaller homogeneous compartments within which the fate of the drug may be observed. The simplest of such models is the one-compartment model which assumes rapid equilibrium within the compartment. In a one-compartment PK model, we assume that a change in the blood plasma concentration reflects a concurrent change in tissue/organ concentration [37]. The rate of change of the drug concentration in the compartment follows a first-order process and can be written as

$$\frac{dC(t)}{dt} = -kC(t), \tag{1.16}$$

with solution

$$C(t) = C_0 e^{-k(t-t_0)}. \tag{1.17}$$

$C(t)$ is the concentration of the drug at time t, C_0 is the initial concentration of the drug at time t_0, and k is the elimination rate constant. In the simplest case, the one-compartment

model assumes the body to be a simple homogenous unit within which the drug undergoes the ADME processes. The model does not account for the intricacies that may arise as the drug flows from one part of the body to the other, which may affect its overall PK. In figure 1.2, k_{10} is the rate of elimination of the drug from the body. Assuming a first-order process, the rate of change of concentration with time in figure 1.2(a) can be written in the form of equation 1.16, with k replaced by k_{10}. The solution can be written in terms of the volume of distribution V_d, which relates the amount of drug in plasma to the amount in the body and dosage D of the drug as

$$C(t) = \frac{D}{V_d} e^{-k_{10}(t-t_D)}. \tag{1.18}$$

In equation 1.18, t_D is the time of drug administration and $t \geq t_D$ for all t. k_{10} is the rate of elimination from compartment 1 into a compartment 0.

For the second case, assuming a drug is infused into the body at a constant rate I, shown in figure 1.2(b), the concentration profile may be written during the infusion as

$$\frac{dC(t)}{dt} = I(t) - k_{10}C(t). \tag{1.19}$$

The solution is

$$C(t) = C_0 e^{-k_{10}(t-t_i)} + \frac{I}{k_{10}}(1 - e^{-k_{10}(t-t_i)}), \tag{1.20}$$

where

$$I(t) = \begin{cases} \frac{D}{t_{inf}}, & \text{if } t_i \leq t \leq t_f. \\ 0, & \text{otherwise.} \end{cases} \tag{1.21}$$

$I(t)$ is the time-dependent rate of infusion, t_i and t_f are the start and end times of the infusion. t_{inf} is the infusion length ($t_{inf} = t_f - t_i$), and t is any post-infusion time. D is the administered dose. If $t > t_f$, equation 1.18 is also the solution of equation 1.19.

We can observe from equation 1.19 that during the infusion phase of the drug, the

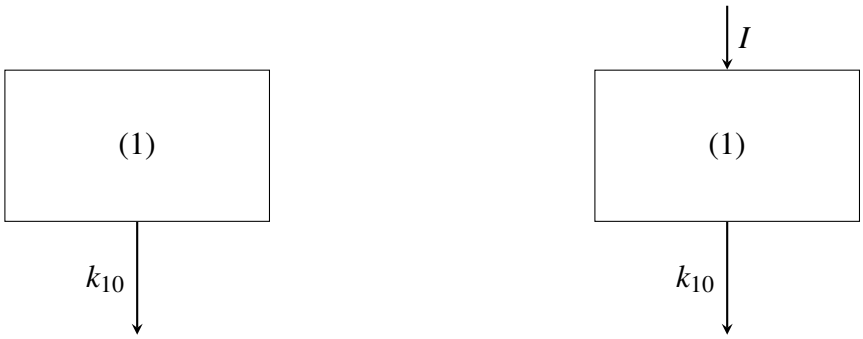

(a) Without infusion (b) With infusion

Figure 1.2: A simple one-compartment system

change in concentration depends on the zeroth order rate of infusion I and the linear elimination constant $-k_{10}C(t)$. Equation 1.16 represents a classical kinetic model of drug in a single compartment model. The model assumes compartmental homogeneity and a well-stirred medium. However, biological systems are characterized by spatial heterogeneity even at the intracellular scale. The heterogeneity results from overcrowding due to the high macromolecular concentrations. Thus, within such a crowded media, the rate of reaction takes a time-dependency [46] given by:

$$k = k_o t^{-\eta}. \tag{1.22}$$

The resulting rate equation can be expressed as

$$\frac{dC(t)}{dt} = -k_o t^{-\eta} C, \tag{1.23}$$

with the solution

$$C(t) = \begin{cases} C_o \left[\frac{t_o}{t}\right]^k & \text{if } \eta = 1 \\ C_o \exp\left[-\frac{k_o}{1-\eta}[t^{1-\eta} - t_o^{1-\eta}]\right] & \text{if } \eta \neq 1. \end{cases} \tag{1.24}$$

1.6.3 Multi-Compartment Models

In a multi-compartment model, we think of the activities within the body as a discrete set of compartments, each with specific characteristics, and the assumption of homogeneity within individual compartments. Again, the molecule is absorbed in the principal compartment but may be eliminated from within any of the compartments. The molecule may also be exchanged between any number of compartments depending on the purpose and design of the model. The most common multi-compartment PK model is the two-compartment model, where the drug is absorbed and eliminated through the principal compartment, and is distributed to and metabolized in the peripheral compartment. This model is significantly more precise than the one-compartment model due to the non-homogenous nature of biological systems and because the single compartment is assumed to be instantaneously well-mixed.

Figure 1.3 shows two types of two-compartment models. In the first case, figure 1.3(a), the infused molecule in compartment 1 is eliminated into an external compartment 0, and distributed to and from compartment 2. The interaction of compartments 1 and 2 may be thought of in terms of a reversible reaction with rate constants k_{12} and k_{21} respectively. A second type of two-compartment model is shown in Figure 1.3(b). There, the molecule infused in compartment 1 is distributed reversibly to compartment two. The molecule in compartment two is also able to flow to an external compartment 0, which represents the elimination from the system. In figure 1.3, k_{12}, k_{21}, k_{10}, and k_{20} are rate constants of the form k_{ij}, each of these describes the rate of flow from compartment i to j. The rate of change of concentration, $\frac{dC(t)}{dt}$, for the drug in compartments 1 and 2 in figure 1.3(a) are given as

$$\frac{dC_1(t)}{dt} = k_{21}C_2(t) - k_{12}C_1(t) - k_{10}C_1(t) \tag{1.25}$$

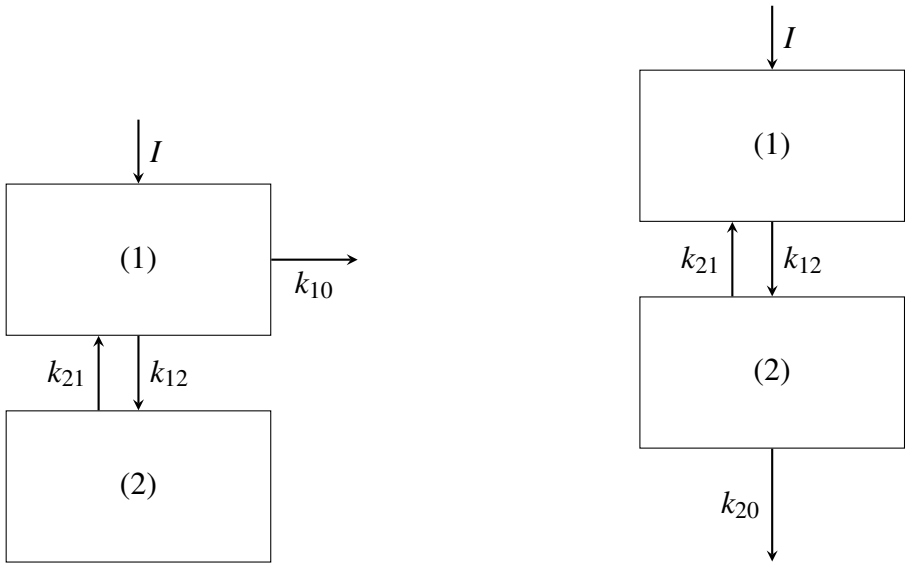

(a) With infusion and elimination from compartment (1)

(b) With infusion from compartment (1) and elimination from compartment (2).

Figure 1.3: A simple two-compartment system.

and

$$\frac{dC_2(t)}{dt} = k_{12}\,C_1(t) - k_{21}\,C_2(t), \tag{1.26}$$

assuming the end of infusion. If all the drug is initially within compartment (1), then the solutions are

$$C_1(t) = \frac{C_0(\alpha - k_{21})}{(\alpha - \beta)}\,e^{-\alpha\delta t} + \frac{C_0(k_{21} - \beta)}{(\alpha - \beta)}\,e^{-\beta\delta t} \tag{1.27}$$

and

$$C_2(t) = \frac{C_0 \cdot k_{12}}{(\alpha - \beta)}(e^{-\alpha\delta t} - e^{-\beta\delta t}), \tag{1.28}$$

where $C_0 \neq 0$, $\Delta t = t - t_o$, and

$$\alpha = \frac{1}{2}\left[(k_{10}+k_{21}+k_{12}) + \sqrt{(k_{10}+k_{21}+k_{12})^2 - 4k_{10}k_{21}}\right] \tag{1.29}$$

$$\beta = \frac{1}{2}\left[(k_{10}+k_{21}+k_{12}) - \sqrt{(k_{10}+k_{21}+k_{12})^2 - 4k_{10}k_{21}}\right]. \tag{1.30}$$

1.6.4 Saturable Kinetics

Biological reactions occur under spatially constrained conditions. These constraints are due to the fractal-like nature of the surfaces of biological systems. Kopelman [46] proposed that for a reaction within a non-homogenous medium, the kinetics is fractal-like and can be described by the time-dependent rate constant

$$k = k_o t^{-h}, \tag{1.31}$$

where $-h$ is the slope when k is plotted against t on a log-log scale. At steady-state, the rate of reaction is proportional to an anomalous reaction order X, written as:

$$\frac{dC}{dt} = kC^X, \tag{1.32}$$

where X can be written in terms of the spectral dimension $1+2/d_s$, and $d_s = 1+(1-h)^{-1}$. Therefore, for a heterogenous medium, assuming the reaction in equation 1.7, the rate of the forward reaction can be written as

$$\frac{d[ES]}{dt} = k_1[E][S]^X - (k_2+k_{-1})[ES] = 0. \tag{1.33}$$

Therefore,

$$k_1[E][S]^X = (k_2+k_{-1})[ES]. \tag{1.34}$$

Rearranging terms we have:

$$\frac{[E][S]^X}{[ES]} = \frac{k_2+k_{-1}}{k_1}. \tag{1.35}$$

Substituting $K_M = \frac{k_2+k_{-1}}{k_1}$, equation 1.35 can be written as a form of equation 1.12. The resulting equation represents the steady-state enzyme kinetics

$$\begin{aligned} v &= k_2 \frac{[E]_T [S]^X}{K_M + [S]^X} \\ &= V_{max} \frac{[S]^X}{K_M + [S]^X}. \end{aligned} \tag{1.36}$$

A single compartment saturable model with fractal effects can be modelled with a slightly modified form of equation 1.36 [47]. The rate of change of concentration with time is given as

$$\frac{dX}{dt} = -\frac{V_{max} X^a}{K_M + X^b}, \tag{1.37}$$

where a and b are the reaction orders, which are unique for individual processes. The solution to equation 1.37 depends on the unique values of a and b. For the special case where $a = 1$ and $b \neq 0$,

$$K_M \ln\left[\frac{X}{X_o}\right] + \frac{X^b}{b} = V_{max}(t - t_o). \tag{1.38}$$

Another special case is when $a = 1 + b$; the solution is

$$\frac{K_M}{1-a}\left[X^{1-a} - X_o^{1-a}\right] + \ln\left[\frac{X}{X_o}\right] = V_{max}(t - t_o). \tag{1.39}$$

1.7 Anthracyclines

The primary drug used in this study is DOX. DOX belongs to the drug class anthracyclines, which were first discovered when daunomycin was isolated from *Streptomyces peucetius* in the early 1960's. Since then, several other members of this drug class have been discovered and have found significant clinical use. Anthracyclines are indicated in more types of cancer treatment than any other drug class [31]. Their derivatives have also been found to be active against particular types of tumours [48]. Several mechanisms for anthracycline cytotoxicity have been proposed, although a lot of these have been debated

and are currently a subject of controversy. However, the widely accepted mechanisms of action for members of the drug class includes the intercalation of the drugs between DNA base pairs, thus inhibiting the replication of DNA. This results in the inability to form daughters in quickly dividing tumour cells [49]. Anthracyclines also inhibit the enzyme Topoisomerase II and by extension, the ability of DNA to replicate [50], causing the initiation of apoptosis by a cellular arrest in the S-phase [51]. Other possible mechanisms of actions of DOX have been proposed, including the action of free radicals in inducing cell membrane damage, causing oxidative stress through the oxidation of the drug to semiquinone [52]. This reaction releases reactive oxygen species (ROS), which have been linked to DNA damage [53]. Gewirtz [54] suggested that the various mechanisms of action ascribed to DOX may be concentration-dependent, with concentrations close to the peak plasma concentration favouring the topoisomerase II inhibition mechanism, and those ranging from 2 $\mu mol \cdot l^{-1}$ to 4 $\mu mol \cdot l^{-1}$ preferring the free radical mechanism.

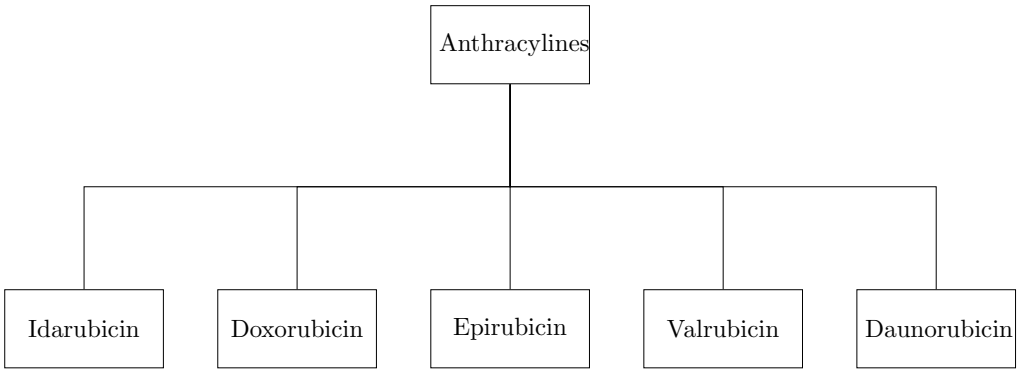

Figure 1.4: Anthracycline Drug Class

Figure 1.4 shows some of the drugs within this class. Idarubicin is used in the treatment of leukemia and advanced breast cancer. Valrubicin is used in the treatment of bladder cancer. Epirubicin and daunorubicin are used in the treatment of several types of cancers including breast cancer, non-Hodgkin's lymphoma, leukemia and Ewing's sarcoma. Although anthracyclines are widely used in clinical practice, their effectiveness is affected by their associated cytotoxicity to healthy body cells. Cardiotoxicity is the main cytotoxic

effect following long term administration of anthracyclines. The underlying mechanism responsible for the cardiotoxicity has been suggested to be the same one responsible for the apoptosis of cancer cells, and the severity of toxicity is related to the cumulative dose of anthracyclines taken within any therapeutic window.

1.7.1 Doxorubicin

DOX, also known as adriamycin, is the most widely used anthracycline and is used in the treatment of solid tumours such as breast, lung, and various types of sarcomas. The chemical structure of DOX consists of a hydrophobic tetracyclic aglycone and a daunosamine sugar attached by a glycosidic bond (Figure 1.5). DOX intercalates into DNA by the interaction of its aglyconic moiety with the DNA base pairs, with the daunosamine ring acting as a minor groove binding agent [55]. DOX is usually administered intravenously resulting in 100% bioavailability, which implies that the total administered dose is available for systemic distribution. Other forms of DOX administration have been examined [56, 57], with lower levels of bioavailability due to factors such as the reduced binding of DOX to the CYP450 enzymes and the over-expression of efflux proteins in the gut [58].

After infusion, DOX is characterized by high plasma concentration, which is immediately followed by a sharp drop in concentration as the drug is distributed into tissues and metabolized via the liver. Green *et al.* [59] reported that $74 \pm 1.7\%$ of the total plasma DOX was bound to plasma protein, with a constant $20 \pm 5\%$ available for distribution over measured concentrations of 20 nmol to 2 μmol. DOX is extensively bound to cells following distribution, with up to 350-times higher concentration of the drug observed in mononuclear cells than that observed in plasma [61]. Other studies have shown a heart-to-plasma concentration ratio of 40 in rats 24 hours after infusion [62]. Most of the DOX available for distribution is deposited in the liver where it is metabolized into doxorubicinol (DOL) and other metabolites [63]. Benjamin *et al.* [64] suggested that the rapid metabolism of DOX into its metabolites results from a single passage through the liver. DOX is metabolized

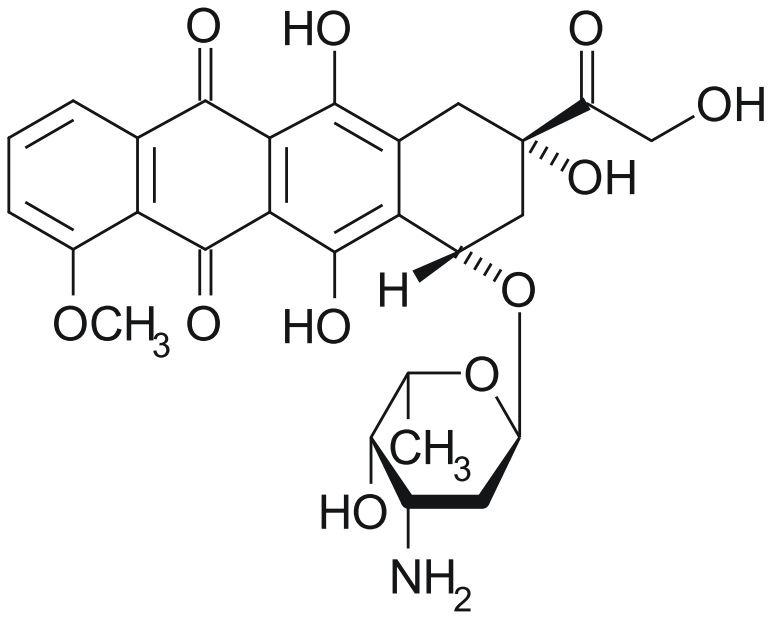

Figure 1.5: DOX chemical structure showing the aglycone and sugar rings [60].

into DOL, a toxic metabolite, via enzymatic reduction by aldoketoreductases which are present in high concentrations in liver and kidney cells [53]. Studies have suggested that the aglycone metabolites may be responsible for the associated DOX related cardiotoxicity by altering mitochondrial function and increasing the permeability of the inner membrane to small molecules [65]. The primary route of DOX elimination is through the bile [66], with up to 45% of the administered drug eliminated via the bile 7 days post-infusion. Urinary excretion of DOX accounts for about 3.3% of the administered dose 5 days after administration [63]. A combined 3-fold increase in total biliary and urinary excretion has been observed in patients with renal insufficiencies [67, 68]. Large inter-individual variations in PK behaviours characterize DOX [69], with up to 10-fold variation in the dose-normalized area under the curve (AUC) observed. The plasma elimination of DOX has been characterized by a biphasic [63] and triphasic elimination curve [64, 61, 70]. DOX exhibits a short half-life of 12 ± 8 minutes, an intermediate half-life of 3.3 ± 2.2 hours, and a long half-life of 29.6 ± 13.5 hours post-infusion. However, later studies have suggested a dose-

related elimination pattern for the drug, suggesting that at low doses, the drug undergoes a bi rather than a tri-exponential elimination pattern [71]. This implies that above a certain dose threshold, it is possible to observe an extra elimination phase. DOX undergoes linear kinetics with dose-dependent absorption, distribution and elimination. The AUC of the drug, which is a measure of the total drug exposure, appears to be independent of the maximum concentration with the terminal elimination phase contributing up to 75% of the total AUC [59].

1.7.2 Doxorubicin Related Toxicity

Although DOX is used in the treatment of a wide range of cancers, its use is limited by its associated toxicities. The more common side effects such as nausea, vomiting, and baldness have been well-documented [72]. However, more lethal toxicities occur as the dose is increased. Some of these adverse effects may pose more threat to the patient than the cancer itself. Cardiomyopathy, the most common side effect, with a mortality rate of 50% has been correlated to DOX cumulative dose above 550 $\mathrm{mg} \cdot \mathrm{m}^{-2}$ [73]. Studies have suggested the likelihood of acute DOX cardiomyopathy of 11% and occurrence is usually two to three days after drug administration. DOX cardiological toxicity occurs in 2% of treated patients. Currently, the mechanism of cardiotoxicity of DOX is unclear, although recent studies have suggested DOX risk-factors which may potentially increase the occurrence of severe toxicities; these risk factors include age, lifestyle choices, the combination with cardiotoxic anti-tumour drugs, and prior radiation therapy [74].

1.7.3 Single Agent Doxorubicin

DOX is effective as a single drug or when administered concomitantly with other active agents as a first-line or adjuvant treatment. DOX chemotherapy is characterized by its response rate, which can reach as high as 70%. The response rate is a measure of tumour progression after treatment. Studies involving liposomal DOX administered to breast cancer patients have recorded response rates of 36% as a single agent, and 47% in combination

with paclitaxel [75]. As a single agent, DOX has been found to show large inter-individual PK variations in patients treated with two or more courses of the drug [76]. Much of this variation has been observed from the ratio of DOX metabolized relative to the time after dose administration, and from patients without known renal or liver insufficiencies [77].

1.7.4 Dose-Response Relationship of Doxorubicin

The major considerations when establishing a dose-response relationship is whether the specific agent is solely responsible for the response, and how quantifiable the response is. Previous studies on single-agent administration of DOX to patients with solid tumours showed that dosages of up to 60 mg/m^2 administered over three to four weeks are most efficient for the tumour-killing effect of the drug. Consequently, increasing this tolerable dosing limit may result in achieving a maximum cumulative dose, which increases side-effects and may result in acute toxicities. Much research has focused on administering smaller dosages of DOX over a longer period, which produces an increased exposure to the drug without a loss in effectiveness; however, due to the severe side effects associated with anti-cancer drug toxicity, the need for an effective dose remains a challenge for oncologists. Studies using in vivo and in vitro methods have determined the maximum tolerated dose of the drug, above which there exists an onset of acute toxicities. Bryan *et al.* [78] studied the dose-response relationship of DOX using a 6-dose schedule for patients in 5 risk levels. The study could not establish a relationship between dose schedule and remission induction time - with different types of tumour producing a different response when treated with any of the six dosing cycles. However, over a cumulative dose of 500 mg/m^2, severe toxicities were observed in patients in the low-risk categories. In the study, the 60 mg/m^2 dosage group showed the greatest remission rate, while the 45 mg/m^2 dosage group produced the longest remission from observed subjects. This is similar to the observed response rate of single-agent DOX in the treatment of histological sarcomas, where complete and partial remissions occurred in 9% and 32% of subjects respectively, resulting in a response rate of

25% observed in patients treated with 60 mg/m^2 of DOX[63].

1.8 Alternative Doxorubicin Formulations

To maintain the overall significance of anthracyclines as anticancer agents, studies in the past decade have targeted the need to preserve drug efficacy and limit associated toxicity; this is even more important since tumour-kill and toxicity have different mechanisms. A result of this effort is the development of novel drugs which are prodrugs or alternative formulations of known antineoplastic agents. These provide a balance between efficacy and safety.

Liposomal DOX formulations were developed to improve the conventional DOX therapeutic index by altering its biodistribution and PK [79, 80]. Liposomes are made of an aqueous core and a surrounding lipid bilayer. The active drug is enclosed within the lipid membrane or loaded into the aqueous core. They are alternatively referred to as nanoparticle formulations due to their distinctly small size ($\leq$ 100 nm). Liposomal DOX is further classified into two depending on the presence of polyethylene glycol (PEG). In the pegylated liposomal DOX (PLD) formulation, the lipid bilayer is coated with PEG, in a process called pegylation. The PEG coating reduces the binding of the liposome and proteins within the tumour microenvironment, ensuring that the circulation time of the drug in the blood is increased, and more of the drug is delivered to the tumour site. The two major encapsulated formulations of DOX in clinical use today are Myocet (MYO), which is referred to as conventional liposomal DOX, and Doxil/Caelyx (PLD), which is referred to as stealth liposomal DOX.

The mechanism of drug transport in liposomal DOX follows from the leaky vasculature of tumour cells. DOX molecules escape from the liposome carrier into the surrounding environment in a process known as extravasation. In the tumour site, extravasation is responsible for the release of free DOX to the tumour cells. The rapid, uncontrolled division of cancer cells leads to an incomplete vascular architecture, and leaky blood vessels. Thus,

the drug can bypass the heart and gastrointestinal cells which have tighter cell-cell junctions and prevent the passage of liposomes through them. The lack of functional lymphatic drainage also ensures that extravasated liposomes are retained within the vascular space, leading to an accumulation of the drug in the tumour site. The activity of liposomal formulations of DOX has been studied in several cancer types. In a phase III study of 509 breast cancer patients using MYO and PLD, O'Brien *et al.* [81] observed that compared with MYO (58 mg/m^2 every three weeks), PLD (48 mg/m^2 every four weeks) treated patients showed $7-$fold less risk of attaining cardiotoxicity with similar response and survival profiles. Other studies using encapsulated DOX formulations have shown a considerable reduction in the mild side effects of DOX when compared with conventional DOX. Cowens *et al.* [82] reported markedly less gastrointestinal abnormalities using PLD than the free drug. Mross *et al.* [83] showed that for patients treated with MYO, the concentration profiles suggested that up to 85% of DOX in plasma was in encapsulated form, ensuring that the risk of reaching peak plasma concentration(C_{max}), which has been indicated in the occurrence of DOX toxicity, was markedly reduced.

The PK of PLD has been studied in patients with solid tumours [84], where it was observed that the concentration of free DOX in plasma was negligible compared with the encapsulated form. The study provided evidence of a dose-dependent PLD AUC and concentration with a dose-independent clearance. The drug was characterized by a smaller steady-state volume of distribution (V_{SS}) indicating greater stability of the drug within the plasma. Likewise, minor DOX toxicities such as nausea, alopecia and myelosuppression were markedly reduced compared to conventional DOX administration. The terminal half-life of PLD after administration was up to 70 hours, which is consistent with animal studies of mice imbued with colon cancer cell strains where, after an initial long plasma circulation phase, liposomes were observed in the tumour-surrounding extracellular space [85]. Other animal models have shown an increased AUC, as well as reduced clearance and distribution volume (V_d) compared to free DOX administration in dogs and rabbits treated with

PLD [85]. Gabizon *et al.* [86], in a study aimed at correlating animal PLD observations with human subjects, explored the PK of PLD and conventional DOX in sixteen cancer patients. They observed a striking difference between the plasma clearance rate of free DOX between the PLD and conventional DOX treated groups. At all times that blood samples were considered, encapsulated and total (encapsulated + free) DOX concentrations were superimposable, suggesting that almost all the DOX available in plasma existed in the encapsulated form. As was observed from previous studies, the clearance rate between two PLD dose groups (25 mg/m^2 and 50 mg/m^2) were identical, suggesting a dose-independent behaviour. Perhaps, the most important observation from the study was the concentration of DOX in the malignant effusions of twelve patients, where peak concentrations of the drug were observed in the pleural fluid several days after PLD administration. The drug levels obtained after conventional DOX were found to be 16-fold less than in PLD treated patients. This study suggests that while both drugs undergo similar metabolic patterns, the rate of metabolite formation after PLD is markedly slower than after DOX administration due to the rate of metabolism being slower than that of elimination.

1.9 Objectives

The current focus of oncological research involves a more patient-based approach to cancer treatment. In doing this, unique patient characteristics such as cancer types, and factors such as age are matched with the genetic profile of the patient to suggest the most accurate and effective treatment [87]. In this thesis, a population pharmacokinetic model is introduced to predict the plasma concentration and important pharmacokinetic parameters of DOX and DOL in cancer patients. The approach used in this work considers the possibility of non-first-order kinetics of DOX and its metabolites using a series of compartmental models to describe unique PK processes. The main focus of this research is to find the most effective dosing plan for patients in any of these groups. Along with these, this thesis aims to achieve the following objectives:

- To develop a physical model of anticancer drug flow in the body.
- To incorporate drug release for the case of the encapsulated drug into the model.
- To obtain mathematical expressions for the different rates of the PK processes.

Chapter 2

Methodology

Truth has nothing to do with the conclusion,

and everything to do with the methodology.

– L. Fleinhardt

2.1 The Model

The model design used in this thesis is the four-compartment model as illustrated in figure 2.1. In this model, we assume a well-mixed central compartment (1) which represents the blood plasma and the compartment where the molecule concentrations are measured. This compartment represents the plasma volume of the molecules used in this work. The metabolization and elimination organs such as the liver and kidney compartment denoted by number (2), represents the drug's metabolism, activation and elimination. The healthy cells are represented by compartment (3), and the tumour cells by compartment (4). Compartments (3) and (4) allow for measurement of the amount of drug that is available to the healthy and tumoured cells respectively. These can be compared to experimental estimates to provide a measure of the toxicity of the drug to both cell types. This simple model representation of our biological system is sufficient for this work as we are more interested in the drug's behaviour in vivo. Table 2.1 shows the molecules used in the model and the compartments within which they are active. In total, there are five representative types of molecules in the model. The primary molecule, with index (d_1), represents the drug DOX, the active cytotoxic drug. The major metabolite suggested to be responsible for acute toxi-

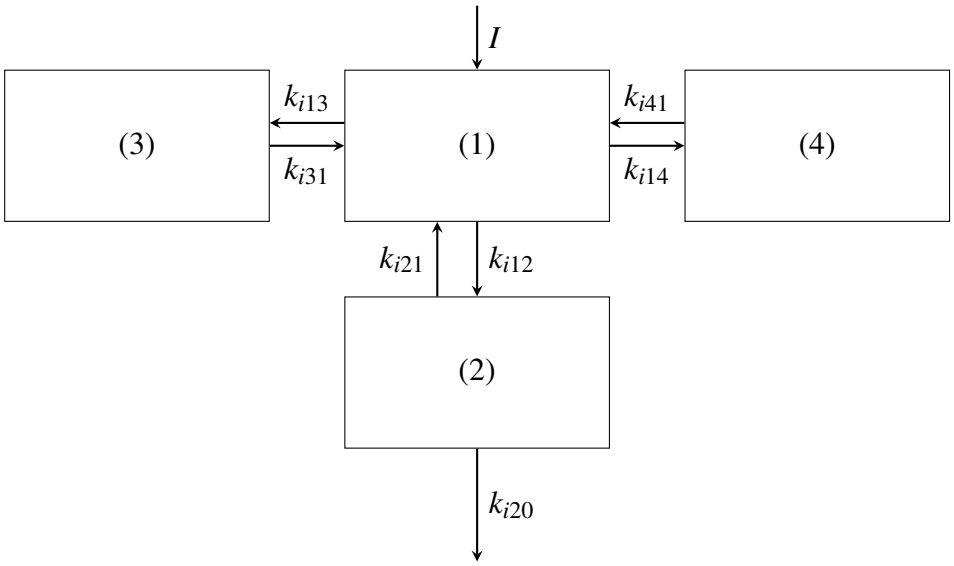

Figure 2.1: The four-compartment system used in this work.

Table 2.1: Molecules used in the model and their active compartments

Molecule (index)	Compartment
DOX (d_1)	0-4
DOL (d_2)	0-4
CBR1 (d_3)	2
DOX-CBR1 (d_4)	2
Encapsulated DOX (d_5)	0-2

Compartment 0 here is the environment external to the body and is representative of the elimination of a molecule from the body.

city, DOL, is assigned index (d_2). The carbonyl reductase enzyme (CBR1) responsible for DOX metabolism is represented by the molecule index (d_3). The enzyme-substrate complex DOX-CBR1, formed by the interaction of DOX with CBR1 is assigned the molecule index (d_4). DOX administered in encapsulated form is represented by molecule index (d_5). The model herein described is represented by a series of ordinary differential equations written as

$$\frac{dX_{di,ci}}{dt} = I_{di,ci} + \sum_{j=1}^{4} \frac{dX_{di,ci}^{(j)}}{dt}, \tag{2.1}$$

where $I_{di,ci}$ is the time-dependent rate of infusion of molecule di into compartment ci, and the $X_{di,ci}$ is the time-dependent amount of molecule di in compartment ci. The sum within

the differential equation is unique for each type of molecule and each compartment. In compartment ci the concentration of the molecule di is

$$C_{di,ci} = \frac{X_{di,ci}}{V_{d,di,ci}}, \tag{2.2}$$

where $V_{d,di,ci}$ is the volume of distribution of molecule di within compartment ci. The differential components of the RHS of equation 2.1 describe four main reactions occurring within the model and are described below assuming N types of molecules and M compartments. In our analysis in the next chapter, we will allow N to vary from 1 to 5 and M from 0 to 4, with $M = 0$ representing the environment exterior to the body.

2.1.1 The kinetic flows between compartments

The first term in the sum within equation 2.1 is the flow of molecules between the compartments

$$\frac{dX^{(1)}_{di,ci}}{dt} = \sum_{cj\neq ci}^{M}\sum_{p=0}^{2}\left[\frac{\bar{k}^{(1,p)}_{di,cj,ci}X^{A^{(1,p)}_{di,cj,ci}}_{di,cj}}{1+\Gamma^{(1,p)}_{di,cj,ci}X^{B^{(1,p)}_{di,cj,ci}}_{di,cj}} - \frac{\bar{k}^{(1,p)}_{di,ci,cj}X^{A^{(1,p)}_{di,ci,cj}}_{di,ci}}{1+\Gamma^{(1,p)}_{di,ci,cj}X^{B^{(1,p)}_{di,ci,cj}}_{di,ci}}\right], \tag{2.3}$$

where

$$\begin{aligned}\bar{k}^{(1,p)}_{di,ci,cj} &= k^{(1,p)}_{di,ci,cj}\left[1+\sum_{dj=1}^{N}\sum_{ck=1}^{M}\sum_{pi=0}^{2}\frac{\alpha^{(1,p,pi)}_{di,ci,cj,dj,ck}X^{C^{(1,p,pi)}_{di,ci,cj,dj,ck}}_{dj,ck}}{1+\beta^{(1,p,pi)}_{di,ci,cj,dj,ck}X^{D^{(1,p,pi)}_{di,ci,cj,dj,ck}}_{dj,ck}}\right]H\left(X_{di,ci}\right)\\ &\times H\left(1+\sum_{dj=1}^{N}\sum_{ck=1}^{M}\sum_{pi=0}^{2}\frac{\alpha^{(1,p,pi)}_{di,ci,cj,dj,ck}X^{C^{(1,p,pi)}_{di,ci,cj,dj,ck}}_{dj,ck}}{1+\beta^{(1,p,pi)}_{di,ci,cj,dj,ck}X^{D^{(1,p,pi)}_{di,ci,cj,dj,ck}}_{dj,ck}}\right).\end{aligned} \tag{2.4}$$

$k^{(1,p)}_{di,ci,cj}$ and $\Gamma^{(1,p)}_{di,ci,cj}$ are the kinetic rate coefficient and saturable kinetics coefficient for molecule di flowing from compartment ci into cj for kinetic process p respectively. The $\alpha^{(1,p,pi)}_{di,ci,cj,dj,ck}$ and $\beta^{(1,p,pi)}_{di,ci,cj,dj,ck}$ terms are the interaction kinetics parameters due to the influence of molecule dj in compartment ck on the kinetics of molecule di in compartment ci. They

provide a measure of the effect of molecule *dj* in compartment *ck* on the flow of *di* from *ci* to *cj*. The $\bar{k}^{(1,p)}_{di,ci,cj}$ term has been used for convenience to represent the effective rate constant. The *A*, *B*, *C*, and *D* terms are the fractal exponents of the reaction and describes the heterogeneity of the system. The superscript *p* represents the process which determines the exponent. These exponents are free fitting parameters with initial values of: $p = 0$, $A^{(1,0)}_{di,ci,cj} = B^{(1,0)}_{di,ci,cj} = 0$, for a zeroth-order process; $p = 1$, $A^{(1,1)}_{di,ci,cj} = B^{(1,1)}_{di,ci,cj} = 1$, for a first-order process; and $p = 2$, $A^{(1,2)}_{di,ci,cj} = B^{(1,2)}_{di,ci,cj} = 2$, for a second order process. The $H\left(X_{di,ci}\right)$ function represents the Heaviside step function, which is zero for negative argument and one for a positive argument.

2.1.2 The conversion of one molecule into another

The second term in the sum within equation 2.1 is the conversion of one type of molecule into a different type of molecule. Figure 2.2 shows molecule *dj* within compartment *cj* being converted into molecule *di* in compartment *ci*.

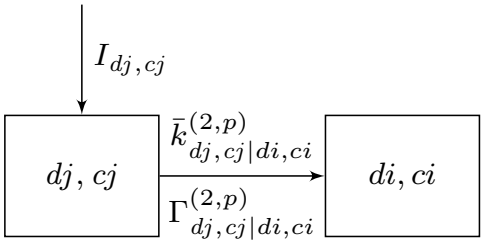

Figure 2.2: The conversion of molecule *dj* in compartment *cj* to d_i in compartment c_i.

The equation that describes this process is:

$$\frac{dX^{(2)}_{di,ci}}{dt} = \sum_{dj=1}^{N}\sum_{cj=1}^{M}\sum_{p=0}^{2}\left[\frac{\delta^{(1,p,di,ci)}_{dj,cj|di,ci}\bar{k}^{(2,p)}_{dj,cj|di,ci}X^{A^{(2,p)}_{dj,cj|di,ci}}_{dj,cj}}{1+\Gamma^{(2,p)}_{dj,cj|di,ci}X^{B^{(2,p)}_{dj,cj|di,ci}}_{dj,cj}} - \frac{\delta^{(1,p,di,ci)}_{di,ci|dj,cj}\bar{k}^{(2,p)}_{di,ci|dj,cj}X^{A^{(2,p)}_{di,ci|dj,cj}}_{di,ci}}{1+\Gamma^{(2,p)}_{di,ci|dj,cj}X^{B^{(2,p)}_{di,ci|dj,cj}}_{di,ci}}\right], \quad (2.5)$$

where the δ's are the stoichiometric coefficients of the reaction. For example, 2 moles of (dj,cj) becoming 4 moles of (di,ci) would be $\delta^{(1,p,dj,cj)}_{dj,cj|di,ci} = 2$ mol and $\delta^{(1,p,di,ci)}_{dj,cj|di,ci} = 4$ mol.

The effective rate constant for this reaction is

$$\begin{aligned}\overline{k}^{(2,p)}_{dj,cj|di,ci} &= k^{(2,p)}_{dj,cj|di,ci}\left[1+\sum_{dk=1}^{N}\sum_{ck=1}^{M}\sum_{pi=0}^{2}\frac{\alpha^{(2,p,pi)}_{dj,cj|di,ci||dk,ck}X^{C^{(2,p,pi)}_{dj,cj|di,ci||dk,ck}}_{dk,ck}}{1+\beta^{(2,p,pi)}_{dj,cj|di,ci||dk,ck}X^{D^{(2,p,pi)}_{dj,cj|di,ci||dk,ck}}_{dk,ck}}\right]H\left(X_{dj,cj}\right)\\ &\times H\left(1+\sum_{dk=1}^{N}\sum_{ck=1}^{M}\sum_{pi=0}^{2}\frac{\alpha^{(2,p,pi)}_{dj,cj|di,ci||dk,ck}X^{C^{(2,p,pi)}_{dj,cj|di,ci||dk,ck}}_{dk,ck}}{1+\beta^{(2,p,pi)}_{dj,cj|di,ci||dk,ck}X^{D^{(2,p,pi)}_{dj,cj|di,ci||dk,ck}}_{dk,ck}}\right). \qquad (2.6)\end{aligned}$$

$k^{(2,p)}_{dj,cj|di,ci}$ and $\Gamma^{(2,p)}_{dj,cj|di,ci}$ are the kinetic rate coefficient and saturable kinetics coefficient of molecule dj in compartment cj converting into di in ci. The $\alpha^{(2,p,pi)}_{dj,cj|di,ci||dk,ck}$ and $\beta^{(2,p,pi)}_{dj,cj|di,ci||dk,ck}$ terms are the interaction kinetics coefficients which describe the effect of molecule dk in compartment ck on the conversion process. The terms in the subscripts are split by 'I' to signify a change in the type of molecules involved in the reaction. The type of molecules on the left of the break is being converted to the type on the right. The second break 'II' in the subscripts within equation 2.6 signifies the molecules on the right are enhancing or inhibiting the reaction, this represents possible drug-drug interaction effects for a multi-drug system.

We shall assume all the conversion processes occur in compartment 2, hence $cj = ci = 2$, doing this equation 2.5 can be written as

$$\frac{dX^{(2)}_{di,2}}{dt} = \sum_{dj=1}^{N}\sum_{p=0}^{2}\left[\frac{\delta^{(1,p,di)}_{dj|di}\overline{k}^{(2,p)}_{dj|di}X^{A^{(2,p)}_{dj|di}}_{dj,2}}{1+\Gamma^{(2,p)}_{dj|di}X^{B^{(2,p)}_{dj|di}}_{dj,2}} - \frac{\delta^{(1,p,di)}_{di|dj}\overline{k}^{(2,p)}_{di|dj}X^{A^{(2,p)}_{di|dj}}_{di,2}}{1+\Gamma^{(2,p)}_{di|dj}X^{B^{(2,p)}_{di|dj}}_{di,2}}\right] \qquad (2.7)$$

2.1.3 The conversion of a complex into two molecules

The third term in the sum within equation 2.1 is the dissociation of a molecule into two types of molecules. Figure 2.3 shows the release of molecules dj in compartment cj and dk in compartment ck following the dissociation of di in compartment ci. The rates can be modelled by:

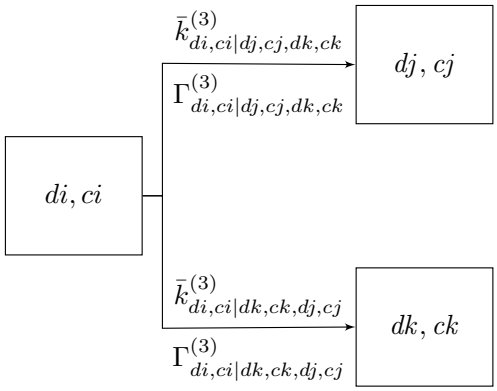

Figure 2.3: The conversion of molecule di in compartment ci into molecules dj and dk in compartments cj and ck respectively.

$$\frac{dX^{(3)}_{di,ci}}{dt} = \sum_{dj,dk=1}^{N}\sum_{cj,ck=1}^{M}\sum_{p=0}^{2}\left\{\frac{-\delta^{(2,p,di,ci)}_{di,ci|dj,cj,dk,ck}\bar{k}^{(3,p)}_{di,ci|dj,cj,dk,ck}X^{A^{(3,p)}_{di,ci|dj,cj,dk,ck}}_{di,ci}}{1+\Gamma^{(3,p)}_{di,ci|dj,cj,dk,ck}X^{B^{(3,p)}_{di,ci|dj,cj,dk,ck}}_{di,ci}}\right.$$
$$+\frac{\delta^{(2,p,dk,ck)}_{dk,ck|di,ci,dj,cj}\bar{k}^{(3,p)}_{dk,ck|di,ci,dj,cj}X^{A^{(3,p)}_{dk,ck|di,ci,dj,cj}}_{dk,ck}}{1+\Gamma^{(3,p)}_{dk,ck|di,ci,dj,cj}X^{B^{(3,p)}_{dk,ck|di,ci,dj,cj}}_{dk,ck}}$$
$$\left.+\frac{\delta^{(2,p,dj,cj)}_{dj,cj|dk,ck,di,ci}\bar{k}^{(3,p)}_{dj,cj|dk,ck,di,ci}X^{A^{(3,p)}_{dj,cj|dk,ck,di,ci}}_{dj,cj}}{1+\Gamma^{(3,p)}_{dj,cj|dk,ck,di,ci}X^{B^{(3,p)}_{dj,cj|dk,ck,di,ci}}_{dj,cj}}\right\}, \tag{2.8}$$

where $\delta^{(2,p,di,ci)}_{di,ci|dj,cj,dk,ck}$, $\delta^{(2,p,dk,ck)}_{dk,ck|di,ci,dj,cj}$ and $\delta^{(2,p,dj,cj)}_{dj,cj|dk,ck,di,ci}$ are the stoichiometric coefficients, and the effective rate constant is written as;

$$\bar{k}^{(3,p)}_{di,ci|dj,cj,dk,ck} = k^{(3,p)}_{di,ci|dj,cj,dk,ck}\left[1+\sum_{dl=1}^{N}\sum_{cl=1}^{M}\sum_{pi=0}^{2}\frac{\alpha^{(3,p,pi)}_{di,ci|dj,cj,dk,ck\|dl,cl}X^{C^{(3,p,pi)}_{di,ci|dj,cj,dk,ck\|dl,cl}}_{dl,cl}}{1+\beta^{(3,p,pi)}_{di,ci|dj,cj,dk,ck\|dl,cl}X^{D^{(3,p,pi)}_{di,ci|dj,cj,dk,ck\|dl,cl}}_{dl,cl}}\right]$$
$$\times\; H\left(X_{di,ci}\right)H\left(1+\sum_{dl=1}^{N}\sum_{cl=1}^{M}\sum_{pi=0}^{2}\frac{\alpha^{(3,p,pi)}_{di,ci|dj,cj,dk,ck\|dl,cl}X^{C^{(3,p,pi)}_{di,ci|dj,cj,dk,ck\|dl,cl}}_{dl,cl}}{1+\beta^{(3,p,pi)}_{di,ci|dj,cj,dk,ck\|dl,cl}X^{D^{(3,p,pi)}_{di,ci|dj,cj,dk,ck\|dl,cl}}_{dl,cl}}\right). \tag{2.9}$$

The $k^{(3,p)}_{di,ci|dj,cj,dk,ck}$ and $\Gamma^{(3,p)}_{di,ci|dj,cj,dk,ck}$ terms are the complex dissociation rate coefficient and saturable kinetics coefficient of molecule *di* in compartment *ci* breaking down into molecules *dj* in compartment *cj* and *dk* in compartment *ck*. The $\alpha^{(3,p,pi)}_{di,ci|dj,cj,dk,ck||dl,cl}$ and $\beta^{(3,p,pi)}_{di,ci|dj,cj,dk,ck||dl,cl}$ are the interaction kinetics coefficients which describe the effect of molecule *dl* in compartment *cl* on the process.

A simplified form of equation 2.8 can be written as follows, assuming all dissociation occurs in compartment 2:

$$\frac{dX^{(3)}_{di,2}}{dt} = \sum_{dj,dk=1}^{N}\sum_{p=0}^{2}\left[-\frac{0.5\bar{k}^{(3,p)}_{di|dj,dk}X^{A^{(3,p)}_{di|dj,dk}}_{di,2}}{1+\Gamma^{(3,p)}_{di|dj,dk}X^{B^{(3,p)}_{di|dj,dk}}_{di,2}} + \frac{0.5\bar{k}^{(3,p)}_{dj|di,dk}X^{A^{(3,p)}_{dj|di,dk}}_{dj,2}}{1+\Gamma^{(3,p)}_{dj|di,dk}X^{B^{(3,p)}_{dj|di,dk}}_{dj,2}} + \frac{0.5\bar{k}^{(3,p)}_{dk|dj,di}X^{A^{(3,p)}_{dk|dj,di}}_{dk,2}}{1+\Gamma^{(3,p)}_{dk|dj,di}X^{B^{(3,p)}_{dk|dj,di}}_{dk,2}}\right], \tag{2.10}$$

where 0.5 is to account for double counting since $\bar{k}^{(3,p)}_{dj|di,dk} = \bar{k}^{(3,p)}_{dj|dk,di}$.

2.1.4 The formation of a complex from two molecules

The last term in the sum within equation 2.1 pertains to the interaction of two molecules to form a third molecule. Figure 2.4 shows the binding of molecules *di* in compartment *ci* and *dj* in compartment *cj* to form *dk* in compartment *ck*.

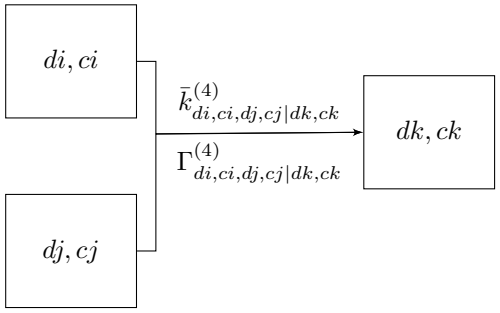

Figure 2.4: The formation of molecule *dk* from the binding of *di* and *dj*.

The differential equation describing the process is shown below:

$$\begin{aligned}\frac{dX^{(4)}_{di,ci}}{dt} &= \sum_{dj,dk=1}^{N}\sum_{cj,ck=1}^{M}\sum_{pi,pj=0}^{2}\left\{\frac{\overline{k}^{(4,pi,pj)}_{dj,cj,dk,ck|di,ci}X^{A^{(4,pi)}_{dj,cj,dk,ck|di,ci}}_{dj,cj}X^{A^{(5,pj)}_{dj,cj,dk,ck|di,ci}}_{dk,ck}}{1+\Gamma^{(4,pi,pj)}_{dj,cj,dk,ck|di,ci}X^{B^{(4,pi)}_{dj,cj,dk,ck|di,ci}}_{dj,cj}X^{B^{(5,pj)}_{dj,cj,dk,ck|di,ci}}_{dk,ck}}\right.\\
&- \frac{\overline{k}^{(4,pi,pj)}_{dj,cj,di,ci|dk,ck}X^{A^{(4,pi)}_{dj,cj,di,ci|dk,ck}}_{dj,cj}X^{A^{(5,pj)}_{dj,cj,di,ci|dk,ck}}_{di,ci}}{1+\Gamma^{(4,pi,pj)}_{dj,cj,di,ci|dk,ck}X^{B^{(4,pi)}_{dj,cj,di,ci|dk,ck}}_{dj,cj}X^{B^{(5,pj)}_{dj,cj,di,ci|dk,ck}}_{di,ci}}\\
&\left.- \frac{\overline{k}^{(4,pi,pj)}_{di,ci,dk,ck|dj,cj}X^{A^{(4,pi)}_{di,ci,dk,ck|dj,cj}}_{di,ci}X^{A^{(5,pj)}_{di,ci,dk,ck|dj,cj}}_{dk,ck}}{1+\Gamma^{(4,pi,pj)}_{di,ci,dk,ck|dj,cj}X^{B^{(4,pi)}_{di,ci,dk,ck|dj,cj}}_{di,ci}X^{B^{(5,pj)}_{di,ci,dk,ck|dj,cj}}_{dk,ck}}\right\}. \qquad (2.11)\end{aligned}$$

The effective rate constant can be written as;

$$\begin{aligned}\overline{k}^{(4,pi,pj)}_{di,ci,dj,cj|dk,ck} &= \delta^{(3,pi,pj,di,ci)}_{di,ci,dj,cj|dk,ck}k^{(4,pi,pj)}_{di,ci,dj,cj|dk,ck}H\left(X_{di,ci}\right)H\left(X_{dj,cj}\right)\\
&\times H\left(1+\sum_{dl=1}^{N}\sum_{cl=1}^{M}\sum_{pk=0}^{2}\frac{\alpha^{(4,pi,pj,pk)}_{di,ci,dj,cj|dk,ck||dl,cl}X^{C^{(4,pi,pj,pk)}_{di,ci,dj,cj|dk,ck||dl,cl}}_{dl,cl}}{1+\beta^{(4,pi,pj,pk)}_{di,ci,dj,cj|dk,ck||dl,cl}X^{D^{(4,pi,pj,pk)}_{di,ci,dj,cj|dk,ck||dl,cl}}_{dl,cl}}\right)\\
&\times \left[1+\sum_{dl=1}^{N}\sum_{cl=1}^{M}\sum_{pk=0}^{2}\frac{\alpha^{(4,pi,pj,pk)}_{di,ci,dj,cj|dk,ck||dl,cl}X^{C^{(4,pi,pj,pk)}_{di,ci,dj,cj|dk,ck||dl,cl}}_{dl,cl}}{1+\beta^{(4,pi,pj,pk)}_{di,ci,dj,cj|dk,ck||dl,cl}X^{D^{(4,pi,pj,pk)}_{di,ci,dj,cj|dk,ck||dl,cl}}_{dl,cl}}\right]. \qquad (2.12)\end{aligned}$$

The $k^{(4,pi,pj)}_{dj,cj,di,ci|dk,ck}$ and $\Gamma^{(4,pi,pj)}_{dj,cj,di,ci|dk,ck}$ terms are the complex formation rate coefficient and saturable kinetics coefficient of molecules *dj* in compartment *cj* and *di* in compartment *ci* combining to form *dk* in compartment *ck*. The $\alpha^{(4,pi,pj,pk)}_{di,ci,dj,cj|dk,ck||dl,cl}$ and $\beta^{(4,pi,pj,pk)}_{di,ci,dj,cj|dk,ck||dl,cl}$ are the interaction kinetics coefficients which describe the effect of molecule *dl* in compartment *cl* on the reaction. The $\delta^{(3,pi,pj,di,ci)}_{di,ci,dj,cj|dk,ck}$ terms are the stoichiometric coefficients. In this model, the process occurs within a single compartment, hence the $ci = cj = ck = 2$.

A simplified form of equation 2.11 can be written as follows:

$$\frac{dX^{(4)}_{di,2}}{dt} = \sum_{dj,dk=1}^{N} \sum_{pi,pj=0}^{2} \left[\frac{0.5\bar{k}^{(4,pi,pj)}_{dj,dk|di} X^{A^{(4,pi)}_{dj,dk|di}}_{dj,2} X^{A^{(5,pj)}_{dj,dk|di}}_{dk,2}}{1+\Gamma^{(4,pi,pj)}_{dj,dk|di} X^{B^{(4,pi)}_{dj,dk|di}}_{dj,2} X^{B^{(5,pj)}_{dj,dk|di}}_{dk,2}} \right.$$
$$- \frac{0.5\bar{k}^{(4,pi,pj)}_{di,dj|dk} X^{A^{(4,pi)}_{di,dj|dk}}_{di,2} X^{A^{(5,pj)}_{di,dj|dk}}_{dj,2}}{1+\Gamma^{(4,pi,pj)}_{di,dj|dk} X^{B^{(4,pi)}_{di,dj|dk}}_{di,2} X^{B^{(5,pj)}_{di,dj|dk}}_{dj,2}} - \left. \frac{0.5\bar{k}^{(4,pi,pj)}_{di,dk|dj} X^{A^{(4,pi)}_{di,dk|dj}}_{di,2} X^{A^{(5,pj)}_{di,dk|dj}}_{dk,2}}{1+\Gamma^{(4,pi,pj)}_{di,dk|dj} X^{B^{(4,pi)}_{di,dk|dj}}_{di,2} X^{B^{(5,pj)}_{di,dk|dj}}_{dk,2}} \right], \tag{2.13}$$

where 0.5 is to account for double-counting since $\bar{k}^{(4,pi,pj)}_{di,dj|dk} = \bar{k}^{(4,pi,pj)}_{dj,di|dk}$.

2.2 The Pharmacokinetic Parameters

The model used here is entirely predictive and depends on the parameter values described above and how they fit with the clinical data. The parameters in equations 2.3 to 2.13 and the $V_{d,di,ci}$ of the molecules are obtained by minimizing the variance. The weighted variance and weighted percentage variance are adapted from Vos et al. [47] and are given as

$$S_a = \frac{1}{N_p} \sum_{i,j,l,m} P_{i,j,l,m} \left[\frac{X^{(m)}_{i,j}(t_l)}{V_{D,i}} - C^{(l)}_{i,j}(t_l) \right]^2 \tag{2.14}$$

$$S_p = \frac{4}{N_p} \sum_{i,j,l,m} P_{i,j,l,m} \left[\frac{X^{(m)}_{i,j}(t_l) - V_{D,i} C^{(l)}_{i,j}(t_l)}{X^{(m)}_{i,j}(t_l) + V_{D,i} C^{(l)}_{i,j}(t_l)} \right]^2, \tag{2.15}$$

where $X^{(m)}_{i,j}(t_l)$ is the theoretical amount of molecule i in compartment j at time t_l using the dosage and infusion time from the clinical study m. $C^{(l)}_{i,j}(t_l)$ is the clinical concentration of molecule i in compartment j at time t_l from clinical study m. The $P_{i,j,l,m}$ terms represent a weighting coefficient, which is the number of patients represented in study m at time t_l for which the molecule concentration is known. The N_p is the number of patients multiplied by the number of data points summed over all the clinical studies.

All the datasets used for the theoretical comparisons were obtained from published clin-

ical studies using DOX, DOL and encapsulated DOX. In the case of multi-drug treatment, only the DOX PK profile was considered. Clinical concentrations were obtained by digitizing concentration-time graphs from previous studies and converting the concentration data into units of micromols per liter ($\mu\text{mol}\cdot\text{l}^{-1}$). Data from Andersen et al. [61], Benjamin et al. [64, 63], Gianni et al. [88], Greene et al. [59] and Moriera et al. [89] were used to determine the parameters within the model. The choice of these datasets represents the contribution from different patient groups, each with specific tumour types, dose, and infusion length. The total number of patients in the baseline dataset was 81 for DOX and 37 data points with $N_p = 960$. The total number of DOL data points was 41, with 83 patients and $N_p = 710$. Data from PLD and MYO studies were also used to obtain the PK variables. The total number of PLD data points used was 27 and 22 patients with $N_p = 594$, and with 18 data points and 16 patients used to model MYO, $N_p = 288$. The other data sets were used for comparison. The infusion for the studies are listed in table 2.2 and have units of $\mu\text{mol}/(\text{m}^2\cdot\text{min})$, which implies that the unit of $X_{i,j}(t_l)$ in the theory from equations 2.14 and 2.15 is $\mu\text{mol}/\text{m}^2$. The studies have dosages with the units of $\mu\text{mol}\cdot\text{m}^{-2}$, and we left the theoretical calculations in these units. The clinical studies with infusion having units of $\mu\text{mol}/\text{min}$ or $\mu\text{mol}/\text{kg}\cdot\text{min}$ have been treated separately. Table 2.2 shows the data sets used to compare DOX PK to the theoretical models developed here. The table also shows the administered dose, infusion time, rate of infusion, and the number of patients for each data set.

The AUC was calculated using the linear trapezoidal method. In all cases, the AUC values were calculated up to infinity, $AUC_{0\to\infty}$, using

$$AUC_{0\to\infty} = \int_{t=0}^{t=\infty} X_{i,j}(t)dt. \tag{2.16}$$

The maximum concentration, $C_{\max}$, after infusion of the molecules for each dataset was also determined as the maximum predicted concentration over every time point. The distribution half-life, $t^d_{1/2}$, was estimated as the time taken for the concentration to reach half

Table 2.2: Papers used to model DOX showing the dosage, length of infusion and the number of data points from each study.

Reference	Dosage($\frac{mg}{m^2}$)	T_{inf} (min)	Inf($\frac{\mu\text{mol}}{\text{m}^2\,\text{min}}$)	n_p	Data points
Andersen et al. [61]	50	10	9.1996	24	8
Greene et al. [59]	75	15	9.1996	10	11
Wurtz et al. [90]	60	15	7.3597	11	11
Gianni et al. [88]	60	5	22.0791	8	9
Speth et al. [91]	30	1	55.1978	9	12
Rodvold et al. [92]a.	67	60	2.0545	7	11
Rodvold et al. [92]b.	64	60	1.9626	7	8
Rodvold et al. [92]c.	60	60	1.8399	7	11
Twelves et al. [93]a.	75	6.6	20.9083	6	9
Twelves et al. [93]b.	25	2.2	20.9083	5	8
Wihlm et al. [94]	120	360	0.6133	9	11
Erttmann et al. [95]	15	5	5.5198	8	12
Barpe et al. [96]a.	60	39.6	2.7878	3	4
Barpe et al. [96]b.	60	39.6	2.7878	7	4
Moriera et al. [89]	60	5	22.0791	28	10
Benjamin et al. [64]	60	10	11.0396	13	10
Benjamin et al. [63]	60	5	22.0791	16	9
Jacquet et al. [97]a.	51	10.2	9.2664	1	10
Jacquet et al. [97]b.	51	15	6.2705	1	10

[92]a,b,c corresponds to the normal weight, mildly obese and obese patients data respectively.

[93]a,b corresponds to 75mg/m^2 and 25mg/m^2 dose data respectively.

[96]a,b corresponds to normal and overweight patients data respectively.

[97]a,b corresponds to data from patient GON and BOU respectively.

the maximum concentration after infusion. The calculation of the elimination half-life $t^e_{1/2}$, which is the time required for the plasma concentration of the molecule to reach half its initial value in the elimination phase, depended on the model used. In the classical kinetic models, $t^e_{1/2}$ is calculated as

$$t^e_{1/2} = 0.693/k_{el}, \tag{2.17}$$

where k_{el} is the elimination rate constant, which describe the terminal phase of the kinetics. In the saturable kinetics models with exponents $A \neq 1$ and $B \neq A-1$, the elimination half-

life of molecule i in compartment j can be written in terms of the PK parameters as

$$t^{e}_{1/2} = \frac{1}{k_{el}} \left\{ \frac{1}{X^{A-1}_{ij}(A-1)} \left[2^{A-1} - 1\right] + \frac{\Gamma X^{1+B-A}_{ij}}{1+B-A}, \left[1 - \frac{1}{2^{1+B-A}}\right] \right\}. \tag{2.18}$$

Similarly, the transition amount and concentration are calculated using

$$\begin{aligned} X^{T,cj}_{di,ci} &= \frac{1}{\left[\Gamma_{di,ci,cj}\right]^{1/B_{di,ci,cj}}} \\ C_{di,ci} &= \frac{X^{T,cj}_{di,ci}}{V_{d,di,ci}}, \end{aligned} \tag{2.19}$$

where T is the transition time and $V_{d,di,ci}$ is the distribution volume. This concentration represents the transition of the kinetics from a low concentration phase to a high concentration phase. Where applicable, the times corresponding to the transition from low to high and high to low are recorded and represent the time interval when the influence of the saturation coefficient is greatest.

2.3 Numerical Methods

2.3.1 Overview

In this work, the weighted percentage variance, S_p, was minimized to obtain the parameters that described the PK of the molecules within each model. The choice of the S_p model was because it assigns equal weight to all the available data points, resulting in a better estimate of concentration over a broad range of time. Considering that the PK of DOX is characterized by long residence time, our model of choice must be able to accurately estimate the long-term concentrations of DOX. The S_a models were also considered for completeness and were used to compare the results of the two measures over the same data sets.

2.3.2 Runge-Kutta Method

The choice of numerical method used to solve the set of non-linear differential equations in this work was the fourth order Runge-Kutta (RK) method. The RK methods of solving initial value problems have the advantage of producing stable solutions in an efficient manner. The differential equations in the model assumed the form of a coupled vector field:

$$\dot{\bar{x}} = \begin{bmatrix} \dot{x}_1 \\ \dot{x}_2 \\ \dot{x}_3 \\ \vdots \\ \dot{x}_n \end{bmatrix} = \begin{bmatrix} f_1(t,x_1,x_2,x_3,\ldots,x_n) \\ f_2(t,x_1,x_2,x_3,\ldots,x_n) \\ f_3(t,x_1,x_2,x_3,\ldots,x_n) \\ \vdots \\ f_n(t,x_1,x_2,x_3,\ldots,x_n) \end{bmatrix} \tag{2.20}$$

$\dot{x_1}\ldots\dot{x_n}$ is the time derivative of molecule type $1\ldots n$ and corresponds to all of the molecules in the compartments of the system. n is the product of the total number of molecules and compartments. Each differential equation is represented as a function $f_n(t,x_1(t)\ldots x_n(t))$, where t is the current time for which the concentration is known, and $x_n(t)$ is the amount of molecule n at that time. The midpoints of the fourth-order RK method for the differential equations were written considering the coupled terms as:

$$T_1^{(i)} = f_i(t,x_1(t),x_2(t),x_3(t),\ldots,x_n(t)) \tag{2.21}$$

$$T_2^{(i)} = f_i(t+\frac{h}{2},x_1(t)+\frac{h}{2}T_1^{(1)},x_2(t)+\frac{h}{2}T_1^{(2)},x_3(t)+\frac{h}{2}T_1^{(3)},\ldots,x_n(t)+\frac{h}{2}T_1^{(n)}) \tag{2.22}$$

$$T_3^{(i)} = f_i(t+\frac{h}{2},x_1(t)+\frac{h}{2}T_2^{(1)},x_2(t)+\frac{h}{2}T_2^{(2)},x_3(t)+\frac{h}{2}T_2^{(3)},\ldots,x_n(t)+\frac{h}{2}T_2^{(n)}) \tag{2.23}$$

$$T_4^{(i)} = f_i(t+h,x_1(t)+hT_3^{(1)},x_2(t)+hT_3^{(2)},x_3(t)+hT_3^{(3)},\ldots,x_n(t)+hT_3^{(n)}). \tag{2.24}$$

And the solution after a step size h is:

$$x_i(t+h) = x_i(t) + \frac{h}{6}(T_1^{(i)} + 2T_2^{(i)} + 2T_3^{(i)} + T_4^{(i)}), \tag{2.25}$$

where h is a small increment in time, which is kept small enough to limit the error in the approximation. $T_1^{(i)} - T_4^{(i)}$ are the midpoints of the RK method for differential equation index i, and $x_i(t+h)$ is the new approximation of the amount of molecule index i at time $t+h$.

2.3.3 Powell's Method in Multidimensions

Powell's method is one of the choice tools used to minimize a function in multidimensional space. This is due to how quickly it computes the local minimums, and because it is derivative-free. The choice of this method of minimizing the variance was necessary because there is no explicit functional form for the variance. Therefore, Powell's method offers a trustworthy optimizer able to approach the global minimum with little computational overhead. A summarized Powell's algorithm from Yan et al. [98] is shown below.

1. Consider a vector $X^0 = \left[k_1, \Gamma_1, A_1, B_1, \alpha_1, \beta_1, C_1, D_1, \ldots, k_n, \Gamma_n, A_n, B_n, \alpha_n, \beta_n, C_n, D_n\right]^T \in R^{8n}$ which represents the system variables. Let $L = 8 * n$ be the dimension of vector X^0, X^0 is the starting point of the minimization, and a set of linearly independent search directions $\{P^0, P^1, P^2, \ldots, P^{L-1}\}$ which forms an L×L unit matrix are chosen.

2. Begin the search along each direction starting at $Y^0 = X^0$ where Y^i is the average direction moved during each iteration of vector i. Using Y^i find a scalar η_i such that

$$f(Y^{i-1} + \eta_i P^i) = \min_{\eta} f(Y^{i-1} + \eta P^i), \tag{2.26}$$

   where $i = 1, 2, 3, \ldots, L$ and $\eta > 0$. Set $Y^i = Y^{i-1} + \eta_i P^i$ where η_i minimizes the function $f(Y^{i-1} + \eta_i P^i)$.

3. Choose a new direction where the function converges to the minimum by setting $P^i = P^{i+1}$ and $P^L = Y^L - Y^0$. If $|P^i| \leq \varepsilon$ stop the search and output the result $X^{k+1} = Y^L$, else go to 4.

4. Determine the next direction to be minimized by finding an index m such that

$$f(Y^{m-1}) - f(Y^m) = \max\{f(Y^{i-1}) - f(Y^i)\} \text{for } i = 1, 2, \ldots, L \tag{2.27}$$

   If $f(Y^0) - 2f(Y^L) + f(2Y^L - Y^0) < 2(F(Y^{m-1}) - F(Y^m)$ is true go to step 5 else go to step 6.

5. Adjust the search group to find $\min_{\eta} f(Y^{L-1} + \eta_L P^L)$ and $X^{k+1} = Y^0 + \eta P^L$.

6. Ignore the searched groups and finish searching at unadjusted directions. Let $X^{k+1} = Y^L$, increase k by 1 and go to step 2.

Although there are several implementations of Powell's method within different frameworks, the Dlib C++ Library [99] was used in this thesis because it offers a framework to perform constrained and unconstrained minimization of many variable functions, having many local minima through the *BOBYQA* method [100]. The library uses a set of interpolating points to choose a search direction using a trust-region algorithm while preserving system constraints. The constraints are necessary in the model because some of the variables take unique values, or in some cases, bounds on some variables were chosen to ensure consistency with clinical observations. For instance, k, Γ, β, A, B, C and D were only allowed to be positive real number values, while the α parameters from our model were allowed to take positive or negative values depending on the model considered. When modelling the drug combinations, the model also allowed for specific considerations such as the fraction of the infused drug that is eliminated through the liver which is clinically known to be $\approx 40\%$ [56], and $\approx 5\%$ in urine within 7 days after administration [66].

Chapter 3

Parameter Development

Some drugs have been appropriately called 'wonder drugs'

in that one wonders what they'll do next.

– Annals of Internal Medicine

3.1 Objective

The process of building a model involves several steps, which include parameter development, parameter sensitivity testing, and validation of the model against other models. In this chapter, we will apply the model described in chapter 2 to the PK of DOX, DOL and encapsulated DOX. The four-compartment model is broken down into several smaller models to test each model's ability to describe the molecule's PK parameters appropriately. The model parameters were estimated within the context of the model considered. The sections follow a numerical order based on the number of molecules considered in each model.

The first type of models considered were those involving DOX PK. In that model, the parameters that describe the kinetic flow of the drug between the compartments are developed. The second type of model considered the release of DOX from the encapsulated prodrug. In this model, the parameters that describe the PK of free and encapsulated drugs are developed. In cases where data for one of the drugs is unavailable, the parameters of the available drug are developed. In the last type of model, the parameters describing the distribution, metabolism and elimination of DOX and DOL are developed.

3.2 Parameter Development

3.2.1 Michaelis-Menten Type Processes

In this chapter, we have assigned specific notations to differentiate between different cases. Case 1 refers to the model where the exponents A and B are fixed at one and the rate coefficients are allowed to vary. Case 1.1 refers to the case where zeroth-order rate coefficients were allowed to vary in addition to the first-order processes, this is done to examine the effect of the zeroth-order perturbation on the Michaelis-Menten model. Like the single-process case, the exponents are fixed at zero, and only the rate coefficients allowed to vary. Case 1.2 is similar to case 1.1 but with second-order process perturbations. The exponents are fixed at two, and only the rate parameters varied. Case 1.3 considered a model where all three processes can describe the PK of DOX. All the exponents remained fixed and the rate coefficients of the three processes were varied.

3.2.2 Saturable Kinetic Processes

The more parameterized models involving all the parameters are denoted by cases 2, 2.1 and 2.2. Case 2 refers to the single process case where A and B are varied alongside the rate parameters. Case 2.1 describes a second process correction to the single-process model. In this case, a second set of rate parameters and exponential terms are allowed to vary alongside the case 2 parameters. Case 2.2 describes the fit of three processes. It describes a model with the two correction processes that produced the lowest variance. The sets of parameters are varied alongside the case 2 parameters.

3.2.3 Interaction Processes

Cases 3.0, 3.1 and 3.2 refer to the effect of the interaction parameters on the single-process rate terms. In each of these cases, the terms describing the effective rate coefficients were developed. Case 3.0 describes the influence of zeroth-order interaction on the case 2 parameters. Case 3.1 describes the influence of first-order interaction on the case 2 parame-

ters. Case 3.2 describes the influence of second-order interaction on the case 2 parameters. Case 3.3 describes the influence of the two best interactions on the case 2 parameters.

3.3 One-Molecule Fixed-Order Models

3.3.1 One-Molecule, One-Compartment Model

The simplest model is the single molecule, one-compartment model illustrated in figure 3.1. In this case, only DOX PK was considered; thus the initial model focused on developing the parameters that described the flow of DOX from compartment 1 into compartment 0, which is external to the body. The numerical values of the parameters that best fit the clinical data were obtained by minimizing the variance given in equation 2.15.

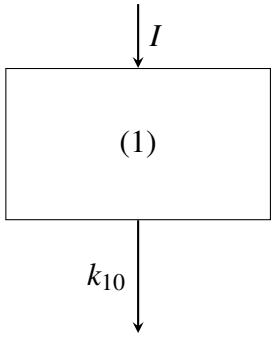

Figure 3.1: Schematic Representation of a One-Compartment System.

Classical PK models use a series of first-order processes to describe the PK of DOX. Therefore, the values of our exponents A and B were initially set to one. This model represents a Michaelis-Menten's type PK of DOX. Table 3.1 shows the parameters from the one-molecule, one-compartment model for DOX with A and B fixed at one from single studies. Using the model, we observe that DOX PK is described by an elimination rate constant and a large volume of distribution. The numbers in the brackets are the deviations in the parameters that produced a 1% change in S_p. The result was a poor fit of the theoretical curves to the clinical concentrations shown in Figure 3.2. In the figure we notice that the curves fit poorly to the data over the range of concentrations. There is significantly large difference in the measured and simulated maximum concentrations for all the datasets.

Table 3.1: One-compartment model case 1 parameters for modelling DOX using single datasets ($A = B = 1$).

Parameter	Benjamin et al. [63]	Benjamin et al. [64]	Moriera et al. [89]
$\boldsymbol{k}^{(1)}_{DOX,10}$ [a]	0.00091 (23)	0.0009 (12)	0.0013 (17)
$\boldsymbol{\Gamma}^{(1)}_{DOX,10}$ [b]	0.0000 (30)	0.0000 (23)	0.0000 (22)
$V_{d,DOX}$ [c]	1039.94 (65)	614.58 (54)	895.38 (55)
S_p	0.1261	0.1594	0.1976

units of:
[a] min^{-1} [b] $\left[\frac{\mu\mathrm{mol}}{\mathrm{m}^2}\right]^{-1}$ [c] $\left[\mathrm{L}\cdot\mathrm{m}^{-2}\right]$

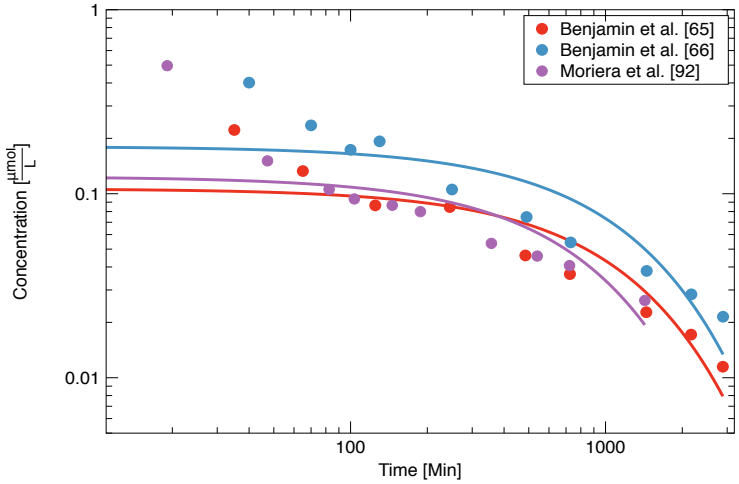

Figure 3.2: Comparison of theoretical and experimental concentrations of DOX using the parameters from Table 3.1. The curves represent the theoretical estimates of the concentrations from Moriera *et al.* [89] (purple), Benjamin *et al.* [63] (red) and Benjamin *et al.* [64] (blue).

In this work, the maximum number of parameters allowed to vary for each model is the number of data points minus one. A subset of the available clinical data set with a sufficient variation in the number, age, gender and type of cancer between patients was selected as a baseline for modelling the DOX PK. The baseline datasets represent a balanced distribution of patients' characteristics between different studies and are shown in Table 3.2.

Using the baseline datasets, the parameters that described the one-compartment PK of DOX were developed. Table 3.3 shows the parameters from cases 1, 1.1, 1.2 and 1.3 in their respective columns. In the first column, it is observed that in the single-process case, the elimination of DOX occurs at a fixed linear rate. The result of the fixed-rate constant

Table 3.2: Patients distribution in the baseline datasets for modeling DOX PK.

Data set	Age [yr]	No. of Patients	Cancer Type	Gender (M : F)
Andersen *et al.* [61]	54[a]	24	Malignant Lymphoma	17:7
Moriera *et al.* [89]	≤ 60[b]	28	Breast Cancer	0 : 28
Gianni *et al.* [88]	52[a]	8	Breast Cancer	0 : 8
Benjamin *et al.* [64]	-	13	Refractory Acute Leukamia	-
Greene *et al.* [59]	-	10	Metastatic Soft Tissue Sarcoma Breast Cancer	-
Benjamin *et al.* [63]	-	16	Disseminated Solid Tumours Acute Lymphocytic Lymphoma	-

[a] mean value [b] range

is a large volume of distribution, which may imply that the drug is slowly eliminated from the body. The second column shows the addition of a zeroth-order process, which does not appear to influence the first-order process parameters. The volume of distribution and the variance are the same in both cases. In the third and fourth columns, the parameters show that introducing higher order elimination terms reduces the variance slightly. The higher-order kinetics is described by a Michaelis-Menten type process, which is zeroth-order at high concentrations and second-order at low concentrations. One possible explanation of the zeroth-order effect is the over saturation of the elimination mechanism with the drug. The large volume of distribution suggests that a large concentration of DOX is distributed within the compartment. The model variance is reduced 7.93% from case 1 to case 1.2. The high variance of the fixed-order models implies a poor fit to the clinical concentrations.

Table 3.3: One-compartment parameters for modelling DOX.

Parameter	Case 1	Case 1.1	Case 1.2	Case 1.3
$k^{(1,1)}_{DOX,10}[\mathrm{min}^{-1}]$	0.00152(17)	0.00152(17)	0.0015(34)	0.000(21)
$\Gamma^{(1,1)}_{DOX,10}[\frac{\mu\mathrm{mol}}{\mathrm{m}^2}]^{-1}$	0.0000(12)	0.0000(12)	N/A**	0.0003(19)
$k^{(1,0)}_{DOX,10}[\frac{\mu\mathrm{mol}}{\mathrm{m}^2}]\mathrm{min}^{-1}$	-	0.00000(23)	-	0.0000(20)
$k^{(1,2)}_{DOX,10}[\frac{\mu\mathrm{mol}}{\mathrm{m}^2}]^{-1}\mathrm{min}^{-1}$	-	-	0.00003(29)	0.000041(29)
$\Gamma^{(1,2)}_{DOX,10}[\frac{\mu\mathrm{mol}}{\mathrm{m}^2}]^{-2}$	-	-	0.000(15)	0.000051(15)
$V_{d,DOX}[\mathrm{L}\cdot\mathrm{m}^{-2}]$	840.70(20)	840.70(20)	820.78(21)	820.78(21)
S_p	0.8842	0.8842	0.8141	0.8141

** The parameter is indeterminate because the rate constant is zero.

Figure 3.3 shows the simulated concentration curves of DOX using the parameters from

the one-compartment case 1.2 model. Like the single dataset models, the poor fit to the data is noticeable over the whole range of concentrations. The high concentration-fit of this model is similar to the single dataset model in figure 3.2. There is a noticeable underestimation of the maximum concentrations for all the datasets.

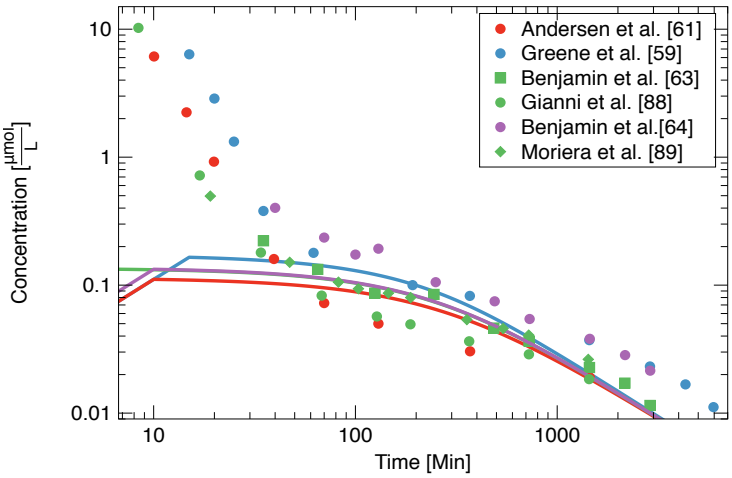

Figure 3.3: Comparison of theoretical and experimental concentrations of DOX using the parameters from Table 3.3. The clinical data and curves are for an infusion of 9.19 $\mu mol \cdot m^{-2} \cdot min^{-1}$ (red and blue), 22.08 $\mu mol \cdot m^{-2} \cdot min^{-1}$ (green) and 11.04 $\mu mol \cdot m^{-2} \cdot min^{-1}$ (purple).

3.3.2 One-Molecule, Two-Compartment Model Version A

The next sets of parameters developed corresponds to the one-molecule two-compartment model where DOX is infused and eliminated from the principal compartment (figure 1.3(a)). In this model, DOX is allowed to flow between compartments one and two, and eliminate via compartment one. The DOX in compartment zero is not allowed to interact with the system. The model mirrors the activity of the drug in the blood, and how it is distributed in and out of tissues and organs, which are represented by compartment two. The presence of this compartment allows us to parameterize the distribution and elimination of DOX from the tissues, cells and the body. In studying the two-compartment models, we begin with a Michaelis-Menten model with first-order process even though the one-compartment model is not a first-order process. The parameters that describe this model are shown in

Table 3.4. We notice that the PK of DOX in compartment one is characterized by the elimination or distribution to the tissue compartment. The elimination process, which may be via metabolism or renal elimination, accounts for 45% of the total rate of drug release from the compartment. The rate parameter of elimination of DOX from compartment one ($k^{(1)}_{DOX,10}$) in Table 3.4 is approximately forty times the one-compartment elimination rate constant in Table 3.3. The volume of distribution is reduced over eighty-fold from Table 3.3 which suggests extensive distribution of DOX to compartment two. The very small rate constant of redistribution of the drug in compartment two suggests that most of the absorbed drug is retained in the compartment. The variance is reduced four-fold between the one and two-compartment models. The saturation parameters are all zero suggesting that the rate processes do not change with the concentration of the molecule.

Table 3.4: Two-compartment model (version A) case 1 parameters of DOX.

$\boldsymbol{k}^{(1)}_{DOX,10}$ [a]	$\boldsymbol{\Gamma}^{(1)}_{DOX,10}$ [b]	$\boldsymbol{k}^{(1)}_{DOX,12}$ [a]	$\boldsymbol{\Gamma}^{(1)}_{DOX,12}$ [b]	$\boldsymbol{k}^{(1)}_{DOX,21}$ [a]	$\boldsymbol{\Gamma}^{(1)}_{DOX,21}$ [b]	$V_{d,DOX}$ [c]	S_p
0.0666 (87)	0.000 (28)	0.0830 (13)	0.00000(21)	0.003(77)	0.000000(23)	10.86(32)	0.2144

units of:
[a] min^{-1} [b] $\left[\frac{\mu\mathrm{mol}}{\mathrm{m}^2}\right]^{-1}$ [c] $\left[\mathrm{L}\cdot\mathrm{m}^{-2}\right]$

Figure 3.4 shows the simulated plasma concentration of DOX using the parameters in Table 3.4. The curves show a better fit than figure 3.3. However, there is a poor fit at high and low concentrations.

3.3.3 One-Molecule, Two-Compartment Model Version B

The second type of two-compartment model considered allows the molecules to flow between compartments one and two and to be eliminated from the system via the flow from compartment two to compartment zero as seen in figure 1.3(b). The molecule is infused into compartment one from where it disperses into compartment two, which then controls the reverse flow to compartment one or flow into compartment zero. For this version, compartment one relates exclusively to the activities of the drug within the plasma, and compartment two describes the drug activities within tissues and organs. The param-

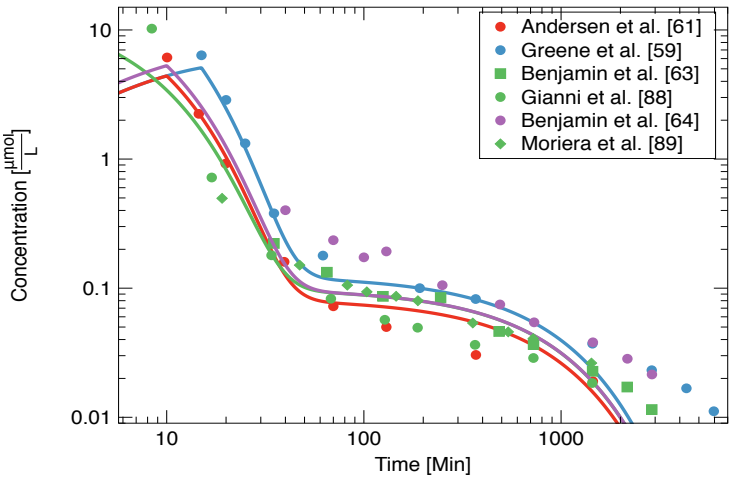

Figure 3.4: Comparison of theoretical and experimental concentrations of DOX using the parameters from Table 3.4. The clinical data and curves are for an infusion of 9.19 $\mu mol \cdot m^{-2} \cdot min^{-1}$ (red and blue), 22.08 $\mu mol \cdot m^{-2} \cdot min^{-1}$ (green) and 11.04 $\mu mol \cdot m^{-2} \cdot min^{-1}$ (purple).

eters that describe the model are presented in Table 3.5. The parameters show that the PK processes do not change relative to the amount of drug using the Michaelis-Menten type process. The rate of distribution of DOX from compartment one to compartment two is approximately twice the rate in Table 3.4. This suggests a significant distribution from plasma to the metabolism site. The distribution of DOX to the peripheral compartment increases 100 times from the one-compartment model in Table 3.3. The rate of plasma elimination is approximately the same as the total rate of drug release from the plasma in Table 3.4. In compartment two, the PK of DOX is in competition between drug elimination and redistribution. The rate of distribution is approximately 55% of the total drug elimination from compartment two. This suggests that within compartment two, approximately 45% of available DOX is retained, metabolized or eliminated. The volume of distribution is approximately eighty-fold less than Table 3.3 suggesting a greater distribution of DOX in the two-compartment model. The model produced a four-fold decrease in S_p from Table 3.3.

Figure 3.5 shows the simulated plasma concentration of DOX using the parameters in Table 3.5. The curves are similar to figure 3.4 over the range of concentrations. The curves retain a poor fit of the first-order models at high and low concentrations.

Table 3.5: Two-compartment model (version B) case 1 parameters of DOX.

$k^{(1)}_{DOX,12}$ [a]	$\Gamma^{(1)}_{DOX,12}$ [b]	$k^{(1)}_{DOX,20}$ [a]	$\Gamma^{(1)}_{DOX,20}$ [b]	$k^{(1)}_{DOX,21}$ [a]	$\Gamma^{(1)}_{DOX,21}$ [b]	$V_{d,DOX}$ [c]	S_p
0.1504 (10)	0.000 (30)	0.0012 (10)	0.0000 (21)	0.0015 (17)	0.00000 (50)	10.744 (26)	0.2144

units of:
[a] min^{-1} [b] $\left[\frac{\mu\text{mol}}{\text{m}^2}\right]^{-1}$ [c] $\left[\text{L}\cdot\text{m}^{-2}\right]$

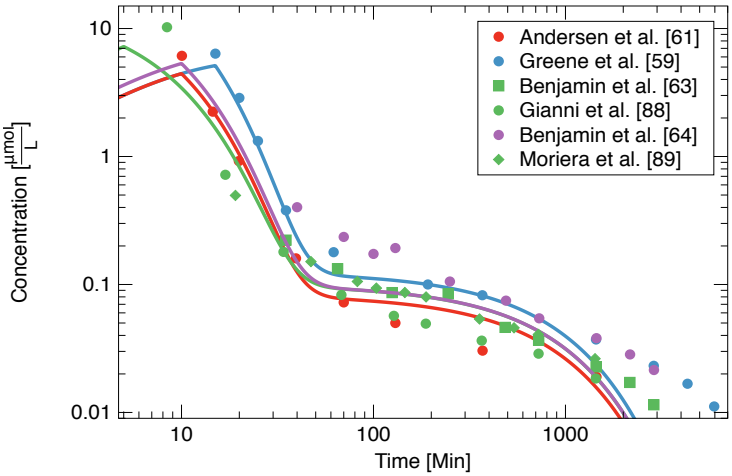

Figure 3.5: Comparison of theoretical and experimental concentrations of DOX using the parameters from Table 3.5. The clinical data and curves are for an infusion of 9.19 $\mu\text{mol}\cdot\text{m}^{-2}\cdot\text{min}^{-1}$ (red and blue), 22.08 $\mu\text{mol}\cdot\text{m}^{-2}\cdot\text{min}^{-1}$ (green) and 11.04 $\mu\text{mol}\cdot\text{m}^{-2}\cdot\text{min}^{-1}$ (purple).

3.3.4 One-Molecule, Three-Compartment Model

The next model considered is the one-molecule, three-compartment model. In this model, a third compartment was added to the two-compartment case. The purpose of the model was to give a more realistic model that separated distribution, elimination and the cells. In this model, the molecule is infused into compartment one from where it distributes into compartments two and three and back into one. Compartment two represents the liver and the renal cells compartment where metabolism and drug elimination occurs. For elimination, the drug flows irreversibly from compartment two to compartment zero. The third compartment may be thought of as the cells and organs where the drug is deposited via regional blood flow. The clinical concentrations of DOX within these organs are not readily available, hence the concentration at any time in compartment three is assumed to be that available for distribution into body tissues and organs. The model assumed a first-order

process ($A = B = 1$) of three compartments. The parameters that minimized the variance are shown in Table 3.6. The three-compartment model resulted in a better fit to the variance than the one and two-compartment models. According to the parameters, the distribution of the drug in compartment one to compartment two is saturable, and is zeroth-order at high concentrations. The distribution of the drug in compartment one to three occurs at a first-order rate throughout the range of concentrations. Likewise, the elimination parameters suggest a saturable elimination process of DOX from the body, which may occur due to the saturation of the binding sites when the amount of DOX in the elimination and metabolism site is significantly more than the amount of enzymes available. The volume of distribution is unchanged from Table 3.5.

Table 3.6: Three-compartment model case 1 parameters of DOX.

Parameters	1,2	2,0	2,1	1,3	3,1	$V_{d,DOX}$ [c]	S_p
$\boldsymbol{k}^{(1)}_{DOX,ci,cf}$ [a]	0.1059 (49)	0.01399 (98)	0.00462 (98)	0.0784 (49)	0.00331 (98)	10.747 (30)	0.1605
$\boldsymbol{\Gamma}^{(1)}_{DOX,ci,cf}$ [b]	0.0064 (29)	0.0186 (49)	0.00000 (98)	0.00000 (98)	0.02167 (98)		

units of:
[a] min^{-1} [b] $\left[\frac{\mu\mathrm{mol}}{\mathrm{m}^2}\right]^{-1}$ [c] $\left[\mathrm{L}\cdot\mathrm{m}^{-2}\right]$

Figure 3.6 shows the simulated plasma concentration of DOX using the parameters in Table 3.6. The curves are similar to figure 3.4 over the range of concentrations. The curves retain the poor fit of the first-order models at high concentrations.

3.4 One-Molecule Variable-Order Models

The poor fit from the fixed-order models and analysis of DOX concentration-time curves suggested that a series of competing processes describe the PK of DOX, notably, the presence of a time-dependent power-law relationship of the concentration. A power-law relationship between concentration, C, and time, t, can be defined by

$$C(t) \propto t^{\alpha}, \tag{3.1}$$

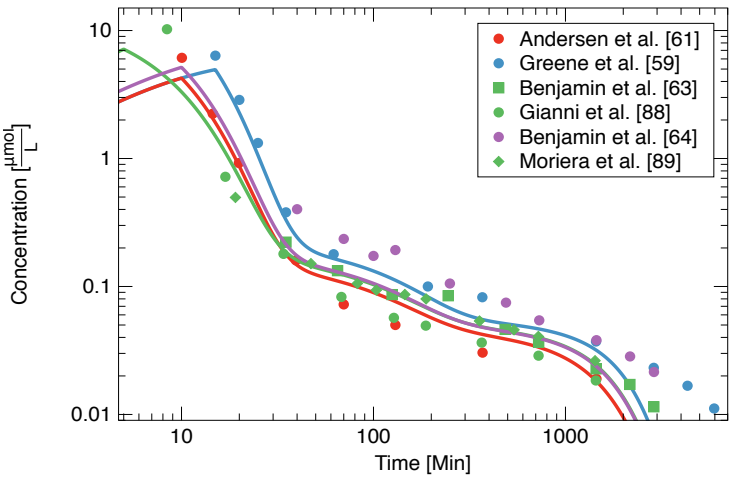

Figure 3.6: Comparison of theoretical and experimental concentrations of DOX using the parameters from Table 3.6. The clinical data and curves are for an infusion of 9.19 $\mu mol \cdot m^{-2} \cdot min^{-1}$ (red and blue), 22.08 $\mu mol \cdot m^{-2} \cdot min^{-1}$ (green) and 11.04 $\mu mol \cdot m^{-2} \cdot min^{-1}$ (purple).

which can also be written as

$$C(t) = ft^{\alpha}, \tag{3.2}$$

where f is a constant of proportionality that relates the variables, and α describes the magnitude of the relationship between C and t. Generally, this relationship is applicable to values above some minimum value of the independent variable. The exponent α can be estimated by evaluating the slope of the log-log plot of $c(t)$ against t. In that case, equation 3.2 reduces to

$$\log c = \log(f) + \alpha \log t. \tag{3.3}$$

The post-infusion differential equation describing our one-molecule one-compartment model takes two forms depending on the magnitude of the dependent variable.

$$\frac{dX_{\mathrm{DOX},1}}{dt} = \begin{cases} -k^{(1)}_{\mathrm{DOX},1,0} X^{A^{(1)}_{\mathrm{DOX},1,0}}_{DOX,1} & \text{at low } X \\ -\frac{k^{(1)}_{\mathrm{DOX},1,0}}{\Gamma^{(1)}_{\mathrm{DOX},1,0}} X^{A^{(1)}_{\mathrm{DOX},1,0} - B^{(1)}_{\mathrm{DOX},1,0}}_{DOX,1}. & \text{at high } X \end{cases} \tag{3.4}$$

Integrating both forms of equation 3.4, one can write a form of equation 3.2 where

$$\alpha = \begin{cases} \frac{1}{1-A^{(1)}_{\mathrm{DOX},1,0}} & \text{at low } X. \\ \frac{1}{1-A^{(1)}_{\mathrm{DOX},1,0}+B^{(1)}_{\mathrm{DOX},1,0}} & \text{at high } X. \end{cases} \tag{3.5}$$

The slopes of the power-law regions of the log-log concentration vs time graphs from the individual data sets were then estimated to obtain the estimates of A and B.

Table 3.7: Calculated values of the fractal estimates from the data set.

Reference	Initial Slope	R^2	long-term Slope	R^2	A	B
[89]	-0.8768	0.9365	-0.5315	0.9931	2.8813	0.7408
[64]	-0.686	0.8755	-0.6384	0.9924	2.5664	0.1087
[88]	-2.2725	0.9336	-0.4533	0.9875	3.2060	1.7660

The new model with A and B set to the new values and varied was then simulated for all the datasets to observe the fit relative to the fixed-order model. The variance in Table 3.8 is approximately ten times smaller than the variance in Table 3.1 implying a better fit to the clinical data. The parameters in Table 3.8 show a large variation between datasets implying the presence of a high degree of variability of DOX PK between datasets. Figure 3.7 shows the log-log plot of the results of concentration vs time using the parameters obtained by simulating the individual datasets shown in Table 3.8.

Table 3.8: One-compartment parameters for modelling DOX.

Data set	$k^{(1)}_{DOX,10}$ [a]	$\Gamma^{(1)}_{DOX,10}$ [b]	$A^{(1)}_{DOX,10}$	$B^{(1)}_{DOX,10}$	$V_{d,DOX}$ [c]	S_p
Greene *et al.* [59]	0.01932 (13)	0.123 (25)	3.0336 (48)	1.908 (25)	4.503 (42)	0.0330
Gianni *et al.* [88]	0.06182 (40)	0.03962 (40)	3.0995 (25)	2.6775 (21)	4.48321 (10)	0.0059
Moriera et al. [89]	0.03572 (11)	0.0143721 (98)	3.2862 (11)	3.010424 (30)	4.352044 (20)	0.0028
Benjamin et al. [64]	0.006321 (29)	0.0000 (25)	2.6181 (25)	N/A**	5.3067 (30)	0.0185

units of:

[a] $\left[\frac{\mu\mathrm{mol}}{\mathrm{m}^2}\right]^{1-A^{(1)}_{DOX,10}}\mathrm{min}^{-1}$ [b] $\left[\frac{\mu\mathrm{mol}}{\mathrm{m}^2}\right]^{-B^{(1)}_{DOX,10}}$ [c] $\left[\mathrm{L}\cdot\mathrm{m}^{-2}\right]$

** The parameter is indeterminate because the rate parameter is zero.

As shown in figures 3.7(a) to (d), the parameters produce theoretical concentrations that generally agree with clinical concentrations over a wide range of data from several studies.

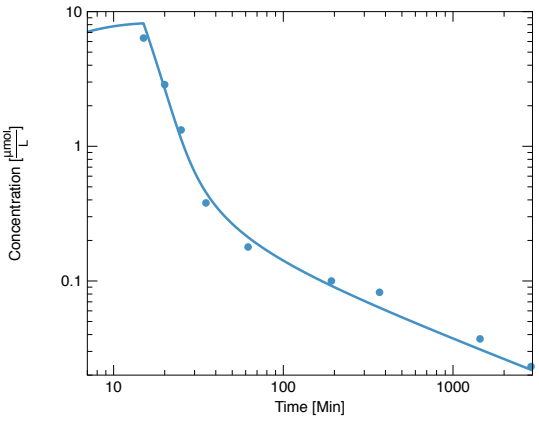

(a) Greene *et al.* [59]

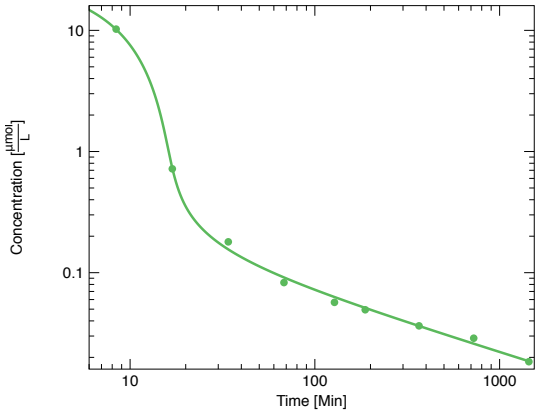

(b) Gianni *et al.* [88]

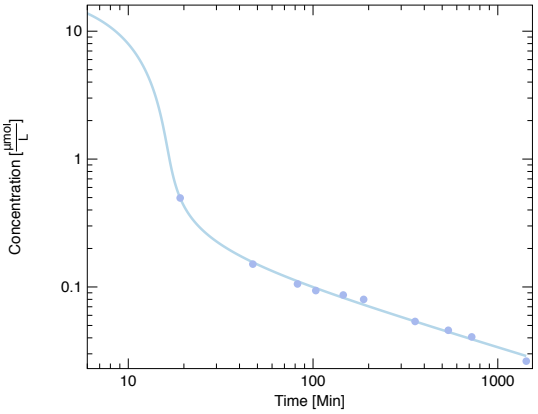

(c) Moriera *et al.* [89]

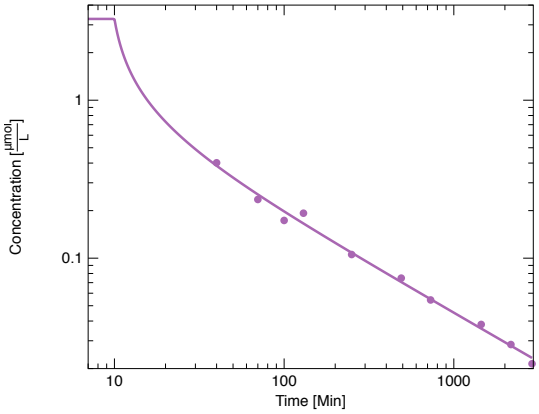

(d) Benjamin *et al.* [64]

Figure 3.7: Comparison of the theoretical and clinical concentrations of DOX using parameters developed from the single data sets model.

The predictive ability of the model over a broad range of datasets was then evaluated by developing the baseline parameters corresponding to large patient populations.

3.4.1 One-Molecule, One-Compartment Model

The set of parameters that best describe the one-compartment model of DOX with all the parameters varied are shown in Table 3.9. The parameters suggest that the elimination of DOX from compartment one is an approximately first-order process ($A - B \approx 0.77$) at high concentrations and a third-order process ($A \approx 3.24$) at low concentrations. There is an over 100-fold decrease in the volume of distribution from Table 3.3. This suggests that the amount of DOX in the body at any time is significantly less than the linear model amount

suggesting that excess drug is eliminated from the compartment volume. The variance is approximately eight times better than case 1 implying a more accurate fit to the clinical data.

Table 3.9: One-compartment model case 2 parameters of DOX.

$\boldsymbol{k}^{(1)}_{DOX,10}$ [a]	$\boldsymbol{\Gamma}^{(1)}_{DOX,10}$ [b]	$\boldsymbol{A}^{(1)}_{DOX,10}$	$\boldsymbol{B}^{(1)}_{DOX,10}$	$V_{d,DOX}$ [c]	S_p
0.0200 (10)	0.0450 (29)	3.2429 (68)	2.477 (19)	6.017 (75)	0.0929

units of:
[a] $\left[\frac{\mu\text{mol}}{\text{m}^2}\right]^{1-A^{(1)}_{DOX,10}}\text{min}^{-1}$ [b] $\left[\frac{\mu\text{mol}}{\text{m}^2}\right]^{-B^{(1)}_{DOX,10}}$ [c] $\left[\text{L}\cdot\text{m}^{-2}\right]$

In Table 3.10, we present the transition concentrations and times. We observe that in all the data sets considered, the transition from a low concentration to high concentration kinetics begins quickly after the start of the infusion. This high concentration phase lasts approximately twenty minutes, after which the kinetics returns to the low concentration phase.

Table 3.10: Calculated transition values using the one-compartment case 2 model parameters.

Inf[a](Dose)[b]	$A-B$	$X^{T,0}_{DOX,1}$ [c]	$C^{T,0}_{DOX,1}$ [d]	$T^{(1)}$ [e]	$T^{(2)}$ [e]
9.19 (50)	0.7659	3.4972	0.5812	0.39	21.36
9.19 (75)				0.38	27.11
11.04 (60)				0.32	22.53
22.08 (60)				0.16	19.79

upits of
[a] $\left[\mu\text{mol}\cdot\text{m}^{-2}\cdot\text{min}^{-1}\right]$ [b] $\left[\text{mg}\cdot\text{m}^{-2}\right]$ [c] $\left[\mu\text{mol}\cdot\text{m}^{-2}\right]$ [d] $\left[\mu\text{mol}\cdot\text{l}^{-1}\right]$ [e] $\left[\text{min}\right]$

Figure 3.8 shows the log-log plot of the concentration against time using the parameters presented in Table 3.9. In the figure, we notice the existence of two power-law regions in the curve of DOX PK. The first power-law region, which shows an approximately first order behavior that appears to depend on the length of infusion, with the longer infusion showing a steeper drop after reaching $C_{\max}$. A second power-law region begins at $\approx$ 70 mins after infusion begins, and is approximately third-order. There is a better fit of the curves to clinical data when compared to figure 3.3.

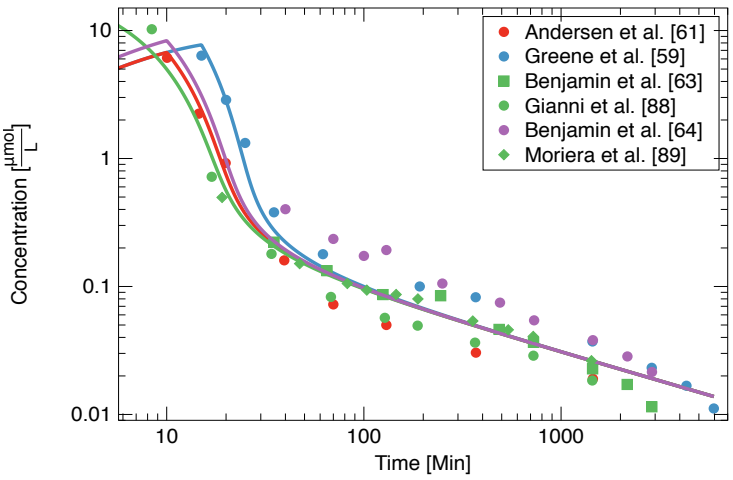

Figure 3.8: Comparison of theoretical and experimental concentrations of DOX using the parameters from Table 3.9. The clinical data and curves are for an infusion of 9.19 $\mu mol \cdot m^{-2} \cdot min^{-1}$ (red and blue), 22.08 $\mu mol \cdot m^{-2} \cdot min^{-1}$ (green) and 11.04 $\mu mol \cdot m^{-2} \cdot min^{-1}$ (purple).

3.4.2 Multi-Process Model

The model in chapter 2 allows for three processes, however only two processes produced a change in the variance. The extra terms were included to observe any competing processes in the elimination of DOX from the body. The third process had a flow rate constant equal to zero. Table 3.11 shows the parameters when all three processes are introduced in the model. The parameters show the presence of an extra process in the plasma disappearance of DOX. At high plasma concentration levels, the kinetics of DOX retains the approximately first-order behaviour of the single-process model. This is because the extra process parameters are significantly less than the main process. The flow and saturation kinetics coefficients are similar to Table 3.9. The parameters suggest that at concentrations below 0.01 $\mu mol \cdot l^{-1}$, the elimination PK of DOX has an exponent ($A \approx 0.79$). The implication of this is reduced plasma levels of the molecule at the terminal phase. The volume of distribution is slightly reduced as the terminal elimination rate increases. There is a slight improvement in the variance between cases 2 and 2.1 suggesting that the extra process does not influence the PK significantly.

In Table 3.12, we show the transition concentrations and times calculated using the

Table 3.11: One-compartment model case 2.1 parameters of DOX.

$\boldsymbol{k}^{(1,A)}_{DOX,10}$ [a]	$\boldsymbol{\Gamma}^{(1,B)}_{DOX,10}$ [b]	$\boldsymbol{A}^{(1)}_{DOX,10}$	$\boldsymbol{B}^{(1)}_{DOX,10}$	$V_{d,DOX}$ [c]	S_p
0.0200 (19)	0.0470 (54)	3.256 (14)	2.4758 (24)	6.0039 (32)	0.0928
0.000023 (10)	0.0461 (11)	0.798 (30)	0.985 (15)		
0.0000 (68)	N/A**	2.0337**	N/A**		

units of:
[a] $\left[\frac{\mu\text{mol}}{\text{m}^2}\right]^{1-A^{(1)}_{DOX,10}}\text{min}^{-1}$ [b] $\left[\frac{\mu\text{mol}}{\text{m}^2}\right]^{-B^{(1)}_{DOX,10}}$ [c] $\left[\text{L}\cdot\text{m}^{-2}\right]$
** The parameter is indeterminate because the rate coefficient is zero.

parameters in Table 3.11. The table shows the values corresponding to both processes in the model. The primary process transitions to high concentration kinetics less than a minute after drug infusion. Like the single process model, the primary process remains in this phase for approximately 20 minutes.

Table 3.12: Calculated transition values using the one-compartment case 2 model parameters.

Inf[a](Dose)[b]	$A-B$		$X^{T,0}_{DOX,1}$ [c]		$C^{T,0}_{DOX,1}$ [d]		$T^{(1)}$ [e]		$T^{(2)}$ [e]	
	p1	p2	p1	p2	p1	p2				
9.19 (50)	0.7802	-0.187	3.4384	22.7326	0.5727	3.7863	0.37	3.56	21.50	12.91
9.19 (75)							0.37	3.56	27.22	21.50
11.04 (60)							0.35	2.75	22.63	14.00
22.08 (60)							0.17	1.14	19.92	11.26

units of
[a] $\left[\mu\text{mol}\cdot\text{m}^{-2}\cdot\text{min}^{-1}\right]$ [b] $\left[\text{mg}\cdot\text{m}^{-2}\right]$ [c] $\left[\mu\text{mol}\cdot\text{m}^{-2}\right]$ [d] $\left[\mu\text{mol}\cdot\text{l}^{-1}\right]$ [e] $\left[\text{min}\right]$

The plasma concentration profile of DOX shown in figure 3.9 corresponds to the case where a first-order process contributes at low concentrations and influences the single process parameters from Table 3.9. It is observed from the figure that the terminal phase of the curves tends downwards due to the increased terminal elimination rate. There is no noticeable change in the high concentration fits of the curves.

3.4.3 One-Molecule, Two-Compartment Model Version A

Table 3.13 shows the model parameters when A and B were varied. The starting point of the model is the one-compartment model parameters from Table 3.9. The starting values of the parameters assumed that the elimination and distribution processes contribute

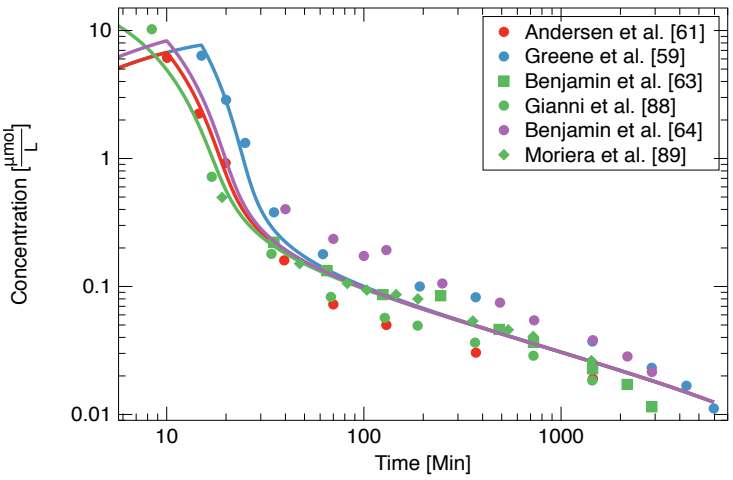

Figure 3.9: Comparison of theoretical and experimental concentrations of DOX using the parameters from Table 3.11. The clinical data and curves are for an infusion of 9.19 $\mu mol \cdot m^{-2} \cdot min^{-1}$ (red and blue), 22.08 $\mu mol \cdot m^{-2} \cdot min^{-1}$ (green) and 11.04 $\mu mol \cdot m^{-2} \cdot min^{-1}$ (purple).

equally to the plasma PK of DOX. The new variance is only slightly better than the one-compartment model result in Table 3.9. The flow of DOX out of compartment one appears to be independent of the final compartment. The parameters show that the model behaves like an extension of the one-compartment case 2 model. The PK of DOX in compartment one is a competition between the elimination and distribution to compartment two. Comparing of the total rate coefficient of elimination of the drug from compartment one, $k_{el} = k^{(1,A)}_{DOX,1,0} + k^{(1,A)}_{DOX,1,2}$, shows that the parameter is comparable to the rate coefficients in Tables 3.9 and 3.11. The rate coefficient of flow from compartment two to one is zero, implying that compartment two represents an irreversible process in DOX PK. The parameters suggest that like the one-compartment case, the elimination kinetics of DOX from plasma is characterized by exponent ($A - B \approx 0.77$) at high concentrations and $A \approx 3.24$ at low concentrations regardless of the process occurring. The high concentration kinetics of the flow to compartment zero begins approximately 4.46 minutes after the start of infusion when the amount of DOX in compartment one is 3.57 $\mu mol \cdot m^{-2}$. For the distribution phase, the high concentration kinetics of the distribution to compartment two begins approximately 4.06 minutes after infusion, which corresponds to DOX amount of 3.37 $\mu mol \cdot m^{-2}$. Com-

paring the rate coefficients of both processes in compartment one, we notice that elimination accounts for nearly 60% of the PK in compartment one. There is no change in the variance of the model over the single-compartment model.

Table 3.13: Two-compartment model (version A) case 2 model parameters of DOX.

ci,cf	$\boldsymbol{k}^{(1,A)}_{DOX,ci,cf}$ [a]	$\boldsymbol{\Gamma}^{(1,B)}_{DOX,ci,cf}$ [b]	$\boldsymbol{A}^{(1)}_{DOX,ci,cf}$	$\boldsymbol{B}^{(1)}_{DOX,ci,cf}$	$V_{d,DOX}$ [c]	S_p
1,0	0.0119 (10)	0.0434 (49)	3.2416 (12)	2.4724 (32)	6.0190 (75)	0.0928
1,2	0.0080 (10)	0.0494 (88)	3.2463 (19)	2.4754 (50)		
2,1	0.0000 (68)	N/A**	0.537**	N/A**		

units of
[a] $\left[\frac{\mu\text{mol}}{\text{m}^2}\right]^{1-A^{(1)}_{DOX,ci,cf}}\text{min}^{-1}$ [b] $\left[\frac{\mu\text{mol}}{\text{m}^2}\right]^{-B^{(1)}_{DOX,ci,cf}}$ [c] $\left[\text{L}\cdot\text{m}^{-2}\right]$
**The parameter is indeterminate because the rate constant is zero.

Table 3.14 shows the transition concentrations and times calculated using the parameters in Table 3.13. The table shows that the elimination and distribution of DOX in compartment one to zero and two are in the high concentration phase between 0.16 and 27 minutes.

Table 3.14: Calculated transition values using the two-compartment version A case 2 model parameters.

Inf[a](Dose)[b]	ci,cf	$A-B$	$X^{T,cf}_{DOX,ci}$ [c]	$T^{(1)}$ [e]	$T^{(2)}$ [e]	$X^{T}_{DOX,1}$ [c]	$C^{T}_{DOX,1}$ [d]
9.19 (50)	1, 0	0.7692	3.5570	0.40	20.09	3.5570	0.5910
	1, 2	0.7709	3.3705	0.41	20.47	3.3705	0.5599
	2, 1	N/A	N/A	N/A	N/A	N/A	N/A
9.19 (75)	1, 0	0.7692	3.5570	0.40	26.79	3.5570	0.5910
	1, 2	0.7709	3.3705	0.41	27.30	3.3705	0.5599
	2, 1	N/A	N/A	N/A	N/A	N/A	N/A
11.04 (60)	1, 0	0.7692	3.5570	0.32	22.10	3.5570	0.5910
	1, 2	0.7709	3.3705	0.33	22.67	3.3705	0.5599
	2, 1	N/A	N/A	N/A	N/A	N/A	N/A
22.08 (60)	1, 0	0.7692	3.5570	0.16	20.79	3.5570	0.5910
	1, 2	0.7709	3.3705	0.16	21.30	3.3705	0.5599
	2, 1	N/A	N/A	N/A	N/A	N/A	N/A

upits of
[a] $\left[\mu\text{mol}\cdot\text{m}^{-2}\cdot\text{min}^{-1}\right]$ [b] $\left[\text{mg}\cdot\text{m}^{-2}\right]$ [c] $\left[\mu\text{mol}\cdot\text{m}^{-2}\right]$ [d] $\left[\mu\text{mol}\cdot\text{l}^{-1}\right]$ [e] $\left[\text{min}\right]$
N/A: Not applicable because the coefficient is zero.

Figure 3.10 shows the concentration curves of DOX using the parameters shown in Table 3.13. The curves are similar to the one-compartment model fits at high and low

plasma concentrations. This is due to the absence of a reverse flow from compartment two. The model behaves like a one-compartment model with two elimination processes.

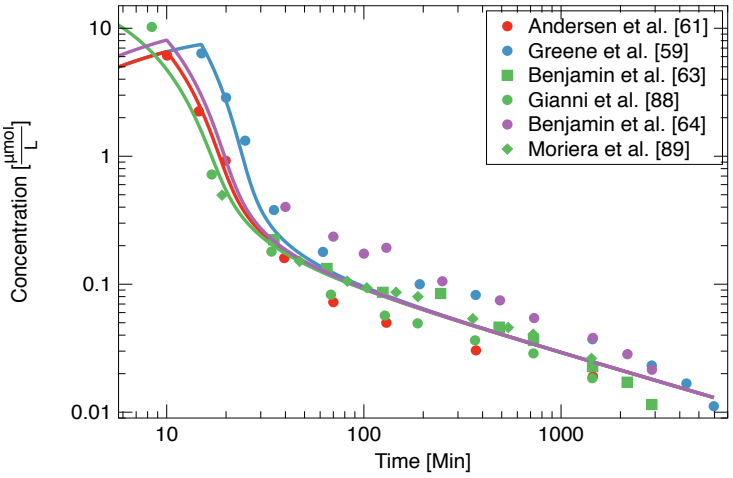

Figure 3.10: Comparison of theoretical and experimental concentrations of DOX using the parameters from Table 3.13. The clinical data and curves are for an infusion of 9.19 $\mu mol \cdot m^{-2} \cdot min^{-1}$ (red and blue), 22.08 $\mu mol \cdot m^{-2} \cdot min^{-1}$ (green) and 11.04 $\mu mol \cdot m^{-2} \cdot min^{-1}$ (purple).

3.4.4 Multi-Process Models for Two-Compartment Version A

To investigate the influence of other processes on the two-compartment model, a second process was added to the single process case. The new model resulted in a 1.29% decrease in the variance, and the parameters are presented in Table 3.15. The table shows the presence of an extra process to describe the flow of DOX to compartment zero. The elimination of DOX from compartment one may be described by two competing processes. The dominant process has an exponent $A - B \approx 0.77$ at high concentrations. The flow rate of the drug from compartment one to zero is increased slightly from the single-process case due to the extra process, which is zeroth-order ($A - B \approx 0.00$), and contributes minimally to the PK. At low concentrations, there is a competition between both processes, with the secondary process, which is approximately second-order ($A \approx 1.99$) dominating at concentrations below 0.01 $\mu mol \cdot l^{-1}$. Conversely, the rate of distribution to compartment two is reduced by about forty times the rate in Table 3.13. The distribution of the drug from compartment two

is a second-order process at low concentrations and a constant rate at high concentrations. The volume of distribution is unchanged from the single-process two-compartment model.

Table 3.15: Two-compartment model (version A) case 2.1 parameters for DOX.

ci, cf	$\boldsymbol{k}^{(1,A)}_{DOX,ci,cf}$ [a]	$\boldsymbol{\Gamma}^{(1,B)}_{DOX,ci,cf}$ [b]	$\boldsymbol{A}^{(1)}_{DOX,ci,cf}$	$\boldsymbol{B}^{(1)}_{DOX,ci,cf}$	$V_{d,DOX}$ [c]	S_p
1,0	0.0174 (10)	0.0397 (46)	3.2198 (19)	2.4486 (35)	6.019 (64)	0.0916
1,0	0.01096 (24)	0.984 (82)	1.9904 (10)	1.9934 (62)		
1,2	0.0002 (23)	0.039 (25)	3.2416 (17)	2.4360 (49)		
1,2	0.000000(93)	N/A**	2.0057**	N/A**		
2,1	0.00000000(48)	N/A**	0.5439**	N/A**		
2,1	0.0031 (15)	1.0150 (20)	1.99854 (19)	1.9936 (82)		

units of:

a $\left[\frac{\mu\text{mol}}{\text{m}^2}\right]^{1-A^{(1)}_{DOX,ci,cf}}\text{min}^{-1}$ b $\left[\frac{\mu\text{mol}}{\text{m}^2}\right]^{-B^{(1)}_{DOX,ci,cf}}$ c $\left[\text{L}\cdot\text{m}^{-2}\right]$

**The parameter is indeterminate because the rate coefficient is zero.

The parameters in Table 3.16 are obtained from fitting the baseline datasets to the two-compartment case 2.2 model. The presence of the extra processes does not significantly change the elimination and distribution processes at high DOX concentrations. The dominant processes of distribution and elimination from compartment one both have exponent $A-B \approx 0.78$ at high concentrations. At low concentrations, the extra processes are approximately first-order. At high concentrations, elimination accounts for over 60% of DOX PK. However, at low concentrations, elimination accounts for less than 20% of the PK. There is a twenty-fold increase in the total clearance from Table 3.13 at concentrations below 0.1 $\mu\text{mol}\cdot\text{l}^{-1}$. Like the single process case, the drug in compartment two appears to be retained within the compartment. There is no change in the distribution volume from case 2.1. The variance is slightly improved from cases 2 and 2.1. Figure 3.11 shows the plasma concentration profile of DOX using parameters from case 2.2 in table 3.16, the curves are slightly shifted downwards at concentrations below 0.05 $\mu\text{mol}\cdot\text{l}^{-1}$ due to the increased elimination rates at low drug levels.

Table 3.16: Two-compartment model (version A) case 2.2 parameters of DOX.

ci, cf	$\boldsymbol{k}^{(1,A)}_{DOX,ci,cf}$ [a]	$\boldsymbol{\Gamma}^{(1,B)}_{DOX,ci,cf}$ [b]	$\boldsymbol{A}^{(1)}_{DOX,ci,cf}$	$\boldsymbol{B}^{(1)}_{DOX,ci,cf}$	$V_{d,DOX}$ [c]	S_p
1,0	0.01193 (67)	0.0434 (27)	3.2417 (13)	2.4724 (16)	6.019 (16)	0.0912
1,0	0.0000 (68)	N/A**	1.9906**	N/A**		
1,0	0.00000190 (40)	0.995 (19)	0.994 (43)	0.998 (16)		
1,2	0.00804 (68)	0.0494 (21)	3.246 (17)	2.475 (20)		
1,2	0.00000 (68)	N/A**	2.0054**	N/A**		
1,2	0.0000121 (80)	1.0013 (11)	0.978 (30)	1.0101 (18)		
2,1	0.0000 (20)	N/A**	0.5441**	N/A**		
2,1	0.0000 (19)	N/A**	1.9994**	N/A**		
2,1	0.0000 (19)	N/A**	1.0083**	N/A**		

units of:
[a] $\left[\frac{\mu\text{mol}}{\text{m}^2}\right]^{1-A^{(1)}_{DOX,ci,cf}}\text{min}^{-1}$ [b] $\left[\frac{\mu\text{mol}}{\text{m}^2}\right]^{-B^{(1)}_{DOX,ci,cf}}$ [c] $\left[\text{L}\cdot\text{m}^{-2}\right]$
**The parameter is indeterminate because the rate parameter is zero.

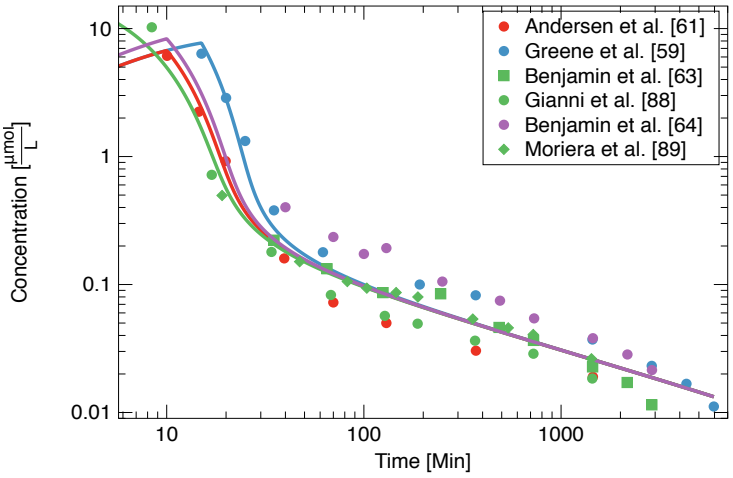

Figure 3.11: Comparison of theoretical and experimental concentrations of DOX using the parameters from Table 3.16. The clinical data and curves are for an infusion of 9.19 $\mu\text{mol}\cdot\text{m}^{-2}\cdot\text{min}^{-1}$ (red and blue), 22.08 $\mu\text{mol}\cdot\text{m}^{-2}\cdot\text{min}^{-1}$ (green) and 11.04 $\mu\text{mol}\cdot\text{m}^{-2}\cdot\text{min}^{-1}$ (purple).

3.4.5 One-Molecule, Two-Compartment Model Version B

Table 3.17 shows the parameters developed from the model when A and B were allowed to vary. In the table, *ci* and *cf* are the initial and the final compartments. The distribution of DOX in compartment one into compartment two retains the saturable kinetics, which is characterized by exponent $A - B \approx 0.81$ at high concentrations. Within compartment two, the flow kinetics to compartment zero is not saturable and follows an order $A \approx 1.59$. This

implies that the distribution kinetics of DOX in the compartment occurs much faster than elimination at high concentrations. At low concentrations, the parameters suggest that the kinetics may be a competition between elimination and distribution within the compartment. In this phase, the elimination coefficient accounts for nearly 55% of the total drug PK. The high concentration kinetics of the flow of the molecule in compartment one to compartment two begins approximately 3.30 minutes after the start of infusion when the amount of DOX in the compartment is 2.85 $\mu\text{mol} \cdot \text{m}^{-2}$, while the kinetics of the molecule in compartment two appears to be predominantly in the low-concentration phase. This model is characterized by a reduced volume of distribution of the molecule in compartment one due to the elimination from the secondary compartment. The change in the variance from Table 3.13 is negligible.

Table 3.17: Two-compartment model (version B) case 2 model parameters of DOX.

ci, cf	$\boldsymbol{k}^{(1,A)}_{DOX,ci,cf}$ [a]	$\boldsymbol{\Gamma}^{(1,B)}_{DOX,ci,cf}$ [b]	$\boldsymbol{A}^{(1)}_{DOX,ci,cf}$	$\boldsymbol{B}^{(1)}_{DOX,ci,cf}$	$V_{d,DOX}$ [c]	S_p
1,2	0.0484 (41)	0.0753 (11)	3.2730 (21)	2.4734 (42)	5.2144 (57)	0.0926
2,0	1.2431 (24)	0.000 (17)	1.5906 (15)	N/A**		
2,1	0.96562 (44)	0.2667 (66)	1.6021 (46)	1.0903 (18)		

units of:
[a] $\left[\frac{\mu\text{mol}}{\text{m}^2}\right]^{1-A^{(1)}_{DOX,ci,cf}} \text{min}^{-1}$ [b] $\left[\frac{\mu\text{mol}}{\text{m}^2}\right]^{-B^{(1)}_{DOX,ci,cf}}$ [c] $\left[\text{L} \cdot \text{m}^{-2}\right]$
**The parameter is indeterminate because the rate coefficient is zero.

Table 3.18 shows the transition concentrations and times calculated using the parameters in Table 3.17. We see that while the elimination of the molecule from the body remains in the low-concentration phase regardless of the amount infused, the distribution and redistribution processes change with the concentration. In compartment one, the high concentration phase begins immediately following the start of the infusion and continues for approximately twenty minutes. Depending on the dose of the drug, the redistribution process from compartment two to one may transition between the high and low concentration phase or remain in an approximately low concentration phase.

Figure 3.12 shows the DOX concentration curves using parameters from Table 3.17. The curves show a slight shift downwards, implying a small change in the $C_{\max}$ as the

Table 3.18: Calculated transition values using the two-compartment version B case 2 model parameters.

Inf[a](Dose)[b]	ci,cf	$A-B$	$X^{T,cf}_{DOX,ci}$ [c]	$T^{(1)}$ [e]	$T^{(2)}$ [e]	$X^{T}_{DOX,1}$ [c]	$C^{T}_{DOX,1}$ [d]
9.19 (50)	1, 2	0.7996	2.8452	0.33	21.49	2.8452	0.5456
	2, 0	N/A	N/A	N/A	N/A	N/A	N/A
	2, 1	0.5118	3.3608	N/A	N/A	N/A	N/A
9.19 (75)	1, 2	0.7996	2.8452	0.33	26.88	2.8452	0.5456
	2, 0	N/A	N/A	N/A	N/A	N/A	N/A
	2, 1	0.5118	3.3608	13.01	15.28	38.69	7.42
11.04 (60)	1, 2	0.7996	2.8452	0.27	22.46	2.8452	0.5456
	2, 0	N/A	N/A	N/A	N/A	N/A	N/A
	2, 1	0.5118	3.3608	7.22	10.79	38.95	7.47
22.08 (60)	1, 2	0.7996	2.8452	0.13	19.45	2.8452	0.5456
	2, 0	N/A	N/A	N/A	N/A	N/A	N/A
	2, 1	0.5118	3.3608	2.45	7.79	40.78	7.81

upits of
[a] $\left[\mu mol \cdot m^{-2} \cdot min^{-1}\right]$ [b] $\left[mg \cdot m^{-2}\right]$ [c] $\left[\mu mol \cdot m^{-2}\right]$ [d] $\left[\mu mol \cdot l^{-1}\right]$ [e] $\left[min\right]$
N/A: Not applicable because the coefficient is zero.

molecule is distributed between compartments one and two. At low concentrations, the curves are similar to the one-compartment model and two-compartment version A model estimates.

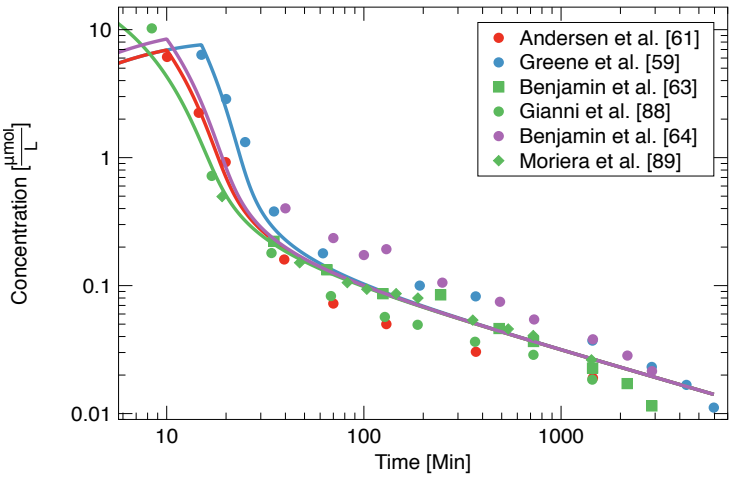

Figure 3.12: Comparison of theoretical and experimental concentrations of DOX using the parameters from Table 3.17. The clinical data and curves are for an infusion of 9.19 $\mu mol \cdot m^{-2} \cdot min^{-1}$ (red and blue), 22.08 $\mu mol \cdot m^{-2} \cdot min^{-1}$ (green) and 11.04 $\mu mol \cdot m^{-2} \cdot min^{-1}$ (purple).

3.4.6 Multi-Process Models for Two-Compartment Version B

To investigate the influence of other processes on the two-compartment (version B) case 2 model, new sets of parameters were added to the model fit from Table 3.17. In the initial model, a second process was added to the model, which resulted in a reduced variance. The parameters are shown in Table 3.19. There, we notice that the distribution of DOX from compartment one can be described by two processes, the dominant process has an exponent $A - B \approx 0.70$ at high concentrations. The secondary process dominates at very low concentrations and suggests an increased terminal rate of distribution. The rate constant of plasma distribution of DOX increased more than eight times from the single process case. The rate constant of elimination from compartment two is reduced threefold in this model, however the PK of DOX in the compartment is characterized by a capacity-limited process of distribution to compartment one. The rate-limiting effect of the plasma redistribution ensures that the maximum rate of distribution occurs at DOX concentrations of $\approx 7\ \mu\text{mol} \cdot \text{l}^{-1}$. Like the single process case in Table 3.17, the low concentration PK of DOX in compartment two suggests a competition between redistribution and elimination. There is a 3% decrease in DOX volume of distribution in compartment one compared to Table 3.17, suggesting an increased delivery of the drug to the cells.

Table 3.19: Two-compartment model (Version B) case 2.1 model parameters of DOX.

ci, cf	$\boldsymbol{k}^{(1,A)}_{DOX,ci,cf}$ [a]	$\boldsymbol{\Gamma}^{(1,B)}_{DOX,ci,cf}$ [b]	$\boldsymbol{A}^{(1)}_{DOX,ci,cf}$	$\boldsymbol{B}^{(1)}_{DOX,ci,cf}$	$V_{d,DOX}$ [c]	S_p
1,2	0.3031 (61)	0.3709 (50)	3.3495 (11)	2.6466 (35)	5.0744 (66)	0.0910
1,2	0.0032 (26)	0.1013 (21)	0.3410 (34)	0.9795 (12)		
2,0	0.4145 (23)	0.0000 (24)	1.2504 (17)	N/A**		
2,0	0.0000 (93)	N/A**	0.9592 (22)	N/A**		
2,1	1.1007 (33)	0.3248 (42)	0.9372 (42)	1.2225 (12)		
2,1	0.0000 (21)	N/A**	0.9833 (89)	N/A**		

units of:
[a] $\left[\frac{\mu\text{mol}}{\text{m}^2}\right]^{1-A^{(1)}_{DOX,ci,cf}} \text{min}^{-1}$ [b] $\left[\frac{\mu\text{mol}}{\text{m}^2}\right]^{-B^{(1)}_{DOX,ci,cf}}$ [c] $\left[\text{L} \cdot \text{m}^{-2}\right]$
**The parameter is indeterminate because the rate constant is zero.

When fitting the parameters in Table 3.19 by adding second-order terms, we notice that some of the parameters do not play a significant role in minimizing the variance and

were been excluded. The new model parameters are shown in Table 3.20. The parameters in Tables 3.19 and 3.20 are similar. The extra parameters are the elimination terms in compartment two. Specifically, the elimination of the drug in compartment two is described by two processes. There is a slight increase in the high and low concentration rate constants of distribution from plasma when compared to Table 3.19. The new terms suggest that there is an approximately second order ($A \approx 1.93$) elimination of DOX from the body at low concentrations. At high concentrations, the new terms enhance the clearance of the drug from compartment two compared to Table 3.19. The addition of the new parameters to the model ensures that when the maximum redistribution rate has been reached the excess DOX in the compartment is cleared quicker. The volume of distribution of DOX is reduced from the two-compartment version B case 2 and 2.1 models, and suggests that there is a slight increase in the amount of drug delivered to compartment two. There is a 3% decrease in the variance from Table 3.17.

Table 3.20: Two-compartment model (Version B) parameters of DOX from case 2.2.

ci, cf	$\boldsymbol{k}^{(1,A)}_{DOX,ci,cf}$ [a]	$\boldsymbol{\Gamma}^{(1,B)}_{DOX,ci,cf}$ [b]	$\boldsymbol{A}^{(1)}_{DOX,ci,cf}$	$\boldsymbol{B}^{(1)}_{DOX,ci,cf}$	$V_{d,DOX}$ [c]	S_p
1,2	0.3138 (41)	0.3945 (46)	3.358 5(21)	2.6616 (35)	5.0274 (66)	0.0900
1,2	0.0011 (26)	0.1112 (21)	0.2959 (34)	0.9775 (21)		
2,0	0.3940 (23)	0.00 (82)	1.2397 (17)	N/A**		
2,0	0.0063 (52)	0.0018 (42)	1.9348 (53)	1.8959 (19)		
2,1	1.0799 (33)	0.3357 (42)	0.9278 (42)	1.2038 (12)		

units of:

[a] $\left[\frac{\mu\text{mol}}{\text{m}^2}\right]^{1-A^{(1)}_{DOX,ci,cf}}\text{min}^{-1}$ [b] $\left[\frac{\mu\text{mol}}{\text{m}^2}\right]^{-B^{(1)}_{DOX,ci,cf}}$ [c] $\left[\text{L}\cdot\text{m}^{-2}\right]$

**The parameter is indeterminate because the rate parameter is zero.

Figure 3.13 shows the concentration curves of DOX using the parameters in Table 3.20. The curves show that the parameters model the data well. There is a notably improved fit of the curves to the clinical data over the range of concentration. The terminal phase of the curve shows an extra process beginning 24 hours after the start of infusion.

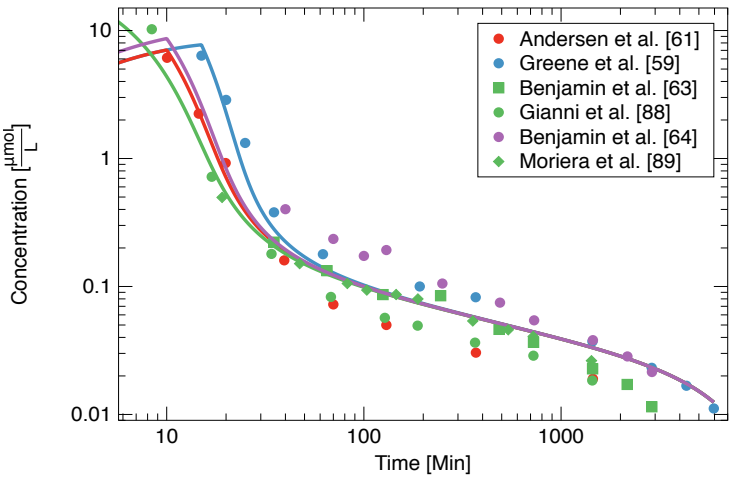

Figure 3.13: Comparison of theoretical and experimental concentrations of DOX using the parameters from Table 3.20. The clinical data and curves are for an infusion of 9.19 $\mu mol \cdot m^{-2} \cdot min^{-1}$ (red and blue), 22.08 $\mu mol \cdot m^{-2} \cdot min^{-1}$ (green) and 11.04 $\mu mol \cdot m^{-2} \cdot min^{-1}$ (purple).

3.4.7 Drug Interaction Effects for Two-Compartment Version B

The two-compartment model also allowed to test the effect of the presence of a drug in a compartment on its flow into the compartment, specifically how the presence of molecule *di* in compartment *cj* affects the rate of flow of the same molecule, *di*, from compartment *ck* into *cj*. A new set of terms were added to the two-molecule two-compartment model, which describe the effect of molecule interactions. These interactions produce the effective rate constants as discussed in chapter 2. The α and β terms represent the molecule interaction and saturation effect, the C and D terms describe the process and the fractal exponents. The two-compartment (version B) model case 2 parameters in Table 3.17 were used to obtain the effect of the interaction parameters. According to the parameters in Table 3.21, the distribution of DOX in compartment one to compartment two is influenced by the amount of the drug in compartment two. However, this effect is noticeable only at very high concentrations of the drug in compartment two. Conversely, the redistribution of DOX to compartment one is reduced with high concentration of the drug in compartment one. The flow parameters and the volume of distribution do not change significantly from the case 2 model. However, the variance is reduced by 1% from Table 3.17, representing

a small change in the variance being larger than the case 2.2 variance. Hence, case 2.2 provides a better model than including these interactions.

Table 3.21: Two-compartment model (Version B) case 3.1 parameters of DOX.

ci, cf	$\boldsymbol{k}^{(1,A)}_{DOX,ci,cf}$ [a]	$\boldsymbol{\Gamma}^{(1,B)}_{DOX,ci,cf}$ [b]	$\boldsymbol{A}^{(1)}_{DOX,ci,cf}$	$\boldsymbol{B}^{(1)}_{DOX,ci,cf}$	$V_{d,DOX}$ [e]
1,2	0.0482 (10)	0.0754 (50)	3.15 (12)	2.4734 (50)	5.2166 (61)
2,0	1.2242 (50)	0.00 (11)	1.595 (55)	1.119 (24)	
2,1	0.9856 (40)	0.2667 (16)	1.5502 (51)	1.1204 (19)	
ci, cf	$\boldsymbol{\alpha}^{(1,C)}_{DOX,ci,cf\|DOX,cf}$ [c]	$\boldsymbol{\beta}^{(1,D)}_{DOX,ci,cf\|DOX,cf}$ [d]	$\boldsymbol{C}^{(1)}_{DOX,ci,cf\|DOX,cf}$	$\boldsymbol{D}^{(1)}_{DOX,ci,cf\|DOX,cf}$	S_p
1,2	0.0004 (50)	0.0001 (15)	1.000 (13)	0.999 (10)	0.0916
1,2	0.0004 (19)	0.00005 (15)	2.0001 (22)	1.997 (24)	
2,1	-0.0002 (16)	0.000053 (34)	1.000 (19)	0.9999 (45)	
2,1	0.00008 (48)	0.0003 (50)	2.00 (23)	2.000 (19)	

units of:

[a] $\left[\frac{\mu\text{mol}}{\text{m}^2}\right]^{1-A^{(1)}_{DOX,ci,cf}}\text{min}^{-1}$ [b] $\left[\frac{\mu\text{mol}}{\text{m}^2}\right]^{-B^{(1)}_{DOX,ci,cf}}$ [c] $\left[\frac{\mu\text{mol}}{\text{m}^2}\right]^{-C^{(1)}_{DOX,ci,cf|DOX,cf}}$ [d] $\left[\frac{\mu\text{mol}}{\text{m}^2}\right]^{-D^{(1)}_{DOX,ci,cf|DOX,cf}}$ [e] $\left[\text{L}\cdot\text{m}^{-2}\right]$

Figure 3.14 shows the concentration-time profile of DOX when the molecule within the compartments are allowed to interact. The plasma PK of DOX does not appear to show any significant change from the case 2 model.

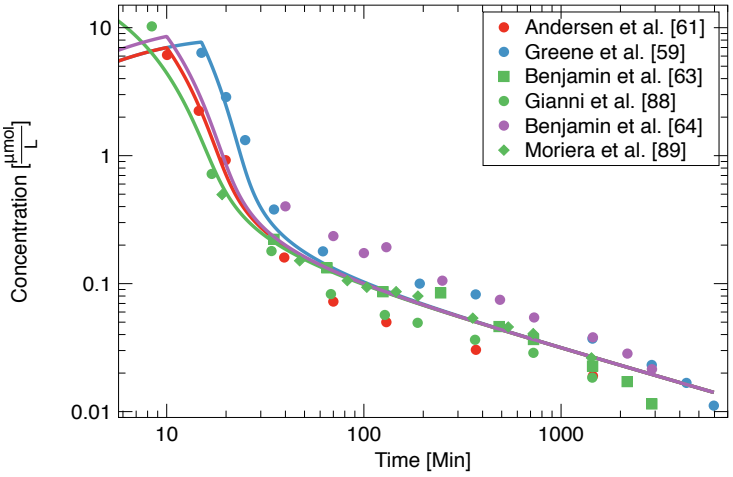

Figure 3.14: Comparison of theoretical and experimental concentrations of DOX using the parameters from Table 3.21. The clinical data and curves are for an infusion of 9.19 $\mu\text{mol}\cdot\text{m}^{-2}\cdot\text{min}^{-1}$ (red and blue), 22.08 $\mu\text{mol}\cdot\text{m}^{-2}\cdot\text{min}^{-1}$ (green) and 11.04 $\mu\text{mol}\cdot\text{m}^{-2}\cdot\text{min}^{-1}$ (purple).

3.4.8 One-Molecule, Three-Compartment Model

The parameters that describe the model with A and B varied are shown in Table 3.22. We observe that the exponents of the rate constants of flow from compartment one to two and three are approximately the same. This suggests that DOX distribution from compartment one retains the one and two-compartment model behaviours at high plasma concentrations with exponent $A - B \approx 0.89$ characterizing the distribution to compartment two, and exponent $A - B \approx 0.79$ characterizing the distribution to compartment three. Plasma distribution to the elimination sites accounts for approximately 97% of the total drug PK in compartment one. This implies that less than 3% of the plasma drug is distributed to the tissues and organs in compartment three. In compartment two, the two processes depend on the concentration of the drug in the compartment, with elimination and metabolism accounting for approximately 95% of the high concentration PK of DOX. When the amount of DOX in compartment two reduces, the redistribution of the drug to the plasma compartment accounts for 70% of the drug PK. The kinetics of plasma redistribution of DOX in compartment three is also concentration-dependent, the process is characterized by exponent $A - B \approx 0.32$ at high concentrations. The high concentration kinetics of the flow of DOX from compartment one to compartment two occurs when the amount of the molecule in compartment one is 2.70 $\mu\text{mol} \cdot \text{m}^{-2}$ and to compartment three when the amount is 3.92 $\mu\text{mol} \cdot \text{m}^{-2}$. The kinetics of the molecule in the other compartments are in the low-concentration phase. The volume of distribution is reduced by 2% from the two-compartment model in Table 3.17 suggesting that the distribution to compartment three contributes minimally to the plasma PK of the drug. The model result in a 1% decrease in the two-compartment (version B) model variance, and is a worse variance than the two-compartment (version B) case 2.2 result.

Table 3.23 shows the transition concentrations and times calculated using the parameters in Table 3.22. The table shows that elimination and redistribution of DOX in compartment two and three respectively remains in a low-concentration phase regardless of

Table 3.22: Three-compartment model case 2 parameters of DOX.

ci, cf	$\boldsymbol{k}^{(1,A)}_{DOX,ci,cf}$ [a]	$\boldsymbol{\Gamma}^{(1,B)}_{DOX,ci,cf}$ [b]	$\boldsymbol{A}^{(1)}_{DOX,ci,cf}$	$\boldsymbol{B}^{(1)}_{DOX,ci,cf}$	$V_{d,DOX}$ [c]	S_p
1,2	0.0665 (12)	0.0831 (23)	3.3909 (14)	2.5044 (75)	5.1221 (32)	0.0915
2,0	0.4593 (49)	0.0011 (87)	1.4828 (51)	1.1151 (82)		
2,1	1.0626 (50)	0.1242 (14)	1.4989 (25)	1.1430 (55)		
1,3	0.000045(12)	0.0326 (63)	3.2906 (48)	2.5062 (18)		
3,1	0.0490 (13)	0.0014 (33)	1.4771 (44)	1.1592 (74)		

units of:
a $\left[\frac{\mu\text{mol}}{\text{m}^2}\right]^{1-A^{(1)}_{DOX,ci,cf}}\text{min}^{-1}$ b $\left[\frac{\mu\text{mol}}{\text{m}^2}\right]^{-B^{(1)}_{DOX,ci,cf}}$ c $\left[\text{L}\cdot\text{m}^{-2}\right]$

the concentration of the molecule in the body. The redistribution of DOX in compartment two to compartment one is fastest when the amount of the molecule in the compartment is 6.2021 $\mu\text{mol}\cdot\text{m}^{-2}$, which corresponds to the DOX plasma concentration of 5.5041 $\mu\text{mol}\cdot\text{l}^{-1}$.

Figure 3.15 shows the plot of concentration against time using the parameters from the three-compartment model. The curves show a good agreement with the clinical data.

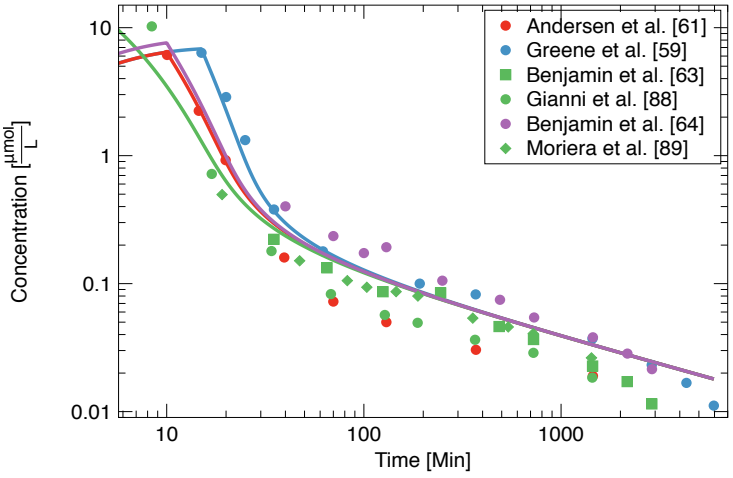

Figure 3.15: Comparison of theoretical and experimental concentrations of DOX using the parameters from Table 3.22. The clinical data and curves are for an infusion of 9.19 $\mu\text{mol}\cdot\text{m}^{-2}\cdot\text{min}^{-1}$ (red and blue), 22.08 $\mu\text{mol}\cdot\text{m}^{-2}\cdot\text{min}^{-1}$ (green) and 11.04 $\mu\text{mol}\cdot\text{m}^{-2}\cdot\text{min}^{-1}$ (purple).

Table 3.23: Calculated transition values using the three-compartment case 2 model parameters.

Inf[a](Dose)[b]	ci,cf	$A-B$	$X^{T,cf}_{DOX,ci}$ [c]	$T^{(1)}$ [e]	$T^{(2)}$ [e]	$X^{T}_{DOX,1}$ [c]	$C^{T}_{DOX,1}$ [d]
9.19 (50)	1, 2	0.8865	2.7000	0.31	24.51	2.7000	0.5272
	2, 0	0.3677	450.0094	N/A	N/A	N/A	N/A
	2, 1	0.3559	6.2021	6.23	11.12	28.1926	5.5041
	1, 3	0.7844	3.9273	0.46	21.07	3.9273	0.7667
	3, 1	0.3179	289.6892	N/A	N/A	N/A	N/A
9.19 (75)	1, 2	0.8865	2.7000	0.30	29.75	2.7000	0.5272
	2, 0	0.3677	450.0094	N/A	N/A	N/A	N/A
	2, 1	0.3559	6.2021	6.25	16.35	28.2335	5.5121
	1, 3	0.7844	3.9273	0.45	26.29	3.9273	0.7667
	3, 1	0.3179	289.6892	N/A	N/A	N/A	N/A
11.04 (60)	1, 2	0.8865	2.7000	0.25	25.15	2.7000	0.5272
	2, 0	0.3677	450.0094	N/A	N/A	N/A	N/A
	2, 1	0.3559	6.2021	4.55	11.83	28.7022	5.6036
	1, 3	0.7844	3.9273	0.38	21.76	3.9273	0.7667
	3, 1	0.3179	289.6892	N/A	N/A	N/A	N/A
22.08 (60)	1, 2	0.8865	2.7000	0.12	21.84	2.7000	0.5272
	2, 0	0.3677	450.0094	N/A	N/A	N/A	N/A
	2, 1	0.3559	6.2021	2.00	8.44	31.9113	6.3213
	1, 3	0.7844	3.9273	0.19	18.36	3.9273	0.7667
	3, 1	0.3179	289.6892	N/A	N/A	N/A	N/A

[a] units of $\left[\mu\text{mol}\cdot\text{m}^{-2}\cdot\text{min}^{-1}\right]$ [b] $\left[\text{mg}\cdot\text{m}^{-2}\right]$ [c] $\left[\mu\text{mol}\cdot\text{m}^{-2}\right]$ [d] $\left[\mu\text{mol}\cdot\text{l}^{-1}\right]$ [e] $\left[\text{min}\right]$

N/A: Not applicable because the coefficient is zero.

3.4.9 Multi-Process Model for the Three-Compartment Model

Like the one and two-compartment single-molecule cases, the influence of the other processes on the single process was investigated. The new model included all the rate processes that influence the PK of DOX. The parameters from the new model are presented in Table 3.24. There are five competing processes in the flow of DOX from compartment one to compartments two and three. The distribution of DOX to the cells is a saturable process. There are first and second-order contributions to the plasma distribution of the drug to the cells and the elimination sites. At high concentrations, the distribution of plasma DOX to the elimination compartment dominates. There are two secondary processes in the distri-

bution from compartment one to two and both processes are approximately zeroth order at high DOX concentrations, and contributes minimally to the PK of the drug in compartment one. The set of terms that describe the distribution of DOX in compartment one to compartment three are both zeroth order processes at high concentrations, and suggests a constant rate of distribution of the drug to the compartment. According to the parameters, the rate of distribution from compartment one to compartments two and three is increased relative to the previous models. The elimination and redistribution of the drug in compartment two are both described by three terms each, the first set of terms are the dominant process, and the secondary terms dominate at low concentrations in the compartment. The volume of distribution is similar to the single process model in Table 3.22. The model results in a 14% decrease in the variance from Table 3.22.

Table 3.24: Three-compartment model case 2.2 parameters of DOX.

ci, cf	$\boldsymbol{k}^{(1,A)}_{DOX,ci,cf}$ [a]	$\boldsymbol{\Gamma}^{(1,B)}_{DOX,ci,cf}$ [b]	$\boldsymbol{A}^{(1)}_{DOX,ci,cf}$	$\boldsymbol{B}^{(1)}_{DOX,ci,cf}$	$V_{d,DOX}$ [c]	S_p
1,2	0.0562 (80)	0.0831 (17)	3.39 (16)	2.5044 (78)	5.14 (49)	0.0788
1,2	0.0102 (11)	0.00489 (41)	0.989 (19)	0.999 (99)		
1,2	0.00941 (94)	0.00390 (37)	1.99 (15)	1.999 (19)		
2,0	0.459 (27)	0.00112 (40)	1.4828 (93)	1.115 (11)		
2,0	0.00157 (13)	0.0018 (20)	1.0026 (13)	1.001 (24)		
2,0	0.0027 (30)	0.000017 (20)	1.9993 (10)	2.0005 (20)		
2,1	1.0626 (66)	0.124 (13)	1.49 (21)	1.143 (14)		
2,1	0.0005 (15)	0.00423 (43)	1.00 (15)	1.000 (12)		
2,1	0.000489 (70)	0.00065 (15)	1.999 (21)	1.997 (10)		
1,3	0.0011 (25)	0.00128 (19)	1.001 (21)	0.999 (16)		
1,3	0.00035 (10)	0.00026 (30)	2.0022 (62)	1.9984 (35)		
3,1	0.000250 (20)	0.0000015 (14)	2.000 (19)	1.99 (13)		

units of:
[a] $\left[\frac{\mu\text{mol}}{\text{m}^2}\right]^{1-A^{(1)}_{DOX,ci,cf}}\text{min}^{-1}$ [b] $\left[\frac{\mu\text{mol}}{\text{m}^2}\right]^{-B^{(1)}_{DOX,ci,cf}}$ [c] $\left[\text{L}\cdot\text{m}^{-2}\right]$

Figure 3.16 shows the concentration curves of DOX using the parameters from Table 3.24. The plasma concentrations of DOX increases relative to the one and two-compartment models. The curves also show an increased terminal plasma concentration as the drug in compartment two is being redeposited in compartment one.

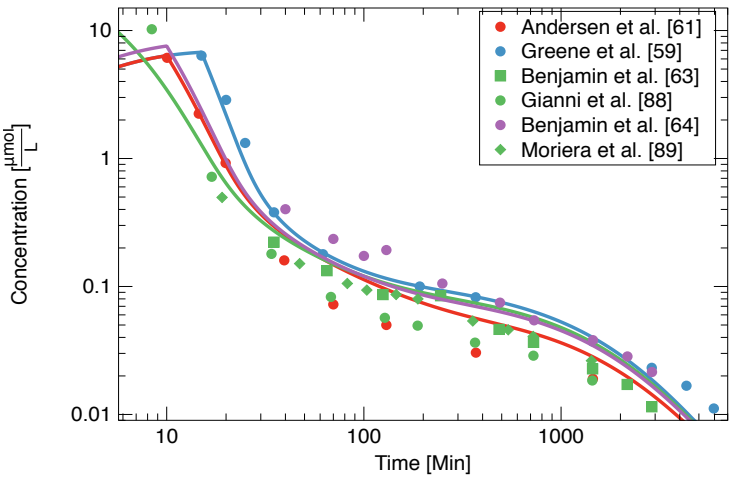

Figure 3.16: Comparison of theoretical and experimental concentrations of DOX using the parameters from Table 3.24. The clinical data and curves are for an infusion of 9.19 $\mu mol \cdot m^{-2} \cdot min^{-1}$ (red and blue), 22.08 $\mu mol \cdot m^{-2} \cdot min^{-1}$ (green) and 11.04 $\mu mol \cdot m^{-2} \cdot min^{-1}$ (purple).

3.4.10 Drug Interaction Effects for the Three-Compartment Model

The model parameters in Table 3.22 were perturbed to obtain the effective rate constants due to the interaction parameters as discussed in Chapter 2. The parameters that produced the best fit to the baseline data set are shown in Table 3.25. According to the parameters, the distribution of DOX from compartment one to compartments two and three may depend on the amount of the drug present in these compartments. The distribution to compartment two and three increases with the amount of the drug in the compartments. The rate of redistribution of DOX in compartment two into compartment one is also slightly increased by the amount of the drug in compartment one. Interestingly, the redistribution of DOX in compartment three to compartment one is limited by the amount of the drug in compartment one, with a slower flow from the compartment to the principal compartment as the amount of drug in the principal compartment increases. This model produced a 3% decrease in the variance from the three-compartment model in Table 3.22.

Figure 3.17 shows the concentration curves of DOX using the parameters from Table 3.25. The curves show good agreement with the clinical data. The high and low concentrations show good agreement with the clinical data.

Table 3.25: Three-compartment model case 3.1 parameters of DOX.

ci,cf	$\boldsymbol{k}^{(1,A)}_{DOX,ci,cf}$ [a]	$\boldsymbol{\Gamma}^{(1,B)}_{DOX,ci,cf}$ [b]	$\boldsymbol{A}^{(1)}_{DOX,ci,cf}$	$\boldsymbol{B}^{(1)}_{DOX,ci,cf}$	$V_{d,DOX}$ [e]
1,2	0.06112 (50)	0.0200 (17)	3.247 (21)	2.6220 (75)	5.1721 (32)
2,0	1.0884 (49)	0.3993 (87)	1.4330 (51)	0.9317 (82)	
2,1	1.1180 (50)	0.0412 (14)	1.6197 (24)	1.6173 (55)	
1,3	0.0002 (12)	0.1150 (63)	3.3335 (48)	2.4620 (18)	
3,1	0.0109 (12)	0.0031 (63)	1.4789 (44)	1.1567 (18)	
ci,cf	$\boldsymbol{\alpha}^{(1,C)}_{DOX,ci,cf\|DOX,cf}$ [c]	$\boldsymbol{\beta}^{(1,D)}_{DOX,ci,cf\|DOX,cf}$ [d]	$\boldsymbol{C}^{(1)}_{DOX,ci,cf\|DOX,cf}$	$\boldsymbol{D}^{(1)}_{DOX,ci,cf\|DOX,cf}$	S_p
1,2	0.0490 (14)	0.0000000 (17)	1.00911 (14)	N/A**	0.0885
1,2	0.0007 (15)	0.0039 (40)	0.0016 (19)	0.00322 (29)	
1,3	0.0005 (13)	0.007923 (50)	0.9987 (52)	1.00282 (10)	
1,3	-0.00174 (10)	0.00145 (44)	0.00142 (28)	0.0016 (34)	
2,1	0.03756 (12)	0.00482 (15)	1.0007 (10)	1.0020 (38)	
2,1	0.00105 (10)	0.0023 (81)	0.0019 (20)	0.00298 (10)	
3,1	-0.02051 (50)	0.00000 (59)	1.0018 (16)	N/A**	
3,1	-0.00064 (10)	0.00010 (50)	0.00042 (25)	0.0004 (12)	

units of:
[a] $\left[\frac{\mu\text{mol}}{\text{m}^2}\right]^{1-A^{(1)}_{DOX,ci,cf}}\text{min}^{-1}$ [b] $\left[\frac{\mu\text{mol}}{\text{m}^2}\right]^{-B^{(1)}_{DOX,ci,cf}}$ [c] $\left[\frac{\mu\text{mol}}{\text{m}^2}\right]^{-C^{(1)}_{DOX,ci,cf|DOX,cf}}$ [d] $\left[\frac{\mu\text{mol}}{\text{m}^2}\right]^{-D^{(1)}_{DOX,ci,cf|DOX,cf}}$ [e] $\left[\text{L}\cdot\text{m}^{-2}\right]$
**The parameter is indeterminate because the rate parameter is zero.

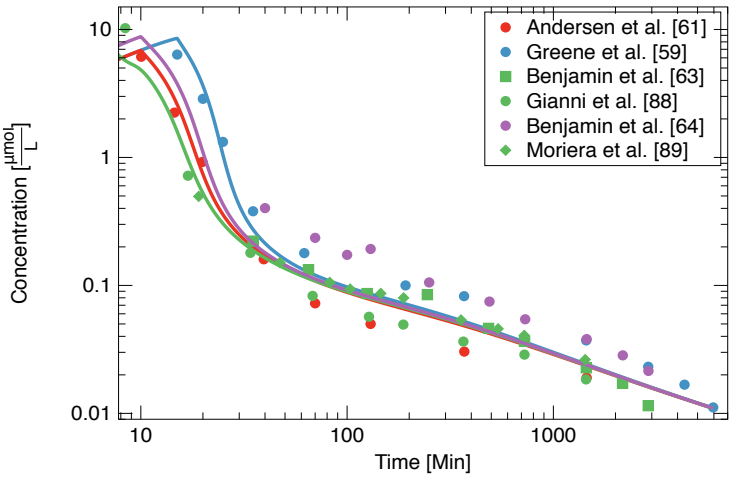

Figure 3.17: Comparison of theoretical and experimental concentrations of DOX using the parameters from Table 3.25. The clinical data and curves are for an infusion of 9.19 $\mu\text{mol}\cdot\text{m}^{-2}\cdot\text{min}^{-1}$ (red and blue), 22.08 $\mu\text{mol}\cdot\text{m}^{-2}\cdot\text{min}^{-1}$ (green) and 11.04 $\mu\text{mol}\cdot\text{m}^{-2}\cdot\text{min}^{-1}$ (purple).

3.4.11 Comparison of the DOX Model Results

The parameters in Table 3.9 to 3.25 describe the variable-order models of DOX. We notice from the plasma concentration curves of DOX that varying the exponents of the pro-

cesses result in a better fit of the model to the clinical data when compared to the model with fixed exponents discussed at the beginning of the chapter. The addition of new terms to the models did not provide any new information about the system although the multi-process models give a reduced variance. Considering that the greatest difference in the variance of the model is 15%, which corresponds to an additional 51 parameters from the simplest model, the choice of the best model to use depends on the specifics of the information needed from the model, and a competition between computational simplicity and accuracy.

3.5 Two-Molecule Models

The second group of models developed describe the two-molecule system. In these models, the infused molecule is in an encapsulated form of DOX, which alters the overall PK by systemically reducing the amount of the free DOX available to distribute to normal body cells and ensuring that the drug is mostly delivered into tumour tissues. This implies that the plasma concentration of the free drug slowly builds up as the drug is released from the carrier before reaching a peak value, C_{max}, hours after administration. The modelling approach used in this section depends on the available concentration data, in cases where plasma concentration data is readily available for free and nanoparticle-encapsulated drug, the PK parameters describing both drugs were obtained. In the instance where only one of the drug plasma concentrations is available, the available drug is modelled as a single-drug system. In all the cases, the total number of parameters allowed to vary is the number of data points available minus one. A simple chemical reaction to depict the process considered here is shown below.

$$\begin{aligned} \text{DOXIL} &\xrightarrow{k^{(2)}_{PLD,i||DOX,i}} \text{DOX} \\ \text{MYOCET} &\xrightarrow{k^{(2)}_{MYO,i||DOX,i}} \text{DOX} \end{aligned} \tag{3.6}$$

In the first reaction, free DOX is released from the PLD [86], and in the second, DOX is released from MYO [101]. An assumption made for this model was that both reactions follow the same pathway so they could be described by the same set of equations without any uniqueness introduced to either molecule. The release of the DOX is assumed to be a non-catalyzed reaction which depends only on the concentration of the encapsulated drug available in the compartment. The subscript i in equation 3.6 represent the activity compartment where the release occurs - in this model assumed to be in compartment two. When modelling only the encapsulated molecule, the parameters of the one-compartment model of DOX were left fixed with the parameters describing the release of DOX from encapsulated DOX and those representing the elimination of encapsulated drug varied. In the models where the free and encapsulated molecules are considered, the parameters that describe the effect of encapsulation on the PK of the free molecule were varied alongside the parameters of the encapsulated molecule.

3.5.1 Two-Molecule, One-Compartment Model of PLD

In the one-compartment model, the PK of PLD and DOX are assumed to occur within the same homogenous compartment. In the first set of tests, the PK parameters of DOX from the one-drug, one-compartment models were kept fixed with the PLD parameters alone varied. In Table 3.26, the parameters that describe the PK of PLD are presented. The parameters suggest that the elimination process is the same order as the release of the free molecule. The high and low concentration PK of PLD is dominated by the release of DOX. At high concentrations of PLD in the body, the release of DOX accounts for over 75% of the PK, which is further enhanced with decreasing concentration. The small elimination term suggests that the release of DOX dominates the low concentration PK of PLD. The high and low concentration PK of PLD is characterized by exponents $A - B \approx 0.42$ and $A \approx 1.40$ respectively.

This model resulted in a poor fit of DOX following the administration of PLD. There-

Table 3.26: One-compartment model case 2 parameters of PLD and DOX.

Type	$\boldsymbol{k}^{(1,p1)}_{\text{Type},2,0}$ [a]	$\boldsymbol{\Gamma}^{(1,p1)}_{\text{Type},2,0}$ [b]	$\boldsymbol{A}^{(1,p1)}_{\text{Type},2,0}$	$\boldsymbol{B}^{(1,p1)}_{\text{Type},2,0}$	$V_{d,Type}$ [e]
DOX	0.0200 (22)*	0.0450 (22)*	3.2429 (62)*	2.477 (18)*	6.02 (22)*
PLD	0.0000042 (19)	0.000064 (10)	1.4045 (22)	0.9881 (25)	2.1439 (57)
$\boldsymbol{k}^{(2,p1)}_{\text{PLD},2\|DOX,2}$ [c]	$\boldsymbol{\Gamma}^{(2,p1)}_{\text{PLD},2\|DOX,2}$ [d]	$\boldsymbol{A}^{(2,p1)}_{\text{PLD},2\|DOX,2}$	$\boldsymbol{B}^{(2,p1)}_{\text{PLD},2\|DOX,2}$		S_p
0.0001 (22)	0.0005 (10)	1.4045 (22)	0.9880 (19)	-	0.2312

units of:
[a] $\left[\frac{\mu\text{mol}}{\text{m}^2}\right]^{1-A^{(1,p1)}_{Type,20}}\text{min}^{-1}$ [b] $\left[\frac{\mu\text{mol}}{\text{m}^2}\right]^{-B^{(1,p1)}_{Type,20}}$ [c] $\left[\frac{\mu\text{mol}}{\text{m}^2}\right]^{1-A^{(2,p1)}_{\text{PLD},2\|DOX,2}}\text{min}^{-1}$ [d] $\left[\frac{\mu\text{mol}}{\text{m}^2}\right]^{-B^{(2,p1)}_{\text{PLD},2\|DOX,2}}$ [e] $\left[\text{L}\cdot\text{m}^{-2}\right]$
* These parameters have are from Table 3.9.

fore, the parameters describing the influence of PLD administration on DOX were varied to test the influence of PLD on the PK of DOX. Table 3.27 shows the parameters of the model when PLD is administered. The parameters in the top row are the rate of elimination of both molecules from the system. In the second row, $\alpha^{(1,p1,p2)}_{\text{DOX},2,0||\text{PLD},2}$ and $\beta^{(1,p1,p2)}_{\text{DOX},2,0||\text{PLD},2}$ describe the effect of PLD on the elimination rate of DOX. This is important since we expect that the administration of PLD will influence the PK of DOX. In the last row, the rate constants of drug release from PLD are presented. We notice the changes to the PLD parameters from Table 3.26. Specifically, the parameters suggest that at high concentrations, the release kinetics account for over 90% of the PLD PK, which represents an increase from Table 3.26. However, at low concentrations the release kinetics account for less than 60% of the PLD PK. This implies that the process of DOX release from PLD slows with decreasing concentration, suggesting that the terminal PK of PLD in the one-compartment model is characterized by increasing elimination of the molecule in its unchanged form. The parameters also suggest that the elimination of DOX from the body is influenced by PLD concentration. At high PLD concentrations, the clearance of DOX is increased, which may be explained by the slow release of DOX relative to the rate of distribution, metabolism and elimination. At low PLD concentrations, the clearance of DOX is the same as Table 3.9, this ensures that the maximum concentration of the free molecule is attained as the concentration of PLD decreases. In this model, the high and low concentration PK of the PLD is characterized by exponent $A \approx 1.40$. DOX's volume of distribution is approximately

three times the distribution volume of PLD. This model resulted in a 62% decrease in the variance from Table 3.26 implying a better fit to the clinical data.

Table 3.27: One-compartment model case 3.1 parameters of PLD and DOX with interactions.

Type	$\boldsymbol{k}^{(1,p1)}_{\text{Type},2,0}$ [a]	$\boldsymbol{\Gamma}^{(1,p1)}_{\text{Type},2,0}$ [b]	$\boldsymbol{A}^{(1,p1)}_{\text{Type},2,0}$	$\boldsymbol{B}^{(1,p1)}_{\text{Type},2,0}$	$V_{d,Type}$ [g]
DOX	0.0200 (10)*	0.0450 (29)*	3.2429 (68)*	2.477 (19)*	6.017 (75)*
PLD	0.000035 (25)	0.0503 (38)	1.409 (55)	0.0040 (17)	2.1444 (18)
$\boldsymbol{\alpha}^{(1,p1,p2)}_{\text{DOX},2,0\|\|\text{PLD},2}$ [c]	$\boldsymbol{\beta}^{(1,p1,p2)}_{\text{DOX},2,0\|\|\text{PLD},2}$ [d]	$\boldsymbol{C}^{(1,p1,p2)}_{\text{DOX},2,0\|\|\text{PLD},2}$	$\boldsymbol{D}^{(1,p1,p2)}_{\text{DOX},2,0\|\|\text{PLD},2}$		S_p
-0.0096 (21)	0.0069 (14)	2.000 (43)	2.007 (25)	-	0.0875
0.0069 (78)	0.000029 (18)	1.0006 (15)	0.99 (13)	-	
$\boldsymbol{k}^{(2,p1)}_{\text{PLD},2\|DOX,2}$ [e]	$\boldsymbol{\Gamma}^{(2,p1)}_{\text{PLD},2\|DOX,2}$ [f]	$\boldsymbol{A}^{(2,p1)}_{\text{PLD},2\|DOX,2}$	$\boldsymbol{B}^{(2,p1)}_{\text{PLD},2\|DOX,2}$		
0.000047 (74)	0.0045 (14)	1.409 (55)	0.00 (21)		

units of:
[a] $\left[\frac{\mu\text{mol}}{\text{m}^2}\right]^{1-A^{(1,p1)}_{Type,20}}\text{min}^{-1}$ [b] $\left[\frac{\mu\text{mol}}{\text{m}^2}\right]^{-B^{(1,p1)}_{Type,20}}$ [c] $\left[\frac{\mu\text{mol}}{\text{m}^2}\right]^{1-C^{(1,p1,p2)}_{\text{DOX},2,0\|\|\text{PLD},2}}$
[d] $\left[\frac{\mu\text{mol}}{\text{m}^2}\right]^{-D^{(1,p1,p2)}_{\text{DOX},2,0\|\|\text{PLD},2}}$ [e] $\left[\frac{\mu\text{mol}}{\text{m}^2}\right]^{1-A^{(2,p1)}_{\text{PLD},2\|DOX,2}}\text{min}^{-1}$ [f] $\left[\frac{\mu\text{mol}}{\text{m}^2}\right]^{-B^{(2,p1)}_{\text{PLD},2\|DOX,2}}$ [g] $\left[\text{L}\cdot\text{m}^{-2}\right]$
*These parameters are from Table 3.9.

Figure 3.18 shows the simulated concentration curves of PLD and DOX. The plot shows that the concentration of DOX increases with decreasing PLD in the body. This ensures that DOX reaches $C_{\max}$ twenty to fifty hours after PLD infusion. The curves of DOX post $C_{\max}$ is similar to the one-molecule model.

3.5.2 Two-Molecule, One-Compartment Model of MYO

Like the PLD model, we initially considered only the PK of the MYO. Here, the only consideration of the DOX in the model is the release rate of the MYO. The model assumed that the MYO and DOX do not interact, therefore the interaction parameters were excluded. Table 3.28 shows the parameters that describe the PK of MYO. According to these parameters, the rate of conversion of MYO is the only process that describes the PK of the molecule after administration. This conversion to DOX is described by an exponent $A \approx 1.31$. The volume of distribution of MYO is similar to the DOX suggesting that both molecules are distributed similarly within the body.

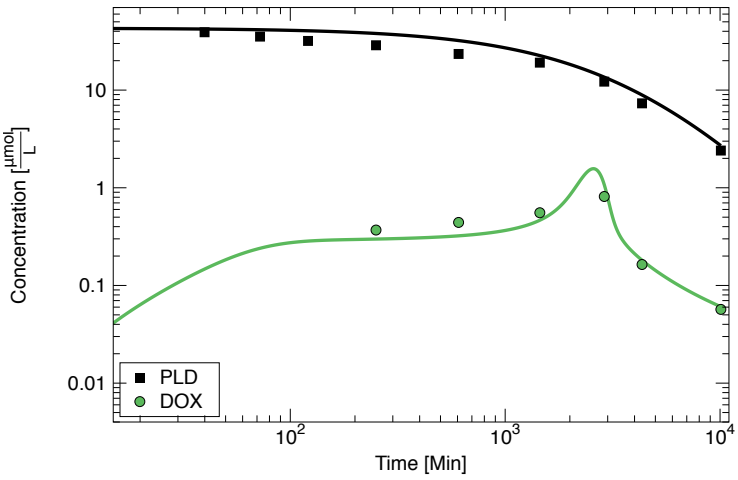

Figure 3.18: Comparison of theoretical and experimental concentrations of PLD and DOX using the parameters from Table 3.27. The curves represent infusions of 50 $\mathrm{mg} \cdot \mathrm{m}^{-2}$ PLD. The clinical data points are from Gabizon *et al.* [86].

Table 3.28: One-compartment model case 2 parameters of MYO.

Type	$\boldsymbol{k}^{(1,p1)}_{\mathrm{Type},2,0}$ [a]	$\boldsymbol{\Gamma}^{(1,p1)}_{\mathrm{Type},2,0}$ [b]	$\boldsymbol{A}^{(1,p1)}_{\mathrm{Type},2,0}$	$\boldsymbol{B}^{(1,p1)}_{\mathrm{Type},2,0}$	$V_{d,Type}$ [e]
DOX	0.0200 (57)*	0.0450 (29)*	3.2429 (68)*	2.477 (19)*	6.017 (75)*
MYO	0.00000 (10)	N/A**	N/A**	N/A**	5.6131 (56)
$\boldsymbol{k}^{(2,p1)}_{\mathrm{MYO},2\|DOX,2}$ [c]	$\boldsymbol{\Gamma}^{(2,p1)}_{\mathrm{MYO},2\|DOX,2}$ [d]	$\boldsymbol{A}^{(2,p1)}_{\mathrm{MYO},2\|DOX,2}$	$\boldsymbol{B}^{(2,p1)}_{\mathrm{MYO},2\|DOX,2}$		S_p
0.0030 (13)	0.0000 (22)	1.3075 (11)	N/A**		0.3063

units of:
[a] $\left[\frac{\mu\mathrm{mol}}{\mathrm{m}^2}\right]^{1-A^{(1,p1)}_{\mathrm{Type},2,0}} \mathrm{min}^{-1}$ [b] $\left[\frac{\mu\mathrm{mol}}{\mathrm{m}^2}\right]^{-B^{(1,p1)}_{\mathrm{Type},2,0}}$ [c] $\left[\frac{\mu\mathrm{mol}}{\mathrm{m}^2}\right]^{1-A^{(2,p1)}_{\mathrm{MYO},2\|DOX,2}} \mathrm{min}^{-1}$ [d] $\left[\frac{\mu\mathrm{mol}}{\mathrm{m}^2}\right]^{-B^{(2,p1)}_{\mathrm{MYO},2\|DOX,2}}$ [e] $\left[\mathrm{L} \cdot \mathrm{m}^{-2}\right]$
*These parameters are from Table 3.9.
**The parameter is indeterminate because the rate constant is zero.

The next model considered the interaction of the molecules within the body. Specifically, we expect that the infusion of MYO should influence the PK of DOX. The parameters that model the PK of MYO and DOX with drug interaction are shown in Table 3.29. According to the parameters, the elimination and release kinetics of MYO can be described by approximately first-order processes ($A = 1.27$). The release kinetics of the molecule accounts for over 90% of the PK in the body. The second row parameters describe the effect of MYO on the clearance of DOX. At high concentrations of MYO, the elimination of DOX is similar to the one-molecule, one-compartment model in Table 3.9. Interestingly, the interaction of the molecule shows a rate-limited behavior. The maximum rate of DOX clearance

occurs when the concentration of MYO is $\approx 4\ \mu\text{mol}\cdot\text{l}^{-1}$. At low MYO concentration, the rate of DOX clearance is up to six times the rate when the DOX is administered. The distribution volume of MYO is increased relative to DOX, which may suggest an identical affinity of both molecules to the cells in the compartment. There is a noticeable decrease in the variance from Table 3.28.

Table 3.29: One-compartment model case 3.1 parameters of MYO and DOX with interaction.

Type	$\boldsymbol{k}^{(1,p1)}_{\text{Type},2,0}$ [a]	$\boldsymbol{\Gamma}^{(1,p1)}_{\text{Type},2,0}$ [b]	$\boldsymbol{A}^{(1,p1)}_{\text{Type},2,0}$	$\boldsymbol{B}^{(1,p1)}_{\text{Type},2,0}$	$V_{d,Ype}$ [c]
DOX	0.0200 (10)*	0.0450 (29)*	3.2429 (68)*	2.477 (19)*	6.017 (75)*
MYO	0.00014 (57)	0.00 (29)	1.2681 (79)	N/A**	7.2969 (56)
Process	$\boldsymbol{\alpha}^{(1,p1,p2)}_{DOX,2,0\|\|MYO,2}$ [d]	$\boldsymbol{\beta}^{(1,p1,p2)}_{DOX,2,0\|\|MYO,2}$ [e]	$\boldsymbol{C}^{(1,p1,p2)}_{DOX,2,0\|\|MYO,2}$	$\boldsymbol{D}^{(1,p1,p2)}_{DOX,2,0\|\|MYO,2}$	S_p
$p2=1$	5.3038 (45)	0.0004 (21)	0.105 (26)	3.24 (51)	0.1524
process	$\boldsymbol{k}^{(2,p1)}_{\text{MYO},2\|DOX,2}$ [f]	$\boldsymbol{\Gamma}^{(2,p1)}_{\text{MYO},2\|DOX,2}$ [g]	$\boldsymbol{A}^{(2,p1)}_{\text{MYO},2\|DOX,2}$	$\boldsymbol{B}^{(2,p1)}_{\text{MYO},2\|DOX,2}$	
$p1=1$	0.0026 (13)	0.00 (46)	1.2681 (11)	N/A**	-

units of:
[a] $\left[\frac{\mu\text{mol}}{\text{m}^2}\right]^{1-A^{(1,p1)}_{\text{Type},2,0}}\text{min}^{-1}$ [b] $\left[\frac{\mu\text{mol}}{\text{m}^2}\right]^{-B^{(1,p1)}_{\text{Type},2,0}}$ [c] $\left[\text{L}\cdot\text{m}^{-2}\right]$ [d] $\left[\frac{\mu\text{mol}}{\text{m}^2}\right]^{-C^{(1,p1,p2)}_{\text{DOX},2,0\|\text{MYO},2}}$ [e] $\left[\frac{\mu\text{mol}}{\text{m}^2}\right]^{-D^{(1,p1,p2)}_{\text{DOX},2,0\|\text{MYO},2}}$ [f] $\left[\frac{\mu\text{mol}}{\text{m}^2}\right]^{1-A^{(2,p1)}_{\text{MYO},2\|DOX,2}}\text{min}^{-1}$
[g] $\left[\frac{\mu\text{mol}}{\text{m}^2}\right]^{-B^{(2,p1)}_{\text{MYO},2\|DOX,2}}$
*These parameters are from Table 3.9.
**The parameter is indeterminate because the rate parameter is zero.

A simulation of the model parameters is shown in figure 3.19. The concentrations are in the clinically observed range [101]. The curves show that due to the increased rate of release of DOX from MYO, DOX attains a maximum plasma concentration quicker than when PLD is administered. However, as the concentration of MYO decreases, there is a concurrent drop in DOX plasma concentration due to increased clearance.

3.5.3 Comparison of the PLD and MYO Model Results

In the two-molecule models, we considered two modeling approaches to describe the PK of the encapsulated and free molecules. The first modeling approach assumes that no interaction exists between both molecules in the body, which implies that the PK of either molecule is independent of the other. The implication of this is that the PK of DOX is unchanged from the single molecule models, and the elimination and conversion parameters

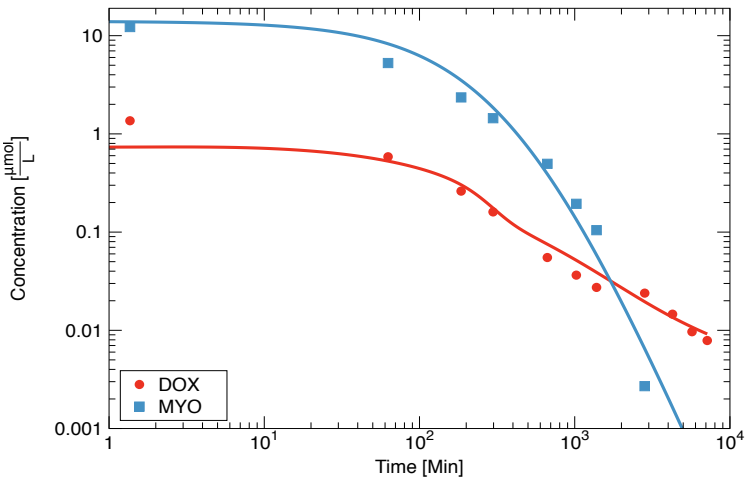

Figure 3.19: Comparison of theoretical and experimental concentrations of MYO using parameters from Table 3.29. The square and circles are the plasma concentrations of MYO and DOX after the infusion of 75 $mg \cdot m^{-2}$ of MYO over 1 h. The data points are from Mross *et al.* [101].

of the encapsulated molecule are of importance. The second modeling approach assumes an interdependence of the PK of both molecules. This implies that the elimination and conversion parameters of the encapsulated molecule, and the terms that describe the interdependence of both molecules are important.

When observing variance and the fit of the theory curves to the clinical data, we notice that for both encapsulated forms of DOX considered, the model with drug interaction produced a smaller variance and a better fit to the data. The PLD variance improved by 60% and the MYO variance improved by 50%. Comparing the parameters of both molecules, we observed interesting behaviors; for PLD, the slower rate of release of free DOX results in a slower terminal clearance of the drug from the body, which ensures a longer exposure of both molecules to the cells. This behavior is reversed in the MYO model, where the clearance of DOX increases with decreasing MYO and a rate-limiting interaction was observed. This behavior for MYO administration may suggest the presence of a maximum concentration of MYO above which the clearance of DOX is reduced. A comparison of the volumes of distributions of the encapsulated molecules show that the volume of distribution of MYO is noticeably larger than that of PLD. This may be due to the biochemical com-

position of both molecules and may be important in explaining the difference in the PK of both molecules.

3.6 Four-Molecule Models

3.6.1 Four-Molecule, One-Compartment Model

In this model, the parameters that describe the PK of DOX were extended to the four-molecule case. The model considered the PK of DOX and DOL following the infusion of DOX. DOX is allowed to bind with metabolizing enzyme and form a complex which breaks down into the enzyme and metabolite. Two approaches were used, in the first, the parameters of the one-compartment DOX model were left fixed with DOL parameters allowed to vary. The parameters of both molecules were also allowed to vary to observe changes to DOX PK due to the presence of DOL and to observe the possibility of a better overall fit to data. The parameters that describe the binding of the enzyme to DOX and complex dissociation from which DOL is formed were also varied. The amount of DOX available to bind with $CBR1$ was fixed at 55% of the total DOX in compartment two, which corresponds to clinical measurement of the amount of DOX not eliminated [64]. Table 3.30 shows the best fit parameters for this model. In the first row, the parameters that describe the elimination of the molecules from the compartment are presented. The parameters in the second row describe the complex dissociation process, and the parameters in the last row describe the rate of binding of the parent drug to the enzyme. According to the parameters, the elimination of DOX and DOL from the body is concentration-dependent and characterized by exponents $A-B \approx 0.77$ and $A-B \approx 1.13$ at high concentrations respectively. At low concentrations, the elimination of both molecules have exponents $A \approx 3.24$ and $A \approx 2.66$. The binding of DOX with CBR1 appears to be nonlinearly dependent on the amount of DOX available and does not change with the amount of enzyme available at the binding site. The rate of complex dissociation is less than the rate of formation, which may be explained by the model assumption that the complex formation reaction is irreversible. The complex dissociation

rate is also concentration dependent and can be described by exponents $A - B \approx 1.27$ at high concentrations, and $A \approx 2.73$ at low concentrations. Analyzing the parameters, we notice that for DOL, the kinetics transitions to a high concentration phase when the amount of the molecule in the compartment is 305.76 $\mu mol \cdot m^{-2}$, likewise the complex molecule transitions to the high-concentration kinetics when the amount of the molecule exceeds 1 $\mu mol \cdot m^{-2}$. The volume of distribution of the metabolite is over twice the parent drug, which may suggest the presence of a greater amount of the metabolite molecule relative to the parent molecule.

Table 3.30: One-compartment model case 2 parameters of DOX and DOL with fixed DOX parameters.

Type	$\boldsymbol{k}^{(1,p1)}_{Type,2,0}$ [a]	$\boldsymbol{\Gamma}^{(1,p1)}_{Type,2,0}$ [b]	$\boldsymbol{A}^{(1,p1)}_{Type,2,0}$	$\boldsymbol{B}^{(1,p1)}_{Type,2,0}$	$V_{d,Type}$ [g]
DOX	0.00902 (81)*	0.0450 (12)*	3.243 (17)*	2.477 (22)*	6.017 (93)*
DOL	0.256 (18)	0.0236 (43)	2.661 (51)	1.5275 (20)	14.269 (20)
Type	$\boldsymbol{k}^{(3,p1)}_{Type,2\|\|d3,2,d2,2}$ [c]	$\boldsymbol{\Gamma}^{(3,p1)}_{Type,2\|\|d3,2,d2,2}$ [d]	$\boldsymbol{A}^{(3,p1)}_{Type,2\|\|d3,2,d2,2}$	$\boldsymbol{B}^{(3,p1)}_{Type,2\|\|d3,2,d2,2}$	S_p
DOXCBR1	0.00058 (72)	0.992 (18)	2.731 (42)	1.468 (22)	0.1263
$k^{(4)}_{DOX,2,CBR1,2\|d4,2}$ [e]	$\Gamma^{(4)}_{DOX,2,CBR1,2\|d4,2}$ [f]	$\boldsymbol{A}^{(4,DOX)}_{DOX,2,CBR1,2\|d4,2}$	$\boldsymbol{B}^{(4,DOX)}_{DOX,2,CBR1,2\|d4,2}$	$\boldsymbol{A}^{(5,CBR1)}_{DOX,2,CBR1,2\|d4,2}$	$\boldsymbol{B}^{(5,CBR1)}_{DOX,2,CBR1,2\|d4,2}$
0.01103 (65)	0.0450 (40)	3.2429 (19)	2.477 (47)	0.0028 (42)	0.0022 (11)

units of:

[a] $\left[\frac{\mu mol}{m^2}\right]^{1-A^{(1,p1)}_{Type,2,0}} min^{-1}$ [b] $\left[\frac{\mu mol}{m^2}\right]^{-B^{(1,p1)}_{Type,2,0}}$ [c] $\left[\frac{\mu mol}{m^2}\right]^{1-A^{(3,p1)}_{Type,2\|d3,2,d2,2}} min^{-1}$ [d] $\left[\frac{\mu mol}{m^2}\right]^{-B^{(3,p1)}_{Type,2\|d3,2,d2,2}}$

[e] $\left[\frac{\mu mol}{m^2}\right]^{1-(A^{(4,DOX)}_{DOX,2,CBR1,2\|d4,2}+A^{(5,CBR1)}_{DOX,2,CBR1,2\|d4,2})} min^{-1}$ [f] $\left[\frac{\mu mol}{m^2}\right]^{-(B^{(4,DOX)}_{DOX,2,CBR1,2\|d4,2}+B^{(5,CBR1)}_{DOX,2,CBR1,2\|d4,2})}$ [g] $\left[L \cdot m^{-2}\right]$

where:

$d2 = DOL$ $d3 = CBR1$ $d4 = DOXCBR1$

*These parameters are from Table 3.11

Figure 3.20 shows the concentration curves of DOX and DOL after the administration of DOX. The figure shows a gradual increase in the concentration of DOL, which is maximum at twenty to forty minutes after DOX infusion. The curve of DOL mirrors DOX's as the concentration of the parent molecule decreases. The model parameters slightly overestimates the amount of DOL present in the body.

The result of varying the complete set of parameters is shown in Table 3.31, and allows to observe the changes to the DOX parameters due to the presence of DOL. We notice that the elimination process of DOX retained the high and low-concentration exponents from Table 3.30, however, the elimination of DOX from the body decreases by 40% at

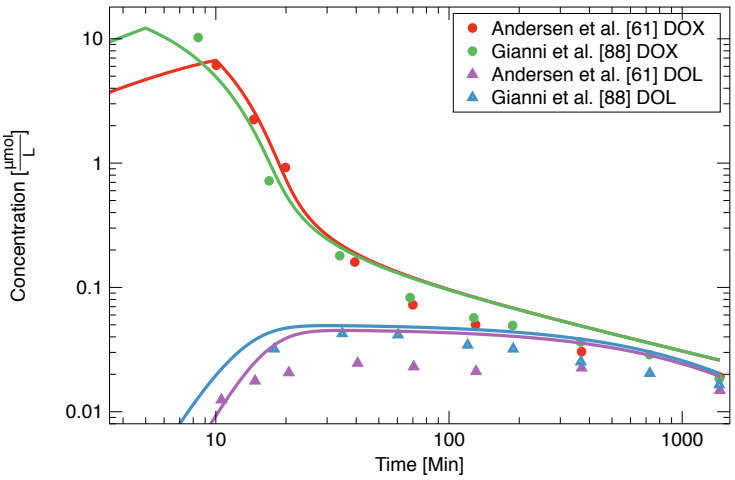

Figure 3.20: Comparison of theoretical and experimental concentrations of DOX and DOL using the parameters from Table 3.30. The curves represent the infusion data from Andersen *et al.* [61](red and purple) and Gianni *et al.* [88](green and blue).

high concentrations and approximately 24% at low concentrations. There was a noticeable change in the DOL PK from Table 3.30. The elimination process of DOL may be described by exponent $A \approx 2.66$ over the range of concentrations. There was no notable change to the binding of DOX to the CBR1, however, the enzyme dissociation rate constant is reduced by 22%, suggesting a slower formation of DOL at high and low complex concentrations when using this model. The reduced volume of distribution of the metabolite results from the slower dissociation of the complex molecule.

Table 3.31: One-compartment model case 2 parameters of DOX and DOL with variable DOX parameters.

Type	$\boldsymbol{k}^{(1,p1)}_{Type,2,0}$ [a]	$\boldsymbol{\Gamma}^{(1,p1)}_{Type,2,0}$ [b]	$\boldsymbol{A}^{(1,p1)}_{Type,2,0}$	$\boldsymbol{B}^{(1,p1)}_{Type,2,0}$	$V_{d,Type}$ [g]
DOX	0.0068 (14)	0.058 (40)	3.235 (21)	2.4887 (40)	6.0207 (40)
DOL	0.319 (25)	0.00 (28)	2.659 (13)	N/A**	10.83 (58)
Type	$\boldsymbol{k}^{(3,p1)}_{Type,2\|\|d3,2,d2,2}$ [c]	$\boldsymbol{\Gamma}^{(3,p1)}_{Type,2\|\|d3,2,d2,2}$ [d]	$\boldsymbol{A}^{(3,p1)}_{Type,2\|\|d3,2,d2,2}$	$\boldsymbol{B}^{(3,p1)}_{Type,2\|\|d3,2,d2,2}$	S_p
DOXCBR1	0.000478 (71)	0.9908 (12)	2.718 (22)	1.5024 (16)	0.1233
$\boldsymbol{k}^{(4)}_{DOX,2,CBR1,2\|d4,2}$ [e]	$\boldsymbol{\Gamma}^{(4)}_{DOX,2,CBR1,2\|d4,2}$ [f]	$\boldsymbol{A}^{(4,DOX)}_{DOX,2,CBR1,2\|d4,2}$	$\boldsymbol{B}^{(4,DOX)}_{DOX,2,CBR1,2\|d4,2}$	$\boldsymbol{A}^{(5,CBR1)}_{DOX,2,CBR1,2\|d4,2}$	$\boldsymbol{B}^{(5,CBR1)}_{DOX,2,CBR1,2\|d4,2}$
0.01065 (39)	0.0417 (21)	3.2632 (40)	2.449 (35)	0.059 (44)	0.0207 (19)

units of:

[a] $\left[\frac{\mu mol}{m^2}\right]^{1-A^{(1,p1)}_{Type,2,0}} min^{-1}$ [b] $\left[\frac{\mu mol}{m^2}\right]^{-B^{(1,p1)}_{Type,2,0}}$ [c] $\left[\frac{\mu mol}{m^2}\right]^{1-A^{(3,p1)}_{Type,2\|\|d3,2,d2,2}} min^{-1}$ [d] $\left[\frac{\mu mol}{m^2}\right]^{-B^{(3,p1)}_{Type,2\|\|d3,2,d2,2}}$

[e] $\left[\frac{\mu mol}{m^2}\right]^{1-(A^{(4,DOX)}_{DOX,2,CBR1,2\|d4,2}+A^{(5,CBR1)}_{DOX,2,CBR1,2\|d4,2})} min^{-1}$ [f] $\left[\frac{\mu mol}{m^2}\right]^{-(B^{(4,DOX)}_{DOX,2,CBR1,2\|d4,2}+B^{(5,CBR1)}_{DOX,2,CBR1,2\|d4,2})}$ [g] $\left[L \cdot m^{-2}\right]$

where:

$d2 = DOL$ $d3 = CBR1$ $d4 = DOXCBR1$

Tables 3.32 and 3.33 show the transition concentrations and times calculated using the parameters in Tables 3.30 and 3.31. Analyzing the DOL values, it can be observed that we can ignore the saturation kinetics coefficient in the compartment, as the molecule kinetic occurs in the low-concentration phase throughout.

Table 3.32: Calculated transition values of DOX and DOL using the one-compartment case 2 model parameters.

Inf[a](Dose)[b]	Type	$A-B$	$X_{Type,2}^{T,0}$ [c]	$C_{Type,2}^{T,0}$ [d]	$T^{(1)}$ [e]	$T^{(2)}$ [e]
9.19 (50)	DOX	0.7659	3.4972	0.5812	0.39	21.36
	DOL	1.1135	11.6197	0.8143	N/A	N/A
9.19 (75)	DOX	0.7659	3.4972	0.5812	0.38	27.11
	DOL	1.1135	11.6197	0.8143	N/A	N/A
11.04 (60)	DOX	0.7659	3.4972	0.5812	0.32	22.53
	DOL	1.1135	11.6197	0.8143	N/A	N/A
22.08 (60)	DOX	0.7659	3.4972	0.5812	0.16	19.79
	DOL	1.1135	11.6197	0.8143	N/A	N/A

[a] $\left[\mu\text{mol}\cdot\text{m}^{-2}\cdot\text{min}^{-1}\right]$ [b] $\left[\text{mg}\cdot\text{m}^{-2}\right]$ [c] $\left[\mu\text{mol}\cdot\text{m}^{-2}\right]$ [d] $\left[\mu\text{mol}\cdot\text{l}^{-1}\right]$ [e] $\left[\text{min}\right]$
N/A: Not applicable because the coefficient is zero.

Table 3.33: Calculated transition values of DOX and DOL using the one-compartment case 2 model parameters.

Inf[a](Dose)[b]	Type	$A-B$	$X_{Type,2}^{T,0}$ [c]	$C_{Type,2}^{T,0}$ [d]	$T^{(1)}$ [e]	$T^{(2)}$ [e]
9.19 (50)	DOX	0.7463	3.1396	0.5215	0.35	21.87
	DOL	N/A	N/A	N/A	N/A	N/A
9.19 (75)	DOX	0.7463	3.1396	0.5215	0.35	28.58
	DOL	N/A	N/A	N/A	N/A	N/A
11.04 (60)	DOX	0.7463	3.1396	0.5215	0.28	23.11
	DOL	N/A	N/A	N/A	N/A	N/A
22.08 (60)	DOX	0.7463	3.1396	0.5215	0.14	20.25
	DOL	N/A	N/A	N/A	N/A	N/A

[a] $\left[\mu\text{mol}\cdot\text{m}^{-2}\cdot\text{min}^{-1}\right]$ [b] $\left[\text{mg}\cdot\text{m}^{-2}\right]$ [c] $\left[\mu\text{mol}\cdot\text{m}^{-2}\right]$ [d] $\left[\mu\text{mol}\cdot\text{l}^{-1}\right]$ [e] $\left[\text{min}\right]$
N/A: Not applicable because the coefficient is zero.

Figure 3.21 shows the concentration curves of DOX and DOL after the administration of DOX. The figure shows a gradual increase in the curves of DOL, which is maximum between eighteen and forty minutes after DOX infusion due to the increased contribution of binding terms. There is no noticeable change in the high and low concentration fits of

both drugs, however, there is a slight shift of the DOX curves downwards midway through the plots.

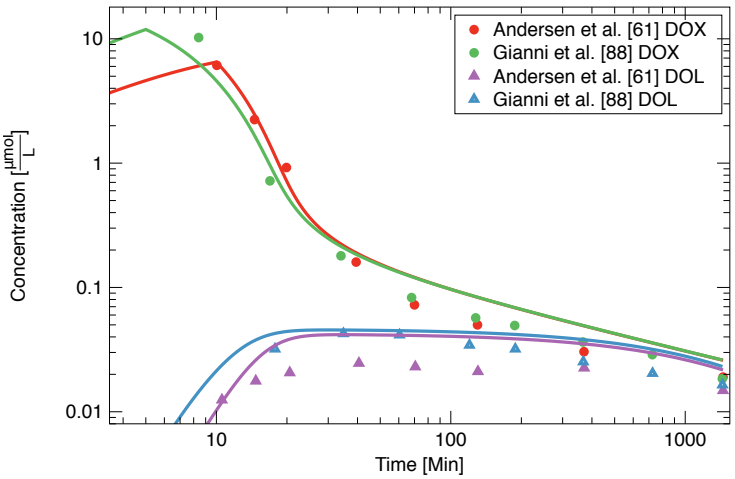

Figure 3.21: Comparison of theoretical and experimental concentrations of DOX and DOL using the parameters from Table 3.31. The curves represent the infusion data from Andersen *et al.* [61](red and purple) and Gianni *et al.* [88](green and blue).

3.6.2 Multi-Process Model for DOX and DOL

Our model allowed us to test the influence of multiple processes on the PK of the molecules. In this case, the parameters from the one-molecule, one-compartment model case 2.1 from Table 3.11 are kept fixed and the DOL parameters varied. The parameters that describe this model are shown in Table 3.34. According to the parameters, the high concentration elimination PK of DOL is described by a dominant process, which has exponent $A - B \approx 1.14$, and a secondary process which is approximately zeroth-order. At low concentrations, the secondary process dominates, and is approximately first-order. Likewise, the dissociation of the complex molecule to form DOL has a first-order contribution that dominates at low concentrations. This implies that the breakdown of the complex to DOL is quicker at low concentrations compared to the single process model in Table 3.30. For DOL, the elimination kinetics in the compartment occurs in a low concentration phase when the amount of the molecule is less than 14.67 $\mu\text{mol} \cdot \text{m}^{-2}$; In the secondary process, the high-concentration phase begins when the amount of the molecule is 102.20 $\mu\text{mol} \cdot \text{m}^{-2}$.

The first-order term increases the rate of elimination at low concentrations and the time to reach $C_{\max}$, resulting in a reduced volume of distribution compared to Table 3.30.

Table 3.34: One-compartment model case 2.1 parameters of DOX and DOL with fixed DOX parameters.

Type	$\boldsymbol{k}^{(1,p1)}_{Type,2,0}$ [a]	$\boldsymbol{\Gamma}^{(1,p1)}_{Type,2,0}$ [b]	$\boldsymbol{A}^{(1,p1)}_{Type,2,0}$	$\boldsymbol{B}^{(1,p1)}_{Type,2,0}$	$V_{d,Type}$ [g]
DOX	0.0090 (33)*	0.0470 (33)*	3.255 (23)*	2.475 (37)*	6.00 (23)*
DOX	0.0000105 (21)*	0.046 (13)*	0.798 (27)*	0.9859 (34)*	
DOL	0.061 (36)	0.0159 (14)	2.6846 (42)	1.542 (23)	12.01 (85)
DOL	0.0725 (99)	0.01 (34)	0.9952 (14)	0.9953 (10)	
Type	$\boldsymbol{k}^{(3,p1)}_{Type,2\|\|d3,2,d2,2}$ [c]	$\boldsymbol{\Gamma}^{(3,p1)}_{Type,2\|\|d3,2,d2,2}$ [d]	$\boldsymbol{A}^{(3,p1)}_{Type,2\|\|d3,2,d2,2}$	$\boldsymbol{B}^{(3,p1)}_{Type,2\|\|d3,2,d2,2}$	S_p
DOXCBR1	0.0002 (33)	0.99 (19)	2.743 (43)	1.469 (43)	0.1078
DOXCBR1	0.0051 (33)	0.183 (90)	0.923 (83)	1.08 (12)	
$\boldsymbol{k}^{(4)}_{DOX,2,CBR1,2\|d4,2}$ [e]	$\boldsymbol{\Gamma}^{(4)}_{DOX,2,CBR1,2\|d4,2}$ [f]	$\boldsymbol{A}^{(4,DOX)}_{DOX,2,CBR1,2\|d4,2}$	$\boldsymbol{B}^{(4,DOX)}_{DOX,2,CBR1,2\|d4,2}$	$\boldsymbol{A}^{(5,CBR1)}_{DOX,2,CBR1,2\|d4,2}$	$\boldsymbol{B}^{(5,CBR1)}_{DOX,2,CBR1,2\|d4,2}$
0.0110 (33)	0.0470 (33)	3.255 (30)	2.476 (23)	0.005 (16)	0.003 (16)
0.0000128 (11)	0.0461 (21)	0.798 (49)	0.985 (34)	0.16 (44)	0.1102 (33)

units of:

[a] $\left[\frac{\mu\text{mol}}{\text{m}^2}\right]^{1-A^{(1,p1)}_{Type,2,0}}\text{min}^{-1}$ [b] $\left[\frac{\mu\text{mol}}{\text{m}^2}\right]^{-B^{(1,p1)}_{Type,2,0}}$ [c] $\left[\frac{\mu\text{mol}}{\text{m}^2}\right]^{1-A^{(3,p1)}_{Type,2\|\|d3,2,d2,2}}\text{min}^{-1}$ [d] $\left[\frac{\mu\text{mol}}{\text{m}^2}\right]^{-B^{(3,p1)}_{Type,2\|\|d3,2,d2,2}}$

[e] $\left[\frac{\mu\text{mol}}{\text{m}^2}\right]^{1-(A^{(4,DOX)}_{DOX,2,CBR1,2\|d4,2}+A^{(5,CBR1)}_{DOX,2,CBR1,2\|d4,2})}\text{min}^{-1}$ [f] $\left[\frac{\mu\text{mol}}{\text{m}^2}\right]^{-(B^{(4,DOX)}_{DOX,2,CBR1,2\|d4,2}+B^{(5,CBR1)}_{DOX,2,CBR1,2\|d4,2})}$ [g] $\left[\text{L}\cdot\text{m}^{-2}\right]$

where:

$d2 = DOL$ $d3 = CBR1$ $d4 = DOXCBR1$

*These parameters are from Table 3.11

Figure 3.22 shows the simulated concentrations of DOX and DOL using the parameters from Table 3.34. The $C_{\max}$ of DOL occurs thirty to fifty minutes after the administration of DOX. The curves show a good agreement with the clinical data points at low DOL concentrations, but a poor fit at the mid-range concentrations.

When relaxing all of the parameters in Table 3.34 to observe changes to the parameters and the possibility of a better overall fit, the model parameters change slightly compared to the initial model. In Table 3.35, the parameters of the model are presented. There were no noticeable changes to the DOL parameters. The parameters show that a single-process was sufficient to describe the PK of DOX when accounting for DOL PK. This model is characterized by a 45% decrease in DOX elimination rate parameter compared to the dominant process in Table 3.34. Conversely, the rate parameter of enzymatic binding increased by 30% from Table 3.30 suggesting an increased metabolism of the parent drug. There is no noticeable change to the other parameters from Table 3.34.

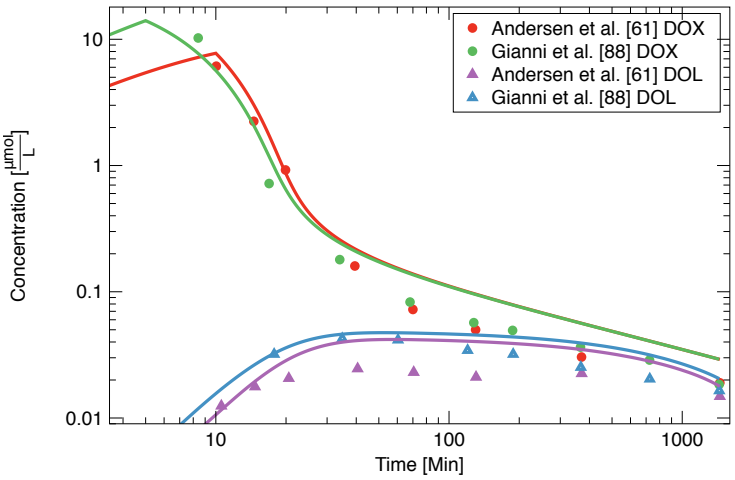

Figure 3.22: Comparison of theoretical and experimental concentrations of DOX and DOL using the parameters from Table 3.34. The curves represent the infusion data from Andersen *et al.* [61](red and purple) and Gianni *et al.* [88](green and blue).

Table 3.35: One-compartment model case 2.1 parameters of DOX and DOL with varied DOX parameters.

Type	$\boldsymbol{k}^{(1,p1)}_{Type,2,0}$ [a]	$\boldsymbol{\Gamma}^{(1,p1)}_{Type,2,0}$ [b]	$\boldsymbol{A}^{(1,p1)}_{Type,2,0}$	$\boldsymbol{B}^{(1,p1)}_{Type,2,0}$	$V_{d,Type}$ [g]
DOX	0.0050 (63)	0.0476 (63)	3.253 (19)	2.477 (44)	6.00 (31)
DOX	0.000000 (10)	N/A**	N/A**	N/A**	
DOL	0.061 (43)	0.0164 (42)	2.6842 (19)	1.5432 (20)	12.0124 (43)
DOL	0.079 (19)	0.01 (24)	0.99 (11)	0.9967 (56)	
Type	$\boldsymbol{k}^{(3,p1)}_{Type,2\|\|d3,2,d2,2}$ [c]	$\boldsymbol{\Gamma}^{(3,p1)}_{Type,2\|\|d3,2,d2,2}$ [d]	$\boldsymbol{A}^{(3,p1)}_{Type,2\|\|d3,2,d2,2}$	$\boldsymbol{B}^{(3,p1)}_{Type,2\|\|d3,2,d2,2}$	S_p
DOXCBR1	0.0002 (64)	0.9 (11)	2.74 (34)	1.468 (31)	0.1078
DOXCBR1	0.0034 (63)	0.18 (14)	0.92 (11)	1.08 (17)	
$\boldsymbol{k}^{(4)}_{DOX,2,CBR1,2\|d4,2}$ [e]	$\boldsymbol{\Gamma}^{(4)}_{DOX,2,CBR1,2\|d4,2}$ [f]	$\boldsymbol{A}^{(4,DOX)}_{DOX,2,CBR1,2\|d4,2}$	$\boldsymbol{B}^{(4,DOX)}_{DOX,2,CBR1,2\|d4,2}$	$\boldsymbol{A}^{(5,CBR1)}_{DOX,2,CBR1,2\|d4,2}$	$\boldsymbol{B}^{(5,CBR1)}_{DOX,2,CBR1,2\|d4,2}$
0.0143 (63)	0.0454 (63)	3.256 (31)	2.4739 (63)	0.007 (31)	0.0015 (63)
0.00000(32)	N/A**	N/A**	N/A**	N/A**	N/A**

units of:

[a] $\left[\frac{\mu\text{mol}}{\text{m}^2}\right]^{1-A^{(1,p1)}_{Type,2,0}}\text{min}^{-1}$ [b] $\left[\frac{\mu\text{mol}}{\text{m}^2}\right]^{-B^{(1,p1)}_{Type,2,0}}$ [c] $\left[\frac{\mu\text{mol}}{\text{m}^2}\right]^{1-A^{(3,p1)}_{Type,2\|\|d3,2,d2,2}}\text{min}^{-1}$ [d] $\left[\frac{\mu\text{mol}}{\text{m}^2}\right]^{-B^{(3,p1)}_{Type,2\|\|d3,2,d2,2}}$

[e] $\left[\frac{\mu\text{mol}}{\text{m}^2}\right]^{1-(A^{(4,DOX)}_{DOX,2,CBR1,2\|d4,2}+A^{(5,CBR1)}_{DOX,2,CBR1,2\|d4,2})}\text{min}^{-1}$ [f] $\left[\frac{\mu\text{mol}}{\text{m}^2}\right]^{-(B^{(4,DOX)}_{DOX,2,CBR1,2\|d4,2}+B^{(5,CBR1)}_{DOX,2,CBR1,2\|d4,2})}$ [g] $\left[\text{L}\cdot\text{m}^{-2}\right]$

**The parameter is indeterminate because the rate constant is zero.

where:

$d2 = DOL$ $d3 = CBR1$ $d4 = DOXCBR1$

Tables 3.36 and 3.37 show the transition concentrations and times calculated using the parameters in Tables 3.34 and 3.35. Like the single process cases, the elimination kinetics of DOL remains in the low-concentration phase. Conversely, the transition concentrations and times of DOX are approximately the same for all the data sets and did not change much from the one-molecule two-compartment model of DOX.

Table 3.36: Calculated transition values of DOX and DOL using the one-compartment case 2.2 model parameters.

Inf[a](Dose)[b]		$A-B$		$X^{T,0}_{Type,2}$ [c]		$C^{T,0}_{Type,2}$ [d]		$T^{(1)}$ [e]		$T^{(2)}$ [e]	
	Type	p1	p2	p1	p2	p1	p2	p1	p2	p1	p2
9.19 (50)	DOX	0.7800	-0.1879	3.4383	22.7178	0.5726	3.7863	0.33	2.90	22.35	13.55
	DOL	1.1426	-0.0001	14.6693	102.1985	1.2214	8.5094	N/A	N/A	N/A	N/A
9.19 (75)	DOX	0.7800	-0.1879	3.4383	22.7178	0.5726	3.7863	0.33	2.90	28.10	19.27
	DOL	1.1426	-0.0001	14.6693	102.1985	1.2214	8.5094	N/A	N/A	N/A	N/A
11.04 (60)	DOX	0.7800	-0.1879	3.4383	22.7178	0.5726	3.7863	0.26	2.27	23.55	14.67
	DOL	1.1426	-0.0001	14.6693	102.1985	1.2214	8.5094	N/A	N/A	N/A	N/A
22.08 (60)	DOX	0.7800	-0.1879	3.4383	22.7178	0.5726	3.7863	0.13	1.13	20.76	11.90
	DOL	1.1426	-0.0001	14.6693	102.1985	1.2214	8.5094	N/A	N/A	N/A	N/A

units of
[a] $\left[\mu mol \cdot m^{-2} \cdot min^{-1}\right]$ [b] $\left[mg \cdot m^{-2}\right]$ [c] $\left[\mu mol \cdot m^{-2}\right]$ [d] $\left[\mu mol \cdot l^{-1}\right]$ [e] $\left[min\right]$

Table 3.37: Calculated transition values of DOX and DOL using the one-compartment case 2.2 model parameters.

Inf[a](Dose)[b]		$A-B$		$X^{T,0}_{Type,2}$ [c]		$C^{T,0}_{Type,2}$ [d]		$T^{(1)}$ [e]		$T^{(2)}$ [e]	
	Type	p1	p2	p1	p2	p1	p2	p1	p2	p1	p2
9.19 (50)	DOX	0.7760	N/A	3.4188	N/A	0.5698	N/A	0.36	N/A	21.45	N/A
	DOL	1.1410	-0.0067	14.3479	101.5364	1.1947	8.4543	N/A	N/A	N/A	N/A
9.19 (75)	DOX	0.7760	N/A	3.4188	N/A	0.5698	N/A	0.36	N/A	29.80	N/A
	DOL	1.1410	-0.0067	14.3479	101.5364	1.1947	8.4543	N/A	N/A	N/A	N/A
11.04 (60)	DOX	0.7760	N/A	3.4188	N/A	0.5698	N/A	0.33	N/A	22.62	N/A
	DOL	1.1410	-0.0067	14.3479	101.5364	1.1947	8.4543	N/A	N/A	N/A	N/A
22.08 (60)	DOX	0.7760	N/A	3.4188	N/A	0.5698	N/A	0.17	N/A	19.85	N/A
	DOL	1.1410	-0.0067	14.3479	101.5364	1.1947	8.4543	N/A	N/A	N/A	N/A

units of
[a] $\left[\mu mol \cdot m^{-2} \cdot min^{-1}\right]$ [b] $\left[mg \cdot m^{-2}\right]$ [c] $\left[\mu mol \cdot m^{-2}\right]$ [d] $\left[\mu mol \cdot l^{-1}\right]$ [e] $\left[min\right]$

Figure 3.23 shows the concentration curves of DOX and DOL using the parameters from Table 3.35. The figure shows the increased terminal concentration of DOX due to the reduced terminal plasma elimination parameters. There is good agreement between the predicted and observed concentrations for both molecules.

3.6.3 Four-Molecule, Two-Compartment Model

In this model, the parameters that describe the PK of DOX and DOL in a two-compartment model are developed. DOX is infused in compartment one and distributes into compartment two where it is either eliminated into compartment zero, metabolized into DOL or redis-

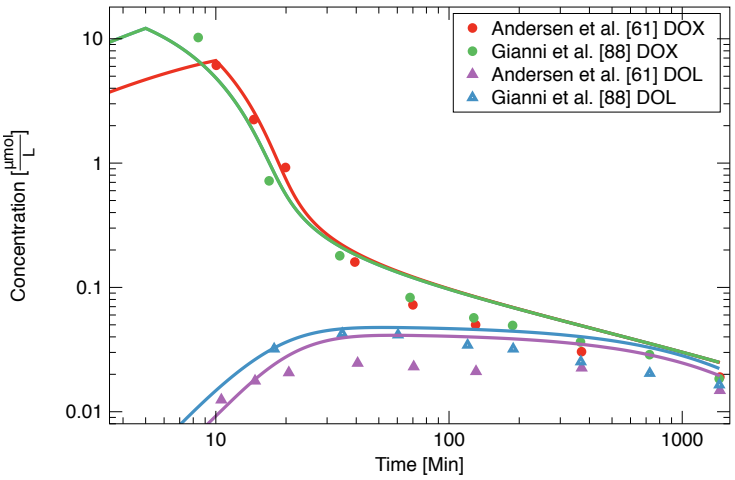

Figure 3.23: Comparison of theoretical and experimental concentrations of DOX and DOL using the parameters from Table 3.35. The curves represent the infusion data from Andersen *et al.* [61](red and purple) and Gianni *et al.* [88](green and blue).

tributed back into compartment one. The activity of the molecules within the plasma is represented by compartment one. The activities of the molecules within individual compartments are uniform implying a constant intra-compartmental distribution rate. In the initial model, we have kept the DOX parameters fixed and varied the parameters for the other molecules in the model. We have retained the assumption of the fraction of DOX converting to the metabolite from clinical studies.

According to the parameters in Table 3.38, following the catabolism of the complex, the distribution of DOL in compartment two to compartment one is characterized by a process with exponent $A \approx 2.75$. Conversely, the elimination kinetics is dependent on the amount of DOL available in compartment two. At high concentrations, the PK of DOL is in competition between elimination and its distribution to compartment one. However, at low concentrations the molecule is eliminated significantly faster than it is distributed to the plasma. The elimination rate is similar to the one-compartment four-molecule model in Table 3.30, which suggests that the molecule is significantly deposited to compartment two. In the plasma, the distribution of DOL can be described by exponent $A - B \approx 1.11$ at high concentrations, and $A \approx 2.66$ at low concentrations. The complex dissociation exponents

are similar to the one-compartment model in Table 3.30. However, the dissociation parameter is increased due to the presence of a principal compartment where DOX is infused. The volume of distribution of DOL is reduced by 12% from Table 3.30, this suggests that the molecule is deposited minimally into the second compartment.

Table 3.38: Two-compartment model case 2 parameters of DOX and DOL with fixed DOX parameters.

Type (ci,cf)	$\boldsymbol{k}^{(1,p1)}_{Type,ci,cf}$ [a]	$\boldsymbol{\Gamma}^{(1,p1)}_{Type,ci,cf}$ [b]	$\boldsymbol{A}^{(1,p1)}_{Type,ci,cf}$	$\boldsymbol{B}^{(1,p1)}_{Type,ci,cf}$	$V_{d,Type}$ [g]
DOX (1,2)	0.0484 (62)*	0.0753 (53)*	3.2730 (42)*	2.473 (19)*	5.21 (23)*
DOX (2,0)	0.559 (31)*	0.000 (43)*	1.590 (31)*	N/A**	
DOX (2,1)	0.96 (16)*	0.266 (44)*	1.60 (13)*	1.09 (18)*	
DOL (1,2)	0.0019 (63)	0.00849 (36)	2.66 (41)	1.5386 (14)	12.52 (24)
DOL (2,0)	0.1564 (63)	0.2447 (63)	2.592 (19)	1.663 (31)	
DOL (2,1)	0.00014 (42)	0.00 (15)	2.751 (44)	N/A**	
Type	$\boldsymbol{k}^{(3,p1)}_{Type,2\|\|d3,2,d2,2}$ [c]	$\boldsymbol{\Gamma}^{(3,p1)}_{Type,2\|\|d3,2,d2,2}$ [d]	$\boldsymbol{A}^{(3,p1)}_{Type,2\|\|d3,2,d2,2}$	$\boldsymbol{B}^{(3,p1)}_{Type,2\|\|d3,2,d2,2}$	S_p
DOXCBR1	0.2570 (13)	0.97 (30)	2.84 (56)	1.40 (12)	0.1016
$\boldsymbol{k}^{(4)}_{DOX,2,CBR1,2\|d4,2}$ [e]	$\boldsymbol{\Gamma}^{(4)}_{DOX,2,CBR1,2\|d4,2}$ [f]	$\boldsymbol{A}^{(4,DOX)}_{DOX,2,CBR1,2\|d4,2}$	$\boldsymbol{B}^{(4,DOX)}_{DOX,2,CBR1,2\|d4,2}$	$\boldsymbol{A}^{(5,DOX)}_{DOX,2,CBR1,2\|d4,2}$	$\boldsymbol{B}^{(5,DOX)}_{DOX,2,CBR1,2\|d4,2}$
0.634 (44)	0.000 (19)	1.539 (56)	1.12 (53)	0.005 (18)	0.000 (24)

units of:
[a] $\left[\frac{\mu\text{mol}}{\text{m}^2}\right]^{1-A^{(1,p1)}_{Type,ci,cf}}\text{min}^{-1}$ [b] $\left[\frac{\mu\text{mol}}{\text{m}^2}\right]^{-B^{(1,p1)}_{Type,ci,cf}}$ [c] $\left[\frac{\mu\text{mol}}{\text{m}^2}\right]^{1-A^{(3,p1)}_{Type,2\|\|d3,2,d2,2}}\text{min}^{-1}$ [d] $\left[\frac{\mu\text{mol}}{\text{m}^2}\right]^{-B^{(3,p1)}_{Type,2\|\|d3,2,d2,2}}$
[e] $\left[\frac{\mu\text{mol}}{\text{m}^2}\right]^{1-(A^{(4,DOX)}_{DOX,2,CBR1,2\|d4,2}+A^{(5,CBR1)}_{DOX,2,CBR1,2\|d4,2})}\text{min}^{-1}$ [f] $\left[\frac{\mu\text{mol}}{\text{m}^2}\right]^{-(B^{(4,DOX)}_{DOX,2,CBR1,2\|d4,2}+B^{(5,CBR1)}_{DOX,2,CBR1,2\|d4,2})}$ [g] $\left[\text{L}\cdot\text{m}^{-2}\right]$
where:
$d2 = DOL$ $d3 = CBR1$ $d4 = DOXCBR1$
**The parameter is indeterminate because the saturation parameter is zero.
*These parameters are from Table 3.17

In Table 3.39, we present the transition concentrations and times of DOX and DOL. It can be seen that for all the datasets, the flow of DOL from compartment one to compartment two and the reverse flow from the compartments occur in a low concentration phase. For both these processes, the saturation coefficients do not affect the kinetics and can be set to zero. The type of elimination kinetics of DOL from the body may, however, depend on the amount of the molecule in compartment two. For DOL amount exceeding 2.3315 $\mu\text{mol}\cdot\text{m}^{-2}$, the kinetics is a high concentration one, and time to reach this value depends on the amount of DOX infused.

Figure 3.24 shows concentration curves of DOX and DOL using the parameters in Table 3.38. The figure shows that the concentrations of DOX and DOL are reduced compared to the single-compartment models. The curves show a good agreement with clinical data

Table 3.39: Calculated transition values of DOX and DOL using the two-compartment version B case 2 model parameters.

Inf[a](Dose)[b]	Type	ci,cf	$A-B$	$X^{T,cf}_{Type,ci}$ [c]	$T^{(1)}$ [e]	$T^{(2)}$ [e]	$X^{T}_{Type,1}$ [c]	$C^{T}_{Type,1}$ [d]
9.19 (50)	DOX	1, 2	0.8000	2.8464	0.32	21.45	2.8464	0.5463
	DOL		1.1214	22.1865	N/A	N/A	22.1865	1.7721
	DOX	2, 0	N/A	N/A	N/A	N/A	N/A	N/A
	DOL		0.9290	2.3315	4.36	22.55	0.0006	0.0001
	DOX	2, 1	0.5100	3.3700	N/A	N/A	N/A	N/A
	DOL		N/A	N/A	N/A	N/A	N/A	N/A
9.19 (75)	DOX	1, 2	0.8000	2.8464	0.32	26.80	2.8464	0.5463
	DOL		1.1214	22.1865	N/A	N/A	22.1865	1.7721
	DOX	2, 0	N/A	N/A	N/A	N/A	N/A	N/A
	DOL		0.9290	2.3315	4.37	28.00	0.0006	0.0001
	DOX	2, 1	0.5100	3.3700	14.30	15.10	39.2969	7.5426
	DOL		N/A	N/A	N/A	N/A	N/A	N/A
11.04 (60)	DOX	1, 2	0.8000	2.8464	0.25	22.41	2.8464	0.5463
	DOL		1.1214	22.1865	N/A	N/A	22.1865	1.7721
	DOX	2, 0	N/A	N/A	N/A	N/A	N/A	N/A
	DOL		0.9290	2.3315	4.00	23.47	0.0006	0.0001
	DOX	2, 1	0.5100	3.3700	7.62	10.69	39.7450	7.6286
	DOL		N/A	N/A	N/A	N/A	N/A	N/A
22.08 (60)	DOX	1, 2	0.8000	2.8464	0.12	19.28	2.8464	0.5463
	DOL		1.1214	22.1865	N/A	N/A	22.1865	1.7721
	DOX	2, 0	N/A	N/A	N/A	N/A	N/A	N/A
	DOL		0.9290	2.3315	3.00	20.47	0.0005	0.00004
	DOX	2, 1	0.5100	3.3700	2.54	7.74	41.9530	8.0524
	DOL		N/A	N/A	N/A	N/A	N/A	N/A

upits of
[a] $\left[\mu\text{mol}\cdot\text{m}^{-2}\cdot\text{min}^{-1}\right]$ [b] $\left[\text{mg}\cdot\text{m}^{-2}\right]$ [c] $\left[\mu\text{mol}\cdot\text{m}^{-2}\right]$ [d] $\left[\mu\text{mol}\cdot\text{l}^{-1}\right]$ [e] $\left[\text{min}\right]$
N/A: Not applicable because the coefficient is zero.

over the range of concentrations. The maximum concentration of DOL can be observed between twenty to fifty minutes after the infusion of DOX.

Table 3.40 shows the model results when the parameters of all the molecules are varied. Most of the parameters did not show any appreciable change from Table 3.38. There is an 8% decrease in the distribution rate constants of DOX at high concentrations and a 6% increase at low concentrations. Conversely the rate constant of binding of DOX to the enzyme is increased by the same magnitude. The greatest change to the parameters

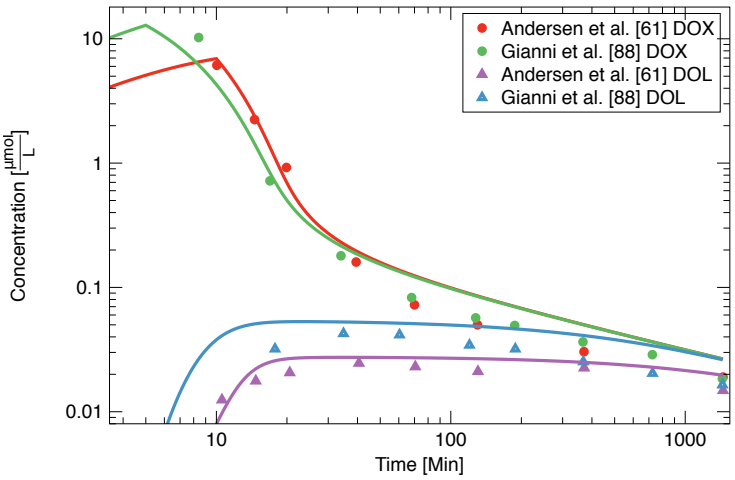

Figure 3.24: Comparison of theoretical and experimental concentrations of DOX and DOL using the parameters from Table 3.38. The curves represent the infusion data from Andersen *et al.* [61](red and purple) and Gianni *et al.* [88](green and blue).

is the elimination of DOX, which has exponent $A - B \approx 0.46$ at high concentrations and $A \approx 1.58$ at low concentrations. The initial PK of unchanged DOX in compartment two is dominated by drug elimination process at high concentrations, accounting for nearly 80% of the drugs's disposition. At low concentrations elimination accounts for 36% of the disposition suggesting a greater exposure of the drug to the compartment. Considering that elimination of unchanged drug in this model can be explained by drug retention or elimination, this result suggests that the retention or elimination mechanisms of DOX dominate at high concentrations while the redistribution mechanisms dominate at low concentrations. The binding parameter of DOX to the enzyme increases slightly when the DOX parameters are allowed to vary. The transition of the flow kinetics from a low to a high phase occurs when amounts of DOX and DOL in compartment one approaches 2.69 $\mu\text{mol} \cdot \text{m}^{-2}$ and 20.75 $\mu\text{mol} \cdot \text{m}^{-2}$ respectively. The elimination of DOL from compartment two transitions to a high concentration kinetics as the amount of the molecule in the compartment approaches 2.30 $\mu\text{mol} \cdot \text{m}^{-2}$. The parameters of DOL and the complex molecule did not change from Table 3.38.

Figure 3.25 shows the concentration curves of DOX and DOL using the parameters in

Table 3.40. The figure shows a slightly increased initial DOX plasma concentration. The curves show a good agreement with clinical data over the range of concentrations.

Table 3.40: Two-compartment model case 2 parameters of DOX and DOL with DOX parameters varied.

Type (ci,cf)	$k^{(1,p1)}_{Type,ci,cf}$ [a]	$\Gamma^{(1,p1)}_{Type,ci,cf}$ [b]	$A^{(1,p1)}_{Type,ci,cf}$	$B^{(1,p1)}_{Type,ci,cf}$	$V_{d,Type}$ [g]
DOX (1,2)	0.0514 (62)	0.0872 (12)	3.281 (42)	2.4656 (12)	5.21 (20)
DOX (2,0)	0.555 (43)	0.036 (14)	1.579 (43)	1.12 (65)	
DOX (2,1)	0.966 (94)	0.267 (81)	1.602 (56)	1.09 (30)	
DOL (1,2)	0.0019 (63)	0.0094 (16)	2.66 (39)	1.539 (40)	12.52 (19)
DOL (2,0)	0.1710 (63)	0.2474 (63)	2.579 (19)	1.678 (18)	
DOL (2,1)	0.0001 (63)	0.0000 (37)	2.759 (44)	N/A**	
Type	$k^{(3,p1)}_{Type,2\|\|d3,2,d2,2}$ [c]	$\Gamma^{(3,p1)}_{Type,2\|\|d3,2,d2,2}$ [d]	$A^{(3,p1)}_{Type,2\|\|d3,2,d2,2}$	$B^{(3,p1)}_{Type,2\|\|d3,2,d2,2}$	S_p
DOXCBR1	0.2570 (13)	0.97 (30)	2.84 (54)	1.39 (12)	0.0998
$k^{(4)}_{DOX,2,CBR1,2\|d4,2}$ [e]	$\Gamma^{(4)}_{DOX,2,CBR1,2\|d4,2}$ [f]	$A^{(4,DOX)}_{DOX,2,CBR1,2\|d4,2}$	$B^{(4,DOX)}_{DOX,2,CBR1,2\|d4,2}$	$A^{(5,CBR1)}_{DOX,2,CBR1,2\|d4,2}$	$B^{(5,CBR1)}_{DOX,2,CBR1,2\|d4,2}$
0.686 (56)	0.000 (32)	1.599 (68)	N/A**	0.0133 (19)	0.0004**

units of:

a $\left[\frac{\mu mol}{m^2}\right]^{1-A^{(1,p1)}_{Type,ci,cf}} min^{-1}$ b $\left[\frac{\mu mol}{m^2}\right]^{-B^{(1,p1)}_{Type,ci,cf}}$ c $\left[\frac{\mu mol}{m^2}\right]^{1-A^{(3,p1)}_{Type,2\|\|d3,2,d2,2}} min^{-1}$ d $\left[\frac{\mu mol}{m^2}\right]^{-B^{(3,p1)}_{Type,2\|\|d3,2,d2,2}}$

e $\left[\frac{\mu mol}{m^2}\right]^{1-(A^{(4,DOX)}_{DOX,2,CBR1,2\|d4,2}+A^{(5,CBR1)}_{DOX,2,CBR1,2\|d4,2})} min^{-1}$ f $\left[\frac{\mu mol}{m^2}\right]^{-(B^{(4,DOX)}_{DOX,2,CBR1,2\|d4,2}+B^{(5,CBR1)}_{DOX,2,CBR1,2\|d4,2})}$ g $\left[L \cdot m^{-2}\right]$

where:

$d2 = DOL$ $d3 = CBR1$ $d4 = DOXCBR1$

**The parameter is indeterminate because the saturation parameter is zero.

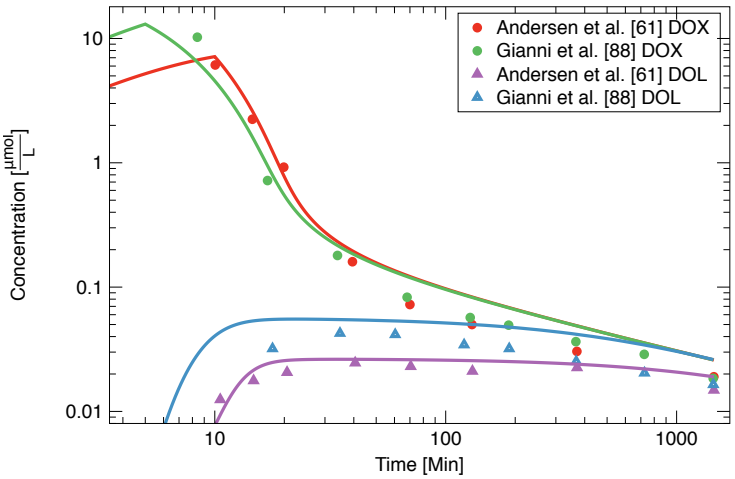

Figure 3.25: Comparison of theoretical and experimental concentrations of DOX and DOL using the parameters from Table 3.40. The curves represent the infusion data from Andersen *et al.* [61](red and purple) and Gianni *et al.* [88](green and blue).

3.6.4 Four-Molecule, Three-Compartment Model

The three-compartment model was used to observe a more realistic depiction of the PK processes of the parent and metabolite molecules. In the initial model, the DOX parameters were kept fixed and parameters of the other molecules were varied. The model parameters are shown in Table 3.41. According to the parameters, the high concentration kinetics of DOL in compartment two is a competition between elimination and redistribution to compartment one. This is likely because the elimination process is limited by the concentration of DOL in the compartment. At low concentrations, elimination of DOL accounts for approximately 90% of the PK in compartment two suggesting that the terminal PK of DOL in the metabolism and elimination sites is dominated by clearance and not redistribution into the plasma volume. The parameters suggest that DOL activity is most prominent in compartments one and two, the rate parameter describing the flow of the molecule from compartment one to three is only a fraction of that from compartment one to two. The reduced volume of distribution can be explained by the reduced rate of flow of DOL to the plasma compartment from the two extra compartments. These parameters suggest that DOL is not distributed to the tissues and organs as much as the parent drug, and is predominantly active only at the metabolism and elimination sites.

Figure 3.26 shows the concentration curves of DOX and DOL using the parameters in Table 3.41. The figure shows a slightly increased initial DOX plasma concentration. The curves show a good agreement with the clinical data over the range of concentrations.

When relaxing the DOX parameters to observe changes to the overall PK, the parameters did not change significantly from the initial model. Table 3.42 shows the new model parameters. The greatest change to the parameters is the rate constant of the binding of DOX to *CBR*1, which increases by 58% at high DOX concentrations from Table 3.41. Similarly, the redistribution of DOL in compartment three to compartment one is zero suggesting that DOL distributed to the tissues and organs are retained in the compartment. Figure 3.27 shows the simulation of the concentrations of DOX and DOL using the parameters in Ta-

Table 3.41: Three-compartment model case 2 parameters of DOX and DOL with fixed DOX parameters.

Type (ci,*cf*)	$k^{(1,p1)}_{Type,ci,cf}$ [a]	$\Gamma^{(1,p1)}_{Type,ci,cf}$ [b]	$A^{(1,p1)}_{Type,ci,cf}$	$B^{(1,p1)}_{Type,ci,cf}$	$V_{d,Type}$ [g]
DOX (1,2)	0.066 (18)*	0.083 (63)*	3.3909 (63)*	2.5044 (31)*	5.122 (17)*
DOX (2,0)	0.2067 (93)*	0.0011 (56)*	1.4828 (18)*	1.1151 (23)*	
DOX (2,1)	1.0626 (31)*	0.1242 (24)*	1.49 (34)*	1.14 (10)*	
DOX (1,3)	0.000043 (62)*	0.0326 (14)*	3.290 (68)*	2.5062 (34)*	
DOX (3,1)	0.0490 (76)*	0.0014 (16)*	1.4771 (23)*	1.1592 (28)*	
DOL (1,2)	0.0030 (63)	0.0015 (23)	2.6808 (39)	1.5458 (12)	9.9932 (12)
DOL (2,0)	0.0198 (26)	0.0294 (12)	2.6919 (31)	1.536 (81)	
DOL (2,1)	0.000070 (62)	0.000 (62)	2.688 (56)	N/A**	
DOL (1,3)	0.000040 (21)	0.0060 (14)	2.7717 (73)	1.447 (12)	
DOL (3,1)	0.000078 (23)	0.0005 (21)	2.7110 (78)	1.5604 (28)	
Type	$k^{(3,p1)}_{Type,2\|\|d3,2,d2,2}$ [c]	$\Gamma^{(3,p1)}_{Type,2\|\|d3,2,d2,2}$ [d]	$A^{(3,p1)}_{Type,2\|\|d3,2,d2,2}$	$B^{(3,p1)}_{Type,2\|\|d3,2,d2,2}$	S_p
DOXCBR1	0.1479 (23)	1.00 (24)	2.7815 (14)	1.453 (81)	0.0987
$k^{(4)}_{DOX,2,CBR1,2\|d4,2}$ [e]	$\Gamma^{(4)}_{DOX,2,CBR1,2\|d4,2}$ [f]	$A^{(4,DOX)}_{DOX,2,CBR1,2\|d4,2}$	$B^{(4,DOX)}_{DOX,2,CBR1,2\|d4,2}$	$A^{(5,CBR1)}_{DOX,2,CBR1,2\|d4,2}$	$B^{(5,CBR1)}_{DOX,2,CBR1,2\|d4,2}$
0.254911 (12)	0.0011 (33)	1.4828 (45)	1.115 (12)	0.0479 (50)	0.001 (10)

units of:

[a] $\left[\frac{\mu mol}{m^2}\right]^{1-A^{(1,p1)}_{Type,ci,cf}}\,min^{-1}$ [b] $\left[\frac{\mu mol}{m^2}\right]^{-B^{(1,p1)}_{Type,ci,cf}}$ [c] $\left[\frac{\mu mol}{m^2}\right]^{1-A^{(3,p1)}_{Type,2\|\|d3,2,d2,2}}\,min^{-1}$ [d] $\left[\frac{\mu mol}{m^2}\right]^{-B^{(3,p1)}_{Type,2\|\|d3,2,d2,2}}$

[e] $\left[\frac{\mu mol}{m^2}\right]^{1-(A^{(4,DOX)}_{DOX,2,CBR1,2\|d4,2}+A^{(5,CBR1)}_{DOX,2,CBR1,2\|d4,2})}\,min^{-1}$ [f] $\left[\frac{\mu mol}{m^2}\right]^{-(B^{(4,DOX)}_{DOX,2,CBR1,2\|d4,2}+B^{(5,CBR1)}_{DOX,2,CBR1,2\|d4,2})}$ [g] $\left[L\cdot m^{-2}\right]$

where:

$d2 = DOL$ $d3 = CBR1$ $d4 = DOXCBR1$

**The parameter is indeterminate because the saturation parameter is zero.

*These parameters are from Table 3.22

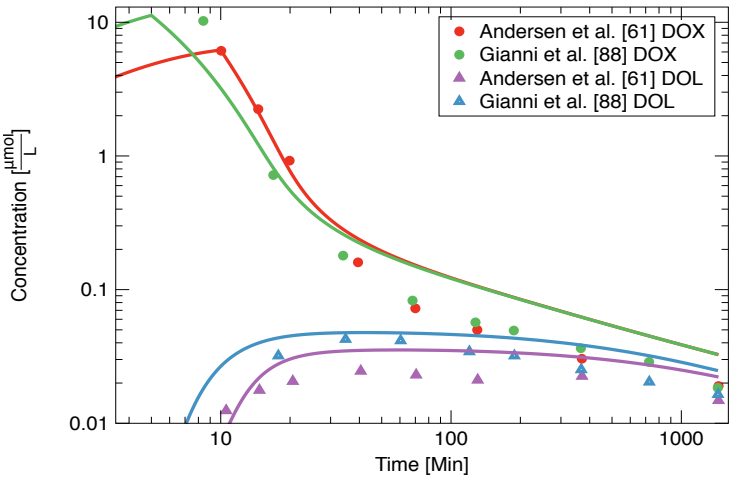

Figure 3.26: Comparison of theoretical and experimental concentrations of DOX and DOL using the parameters from Table 3.41. The curves represent the infusion data from Andersen *et al.* [61](red and purple) and Gianni *et al.* [88](green and blue).

ble 3.42. The figure shows a slightly improved fit to the high and low concentration data points of DOL. The curves show a good agreement for both molecules with the clinical data over the range of concentrations.

Table 3.42: Three-compartment model case 2 parameters of DOX and DOL with varied DOX parameters.

Type (ci,*cf*)	$k^{(1,p1)}_{Type,ci,cf}$ [a]	$\Gamma^{(1,p1)}_{Type,ci,cf}$ [b]	$A^{(1,p1)}_{Type,ci,cf}$	$B^{(1,p1)}_{Type,ci,cf}$	$V_{d,Type}$ [g]
DOX (1,2)	0.0697 (62)	0.0850 (25)	3.3890 (18)	2.505 (44)	5.122 (89)
DOX (2,0)	0.2074 (29)	0.002 (68)	1.481 (19)	1.1121 (30)	
DOX (2,1)	1.062 (62)	0.123 (18)	1.50 (28)	1.142 (68)	
DOX (1,3)	0.000033 (20)	0.0326 (16)	3.291 (10)	2.5062 (18)	
DOX (3,1)	0.0489 (13)	0.0013 (32)	1.47 (25)	1.159 (36)	
DOL (1,2)	0.0030 (62)	0.0010 (18)	2.68 (44)	1.546 (27)	9.99 (74)
DOL (2,0)	0.0188 (64)	0.0351 (54)	2.691 (31)	1.536 (81)	
DOL (2,1)	0.000067 (63)	0.0000 (43)	2.689 (56)	N/A**	
DOL (1,3)	0.000030 (53)	0.0060 (14)	2.7715 (23)	1.4476 (48)	
DOL (3,1)	0.000000 (83)	N/A**	N/A**	N/A**	

Type	$k^{(3,p1)}_{Type,2\|\|d3,2,d2,2}$ [c]	$\Gamma^{(3,p1)}_{Type,2\|\|d3,2,d2,2}$ [d]	$A^{(3,p1)}_{Type,2\|\|d3,2,d2,2}$	$B^{(3,p1)}_{Type,2\|\|d3,2,d2,2}$	S_p
DOXCBR1	0.1479 (53)	1.00 (23)	2.78 (13)	1.4532 (68)	0.0984

$k^{(4,p1,p2)}_{DOX,2,CBR1,2\|d4,2}$ [e]	$\Gamma^{(4,p1,p2)}_{DOX,2,CBR1,2\|d4,2}$ [f]	$A^{(4,p1,p2)}_{DOX,2,CBR1,2\|d4,2}$	$B^{(4,p1,p2)}_{DOX,2,CBR1,2\|d4,2}$	$A^{(5,p1,p2)}_{DOX,2,CBR1,2\|d4,2}$	$B^{(5,p1,p2)}_{DOX,2,CBR1,2\|d4,2}$
0.256 (81)	0.0007 (18)	1.4818 (18)	1.115 (20)	0.056 (56)	0.0009 (63)

units of:

[a] $\left[\frac{\mu mol}{m^2}\right]^{1-A^{(1,p1)}_{Type,ci,cf}} min^{-1}$ [b] $\left[\frac{\mu mol}{m^2}\right]^{-B^{(1,p1)}_{Type,ci,cf}}$ [c] $\left[\frac{\mu mol}{m^2}\right]^{1-A^{(3,p1)}_{Type,2\|\|d3,2,d2,2}} min^{-1}$ [d] $\left[\frac{\mu mol}{m^2}\right]^{-B^{(3,p1)}_{Type,2\|\|d3,2,d2,2}}$

[e] $\left[\frac{\mu mol}{m^2}\right]^{1-(A^{(4,p1,p2)}_{DOX,2,CBR1,2\|d4,2}+A^{(5,p1,p2)}_{DOX,2,CBR1,2\|d4,2})} min^{-1}$ [f] $\left[\frac{\mu mol}{m^2}\right]^{-(B^{(4,p1,p2)}_{DOX,2,CBR1,2\|d4,2}+B^{(5,p1,p2)}_{DOX,2,CBR1,2\|d4,2})}$ [g] $\left[L \cdot m^{-2}\right]$

**The parameter is indeterminate because the rate constant is zero.

where:

$d2 = DOL$ $d3 = CBR1$ $d4 = DOXCBR1$

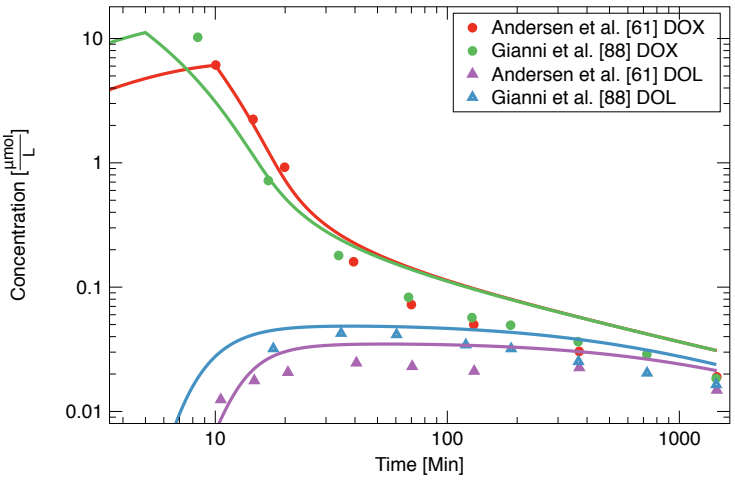

Figure 3.27: Comparison of theoretical and experimental concentrations of DOX and DOL from the baseline datasets. The graphs were plotted using the parameters from Table 3.42. The curves represent the infusion data from Andersen *et al.* [61](red and purple) and Gianni *et al.* [88](green and blue).

3.7 Summary

In this chapter, the parameters that describe the models considered in this thesis have been developed. The parameters have been developed for the one, two and three-compartment

models. In the single molecule case, comparing the predicted concentration fits of our model with those from the Michaelis-Menten type kinetics, it can be seen that our model produced a better result for the variance in all the cases. Analysis of the single-molecule one-compartment parameters show that the elimination of DOX from the body can be described by saturable processes with non-linear exponents. The saturation parameter allows for the modification of the kinetics of the molecule. When introducing the multi-compartment models, we notice that the plasma distribution processes may be described by similar exponents regardless of the final compartments. In multi-compartment systems, the elimination and plasma redistribution processes may be described by similar exponents, which differ from that of plasma distribution. Introducing extra processes to the models produced a better overall fit to the clinical concentration-time data, especially at low concentrations. Conversely, when the interaction terms were introduced to the single-molecule models, the high concentration fits are improved relative to the initial non-interaction models. The variance of these models when compared to the multiprocess models suggest that the multi-process models are a better model than the models with interactions. When modeling the encapsulated form of DOX, the parameters show that the model with drug interactions produced the best fit to the clinical data. The kinetics of DOX is changed by the administration of both encapsulated molecules. When the four-molecule models are considered, the parameters of DOL show that the kinetics is dominated by elimination from the metabolism sites. This suggests that a significant proportion of DOL is removed from the metabolism compartment either through retention or elimination.

Chapter 4

Model Application

Take chances,

make mistakes,

get messy!

– V. F. Frizzle

4.1 Introduction

In Chapter 3 we computed the parameters of the different models considered in this work. In the current chapter, we will apply the model parameters to simulate the concentrations of the molecules from published clinical studies. The analysis of the model will be based on the particular patients' characteristics and other covariates from the chosen study. Where possible, the model parameters will be fitted to the clinical data to observe changes to the parameters due to the covariates. The analysis of the parameters that change in the model should give an insight into the factors responsible for the changes to the predicted concentration values.

4.2 Comparison of the DOX Parameters

Table 4.1 shows the comparison of the PK parameters from the one, two and three-compartment case 2 models of DOX to clinical measurements. The first parameter is the AUC and is the calculated area under the concentration curve from zero to infinity. $C_{\max}$ is the maximum concentration of DOX simulated from the model parameters. $t^d_{1/2}$ is the

distribution half-life and represents the time for the plasma concentration to fall by a factor of two from $C_{\max}$. The unit is minutes, indicative of the rapid initial distribution of the drug. $t^e_{1/2}$ is the elimination half-life and is the time required to eliminate half of the drug in the plasma after reaching pseudo-equilibrium. The unit of the elimination half-life is hours. Table 4.1 shows that the AUC increased with the number of compartments considered in the models. The greatest percentage change in the AUC from the case 2 models using the baseline dataset corresponds to a 14% increase from the one-compartment to the three-compartment model. The AUC shows a good agreement with the clinical estimate for the 11.03 $\mu\text{mol}\cdot\text{m}^{-2}\cdot\text{min}^{-1}$ and 9.19 $\mu\text{mol}\cdot\text{m}^{-2}\cdot\text{min}^{-1}$ infusions. The maximum plasma concentration predicted from the case 2 models also agree well with the measured values from the Gianni *et al.* [88] and Moriera *et al.* [89] studies, but is over twice the measured value from the Benjamin *et al.* [63] study. The parameter decreases from the one-compartment to the three-compartment model. The distribution half-life calculated using the parameters from the models agree with the Gianni *et al.* [88] study and suggest that the initial rapid plasma disappearance occurs within five minutes of DOX administration. However, this estimate is markedly reduced relative to the clinical measurements in the Benjamin *et al.* [63] and Greene *et al.* [59] studies. Comparing the plasma elimination half-lives show that estimates from our models fall within error of the clinical estimates.

Table 4.2 shows the comparison of PK parameters from the case 2.2 models to the clinical estimates. We notice that the addition of extra processes increases the two-compartment AUC, but the AUCs of the one and three-compartment models are reduced from Table 4.1. All of the AUCs are in the clinically measured range for all the models. Comparing the $C_{\max}$ in the table with Table 4.1, we notice that the one and three-compartment model estimates did not change much from Table 4.1, although there is a slight increase in the two-compartment model estimate. Similar to the AUC, the estimated $C_{\max}$ was in the clinically observed range for all the models. The estimated elimination half-life from the two-compartment model was closest to the clinical estimate when using multiple processes. The

Table 4.1: Comparison of the case 2 and clinical parameters of DOX.

	$AUC_{0\to\infty}$ [a]				$C_{\max}$ [b]				$t^d_{1/2}$ [c]				$t^e_{1/2}$ [d]			
Data set	1C2	2C2	3C2	Clin	1C2	2C2	3C2	Clin	1C2	2C2	3C2	Clin	1C2	2C2	3C2	Clin
Moriera *et al.* [89]	4.05	4.06	4.52	2.18 ± 0.86	0.07**	0.07**	0.08**	0.07 ± 0.02**	3.96	3.25	2.77	N/A	32.05	35.79	31.09	35.2 ± 19.5
Gianni *et al.* [88]	4.05	4.06	4.52	3.6 ± 0.8	12.22	12.85	11.48	10.5 ± 1.8	3.96	3.25	2.77	3.8 ± 0.3	32.05	35.79	31.09	48 ± 23
Greene *et al.* [59]	4.36	4.41	4.93	4.43 ± 0.42	7.73	7.62	6.84	N/A	3.55	3.05	3.05	10.0 ± 2.2	40.50	44.99	38.91	30.2 ± 1.9
Benjamin *et al.* [64]	3.97	4.02	4.56	2.66	8.34	8.45	7.61	N/A	3.62	3.10	2.99	11.3	23.70	26.08	22.51	28.1
Benjamin *et al.* [63]	4.05	4.06	4.52	N/A	12.22	12.85	11.48	5.66***	3.96	3.25	2.77	12 ± 8	32.05	35.79	31.09	29.6 ± 13.5

units of:
[a] $\mu mol \cdot l^{-1} \cdot h$ [b] $\mu mol \cdot l^{-1}$ [c] min [d] h N/A = Not provided for the study.
** Measured plasma concentration 3 hours after infusion.
*** Measured plasma concentration in two patients.

Table 4.2: Comparison of the case 2.2 and clinical parameters of DOX.

	$AUC_{0\to\infty}$ [a]				C_{max} [b]				$t_{1/2}^{d}$ [c]				$t_{1/2}^{e}$ [d]			
Data set	1C2.2	2C2.2	3C2.2	Clin	1C2.2	2C2.2	3C2.2	Clin	1C2.2	2C2.2	3C2.2	Clin	1C2.2	2C2.2	3C2.2	Clin
Moriera *et al.* [89]	3.97	4.44	4.11	2.18 ± 0.86	0.07**	0.08**	0.09**	0.07 ± 0.02**	3.92	3.25	2.77	N/A	28.81	35.35	24.35	35.2 ± 19.5
Gianni *et al.* [88]	3.97	4.44	4.11	3.6 ± 0.8	12.20	13.44	11.58	10.5 ± 1.8	3.92	3.15	2.77	3.8 ± 0.3	28.81	35.35	24.35	48 ± 23
Greene *et al.* [59]	4.29	4.75	4.72	4.43 ± 0.42	7.71	7.74	6.76	N/A	3.53	2.91	2.94	10.0 ± 2.2	35.46	41.15	25.90	30.2 ± 1.9
Benjamin *et al.* [64]	3.90	4.37	4.02	2.66	8.32	8.66	7.57	N/A	3.59	2.94	2.95	11.3	21.41	28.11	21.98	28.1
Benjamin *et al.* [63]	3.97	4.44	4.11	N/A	12.20	13.44	11.58	5.66***	3.92	3.15	2.77	12 ± 8	28.81	35.35	24.35	29.6 ± 13.5

units of:
[a] $\mu mol \cdot l^{-1} \cdot h$ [b] $\mu mol \cdot l^{-1}$ [c] min [d] h N/A = Not provided for the study.
** Measured plasma concentration 3 hours after infusion.
*** Measured plasma concentration in two patients.

two-compartment model generally produced $t^e_{1/2}$ estimates greater than the one and three-compartment model estimates. Comparing the parameters in both tables, we can infer that all the models predict the molecule's parameters reasonably well when compared to the clinical calculations.

In figure 4.1, the three-compartment case 2.2 model parameters have been used to simulate the 7.36 $\mu mol \cdot m^{-2} \cdot min^{-1}$ infusion of DOX. The figure shows a reasonable agreement of the theoretical curve to the clinical data. A detailed comparison of the model predicted curves to the clinical concentrations is presented in Appendix C. The model predicted PK parameters are in the clinically observed range as shown in Table 4.3.

Table 4.3: Comparison of the theoretical and clinical parameters of DOX from Wurz *et al.* [90] study.

Parameter	Clinical Est.	Theoretical Est.
$AUC^{theo}_{0\to\infty}$ $(\mu mol \cdot l^{-1} \cdot h)$	3.23	3.69
C_{max} $\mu mol \cdot l^{-1}$	2.68 ± 1.76	5.48
$t^e_{1/2}$ (h)	40.11 ± 9.61	33.22

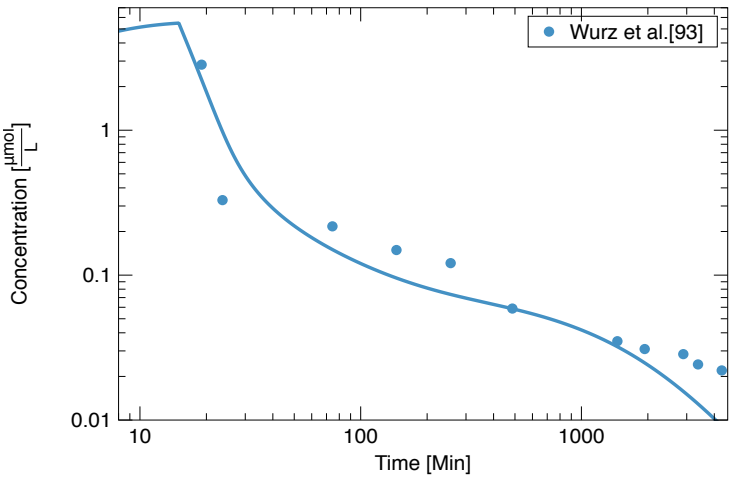

Figure 4.1: Comparison of theoretical and experimental concentrations of DOX using the three-compartment case 2.2 parameters. The curve and data represent DOX infusion of 7.36 $\mu mol \cdot m^{-2} \cdot min^{-1}$. The data points are from Wurz *et al.* [90].

4.3 Effect of Gender on the PK of DOX

The use of anthracyclines as anticancer agents is limited by their associated toxicity. Indeed the most common occurrence of toxicity following anthracycline administration is cardiomyopathy. The long-term effect of DOX treatment is an increase in the possibility of occurrence of adverse effects such as heart-failure [102]. Factors such as age, total cumulative dose, previous radiotherapy and concomitant administration of other anticancer drugs have been correlated with the incidence of anthracycline-induced cardiomyopathy (AIC). Other factors such as liver diseases, diabetes and history of cardiac diseases may also increase the occurrence of AIC. The role of gender on the PK of DOX has not been widely studied. Dobbs *et al.* [103] reported that much of the variability in DOX PK in patients with normal liver function could be explained by the patient's gender. They observed that DOX clearance was greater in men than in women as was the ratio of DOL to DOX AUC. Similarly, Lipshultz *et al.* [104] correlated female gender with the risk of after-treatment cardiac abnormalities of DOX. Liu *et al.* [105] reported that a slower DOL clearance and increased exposure in female cancer patients than males may explain the increased incidence of toxicity. Based on these observations, the four-molecule, one and two-compartment parameters will be used to simulate the concentration profile of DOX and DOL in a subset of the baseline datasets with only female patients [88, 89]. The datasets consist of data from thirty-two female breast cancer patients administered a DOX dose of 60 $\mathrm{mg} \cdot \mathrm{m}^{-2}$ over five minutes. There was no reported alteration to liver biochemistry for all the patients and no drugs were administered concomitantly. The ages of the patients in both studies were less than sixty. Figure 4.2 shows the plasma profile of DOX and DOL simulated from the female patient studies using the four-molecules one and two-compartment models baseline parameters. The green curves are plotted from the one-compartment model parameters, and the red curves are from the two-compartment version B case 2 model. There is no noticeable difference in the DOX curves and the clinical data over the range of concentration. For the DOL curves, the models underestimate the Moriera *et al.* [89] concentration. To in-

vestigate the parameters responsible for the poor fit of DOL concentrations, the one and two-compartment model parameters were fitted to the datasets and the results are shown in Tables 4.4 and 4.5.

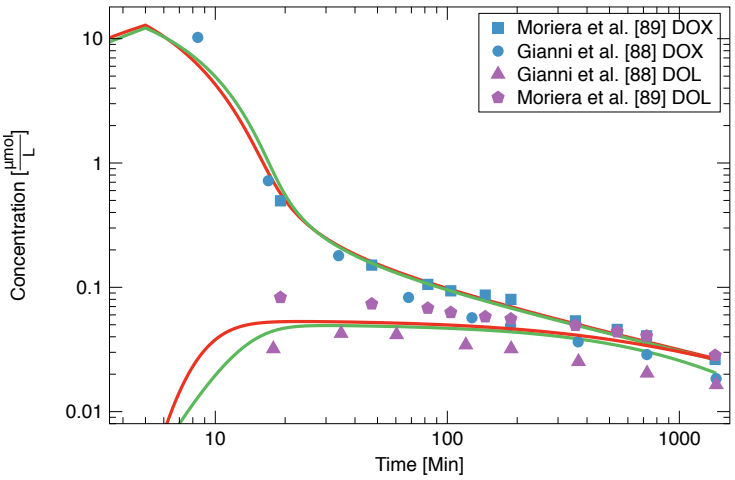

Figure 4.2: Comparison of theoretical and experimental concentrations of DOX and DOL in female cancer patients using the baseline parameters.

Comparing the parameters in Table 4.4 with the baseline shown in Table 3.30 shows interesting changes to some of the parameters. There is a slight increase in the rate constants of elimination and binding of DOX. Conversely, the saturation rate constant of both processes are reduced by 84% from the baseline. The exponent of the saturation term shows the greatest change from the baseline and is characterized by a 21% increase. This results in a high concentration elimination and binding PK of DOX characterized by an exponent $A - B \approx 0.23$. The low concentration PK of DOX is similar to the baseline model, however, the increased rate constants suggest that the the elimination and metabolism of the drug occurs faster in women compared to the baseline. The elimination rate constant of DOL decreased by 12% from the baseline, likewise there is a 97% decrease in the saturation parameters. The elimination exponent of DOL is increased by 28.41% from the baseline. The parameters suggest that the high and low concentration PK of DOL in women changes compared to the baseline.

In Table 4.5, the changes to the parameters of the molecules in female patients compared

Table 4.4: One-compartment model case 2 parameters of DOX and DOL in female breast cancer patients.

Type	$\boldsymbol{k}^{(1,p1)}_{Type,2,0}$ [a]	$\boldsymbol{\Gamma}^{(1,p1)}_{Type,2,0}$ [b]	$\boldsymbol{A}^{(1,p1)}_{Type,2,0}$	$\boldsymbol{B}^{(1,p1)}_{Type,2,0}$	$V_{d,Type}$ [g]
DOX	0.00932 (70)	0.0070 (95)	3.2322 (82)	3.0022 (93)	6.01 (12)
%Δ	3.32	-84.44	-0.33	21.20	-0.12
DOL	0.2230 (34)	0.00062 (13)	3.4171 (21)	1.515 (12)	14.17 (23)
%Δ	-12.89	-97.37	28.41	-0.82	-0.69
Type	$\boldsymbol{k}^{(3,p1)}_{Type,2\|\|d3,2,d2,2}$ [c]	$\boldsymbol{\Gamma}^{(3,p1)}_{Type,2\|\|d3,2,d2,2}$ [d]	$\boldsymbol{A}^{(3,p1)}_{Type,2\|\|d3,2,d2,2}$	$\boldsymbol{B}^{(3,p1)}_{Type,2\|\|d3,2,d2,2}$	S_p
DOXCBR1	0.00076 (93)	1.02 (13)	2.825 (28)	1.41451 (28)	0.04744
%Δ	31.03	2.82	3.44	-3.64	
$\boldsymbol{k}^{(4)}_{DOX,2,CBR1,2\|d4,2}$ [e]	$\boldsymbol{\Gamma}^{(4)}_{DOX,2,CBR1,2\|d4,2}$ [f]	$\boldsymbol{A}^{(4,DOX)}_{DOX,2,CBR1,2\|d4,2}$	$\boldsymbol{B}^{(4,DOX)}_{DOX,2,CBR1,2\|d4,2}$	$\boldsymbol{A}^{(5,CBR1)}_{DOX,2,CBR1,2\|d4,2}$	$\boldsymbol{B}^{(5,CBR1)}_{DOX,2,CBR1,2\|d4,2}$
0.0113 (30)	0.0070 (61)	3.2322 (15)	3.002 (14)	0.00172 (60)	0.0000 (94)
2.45%	-84.44%	-0.33%	21.20%	-38.57%	-100%

units of:
[a] $\left[\frac{\mu\text{mol}}{\text{m}^2}\right]^{1-A^{(1,p1)}_{Type,2,0}}\text{min}^{-1}$ [b] $\left[\frac{\mu\text{mol}}{\text{m}^2}\right]^{-B^{(1,p1)}_{Type,2,0}}$ [c] $\left[\frac{\mu\text{mol}}{\text{m}^2}\right]^{1-A^{(3,p1)}_{Type,2\|\|d3,2,d2,2}}\text{min}^{-1}$ [d] $\left[\frac{\mu\text{mol}}{\text{m}^2}\right]^{-B^{(3,p1)}_{Type,2\|\|d3,2,d2,2}}$
[e] $\left[\frac{\mu\text{mol}}{\text{m}^2}\right]^{1-(A^{(4,DOX)}_{DOX,2,CBR1,2\|d4,2}+A^{(5,CBR1)}_{DOX,2,CBR1,2\|d4,2})}\text{min}^{-1}$ [f] $\left[\frac{\mu\text{mol}}{\text{m}^2}\right]^{-(B^{(4,DOX)}_{DOX,2,CBR1,2\|d4,2}+B^{(5,CBR1)}_{DOX,2,CBR1,2\|d4,2})}$ [g] $\left[\text{L}\cdot\text{m}^{-2}\right]$
where:
$d2 = DOL$ $d3 = CBR1$ $d4 = DOXCBR1$

to the baseline are presented. The greatest change to the DOX parameters corresponds to the saturable elimination and distribution terms. Unlike the combined gender group where the elimination kinetics of DOX does not change regardless of the amount of the molecule in the compartment, in the women group the parameters suggests that the elimination kinetics fluctuates between a high and low concentration phase depending on the amount of DOX in the compartment. This also holds for the metabolism process. In both processes, the high concentration PK can be described by exponents $A - B \approx 0.51$. The reduced saturation term of plasma distribution suggests that the distribution of DOX in women is faster than the baseline average. The changes in the DOL parameters suggest that the high concentration PK of the drug changes in women, and may be characterized by increased plasma distribution, elimination and redistribution. The complex dissociation terms suggest that the DOL is produced more rapidly in women than the baseline. The parameters show that the PK of DOX and DOL is altered by the gender of the patients consistent with Dobbs *et al.* [103] findings. The changes to the baseline parameters suggest that the high concentration PK of DOX have the greatest changes. Conversely, the high and low concentration PK of DOL is altered by patients' gender. Specifically, the redistribution of catalyzed DOL to

plasma, distribution of plasma DOL to tissues and organs, and elimination of DOL, which may describe the entrapment or elimination of the molecule from the body, are all increased in the female group. These, alongside the increased rate of dissociation, may be responsible for the greater exposure to DOL observed by Liu *et al.* [105].

Table 4.5: Two-compartment model case 2 parameters of DOX and DOL in female breast cancer patients.

Type (ci,*cf*)	$\boldsymbol{k}^{(1,p1)}_{Type,ci,cf}$ [a]	$\boldsymbol{\Gamma}^{(1,p1)}_{Type,ci,cf}$ [b]	$\boldsymbol{A}^{(1,p1)}_{Type,ci,cf}$	$\boldsymbol{B}^{(1,p1)}_{Type,ci,cf}$	$V_{d,Type}$ [g]
DOX (1,2)	0.0661 (63)	0.0115 (89)	3.143 (16)	2.957 (16)	5.38 (12)
%Δ	26.77	-554.78	-4.14	1.11	3.16
DOX (2,0)	0.518 (31)	0.285 (43)	1.671 (31)	1.163 (44)	
%Δ	-7.92	100	4.85	4.46	
DOX (2,1)	0.934 (31)	0.263 (16)	1.507 (20)	1.137 (22)	
%Δ	-2.78	-1.14	-6.18	4.13	
DOL (1,2)	0.00267 (63)	0.0000078 (14)	2.71 (43)	1.548 (18)	12.515 (26)
%Δ	28.83	-100	1.85	0.61	-0.04
DOL (2,0)	0.395 (51)	0.2628 (19)	2.5364 (43)	1.761 (11)	
%Δ	60.41	6.89	-2.19	5.57	
DOL (2,1)	0.0009 (62)	0.0000 (30)	2.861 (44)	N/A**	
%Δ	84.44	0	3.84	-0.36	
Type	$\boldsymbol{k}^{(3,p1)}_{Type,2\|\|d3,2,d2,2}$ [c]	$\boldsymbol{\Gamma}^{(3,p1)}_{Type,2\|\|d3,2,d2,2}$ [d]	$\boldsymbol{A}^{(3,p1)}_{Type,2\|\|d3,2,d2,2}$	$\boldsymbol{B}^{(3,p1)}_{Type,2\|\|d3,2,d2,2}$	S_p
DOXCBR1	0.485978 (12)	0.8905 (62)	2.9979 (10)	1.256 (25)	0.0467
%Δ	47.12	-8.93	5.28	-11.46	

$\boldsymbol{k}^{(4)}_{DOX,2,CBR1,2\|d4,2}$ [e]	$\boldsymbol{\Gamma}^{(4)}_{DOX,2,CBR1,2\|d4,2}$ [f]	$\boldsymbol{A}^{(4,DOX)}_{DOX,2,CBR1,2\|d4,2}$	$\boldsymbol{B}^{(4,DOX)}_{DOX,2,CBR1,2\|d4,2}$	$\boldsymbol{A}^{(5,CBR1)}_{DOX,2,CBR1,2\|d4,2}$	$\boldsymbol{B}^{(5,CBR1)}_{DOX,2,CBR1,2\|d4,2}$
0.633 (17)	0.284 (16)	1.670 (19)	1.1627 (31)	0.00324 (23)	0.0000 (24)
-0.16%	100%	4.85%	4.46%	-54.32%	-100%

units of:
[a] $\left[\frac{\mu\text{mol}}{\text{m}^2}\right]^{1-A^{(1,p1)}_{Type,ci,cf}}\text{min}^{-1}$ [b] $\left[\frac{\mu\text{mol}}{\text{m}^2}\right]^{-B^{(1,p1)}_{Type,ci,cf}}$ [c] $\left[\frac{\mu\text{mol}}{\text{m}^2}\right]^{1-A^{(3,p1)}_{Type,2\|\|d3,2,d2,2}}\text{min}^{-1}$ [d] $\left[\frac{\mu\text{mol}}{\text{m}^2}\right]^{-B^{(3,p1)}_{Type,2\|\|d3,2,d2,2}}$
[e] $\left[\frac{\mu\text{mol}}{\text{m}^2}\right]^{1-(A^{(4,DOX)}_{DOX,2,CBR1,2\|d4,2}+A^{(5,CBR1)}_{DOX,2,CBR1,2\|d4,2})}\text{min}^{-1}$ [f] $\left[\frac{\mu\text{mol}}{\text{m}^2}\right]^{-(B^{(4,DOX)}_{DOX,2,CBR1,2\|d4,2}+B^{(5,CBR1)}_{DOX,2,CBR1,2\|d4,2})}$ [g] $\left[\text{L}\cdot\text{m}^{-2}\right]$
where:
$d2 = DOL$ $d3 = CBR1$ $d4 = DOXCBR1$
**The parameter is indeterminate because the saturation parameter is zero.

Figure 4.3 shows the comparison of plasma concentration-time curves of DOX and DOL for both the one-compartment and two-compartment models using parameters from Tables 4.4 and 4.5. The green curves are plotted from the one-compartment model parameters, and the red curves are plotted from the two-compartment model parameters. There is good agreement with the DOL data over all the range of concentration. At the terminal phase of the curves, the DOL concentration slightly exceeds the DOX levels.

Table 4.6 shows the PK parameters of the molecules using the model fits in Tables 4.4

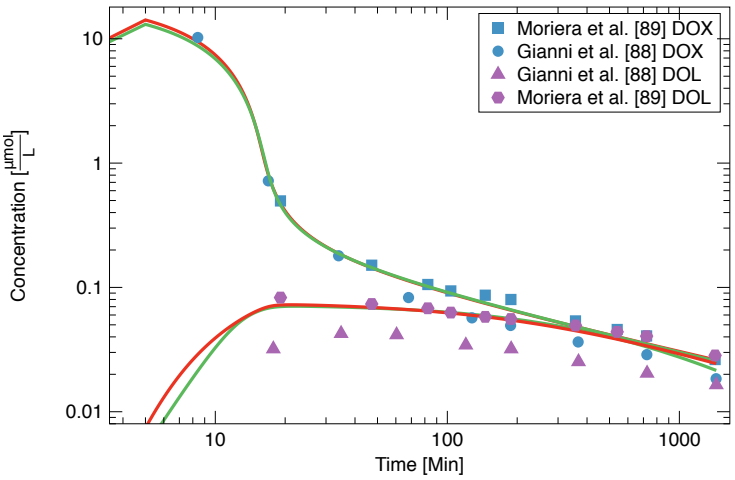

Figure 4.3: Comparison of theoretical and experimental concentrations of DOX and DOL in female cancer patients from the parameter fits.

and 4.5, the values in brackets are the percentage changes to the parameters from the baseline one and two-compartment model calculations in Table 4.1. The table shows that adjusting the DOX and DOL parameters for gender did not result in a noticeable change to the PK parameters from our baseline model.

Table 4.6: Comparison of the theoretical and experimental parameters of DOX and DOL in women.

	Moriera *et al.* [89]			Gianni *et al.* [88]		
Parameter	1C2 (Δ%BL)	2C2 (Δ%BL)	clin	1C2 (Δ%BL)	2C2 (Δ%BL)	clin
DOX						
AUC ($\mu mol \cdot l^{-1} \cdot h$)	4.25 (↑ 4.6)	4.47 (↑ 10.09)	2.19 ± 0.86	4.25 (↑ 4.6)	4.47 (↑ 10.09)	3.6 ± 0.8
C_{max} ($\mu mol \cdot l^{-1}$)	0.067** (↓ 4.29)	0.067** (↓ 4.29)	0.070 ± 0.02**	13.07 (↑ 6.95)	14.17 (↑ 10.27)	10.5 ± 1.8
$t^d_{1/2}$ (min)	5.32 (↑ 34.34)	5.24 (↑ 61.23)	N/A	5.32 (↑ 34.34)	5.24 (↑ 61.23)	3.8 ± 0.3
$t^e_{1/2}$ (h)	37.07 (↑ 15.67)	38.55 (↑ 7.71)	35.2 ± 19.5	37.07 (↑ 15.67)	38.55 (↑ 7.71)	48 ± 23
DOL						
AUC ($\mu mol \cdot l^{-1} \cdot h$)	0.89 (↑ 14.10)	0.90 (↑ 5.88)	0.82 ± 0.21	0.89 (↑ 14.10)	0.90 (↑ 5.88)	0.54 ± 0.2
C_{max} ($\mu mol \cdot l^{-1}$)	0.056** (↑ 30.2)	0.055** (↑ 19.57)	0.06 ± 0.02**	0.071 (↑ 44.16)	0.072 (↑ 37.26)	0.04 ± 0.02
$t^d_{1/2}$ (min)	643.03 (↓ 39.93)	611.83 (↓ 56.19)	N/A	643.03 (↓ 39.93)	611.83 (↓ 56.19)	N/A
$t^e_{1/2}$ (h)	24.16 (↓ 32.78)	32.97 (↑ 14.20)	27.4 ± 14.5	24.16 (↓ 32.78)	32.97 (↑ 14.20)	28 ± 7

N/A = Not provided for the study.
** Measured plasma concentration 3 hours after infusion.

4.4 Effect of Body Weight on DOX PK

One of the factors that may be responsible for DOX related cardiotoxicity is obesity. Obesity may be defined as a condition characterized by excess body weight. Globally,

obesity affects over 13% of the population [106] and has been associated with increased risk of certain types of cancers [107]. Rodvold *et al.* [92] reported reduced clearance of DOX in overweight cancer patients, however, the study did not specify the increase in toxicity profile of these patients. The study included twenty-one adult cancer patients. All the patients received DOX as part of a combined chemotherapy regimen to treat solid tumours. The gender distribution of the study was eight male and thirteen female patients and DOX PK was analyzed based on the percentage ideal bodyweight. In the study, they defined the ideal body weight (IBW) as 110 lb $\pm$ 5 lb per inch above or below 5 feet height for men, and 100 lb $\pm$ 5 lb per inch above or below 5 feet height for women. The patients were grouped into classes depending on their weight category as normal weight ($<$ 115% IBW), mildly obese (115% to 130% IBW), and obese ($>$ 130% IBW), and were administered a DOX dose of 58 ± 10 mg $\cdot$ m^{-2} over one hour. Using the one and two-compartment four-molecule model parameters to simulate DOX infusion, the concentration curves of DOX and DOL for the patients in the study are shown in figure 4.4. The figure shows that the models predict the concentrations of DOX reasonably well for the patient group. However, there is a noticeably poor fit of DOL for all the patients.

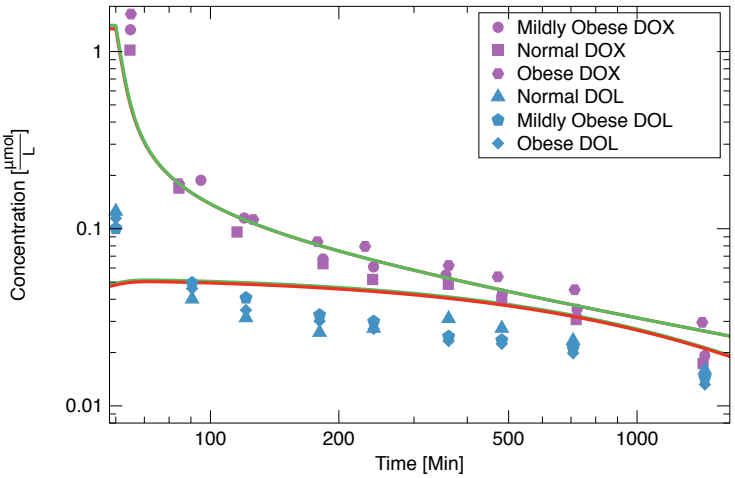

Figure 4.4: Concentrations of DOX and DOL in normal weight and overweight patients using the baseline one (green) and two-compartment (red) case 2 parameters. The curves corresponds to an infusion of 1.84 μmol $\cdot$ m^{-2} $\cdot$ min^{-1} DOX.

The PK parameters of DOX using the one and two-compartment models are shown in Table 4.7. The one-compartment model performs well in predicting the relevant parameters of the molecules in the patients in all weight groups. The two-compartment model resulted in an increased AUC and $C_{\max}$ compared to the one-compartment model.

Table 4.7: Comparison of the theoretical and experimental parameters of DOX and DOL using Rodvold *et al.* [92] study.

	Normal weight			Mildly Obese			Obese		
Parameter	1C2	2C2	clin	1C2	2C2	clin	1C2	2C2	clin
DOX									
AUC (μmol$\cdot$l$^{-1}\cdot$h)	3.00	3.20	2.18 ± 0.44	3.00	3.20	2.68 ± 0.51	3.00	3.20	4.06 ± 2.04
$C_{\max}$ (μmol$\cdot$l^{-1})	1.41	1.56	N/A	1.41	1.56	N/A	1.41	1.56	N/A
$t^d_{1/2}$ (min)	3.03	3.03	N/A	3.03	3.30	N/A	3.03	3.30	N/A
$t^e_{1/2}$ (h)	13.95	16.16	13.0 ± 2.7	13.95	16.16	15.1 ± 5.1	13.95	16.16	20.4 ± 6.6
DOL									
AUC (μmol$\cdot$l$^{-1}\cdot$h)	1.67	3.58	1.29 ± 0.54	1.67	3.58	1.52 ± 0.92	1.67	3.58	1.19 ± 0.51
$C_{\max}$ (μmol$\cdot$l^{-1})	0.05	0.14	N/A	0.05	0.14	N/A	0.05	0.14	N/A
$t^d_{1/2}$ (min)	1038.22	4123.12	N/A	1038.22	4123.12	N/A	1038.22	4123.12	N/A
$t^e_{1/2}$ (h)	40.72	86.63	30.1 ± 16.7	40.72	86.63	30.2 ± 19.7	40.72	86.63	27.1 ± 5.6

N/A = Not provided for the study.

To examine the changes to our model due to body weight, the four-molecule one and two-compartment baseline parameters were fitted to the mildly obese and obese patient groups. The parameters are shown in Table 4.8. According to the parameters, there is a 70% decrease in the saturation parameters of DOX in overweight patients. This suggests that the high-concentration PK of the molecule is most influenced by patient weight. The changes to the DOL and complex parameters suggests that the PK of the molecule may be significantly influenced by patient weight. The elimination and saturation parameters are significantly changed, suggesting that the clearance of DOL is affected by the weight of the patients.

The effect of obesity in female cancer patients can also be observed by fitting the one-compartment case 2 parameters for female patients in Table 4.4 to the obese group. A total of seven female breast cancer patients were included in the study. The new parameters are shown in Table 4.9. The numbers in brackets are the percentage difference from the parame-

Table 4.8: One-compartment model case 2 parameters of DOX and DOL in overweight patients.

Type	$\boldsymbol{k}^{(1,p1)}_{Type,2,0}$ [a]	$\boldsymbol{\Gamma}^{(1,p1)}_{Type,2,0}$ [b]	$\boldsymbol{A}^{(1,p1)}_{Type,2,0}$	$\boldsymbol{B}^{(1,p1)}_{Type,2,0}$	$V_{d,Type}$ [g]
DOX	0.0093 (34)	0.0137 (14)	2.7162 (22)	2.635 (19)	5.7070 (22)
%Δ	3.33	-69.56	-16.24	6.38	-5.15
DOL	0.5678 (42)	0.00 (19)	2.535 (81)	1.5171**	14.24 (14)
%Δ	122.14	-100	-4.93	-0.68	-0.20
Type	$\boldsymbol{k}^{(3,p1)}_{Type,2\|\|d3,2,d2,2}$ [c]	$\boldsymbol{\Gamma}^{(3,p1)}_{Type,2\|\|d3,2,d2,2}$ [d]	$\boldsymbol{A}^{(3,p1)}_{Type,2\|\|d3,2,d2,2}$	$\boldsymbol{B}^{(3,p1)}_{Type,2\|\|d3,2,d2,2}$	S_p
DOXCBR1	0.00039 (53)	0.9841 (13)	2.8482 (22)	1.3669 (13)	0.0741
%Δ	-32.75	-0.80	3.55	-6.89	
$\boldsymbol{k}^{(4)}_{DOX,2,CBR1,2\|d4,2}$ [e]	$\boldsymbol{\Gamma}^{(4)}_{DOX,2,CBR1,2\|d4,2}$ [f]	$\boldsymbol{A}^{(4,DOX)}_{DOX,2,CBR1,2\|d4,2}$	$\boldsymbol{B}^{(4,DOX)}_{DOX,2,CBR1,2\|d4,2}$	$\boldsymbol{A}^{(5,CBR1)}_{DOX,2,CBR1,2\|d4,2}$	$\boldsymbol{B}^{(5,CBR1)}_{DOX,2,CBR1,2\|d4,2}$
0.0113 (12)	0.0137 (44)	2.716 (19)	2.635 (20)	0.0022 (23)	0.0027 (22)
2.45%	-69.56%	-16.24%	6.38%	-21.43%	22.73%

units of:

[a] $\left[\frac{\mu\text{mol}}{\text{m}^2}\right]^{1-A^{(1,p1)}_{Type,2,0}}\text{min}^{-1}$ [b] $\left[\frac{\mu\text{mol}}{\text{m}^2}\right]^{-B^{(1,p1)}_{Type,2,0}}$ [c] $\left[\frac{\mu\text{mol}}{\text{m}^2}\right]^{1-A^{(3,p1)}_{Type,2\|\|d3,2,d2,2}}\text{min}^{-1}$ [d] $\left[\frac{\mu\text{mol}}{\text{m}^2}\right]^{-B^{(3,p1)}_{Type,2\|\|d3,2,d2,2}}$

[e] $\left[\frac{\mu\text{mol}}{\text{m}^2}\right]^{1-(A^{(4,DOX)}_{DOX,2,CBR1,2\|d4,2}+A^{(5,CBR1)}_{DOX,2,CBR1,2\|d4,2})}\text{min}^{-1}$ [f] $\left[\frac{\mu\text{mol}}{\text{m}^2}\right]^{-(B^{(4,DOX)}_{DOX,2,CBR1,2\|d4,2}+B^{(5,CBR1)}_{DOX,2,CBR1,2\|d4,2})}$ [g] $\left[\text{L}\cdot\text{m}^{-2}\right]$

where:

$d2 = DOL$ $d3 = CBR1$ $d4 = DOXCBR1$

**The parameter is indeterminate because the rate parameter is zero.

ters in Table 4.4. According to the parameters, the saturation parameter of DOL showed the greatest change from the women baseline, suggesting that the elimination of the molecule at high concentration is affected by weight in women cancer patients treated with DOX. There is an increased contribution of the enzymes to the metabolism of DOX suggesting increased enzyme activity in overweight patients. Similarly, there is an increased elimination rate constants and saturation parameters of DOL, suggesting that the drug may be eliminated slower at high concentration in overweight female patients. At low concentrations, the parameters suggest a faster terminal clearance of the drug in this group of patients. Likewise, the enzyme dissociation terms show that the dissociation rate constant is reduced from the baseline suggesting that the complex dissociation may be slower in obese patients than the women baseline.

4.5 Effect of Liver Impairment on DOX PK

The liver is the major metabolism site of DOX, therefore the accumulation of the drug due to liver impairment may affect the occurrence of toxicity. Benjamin *et al.* [108] reported

Table 4.9: One-compartment model case 2 parameters of DOX and DOL in female breast cancer patients.

Type	$\boldsymbol{k}^{(1,p1)}_{Type,2,0}$ [a]	$\boldsymbol{\Gamma}^{(1,p1)}_{Type,2,0}$ [b]	$\boldsymbol{A}^{(1,p1)}_{Type,2,0}$	$\boldsymbol{B}^{(1,p1)}_{Type,2,0}$	$V_{d,Type}$ [g]
DOX	0.0100 (12)	0.0125 (22)	3.4560 (13)	3.4818 (22)	5.58 (14)
%Δ	7.30	78.57	6.92	15.97	-7.15
DOL	0.3834 (10)	0.0429 (43)	2.854 (34)	1.462 (70)	14.246 (43)
%Δ	71.93	7688.70	-16.47	-3.50	0.53
Type	$\boldsymbol{k}^{(3,p1)}_{Type,2\|\|d3,2,d2,2}$ [c]	$\boldsymbol{\Gamma}^{(3,p1)}_{Type,2\|\|d3,2,d2,2}$ [d]	$\boldsymbol{A}^{(3,p1)}_{Type,2\|\|d3,2,d2,2}$	$\boldsymbol{B}^{(3,p1)}_{Type,2\|\|d3,2,d2,2}$	S_p
DOXCBR1	0.00033 (10)	0.997 (82)	3.090 (16)	1.032 (24)	0.04012
%Δ	-56.58	-4.90	9.37	-27.04	
$\boldsymbol{k}^{(4)}_{DOX,2,CBR1,2\|d4,2}$ [e]	$\boldsymbol{\Gamma}^{(4)}_{DOX,2,CBR1,2\|d4,2}$ [f]	$\boldsymbol{A}^{(4,DOX)}_{DOX,2,CBR1,2\|d4,2}$	$\boldsymbol{B}^{(4,DOX)}_{DOX,2,CBR1,2\|d4,2}$	$\boldsymbol{A}^{(5,CBR1)}_{DOX,2,CBR1,2\|d4,2}$	$\boldsymbol{B}^{(5,CBR1)}_{DOX,2,CBR1,2\|d4,2}$
0.0122 (32)	0.0125 (18)	3.456 (12)	3.482 (34)	0.0039 (16)	0.0037 (22)
7.96%	78.57%	6.92%	15.97%	126.74%	

units of:

[a] $\left[\frac{\mu\text{mol}}{\text{m}^2}\right]^{1-A^{(1,p1)}_{Type,2,0}}\text{min}^{-1}$ [b] $\left[\frac{\mu\text{mol}}{\text{m}^2}\right]^{-B^{(1,p1)}_{Type,2,0}}$ [c] $\left[\frac{\mu\text{mol}}{\text{m}^2}\right]^{1-A^{(3,p1)}_{Type,2\|d3,2,d2,2}}\text{min}^{-1}$ [d] $\left[\frac{\mu\text{mol}}{\text{m}^2}\right]^{-B^{(3,p1)}_{Type,2\|d3,2,d2,2}}$

[e] $\left[\frac{\mu\text{mol}}{\text{m}^2}\right]^{1-(A^{(4,DOX)}_{DOX,2,CBR1,2\|d4,2}+A^{(5,DOX)}_{DOX,2,CBR1,2\|d4,2})}\text{min}^{-1}$ [f] $\left[\frac{\mu\text{mol}}{\text{m}^2}\right]^{-(B^{(4,CBR1)}_{DOX,2,CBR1,2\|d4,2}+B^{(5,CBR1)}_{DOX,2,CBR1,2\|d4,2})}$ [g] $\left[\text{L}\cdot\text{m}^{-2}\right]$

where:

$d2 = DOL$ $d3 = CBR1$ $d4 = DOXCBR1$

**The parameter is indeterminate because the rate constant is zero.

an increased incidence of DOX-related toxicity in patients with significantly impaired liver function. To investigate the effect of the liver impairment on the PK of DOX compared to the baseline average, the one-compartment model case 2 parameters were used to simulate DOX concentration curves in patients administered 58.7 $\text{mg}\cdot\text{m}^{-2}$ and 59.1 $\text{mg}\cdot\text{m}^{-2}$ DOX over one hour. The curves are compared with the measured concentrations from the Piscitelli *et al.* [67] study of thirty-five small cell lung cancer patients treated with DOX. Four of the patients registered in the study measured bilirubin levels ≥ 1.4 $\text{mg}\cdot\text{dl}^{-1}$ and were classified in the liver impairment group. The curves in Figure 4.5 were plotted using the one-compartment model case 2 parameters. The figure shows a good agreement of our model-predicted concentration with clinical data for patients with normal liver function. The data points of the liver impaired patients show a doubling of the predicted concentrations.

In Table 4.10, the PK parameters of DOX corresponding to the curves in Figure 4.5 are presented. It is seen that the PK parameters from the model agree with the clinical values for the normal liver function group.

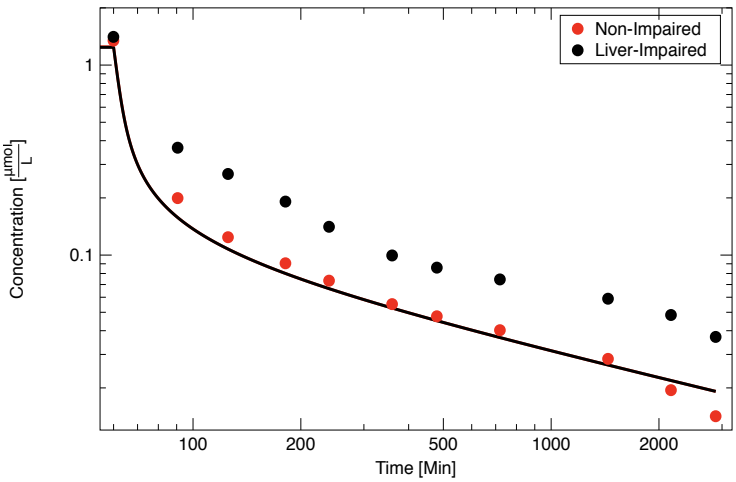

Figure 4.5: Theoretical and experimental concentrations of DOX and DOL using the parameters from Table 3.30. The curves and data points represent infusions of 1.81 $\mu mol/m^2/min$(red) and 1.80 $\mu mol/m^2/min$ (black) DOX over one hour.

Table 4.10: Comparison of the theoretical and experimental parameters of DOX in liver impaired and un-impaired patients.

	Normal		Liver Dysfunction	
Parameter	1C2	clin	1C2	clin
DOX				
AUC $(\mu mol \cdot l^{-1} \cdot h)$	4.83	3.37 ± 1.85	4.82	8.48 ± 3.16
$t^d_{1/2}$ (h)	47.23	25.6 ± 16.9	47.23	49.3 ± 33.4

Due to the limited number of available data points in the study, only the single-molecule one-compartment model case 2 parameters was fitted to the DOX data of the liver-impaired group. The parameters that describe the kinetics of DOX in this group are shown in Table 4.11. Comparing the parameters to the baseline shown in Table 3.9, we see that the elimination and saturation terms of DOX are markedly reduced in liver impaired patients. This suggests that the high and low concentration PK of the drug may be influenced by liver function.

Table 4.11: One-compartment model case 2 parameters of DOX in patients with liver impairment.

$k_{DOX,10}^{(1,p1)}$ [a]	$\Gamma_{DOX,10}^{(1,p1)}$ [b]	$A_{DOX,10}^{(1,p1)}$	$B_{DOX,10}^{(1,p1)}$	$V_{d,DOX}$ [c]	S_p
0.0034 (78)	0.0025 (19)	3.027 (23)	2.317 (70)	6.119 (54)	0.0066
-83.00%	-94.44%	-6.66%	-6.46%	1.70%	

units of:
[a] $\left[\frac{\mu\text{mol}}{\text{m}^2}\right]^{1-A_{DOX,10}^{(1,p1)}}\text{min}^{-1}$ [b] $\left[\frac{\mu\text{mol}}{\text{m}^2}\right]^{-B_{DOX,10}^{(1,p1)}}$ [c] $\left[\text{L}\cdot\text{m}^{-2}\right]$

4.6 Effect of Race on PLD PK

To test for the effect of race on the PK of PLD, the parameters of PLD from Table 3.26 were fitted to the Hong *et al.* [84] concentration-time curve. The new parameters are shown in Table 4.12. The parameters in the table describe the PK of PLD alone, and the PK processes of PLD are assumed to be elimination and release of the free drug. The parameters show that the clearance of PLD is a first-order process ($A \approx 1.00$) in Asian cancer patients. When comparing this result with PLD clearance shown in Table 3.27, we notice interesting changes to the parameters. The saturation term is reduce by 100% suggesting a change in the overall PK. Considering that the volume of distribution of the drug is also reduced by 8%, the parameters suggest that race is a significant covariate in the PK of cancer patients treated with PLD. We were not able to compare the race difference in the PK of DOX due to a lack of clinical data for the drug.

Table 4.12: One-Compartment model case 2 parameters of PLD in Asian subjects.

j,k	$k_{\text{PLD},j,k}^{(1,p1)}$ [a]	$\Gamma_{\text{PLD},j,k}^{(1,p1)}$ [b]	$A_{\text{PLD},j,k}^{(1,p1)}$	$B_{\text{PLD},j,k}^{(1,p1)}$	$V_{d,PLD}$ [c]	S_p
2,0	0.0002 (78)	0.0000 (12)	1.0093(78)	N/A**	1.967(23)	0.0181

units of:
[a] $\left[\frac{\mu\text{mol}}{\text{m}^2}\right]^{1-A_{PLD,10}^{(1,p1)}}\text{min}^{-1}$ [b] $\left[\frac{\mu\text{mol}}{\text{m}^2}\right]^{-B_{PLD,10}^{(1,p1)}}$ [c] $\text{L}\cdot\text{m}^{-2}$
**The parameter is indeterminate because the saturation parameter is zero.

Figure 4.6 shows the plot of PLD concentration against time using the data from Table 4.12. The curves show a first-order elimination of the molecule, and a good fit of theory to clinical data.

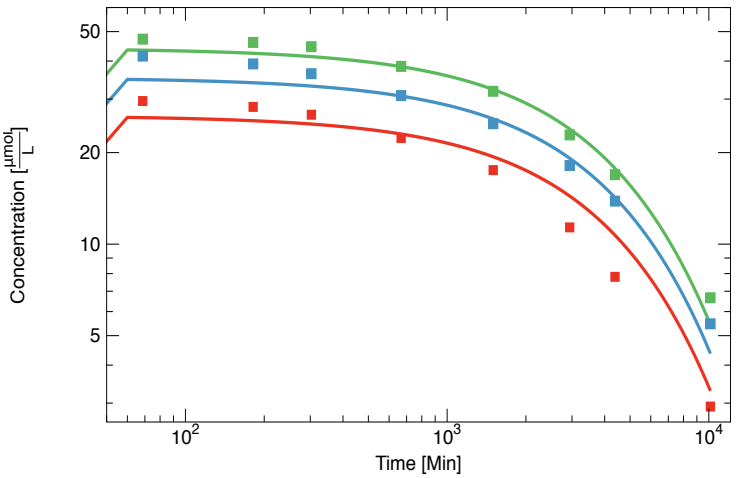

Figure 4.6: Theoretical and clinical concentrations of PLD in Asian subjects. The curves and data points represent PLD infusions of 0.86 $\mu mol/m^2/min$(red), 1.15 $\mu mol/m^2/min$(blue), and 1.43 $\mu mol/m^2/min$(green) over one hour. The data have been digitized from Hong *et al.* [84]. study.

4.7 Summary

In this chapter, the parameters of the model have been used to simulate clinical studies to observe how well the model predicts clinical behaviour in the presence of specific covariates. The four-molecule, one and two-compartment models were simulated for DOX and DOL analysis and the two-molecule, one-compartment model was used to analyze DOX and PLD PK. It is observed that the PK process of DOX and DOL changes when considering covariates such as gender, weight, and liver impairment. However, the baseline model parameters predicted the parameters of both drugs within an acceptable range of the clinical measurements. This suggests that the model can predict the efficacy or toxicity of different dosages of DOX. The parameters that describe the PK of PLD suggests that race affects the overall PK of the molecule. The parameters suggest that the PK of the molecule in Asian patients is a first-order process, and is characterized by a reduced volume of distribution.

Chapter 5

Conclusion

The simplest solution is usually the right one.

– Occam's Razor

The main objective of this thesis was to model DOX and its major metabolite using a saturable model with variable exponents. Previous studies have reported a high degree of variability in the PK of DOX [93, 95], specifically with respect to the inability of models from previous studies to characterize the drug's PK when applied to new sets of patients. In all of these studies, classical kinetic models with first-order elimination and distribution were to categorize the PK of the drug in the body. In this work, we have used a saturable PK model of DOX with fractal effects to fit the parameters of the model against previous clinical values of the drug concentration to gain insight into the PK processes and the important parameters. The one, two and three-compartment model parameters of DOX and DOL have been developed, these parameters are developed to give a clearer understanding of the various PK processes and to analyze the behaviour of the drug within each compartment in the models.

The first step in modelling the PK of DOX was to develop the parameters of a baseline data set, which represents the contribution of several covariates to the PK of DOX over several published studies. The baseline data set represented a range of DOX dose, infusion time, patient characteristics and cancer types, and corresponds to a population PK approach,

which helps to reduce the influence of inter-patient variations on the overall PK. Developing the parameters with the baseline datasets presents a generally accepted description of the body-drug relationship. The baseline data sets were first fitted to the clinical curves using the Michaelis-Menten type kinetic processes for the one, two and three-compartment models. These models produced a poor fit to the baseline in all the cases. Analysis of the concentration-time curves of individual studies showed the presence of a power-law relationship of DOX concentration and time. Therefore, the initial estimates of the initial and final slopes were calculated and provided a useful starting point of the exponents of our models. When modelling the individual data sets, the exponent parameters showed a good agreement with theoretical data for all the datasets. With this result, the single-process parameters of the one, two and three-compartment models were developed for the baseline. These initial processes are consistent regardless of the number of compartments used for the analysis. The addition of extra terms to the single process parameters from the models resulted in a reduced variance, suggesting a better fit to the clinical data than the single-process case, however these did not produce noticeably better fit of the theoretical curves to the clinical data. Likewise, when considering the model drug interactions, we did not notice any obvious improvement in the fit of the DOX theory curves when compared with the clinical measurements.

We find that the most interesting insight from this work is that the PK process of DOX is not exclusively first-order, but a contribution of different processes depending on the concentration of DOX in the compartment. When comparing the PK parameters of the drug in using the multi-compartment models, we observe that the two-compartment and three-compartment models, while fitting better with the $C_{\max}$ data do not improve on the AUC from the single-compartment case.

When modelling DOL using the four-molecule models, we inferred from the parameters that DOL, like DOX, may be described by concentration-dependent PK processes. The one, two and three-compartment parameters modelled DOL reasonably well. The analysis of the

effects of the covariates on DOX and DOL shows that all the covariates tested influenced the parameters of the models. We observed that the high concentration PK parameters of DOX and DOL changed the most when adjusting the parameters for the patient's gender. Likewise, obesity and liver impairment both result in reduced elimination of DOX from the body. Analysis of the PK parameters from the multi-molecule models suggests that the one-compartment, four-molecule model can predict the PK parameters of the drug with an acceptable degree of accuracy in patients.

Some limitations of this work should be mentioned. Firstly, in datasets with varying administered doses, we have taken the average of the recorded doses and used it as the representative dose of those datasets. This may have influenced some of the model results in this work. Secondly, the lack of sufficient clinical concentration data for DOX when encapsulated DOX was administered did not allow for a detailed study of the PK of the drug in this work. Thirdly, the insufficient high concentration data point measurements from clinical studies may have resulted in an underestimation of the maximum concentration of the molecules in this work. Lastly, there was no readily available data on the amount of CBR1 binding to DOX, so we have assumed an initial estimate of 100 μmol.

We have left some additional investigations for the future due to timing constraints. These investigations are related to an in-depth analysis of particular processes, the introduction of new compartments or investigation of the influence of some of the parameters. Some of these include the interaction of DOX with DOL and if the PK of one changes relative to the other. Likewise, we expect to notice interesting insight when adjusting the model parameters for the effect of reduced amount of enzymes on the parameters of DOX and DOL, and the application of the model to a multi-drug PK DOX and other anticancer drugs.

In summary, the model presented in this work has been able to characterize the PK processes of DOX and DOL with a reasonable degree of accuracy. The one, two and three-compartment model parameters have been presented and compared to clinical data;

as well as, an investigation of the effects of covariates such as gender, race, weight and liver-impairment on the PK of the molecules.

Bibliography

[1] A. Jemal, F. Bray, M. M. Center, J. Ferlay, E. Ward, and D. Forman. Global cancer statitics. *CA cancer Journal for clinicians*, 61(2):69–90, 2011.

[2] R. L. Seigel, K. Miller, and A. Jemal. Cancer statitics 2017. *CA Cancer J clin*, 67(1):7–30, 2017.

[3] Canada Cancer Statistics Advisory Board. Canadian cancer statistics 2018. http://www.cancer.ca/Canadian-Cancer-Statistics-2018-EN, 2018.

[4] Kevin Harrington. The biology of cancer. *Medicine*, 44(1):1–5, 2016.

[5] D. Hanahan and R. A. Weinberg. The hallmarks of cancer. *Cell*, 100(1):57–70, 2000.

[6] About Cancer.

[7] W. Zhan, W. Gedroyc, and X. Y. Xu. Mathematical modelling of drug transport and uptake in a realistic model of solid tumour. *Protein Pept Lett*, 21(11):1146–1156, 2014.

[8] Human papillomavirus (HPV) and cervical cancer.

[9] P. George. P53 how crucial is its role in cancer. *International Journal of Current Pharmaceutical Research*, 3(2):19–25, 2011.

[10] R. Kumari, N. Sen, and S. Das. Tumor suppressor p53: Understanding the molecular mechanisms inherent to cancer. *Current Science*, 107(5):786–794, 2014.

[11] J. Mydlo, C. l. Godec, and A. Reese. *Prostate Cancer (Second Edition)*. Academic Press, Oxford, UK, 2016.

[12] Dennis M. Marchiori. *Clinical Imaging*. Elsevier, Amsterdam, Netherlands, 2014.

[13] U. Hamann and C. Ankel. Breast cancer: Diagnostics and therapy - the most important facts for internists. *Dtsch Med Wonchenscher*, 143(4):267–278, 2018.

[14] G. M. Kiebert, A. M. Stiggelbout, J. Kievit, J. W. Leer, C. J. van de Velde, and H. J. de Haes. Choices in oncology: factors that influence patients' treatment preference. *Quality of Life Research: An International Journal of Quality of Life Aspects of Treatment, Care and Rehabilitation*, 3(3):175–182, June 1994.

[15] T. Luo, S. Gaya, F. Johnston, A. Haider, and T. Pawlik. Factors that determine cancer treatment choice among minority groups. *American Society of Clinical Oncology*, 11(3):259–262, 2015.

[16] P Wang, R. Liu, and Z. Jiang. Optimization of combination chemotherapy with dose adjustment using a memetic algorithm. *Information Sciences*, 432:63–78, 2018.

[17] Chemotherapy. https://www.cancer.org/treatment/treatments-and-side-effects/treatment-types/chemotherapy/how-chemotherapy-drugs-work.html.

[18] S. Di Martino, A. Rainone, A. Troise, M. Di Paolo, S. Pugliese, S. Zappavigna, A. Grimaldi, and D. Valente. Overview of fda-approved anti-cancer drugs used for tragetted therapy. *World Cancer Research Journal*, 2(3):1–8, 2015.

[19] S. Jaracz, J. Chen, L. Kuznetsove, and I. Ojima. Recent advances in tumor-targeting anticancer drug conjugates. *Bioorganic and Med Chem*, 13(17):5043–5054, 2005.

[20] A. Gabizon. Liposome circulation time and tumor targeting: implications for cancer chemotherapy. *Advanced Drug Delivery Reviews*, 16(2):285–294, 1995.

[21] F. C. Courtice and D. C. K. Roberts. *The origin of lipoproteins in lymph*. Springer, Boston, MA, 1963.

[22] Y. Matsumura and H. Maeda. A new concept for macromolecular therapeutics in cancer chemotherapy: Mechanism of tumor tropic accumulation of proteins and antitumor agent smancs. *Cancer Research*, 46:6387–6392, 1986.

[23] E. D. Israels and L. G. Israels. The cell cycle. *The Oncologist*, 5(6):510–513, 2000.

[24] K. Collins, T. Jacks, and N Pavletich. The cell cycle and cancer. *PNAS*, 94(7):2778–2779, 1997.

[25] R. Steiner, J. Stewart, M. J. Cantwell, M. Minton, K. Knight, and R. D. Ruben. Adriamycin alone or combined with vincristine in the treatment of advanced breast cancer. *European Journal of Clinical Oncology*, 19(11):1553–1557, 1983.

[26] A. Khodjakov and C. L. Rieder. The nature of cell-cycle checkpoints: facts and fallacies. *Journal of Biology*, 8(10):1–5, 2009.

[27] R. S. Wong. Apoptosis in cancer: from pathogenesis to treatment. *J Exp Clin Cancer Research*, 30:87–95, 2011.

[28] S. Haupt, M. Berger, Z. Goldberg, and Y. Haupt. Apoptosis - the p53 network. *Cell Science*, 116:4077–4085, 2003.

[29] N. Gonen and Y. G. Assaraf. Antifolates in cancer therapy: Structure, activity and mechanisms of drug resistance. *Drug Resistance Updates*, 15(4):183–210, August 2012.

[30] R. Ralhan and J. Kaur. Alkylating agents and cancer therapy. *Expert Opin Ther Pat*, 17(9):1061–1075, 10 2007.

[31] Anthracyclines. https://www.drugbank.ca/categories/DBCAT000874.

[32] N. J. Fauzee. Taxanes: promising anti-cancer drugs. *Asian Pacific journal of cancer prevention : APJCP*, 12(4):837–851, 2011.

[33] R. H. Himes, R. N. Kersey, I. Heller-Bettinger, and F. E. Samson. Action of the Vinca Alkaloids Vincristine, Vinblastine, and Desacetyl Vinblastine Amide on Microtubules in Vitro. *Cancer Research*, 36(10):3798–3802, 1976.

[34] R. Z. Orlowski and D. J. Kuhn. Proteasome Inhibitors in Cancer Therapy: Lessons from the First Decade. *Clinical Cancer Research*, 14(6):1649–1657, March 2008.

[35] R. P. Gehdoo. Anticancer Chemotherapy and it's Anaesthetic Implications (Current Concepts). *Indian Journal of Anaesthesia*, 53(1):18–29, February 2009.

[36] S. B. Kaye. New antimetabolites in cancer chemotherapy and their clinical impact. *British Journal of Cancer*, 78(Suppl 3):1–7, 1998.

[37] Elizabeth Garrett-Mayer, editor. *Fundamental Concepts in Clinical Pharmacology*. Springer New York, New York, NY, 2011.

[38] L. L. Furge and F. P. Guengerich. Cytochrome p450 enzymes in drug metabolism and chemical toxicology. *Biochemistry and Molecular Biology Education*, 34(2):66–74, 2006.

[39] R. S. Foti and K. D. Dalvie. Cytochrome p450 and non–cytochrome p450 oxidative metabolism: Contributions to the pharmacokinetics, safety, and efficacy of xenobiotics. *Drug Metabolism and Disposition*, 44(8):1129–1245, 2016.

[40] R. E. Eliaz, S. Nir, C. Marty, and F. Szoka. Determination and modelling of kinetics of cancer cell killing by doxorubicin and doxorubicin encapsulated in targeted liposomes. *Cancer Research*, 64:711–718, 2004.

[41] WHO. Characterization and application of physiologically based pharmacokinetic models in risk assessment. *International Programme on Chemical Safety*, 2010.

[42] T. Teorell. Kinetics of distribution of substances administered to the body. i.e. the extravascular modes of administration. *Archives Internationales de Pharmacodynamie et de Thérapie*, 57:205–225, 1937.

[43] J. E. Riverie, J. Gabrielsson, M. Fink, and J. Mochel. Mathematical modeling and simulation in animal health. *Vetenary Pharmacoloigy and Therapeutics*, 39(3):213–223, 2016.

[44] L. Michaelis and M. L. Menten. Die kinetik der invertinwirkung. *Biochem Z*, 49:333–369, 1913.

[45] K. A. Johnson and R. S. Goody. The Original Michaelis Constant: Translation of the 1913 Michaelis-Menten Paper. *Biochemistry*, 50(39):8264–8269, October 2011.

[46] R. Kopelman. Fractal reaction kinetics. *Science (New York, N.Y.)*, 241(4873):1620–1626, September 1988.

[47] K. J. Vos, A. G. Martin, M. G. Trimboli, L. Forestell, K. Barakat, and J. A. Tuszynski. A multi-compartment pharmacokinetic model of the interaction between paclitaxel and doxorubicin. *EPJ Nonlinear Biomedical Physics*, 2(1):13, December 2014.

[48] J. Robert. Clinical pharmacokinetics of idarubicin. *Clinical Phamacokinetics*, 24(4):275–288, 1993.

[49] F. Belloc, F. Lacombe, P Domain, F Lopez, P. Bernard, M. Boisseau, and J. Reifers. Intercalation of anthracyclines into living dna analyzed by flow cytometry. *Journal of Quantitative Cell Science*, 13(8):880–885, 1992.

[50] Y. Pommier, E. Leo, H. Zhang, and C. Marchand. Dna topoisomerases and their poisoning by anticancer and antibacterial drugs. *Chemistry and Biology*, 17(5):421 – 433, 2010.

[51] P. Perego, E. Corna, M. De Cesare, L. Gatti, D. Polizzi, G. Pratesi, R. Supino, and F. Zunino. Role of apoptosis and apoptosis-related genes in cellular response and

antitumor efficacy of anthracyclines. *Current Medicinal Chemistry*, 8(1):31–37, January 2001.

[52] H. G. Keizer, H. M. Pinedo, G. J. Schuurhuis, and H. Joenje. Doxorubicin (adriamycin): A critical review of free radical-dependent mechanisms of cytotoxicity. *Pharmacology and Therapeutics*, 47(2):219–231, January 1990.

[53] P. A. Speth, Q. G. van Hoesel, and C. Haanen. Clinical pharmacokinetics of doxorubicin. *Clinical Pharmacokinetics*, 15(1):15–31, July 1988.

[54] D. A. Gewirtz. A critical evaluation of the mechanisms of action proposed for the antitumor effects of the anthracycline antibiotics adriamycin and daunorubicin. *Biochemical Pharmacology*, 57(7):727–741, April 1999.

[55] Fan Yang, Sheila S Teves, Christopher J Kemp, and Steven Henikoff. Doxorubicin, DNA torsion, and chromatin dynamics. *Biochimica et biophysica acta*, 1845(1):84–89, January 2014.

[56] Y. N. Lee, K. K. Chan, P. A. Harris, and J. L. Cohen. Distribution of adriamycin in cancer patients. tissue uptakes, plasma concentration after iv and hepatic ia administration. *Cancer*, 45(9):2231–2239, 1980.

[57] R. F. Ozols, R. C. Young, J. L. Speyer, P. H. Sugarbaker, R. Greene, J. Jenkins, and C. E. Myers. Phase I and Pharmacological Studies of Adriamycin Administered Intraperitoneally to Patients with Ovarian Cancer | Cancer Research. *Cancer Research*, 42(10):4265–4269, October 1989.

[58] A. K. Jain, N. K. Swarnakar, M. Das, C. Godugu, R. P. Singh, P. R. Rao, and S. Jain. Augmented Anticancer Efficacy of Doxorubicin-Loaded Polymeric Nanoparticles after Oral Administration in a Breast Cancer Induced Animal Model. *Molecular Pharmaceutics*, 8(4):1140–1151, August 2011.

[59] R. F. Greene, J. M. Collins, J. F. Jenkins, J. L. Speyer, and C. E. Myers. Plasma Pharmacokinetics of Adriamycin and Adriamycinol: Implications for the Design of in Vitro Experiments and Treatment Protocols. *Cancer Research*, 43(3417-3421):6, 1983.

[60] Wikimedia Commons. Doxorubicin structure, 2008. File: `Doxorubicin-2D-structure.svg`.

[61] A. Andersen, H. Holte, and L. Slordal. Pharmacokinetics and metabolism of doxorubicin after short-term infusions in lymphoma patients. *Cancer Chemother Pharmacol*, 44:422–426, 1999.

[62] M. Weiss. Functional characterization of drug uptake and metabolism in the heart. *Expert Opinion on Drug Metabolism and Toxicology*, 7(10):1295–1306, 2011.

[63] R. S. Benjamin, C. E. Riggs, and N. R. Bachur. Pharmacokinetics and metabolism of adriamycin in man. *Clin Pharmacol Ther.*, 14(4):592–600, 1973.

[64] R. S. Benjamin, C. E. Riggs, and N. R. Bachur. Plasma pharmacokinetics of adriamycin and its metabolites in humans with normal hepatic and renal function. *Cancer Research*, 37(5):1416–1420, 1977.

[65] P. M. Sokolove. Interactions of Adriamycin aglycones with mitochondria may mediate Adriamycin cardiotoxicity. *International Journal of Biochemistry*, 26(12):1341 – 1350, 1994.

[66] G. Di Fronzo, L. Lenaz, and G. Bonadonna. Distribution and excretion of adriamycin in man. *Biomedicine*, 19(4):169–171, 1973.

[67] S. C. Piscitelli, K. A. Rodvold, D. A. Rushing, and D. A. Tewksbury. Pharmacokinetics and pharmacodynamics of doxorubicin in patients with small cell lung cancer. *Clinical Pharmacology & Therapeutics*, 53(5):555–561, 1993.

[68] Kin Tam. The Roles of Doxorubicin in Hepatocellular Carcinoma. *ADMET and DMPK*, 1(3), August 2013.

[69] S. Eksborg. Pharmacokinetics of anthracyclines. *Acta oncol*, 28(6):873–876, 1989.

[70] K. K. Chan, R. T. Chlebowski, M. Tong, H. S. Chen, J. F. Gross, and J. R. Bateman. Clinical pharmacokinetics of adriamycin in hepatoma patients with cirrhosis. *Cancer Research*, 40(4):1263–1268, 1980.

[71] R. C. Boston and D. R. Phillips. Evidence of possible does-dependent doxorubicin plasma kinetics in man. *Cancer Treatment Reports*, 67(1):63–69, Jan 1983.

[72] C. Carvalho, R. X. Santos, S. Cardoso, and S. et al. Correia. Doxorubicin: The good, the bad and the ugly effect. *Current Medicinal Chemistry*, 16(25):3267–3285, 2009.

[73] D. D. Von Hoff, M. W. Layard, P. Basa, H. L. Davis, A. L. Von Hoff, M. Rozencweig, and F. M. Muggia. Risk factors for doxorubicin-induced congestive heart failure. *Annals of Internal Medicine*, 91(5):710–717, November 1979.

[74] K. Chatterjee, J. Zhang, N. Honbo, and J. S. Karliner. Doxorubicin cardiomyopathy. *Cardiology*, 115(2):155–162, 2010.

[75] G. W. Sledge, D. Neuberg, P. Bernardo, J. N. Ingle, S. Martino, E. K. Rowinsky, and W. C. Wood. Phase iii trial of doxorubicin, paclitaxel, and the combination of doxorubicin and paclitaxel as front-line chemotherapy for metastatic breast cancer: An intergroup trial (e1193). *Journal of Clinical Oncology*, 21(4):588–592, 2003. PMID: 12586793.

[76] S. P. Ackland, M. J Ratain, N. J. Vogelzang, K. E. Choi, M. Ruane, and J. A. Sinkule. Pharmacokinetics and pharmacodynamics of long-term continuous-infusion doxorubicin. *Clinical Pharmacology and Therapeutics*, 45(4):340–347, 1989.

[77] G. Freyer, B. Ligneau, B. Tranchand, C. Ardiet, F. Serre-Debeauvais, and V. Trillet-Lenoir. Pharmacokinetic studies in cancer chemotherapy: usefulness in clinical practice. *Cancer Treatment Reviews*, 23(3):153–169, May 1997.

[78] R. M. O'Bryan, L. H. Baker, J. E. Gottlieb, S. E. Rivkin, S. P. Balcerzak, G. N. Grumet, S. E. Salmon, T. E. Moon, and B. Hoogstraten. Dose response evaluation of adriamycin in human neoplasia. *Cancer*, 39(5):1940–1948, 1977.

[79] N. L. Boman, P. R. Cullis, M. B. Bally, and L. D. Mayer. Preclinical and clinical activity of liposomal doxorubicin.

[80] Joyce A. O'Shaughnessy. Pegylated liposomal doxorubicin in the treatment of breast cancer. *Clinical Breast Cancer*, 4(5):318 – 328, 2003.

[81] M. O'Brien, N. Wigler, M. Inbar, R. Rosso, E. Grischke, A. Santoro, R. Catane, D. Kieback, P. Tomczak, S. Ackland, F. Orlandi, L. Mellars, L. Alland, and C. Tendler. Reduced cardiotoxicity and comparable efficacy in a phase iii trial of pegylated liposomal doxorubicin hcl (caelyx/doxil) versus conventional doxorubicin for first-line treatment of metastatic breast cancer. *Annals of oncology : official journal of the European Society for Medical Oncology / ESMO*, 15:440–449, 03 2004.

[82] J. W. Cowens, P. J. Creaven, W. R. Greco, D. E. Brenner, Y. Tung, M. Ostro, F. Pilkiewicz, R. Ginsberg, and N. Petrelli. Initial clinical (phase i) trial of tlc d-99 (doxorubicin encapsulated in liposomes). *Cancer Research*, 53(12):2796–2802, 1993.

[83] K. Mross, P. Maessen, W. J. van der Vijgh, H. Gall, E. Boven, and H. M. Pinedo. Pharmacokinetics and metabolism of epidoxorubicin and doxorubicin in humans. *Journal of Clinical Oncology*, 6(3):517–526, 1988. PMID: 3162516.

[84] R. L. Hong and Y. L Tseng. Phase i and pharmacokinetic study of a stable, polyethylene-glycolated liposomal doxorubicin in patients with solid tumors. *Cancer*, 91(9):1826–1833, 2001.

[85] D. M. Vail, M. A. Amantea, G. T. Colbern, F. J. Martin, R. A. Hilger, and P. K. Working. Pegylated liposomal doxorubicin: Proof of principle using preclinical animal models and pharmacokinetic studies. *Seminars in Oncology*, 31(13):16 – 35, 2004.

[86] A. Gabizon and F. Martin. Polyethylene Glycol-Coated (Pegylated) Liposomal Doxorubicin. *Drugs*, 54(4):15–21, October 1997.

[87] A. Bode and Z. Dong. Recent advances in precision oncology research. *npj Precision Oncology*, 2:1–11, 2018.

[88] L. Gianni, L. Vigano, A. Locatelli, G. Capri, A. Giani, E. Tarenzi, and G. Bonadonna. Human pharmacokinetic characterization and in vitro study of the interaction between doxorubicin and paclitaxel in patients with breast cancer. *Journal of Clinical Oncology: Official Journal of the American Society of Clinical Oncology*, 15(5):1906–1915, May 1997.

[89] A. Moreira, R. Lobato, J. Morais, S. Silva, J. Ribeiro, A. Figueira, D. Vale, C. Sousa, F. Araujo, A. Fernandes, J. Oliveira, and J. L. Passos-Coelho. Influence of the interval between the administration of doxorubicin and paclitaxel on the pharmacokinetics of these drugs in patients with locally advanced breast cancer. *Cancer Chemotherapy and Pharmacology*, 48(4):333–337, October 2001.

[90] G. T. Wurz, L. Soc, V. D. Emshoff, T. B. Cadman, and M. W. DeGregorio. Pharmacokinetic analysis of high-dose toremifene in combination with doxorubicin. *Cancer Chemother Pharmacol*, 42(5):363–366, 1998.

[91] P. A. J. Speth, P. C. M. Linssen, R. S. G. Holdrinet, and C. Haanen. Plasma and cellular concentration of adriamycin in patients with myeloma treated with 96-hrs continuous infusion. *Clinical Pharmacology and Therapeutic*, 41(6):661–665, 1987.

[92] K. A. Rodvold, A. D. Rushing, and D. A. Tewksbury. Doxorubicin clearance in the obese. *Journal of Clinical Oncology*, 6:1321–1327, 1988.

[93] C. J. Twelves, N. A. Dobbs, A. Aldhous, P. G. Harper, R. D. Rubens, and Riehards M. A. Comparative pk of doxorubicin given by different schedules with equal dose intensity in patients with breast cancer. *Journal of Clinical Oncology*, 28:302–307, 1991.

[94] J. Wihlm, J. M. Limacher, D. Leveque, B. Duclos, P. Dufour, J. P. Bergerat, and G. Methlin. Pharmacokinetics of high dose doxorubicin administered as a 6-h iv infusion in breast cancer patients. *Bulletin Du Cancer*, 84(6):603–608, June 1997.

[95] R. Erttmann, N. Erb, A. Steinhoff, and G. Landbeck. Pk of doxorubicin in man: Dose and schedule dependence. *J Cancer Res Clin Oncol*, 88:509–513, 1988.

[96] D.R. Barpe, D.D. Rosa, and P.E. Froehlich. Pk evaluation of doxorubicin plasma levels in normal and overweight patients with breast cancer and simulation of dose adjustment. *Eur J Pharm Sci.*, 41(3):458–463, 2010.

[97] J. M. Jacquet, F. Bressolle, M. Galtier, M. Bourrier, D. Donadio, J. Jourdan, and J. F. Rossi. Doxorubicin and doxorubicinol: intra- and inter-individual variations of pharmacokinetic parameters. *Cancer Chemotherapy and Pharmacology*, 27(3):219–225, 1990.

[98] Y. Yan, H. Shu, X. Bao, L. Luo, and Y. Bai. Clinical treatment planning optimization by Powell's method for gamma unit treatment system. *International Journal of Radiation Oncology, Biology, Physics*, 39(1):247–254, August 1997.

[99] Davis E. King. Dlib-ml: A machine learning toolkit. *Journal of machine Learning Research*, 10:1755–1758, 2009.

[100] J. D Powell. The bobyqa algorithm for bound constrained optimization without derivatives. *Technical Report, Department of Applied Mathematics and Theoretical Physics*, pages 1–39, 01 2009.

[101] K. Mross, B. Niemann, U. Massing, J. Drevs, C. Unger, R. Bhamra, and C. E. Swenson. Pharmacokinetics of liposomal doxorubicin (TLC-D99; Myocet) in patients with solid tumors: an open-label, single-dose study. *Cancer Chemotherapy and Pharmacology*, 54(6):514–524, December 2004.

[102] B. Meiners, C. Shenoy, and B. N. Zordoky. Clinical and preclinical evidence of sex-related differences in anthracycline-induced cardiotoxicity. *Biology of Sex Differences*, 9(1):38, 2018.

[103] N. A. Dobbs, C. J. Twelves, H. Gillies, C. A. James, P. G. Harper, and R. D. Rubens. Gender affects doxorubicin pharmacokinetics in patients with normal liver biochemistry. *Cancer Chemotherapy and Pharmacology*, 36(6):473–476, 1995.

[104] S. E. Lipshultz, S. R. Lipsitz, S. M. Mone, A. M. Goorin, S. E. Sallan, S. P. Sanders, E. J. Orav, R. D. Gelber, and S. D. Colan. Female Sex and Higher Drug Dose as Risk Factors for Late Cardiotoxic Effects of Doxorubicin Therapy for Childhood Cancer. *New England Journal of Medicine*, 332(26):1738–1744, June 1995.

[105] Z. Liu, J. Martin, L. Orme, B. Seddon, J. Desai, W. Nicholls, D. Thomson, D. Porter, G. McCowage, C. Underhill, N. Cranswick, M. Michael, M. Zacharin, A. Herschtal, J. Sivasuthan, and D. M. Thomas. Gender differences in doxorubicin pharmacology

for subjects with chemosensitive cancers of young adulthood. *Cancer Chemotherapy and Pharmacology*, 82(5):887–898, November 2018.

[106] Obesity and Cancer Fact Sheet, February 2017.

[107] J. Y. Sheng, D. Sharma, G. Jerome, and C. A. Santa-Maria. Obese Breast Cancer Patients and Survivors: Management Considerations. *Oncology (Williston Park, N.Y.)*, 32(8):410–417, 2018.

[108] R. Benjamin, P. Wiernik, and N. Bachur. Adriamycin chemotherapy: Efficacy, safety and pharmacologic basis of an intermittent single high-dosage schedule. *Cancer*, 33:19–27, 02 1974.

[109] Shein-Chung Chow. Bioavailability and Bioequivalence in Drug Development. *Wiley interdisciplinary reviews. Computational statistics*, 6(4):304–312, 2014.

[110] National Center for Biotechnology Information, U. S. National Library of Medicine 8600 Rockville Pike, Bethesda MD, and 20894 Usa. *How do cancer cells grow and spread?* Institute for Quality and Efficiency in Health Care (IQWiG), June 2019.

[111] L. Z. Benet. Effect of route of administration and distribution on drug action. *Journal of Pharmacokinetics and Biopharmaceutics*, 6(6):559–585, December 1978.

[112] Pius Fasinu, Patrick J. Bouic, and Bernd Rosenkranz. Liver-based in vitro technologies for drug biotransformation studies - a review. *Current Drug Metabolism*, 13(2):215–224, February 2012.

[113] James Brierley, Mary Gospodarowicz, and Brian O'Sullivan. The principles of cancer staging. *Ecancermedicalscience*, 10:ed61–ed61, November 2016.

[114] Reza Bayat Mokhtari, Tina S Homayouni, Narges Baluch, Evgeniya Morgatskaya, Sushil Kumar, Bikul Das, and Herman Yeger. Combination therapy in combating cancer. *Oncotarget*, 8(23):38022–38043, June 2017.

[115] Sidney Kennedy. Full remission: a return to normal functioning. *Journal of psychiatry & neuroscience : JPN*, 27(4):233–234, July 2002.

[116] Shivaani Kummar, Martin Gutierrez, James H Doroshow, and Anthony J Murgo. Drug development in oncology: classical cytotoxics and molecularly targeted agents. *British journal of clinical pharmacology*, 62(1):15–26, July 2006.

[117] L Hurley. Dna and its associated processes as targets for cancer therapy. *Nature Review*, 2:188–200, 2002.

[118] Geoffrey M. Cooper. The Central Role of Enzymes as Biological Catalysts. *The Cell: A Molecular Approach. 2nd edition*, 2000.

[119] Fran?oise Bressolle, Jeanne-Marie Jacquet, Marc Galtier, Jacques Jourdan, Daniel Donadio, and Jean-Fran?ois Rossi. Doxorubicin and doxorubicinol plasma concentrations and excretion in parotid saliva. *Cancer Chemotherapy and Pharmacology*, 30(3):215–218, 1992.

[120] A S Biebricher, I Heller, R F Roijmans, T P Hoekstra, E J Peterman, and G J L Wuite. The impact of dna intercalators on dna and dna-processing enzymes elucidated through force-dependent binding kinetics. *Nature Communication*, pages 1–12, 2015.

[121] Thomas N Seyfried and Leanne C Huysentruyt. On the origin of cancer metastasis. *Critical reviews in oncogenesis*, 18(1-2):43–73, 2013.

[122] M. Fukuoka and R. Tsuchiya. [Principles for adjuvant and neoadjuvant chemotherapy]. *Gan to Kagaku Ryoho. Cancer & Chemotherapy*, 21 Suppl 3:333–337, October 1994.

[123] Tao Zhu, B. Starling-Emerald, Xin Zhang, Kok-Onn Lee, Peter D. Gluckman, Hichem C. Mertani, and Peter E. Lobie. Oncogenic transformation of human mammary epithelial cells by autocrine human growth hormone. *Cancer Research*, 65(1):317–324, January 2005.

[124] Nicole J Yang and Marlon J Hinner. Getting across the cell membrane: an overview for small molecules, peptides, and proteins. *Methods in molecular biology (Clifton, N.J.)*, 1266:29–53, 2015.

[125] D G Waller and C F George. Prodrugs. *British journal of clinical pharmacology*, 28(5):497–507, November 1989.

[126] S R Mehta, V Suhag, M Semwal, and N Sharma. Radiotherapy: Basic Concepts and Recent Advances. *Medical journal, Armed Forces India*, 66(2):158–162, April 2010.

[127] Y. Fujisaka, A. Horiike, T. Shimizu, N. Yamamoto, Y. Yamada, and T. Tamura. Phase 1 clinical study of pegylated liposomal doxorubicin (JNS002) in Japanese patients with solid tumors. *Japanese Journal of Clinical Oncology*, 36(12):768–774, December 2006.

[128] Y. Matsumura, M. Gotoh, K. Muro, Y. Yamada, K. Shirao, Y. Shimada, M. Okuwa, S. Matsumoto, Y. Miyata, H. Ohkura, K. Chin, S. Baba, T. Yamao, A. Kannami, Y. Takamatsu, K. Ito, and K. Takahashi. Phase I and pharmacokinetic study of MCC-465, a doxorubicin (DXR) encapsulated in PEG immunoliposome, in patients with metastatic stomach cancer. *Annals of Oncology*, 15(3):517–525, March 2004.

[129] P. Chastagner, B. Devictor, B. Geoerger, I. Aerts, P. Leblond, D. Frappaz, J. Gentet, S. Bracard, and N. Andre. Phase I study of non-pegylated liposomal doxorubicin in children with recurrent/refractory high-grade glioma. *Cancer Chemotherapy and Pharmacology*, 76(2):425–432, August 2015.

[130] C. E. Swenson, L. E. Bolcsak, G. Batist, T. H. Guthrie, K. H. Tkaczuk, H. Boxenbaum, L. Welles, S. Chow, R. Bhamra, and P. Chaikin. Pharmacokinetics of doxorubicin administered i.v. as Myocet (TLC D-99; liposome-encapsulated doxorubicin citrate) compared with conventional doxorubicin when given in combination with cyclophosphamide in patients with metastatic breast cancer:. *Anti-Cancer Drugs*, 14(3):239–246, March 2003.

Appendix A

Glossary of Terms

Adjuvant Chemotherapy Additional treatment given to cancer patient after the completion of the primary treatment to lower the chance of disease occurrence [16].

Administration Route The several ways a drug can be administered. The most common ways are oral and intravenous [109].

Apoptosis Mechanism targeted at inducing cell death by a controlled process [28].

Benign Tumours A group of tumours without the ability to spread and metastasize [110].

Bioavialability The degree of availability of a drug at the site of action and a measure of the drug absorption at target site [109].

Biodistribution The extent of distribution of a molecule within the body [111].

Biotransformation The process of transformation of an organic compound into another, usually in the form of a metabolite [112].

Cancer A group of diseases characterized by abnormal cell growth with the ability to metastasize [24].

Cancer Staging The process of determining the tumour extent within a body. This may include the size, location and whether the cancer has spread [113].

Cardiotoxicity A form of cytotoxicity which affects heart muscle cells [65].

Cell Cycle A series of event that occurs during the lifetime of a cell leading to the production of two daughters [23].

Cell Division The process leading to the division of a parent cell into two or more daughters. [9].

Cellular Arrest A phase of the cell-cycle characterized by the termination of cellular division and duplication processes [26].

Checkpoint Proteins Proteins that terminate certain processes that may cause errors in cell properties. They also signal the completion of the different stages of the cell cycle, allowing the initiation of the nest stage [26].

Chemotherapy The treatment of cancer with anti-cancer drugs [17].

Combination Chemotherapy A cancer treatment method that combines two or more anti-cancer agents [114].

Compartment Models A description of the fate of a drug within the body where the pharmacokinetic processes are described by a series of compartments [37].

Complete Remission The period following cancer treatment characterized by an improvement of sufficient magnitude in the response to treatment such that the patients shows virtually no symptoms [115].

Concomitant Administration A mode of treatment where two drugs are given at almost the same time to increase the treatment efficacy or reduce the toxicity of one of the drugs [17].

Cumulative Dose The total amount of a drug administered to a patient over a given period [78].

Cytostatic These are drugs that inhibit cell growth as opposed to killing off the cell [116].

Cytotoxicity Characterized by being toxic to cells [52].

DNA Damage A modification of DNA structure altering the replication mechanism [117].

DNA Replication The process through which a double stranded DNA molecule copies itself to produce two identical copies during cell division [23].

Drug Resistance The ability of cancer cells to develop alternative pathways in response to treatment with a single anticancer drug thereby developing resistance to said drug [114].

Efflux Proteins These are proteins responsible for the transport of toxic substances out of cells [58].

Enhanced Permeability and Retention The process by which drugs accumulate more in tumour tissues than normal tissues [22].

Enzyme Kinetics The rates of enzyme-catalyzed chemical reactions [44].

Enzymatic Reaction	A reaction characterized by the binding of an enzyme with a substate to form a product [118].
Gap1 Phase	The cell cycle phase characterized by the increase in the physical extent of the cell [23].
Gap2 Phase	The cell cycle phase characterized by the synthesis of the protein in preparation for division [23].
in vivo	Processes taking place in living organisms [58].
in vitro	Processes taking place in a simulated environment such as a culture dish or a test tube [58].
Interindividual Variability PK	The differences observed in the pharmacokinetics of a drug between a number of people [119].
Intercalation	The insertion of a molecule into a layered host [120].
Liposome	A spherically-shaped vesicle comprising of a lipid bilayer used as a vehicle to deliver drugs to the body [20].
Lymphatic System	A conduit vessel for transporting extravasated protein-rich fluids back into blood circulation [21].
Malignant Tumours	A group of tumours with the ability to spread and metastasize [110].
Maximum Tolerated Dose	The maximum dose of a drug administered before the onset of side effects [78].
Metastasis	The spread of a cancer cells from their primary site to surrounding tissues and distant organs [121].
Mitotic Phase	The cell cycle phase characterized by the division of the cell into daughter cells [23].
Neo-Adjuvant Chemotherapy	Initial treatment given to cancer patients to shrink the tumour before the main treatment [122].
Oncogenic Transformation	A number of processes involving the accumulation of genetic mutations leading development of cancers [123].
Oxidative Stress	An imbalance between the production of the ROS species and the antioxidants in the body [52].
Partial Remission	The period following cancer treatment characterized by an improvement in the response to treatment but the patient remaining slightly symptomatic [115].
Passive Diffusion	The movement of a molecule across a membrane due to the difference in its concentration gradient [124].

Pegylation	The addition or modification of compounds by the addition of ethylene glycol coating [80].
Phase-Specific Agents	These are drugs that initiate their cytotoxic or cytostatic effects in a specific phase of the cell cycle [17].
Prodrug	Any compound, which when administered is converted or metabolized into a clinically active drug [125].
Radiotherapy	The use of high-energy radiation to kill off cancerous cells and shrink tumours [126].
Reactive Oxygen Specie	An oxygen-containing chemical specie which readily reacts with other cellular molecules [54].
Response Rate	The percentage of patients with a specified reduction in tumour size [78].
Saturable Kinetics	A kinetics of molecule described by a saturable process resulting in a change in the kinetic parameters as a function of concentration [44].
Steady-State kinetics	The state of a chemical reaction where all the variables are constant [45].
Stealth Liposome	A liposome containing an extra layer of polyethylene glycol. The extra layer is added through a process called pegylation [80].
Synthesis Phase	The cell cycle phase characterized by replication of the DNA [23].
Tumour Suppressor gene	Genes encoding proteins that control the progression of the cell cycle stages. [9].

Appendix B

Weighted Variance Model Results

B.1 One-Molecule Models

B.1.1 One-Molecule, One-Compartment Model

The one-compartment model weighted variance, S_a, parameters are shown in Table B.1. According to the parameters, the elimination kinetics of DOX from the compartment is a combination of two processes depending on the drug concentration. At high concentration, the kinetics is almost zeroth-order, $A - B \approx 0.12$, suggesting that the process occurs at a near maximum rate. The elimination kinetics transitions to a process with $A \approx 2.72$ at low drug concentration.

Table B.1: One-compartment model case 2 parameters for DOX with S_a minimized.

$\boldsymbol{k}^{(1)}_{DOX,10}$ [a]	$\boldsymbol{\Gamma}^{(1)}_{DOX,10}$ [b]	$\boldsymbol{A}^{(1)}_{DOX,10}$	$\boldsymbol{B}^{(1)}_{DOX,10}$	$V_{d,DOX}$ [c]	S_a [d]
0.0125 (10)	0.0029 (21)	2.7254 (17)	2.5981 (22)	6.5970 (23)	0.0662

units of:
[a] $\left[\frac{\mu\text{mol}}{\text{m}^2}\right]^{1-A^{(1)}_{DOX,10}}\text{min}^{-1}$ [b] $\left[\frac{\mu\text{mol}}{\text{m}^2}\right]^{-B^{(1)}_{DOX,10}}$ [c] $\left[\text{L}\cdot\text{m}^{-2}\right]$ [d] $\left[\mu\text{mol}\cdot\text{l}^{-1}\right]^2$

Figure B.1 shows an improved high concentration fits of the theoretical curves to the clinical concentrations compared to the figure 3.8. The terminal phase of the curves begins 100 minutes after the start of DOX infusion.

B.1.2 Multi-Process Model for the One-Compartment Model

When investigating the possibility of a better fit of the theoretical to clinical concentrations, the addition of extra elimination terms resulted in a 1.66% decrease in the variance. This is following the addition of an approximately zeroth-order process to the high concentration PK, and a second-order process to the low concentration PK. The new PK suggests a competition between the two approximately zeroth-order processes at high concentrations. At very low concentrations, the second-order terms dominate the elimination kinetics of the molecule, suggesting a faster elimination process than the single-process model. The parameters in the first row of Table B.3 were initialized to the those in Table B.1, and allowed to vary along with the parameters in the second row.

Figure B.2 shows the simulated curves of DOX using the parameters from Table B.2. The new elimination terms produce a better fit of Greene *et al.* [59] at high concentrations. Conversely, the terminal concentrations of the curves were markedly reduced compared to

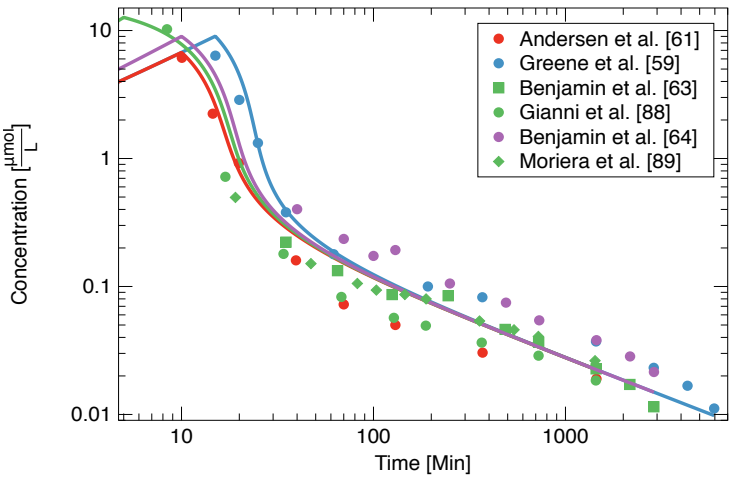

Figure B.1: Comparison of theoretical and experimental concentrations of DOX using the parameters from Table B.1. The clinical data and curves are for an infusion of 9.19 $\mu mol \cdot m^{-2} \cdot min^{-1}$ (red and blue), 22.08 $\mu mol \cdot m^{-2} \cdot min^{-1}$ (green) and 11.04 $\mu mol \cdot m^{-2} \cdot min^{-1}$ (purple).

Table B.2: One-compartment model case 2.1 parameters for DOX with S_a minimized.

$k^{(1,A)}_{DOX,10}$ [a]	$\Gamma^{(1,B)}_{DOX,10}$ [b]	$A^{(1)}_{DOX,10}$	$B^{(1)}_{DOX,10}$	$V_{d,DOX}$ [c]	S_a [d]
0.0114 (11)	0.0023 (22)	2.7074 (24)	2.6132 (18)	6.5818 (37)	0.0651
0.0018 (14)	1.0001 (21)	1.999 (64)	2.003 (23)		

units of:
[a] $\left[\frac{\mu mol}{m^2}\right]^{1-A^{(1)}_{DOX,10}} min^{-1}$ [b] $\left[\frac{\mu mol}{m^2}\right]^{-B^{(1)}_{DOX,10}}$ [c] $[L \cdot m^{-2}]$ [d] $[\mu mol \cdot l^{-1}]^2$

figure B.1. The terminal elimination phase appears to begin approximately 120 minutes after the start of infusion.

B.1.3 One-Molecule, Two-Compartment Model Version A

Table B.3 shows the two-compartment model version A case 2 parameters when S_a was minimized. According to the parameters, the elimination and distribution kinetics of the molecule in compartment one can be described by identical flow and saturation coefficients. At high concentrations, both the elimination and distribution kinetics contribute equally to the PK of the molecule in compartment one. However, the distribution kinetics dominate at low concentrations, culminating in an increased terminal elimination rate compared to the one-compartment model in Table B.1. The coefficient of flow from compartment two to one is zero, suggesting that the compartment acts as an extra elimination compartment for the molecule in compartment one. The addition of the second compartment reduced the model variance by $\approx 27\%$.

Figure B.3 shows the curve of DOX simulated from the one-molecule, two-compartment model version A. The curves agree with the clinical measurements from the studies at high concentrations. At long times, the predicted concentration is reduced from Figure B.1, sug-

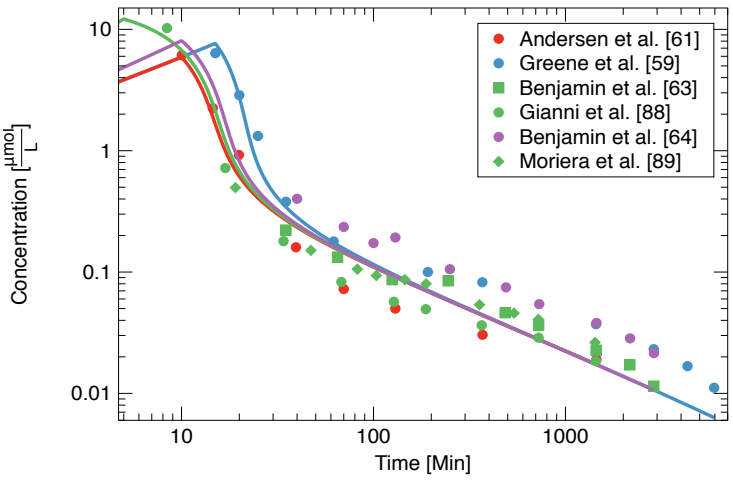

Figure B.2: Comparison of theoretical and experimental concentrations of DOX using the parameters from Table B.2. The clinical data and curves are for an infusion of 9.19 $\mu\text{mol}\cdot\text{m}^{-2}\cdot\text{min}^{-1}$ (red and blue), 22.08 $\mu\text{mol}\cdot\text{m}^{-2}\cdot\text{min}^{-1}$ (green) and 11.04 $\mu\text{mol}\cdot\text{m}^{-2}\cdot\text{min}^{-1}$ (purple).

Table B.3: Two-compartment model version A case 2 parameters of DOX with S_a minimized.

ci,cf	$\boldsymbol{k}^{(1,A)}_{DOX,ci,cf}$ [a]	$\boldsymbol{\Gamma}^{(1,B)}_{DOX,ci,cf}$ [b]	$\boldsymbol{A}^{(1)}_{DOX,ci,cf}$	$\boldsymbol{B}^{(1)}_{DOX,ci,cf}$	$V_{d,DOX}$ [c]	S_a [d]
1,0	0.0060 (13)	0.0028 (21)	2.7250(12)	2.5983(28)	6.5963(89)	0.0484
1,2	0.0061 (45)	0.0028 (58)	2.8546 (72)	2.7250 (50)		
2,1	0.0000 (12)	N/A**	N/A**	N/A**		

units of:
[a] $\left[\frac{\mu\text{mol}}{\text{m}^2}\right]^{1-A^{(1)}_{DOX,ci,cf}}\text{min}^{-1}$ [b] $\left[\frac{\mu\text{mol}}{\text{m}^2}\right]^{-B^{(1)}_{DOX,ci,cf}}$ [c] $\left[\text{L}\cdot\text{m}^{-2}\right]$ [d] $\left[\mu\text{mol}\cdot\text{l}^{-1}\right]^2$
** The parameter is indeterminate because the rate coefficient is zero.

gesting an increased rate of drug elimination from the plasma compartment. The terminal phase of the curves appear to begin $\approx$ 100 minutes after the start of infusion.

B.1.4 One-Molecule, Two-Compartment Model Version B

Table B.4 shows the two-compartment model (version B) case 2 parameters of DOX. According to the parameters, the PK of DOX in compartment one retains the behaviour of the one-compartment model, with exponents $A \approx 2.73$ at low concentrations and $A - B \approx 0.05$ at low concentrations. At high concentrations, the distribution process plays an inhibitory role in the movement of the molecule out of compartment two. At these concentrations, the second process dominates and drives out the molecule from the compartment. The variance of this model is $\approx 15\%$ less than the two-compartment model version A variance, being also $\approx 38\%$ less than the one-compartment model variance.

Figure B.4 shows the graph of DOX using the two-compartment (version B) case 2 parameters. The curves show that the parameters model the high concentration phase of the molecule well over the range of dataset, however, as the redistribution of the molecule in

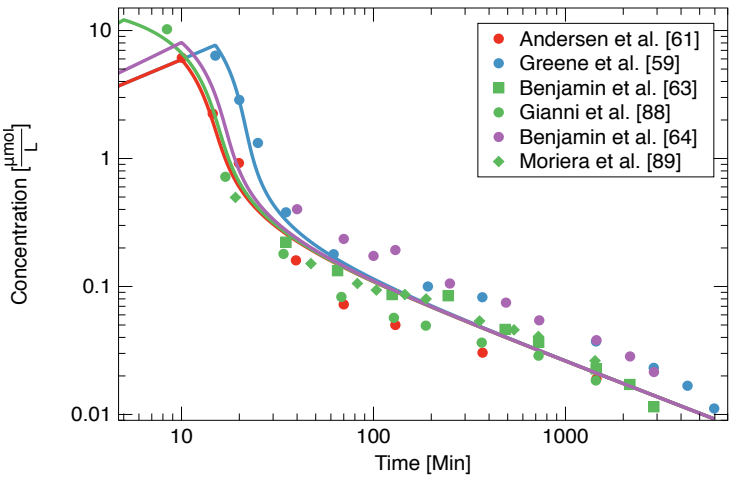

Figure B.3: Comparison of theoretical and experimental concentrations of DOX using the parameters from Table B.3. The clinical data and curves are for an infusion of 9.19 $\mu\text{mol}\cdot\text{m}^{-2}\cdot\text{min}^{-1}$ (red and blue), 22.08 $\mu\text{mol}\cdot\text{m}^{-2}\cdot\text{min}^{-1}$ (green) and 11.04 $\mu\text{mol}\cdot\text{m}^{-2}\cdot\text{min}^{-1}$ (purple).

Table B.4: Two-compartment model version B case 2 parameters of DOX with S_a minimized.

ci,cf	$\boldsymbol{k}^{(1,A)}_{DOX,ci,cf}$ [a]	$\boldsymbol{\Gamma}^{(1,B)}_{DOX,ci,cf}$ [b]	$\boldsymbol{A}^{(1)}_{DOX,ci,cf}$	$\boldsymbol{B}^{(1)}_{DOX,ci,cf}$	$V_{d,DOX}$ [c]	S_a [d]
1,2	0.0401 (10)	0.0016 (13)	3.0093 (28)	2.9636 (45)	5.4160 (48)	0.0412
2,0	1.0323 (66)	0.7452 (28)	2.0557 (30)	1.2153 (19)		
2,1	1.3489 (26)	0.0058 (10)	1.6788 (10)	2.4646 (46)		

units of:
[a] $\left[\frac{\mu\text{mol}}{\text{m}^2}\right]^{1-A^{(1)}_{DOX,ci,cf}}\text{min}^{-1}$ [b] $\left[\frac{\mu\text{mol}}{\text{m}^2}\right]^{-B^{(1)}_{DOX,ci,cf}}$ [c] $\left[\text{L}\cdot\text{m}^{-2}\right]$ [d] $\left[\mu\text{mol}\cdot\text{l}^{-1}\right]^2$

compartment two dominate at long times, the concentration in compartment one increases, producing an increased terminal concentration compared to Figures B.1 and B.3.

B.1.5 Multi-Process Model for the One-Molecule Two-Compartment Version B

The two-compartment version *B* model parameters with multiple processes are shown in Table B.5. According to the parameters, a pair of processes describe the distribution PK of DOX from compartment one, and three processes each describe the PK of the molecule in compartment two. The extra process in compartment one is approximately first-order $A \approx 0.96$ and increases the terminal elimination rate of the molecule. The appears to be an inhibition of the elimination of the molecule from compartment two at high concentrations. This rate-limiting behaviour is also observable in the distribution PK, suggesting that the amount of the molecule retained in compartment two is increased using this model. This model produced a variance that is $\approx 22\%$ less than the variance from Table B.4.

Figure B.5 shows the graph of DOX concentrations using the two-compartment model version B case 2.2 parameters. The curves show a good agreement with the clinical data

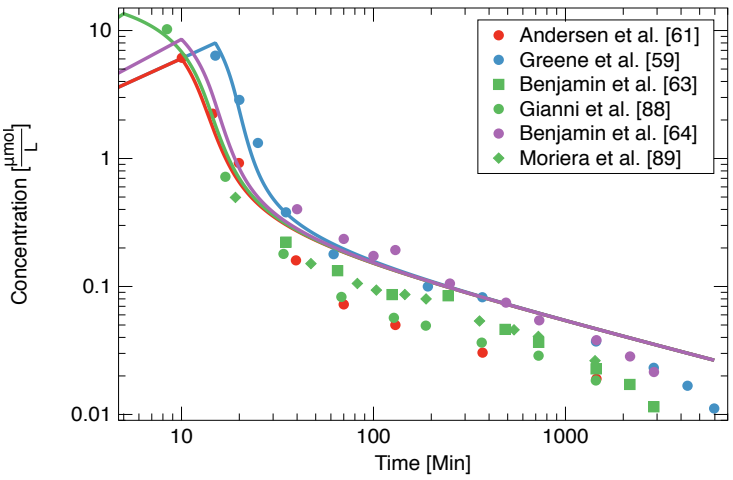

Figure B.4: Comparison of theoretical and experimental concentrations of DOX using the parameters from Table B.4. The clinical data and curves are for an infusion of 9.19 $\mu\text{mol}\cdot\text{m}^{-2}\cdot\text{min}^{-1}$ (red and blue), 22.08 $\mu\text{mol}\cdot\text{m}^{-2}\cdot\text{min}^{-1}$ (green) and 11.04 $\mu\text{mol}\cdot\text{m}^{-2}\cdot\text{min}^{-1}$ (purple).

Table B.5: Two-compartment model version B case 2.2 parameters of DOX with S_a minimized.

ci, cf	$\boldsymbol{k}^{(1,A)}_{DOX,ci,cf}$ [a]	$\boldsymbol{\Gamma}^{(1,B)}_{DOX,ci,cf}$ [b]	$\boldsymbol{A}^{(1)}_{DOX,ci,cf}$	$\boldsymbol{B}^{(1)}_{DOX,ci,cf}$	$V_{d,DOX}$ [c]	S_a [d]
1,2	0.16303 (11)	0.4410 (14)	3.5700 (11)	2.4565 (24)	5.1509 (60)	0.0320
1,2	0.0266 (33)	0.0000 (32)	0.9644 (12)	N/A**		
2,0	0.4026 (18)	0.1875 (29)	1.1427 (23)	1.2887 (53)		
2,0	0.000015 (13)	0.0120 (43)	0.8920 (16)	1.0107 (24)		
2,0	0.5154 (62)	0.0184 (44)	1.773 (31)	2.2999 (18)		
2,1	1.1132 (16)	0.2201 (32)	0.913 (61)	1.2052 (31)		
2,1	0.0797 (22)	0.0356 (32)	1.0071 (14)	1.0505 (42)		
2,1	0.0712 (74)	0.000 (26)	2.2301 (18)	N/A**		

units of:
[a] $\left[\frac{\mu\text{mol}}{\text{m}^2}\right]^{1-A^{(1)}_{DOX,ci,cf}}\text{min}^{-1}$ [b] $\left[\frac{\mu\text{mol}}{\text{m}^2}\right]^{-B^{(1)}_{DOX,ci,cf}}$ [c] $\left[\text{L}\cdot\text{m}^{-2}\right]$ [d] $\left[\mu\text{mol}\cdot\text{l}^{-1}\right]^2$
** The parameter is indeterminate because the saturation coefficient is zero.

points over the range of the datasets considered. The predicted concentrations at long times decrease from Figure B.4 due to the reduced rate of distribution of the molecule in compartment two to compartment one.

B.1.6 Drug Interaction Effects for One-Molecule Two-Compartment Version B

Table B.6 shows the parameters of the two-compartment version B model with drug interactions. The second heading describes the interaction coefficients. In the first two rows, the parameters suggest that two approximately second-order processes enhance the distribution of the molecule to compartment two. The last two rows suggest that two approximately first-order processes enhance the reverse process. These terms suggest that the

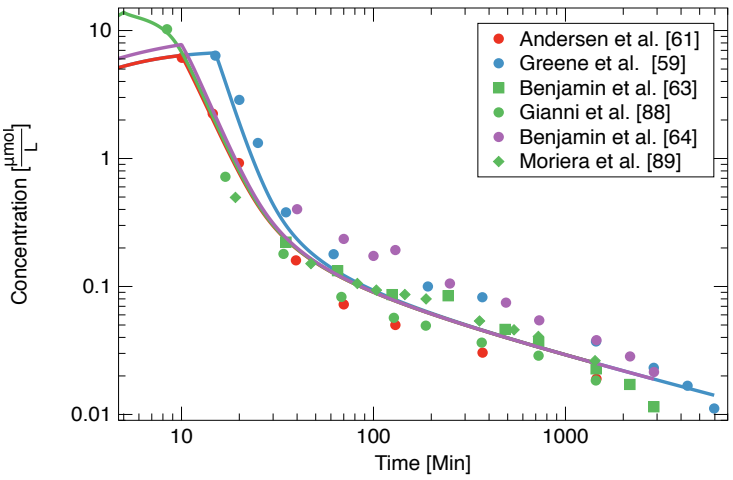

Figure B.5: Comparison of theoretical and experimental concentrations of DOX using the parameters from Table B.5. The clinical data and curves are for an infusion of 9.19 $\mu mol \cdot m^{-2} \cdot min^{-1}$ (red and blue), 22.08 $\mu mol \cdot m^{-2} \cdot min^{-1}$ (green) and 11.04 $\mu mol \cdot m^{-2} \cdot min^{-1}$ (purple).

presence of a molecule in either compartment does inhibit the flow of the same molecule into the compartment. The variance of the model equates to an $\approx 11\%$ decrease in the variance from Table B.4.

Table B.6: Two-compartment model version B case 3.1 parameters of DOX with S_a minimized.

ci, cf	$\boldsymbol{k}^{(1,A)}_{DOX,ci,cf}$ [a]	$\boldsymbol{\Gamma}^{(1,B)}_{DOX,ci,cf}$ [b]	$\boldsymbol{A}^{(1)}_{DOX,ci,cf}$	$\boldsymbol{B}^{(1)}_{DOX,ci,cf}$	$V_{d,DOX}$ [e]
1,2	0.01916 (51)	0.01229 (42)	3.214 (17)	2.4911 (10)	5.2537 (20)
2,0	1.2399 (32)	0.0784 (32)	1.55728 (63)	1.14715 (24)	
2,1	0.98624 (13)	0.23645 (14)	1.60014 (15)	1.10617 (49)	
ci, cf	$\boldsymbol{\alpha}^{(1,C)}_{DOX,ci,cf\|DOX,cf}$ [c]	$\boldsymbol{\beta}^{(1,D)}_{DOX,ci,cf\|DOX,cf}$ [d]	$\boldsymbol{C}^{(1)}_{DOX,ci,cf\|DOX,cf}$	$\boldsymbol{D}^{(1)}_{DOX,ci,cf\|DOX,cf}$	S_a [f]
1,2	0.019401 (83)	0.000014 (22)	2.01878 (25)	2.00453 (67)	0.0365
1,2	0.03785 (16)	0.0012 (42)	1.9729 (27)	1.9745 (91)	
2,1	0.0867 (43)	0.00 (72)	1.0362 (12)	N/A**	
2,1	0.0757 (31)	0.00 (20)	0.9833 (13)	N/A**	

units of:

[a] $\left[\frac{\mu mol}{m^2}\right]^{1-A^{(1)}_{DOX,ci,cf}} min^{-1}$ [b] $\left[\frac{\mu mol}{m^2}\right]^{-B^{(1)}_{DOX,ci,cf}}$

[c] $\left[\frac{\mu mol}{m^2}\right]^{-C^{(1)}_{DOX,ci,cf|DOX,cf}}$ [d] $\left[\frac{\mu mol}{m^2}\right]^{-D^{(1)}_{DOX,ci,cf|DOX,cf}}$

[e] $\left[L \cdot m^{-2}\right]$ [f] $\left[\mu mol \cdot l^{-1}\right]^2$

** The parameter is indeterminate because the saturation coefficient is zero.

Figure B.6 shows the graph of DOX concentrations using the two-compartment model version B case 3.1 parameters. The curves retain a good fit at high concentrations but shift upwards as the more of the molecule is distributed to compartment one from compartment

two.

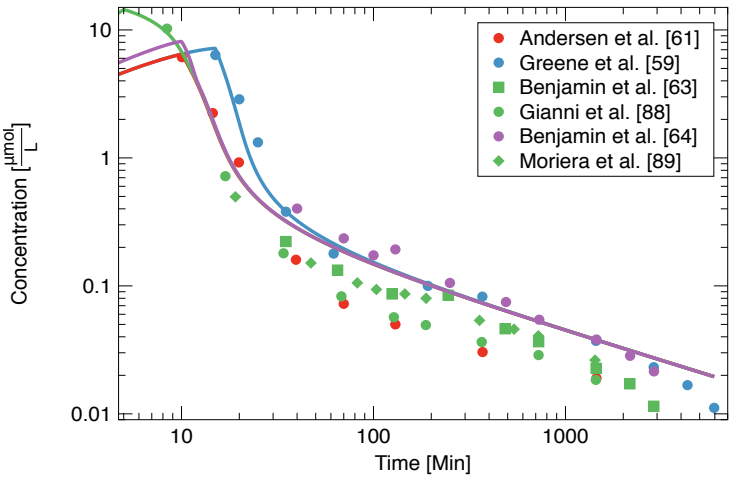

Figure B.6: Comparison of theoretical and experimental concentrations of DOX using the parameters from Table B.6. The clinical data and curves are for an infusion of 9.19 $\mu mol \cdot m^{-2} \cdot min^{-1}$ (red and blue), 22.08 $\mu mol \cdot m^{-2} \cdot min^{-1}$ (green) and 11.04 $\mu mol \cdot m^{-2} \cdot min^{-1}$ (purple).

B.1.7 One-Molecule, Three-Compartment Model

In the high concentration phase, the flow to compartment two appears to be saturable when the amount of the drug in compartment one exceeds a certain threshold, this is no the same for the flow to compartment three as the flow rate does not change in response to the amount of the drug. The distribution of the drug in compartment one is characterized by low concentration kinetics of order $A \approx 2.80$, and high concentration kinetics, to compartment two, of order $A - B \approx 0.50$. This suggests that the molecule in compartment one shows a greater affinity for the disposition into compartment two over compartment three.

The PK of the drug in compartment two suggests that the redistribution and elimination kinetics follow different processes. In the case of elimination, the kinetics is a high concentration one when the amount of the molecule in the compartment, $X_{DOX,2}$, exceeds 2.30 $\mu mol \cdot m^{-2}$. The redistribution kinetics does not appear to saturate in response to the amount of DOX in the compartment. Likewise, the redistribution from compartment three follows a similar kinetic process to the redistribution from compartment two, however, the rate constant is markedly reduced, suggesting a reduced flow of compartment three DOX back to compartment one. The three-compartment model reduced the variance by 32% from Table B.4.

Figure B.7 shows the simulation of DOX concentrations using the three-compartment model case 2 parameters. The curves show a slightly poorer high concentration fit compared to the two-compartment models. There is a noticeably faster rate of elimination at the terminal phase, which may suggests increased influence of drug distribution from compartment one to compartment three.

Table B.7: Three-compartment model case 2 parameters of DOX with S_a minimized.

ci, cf	$\boldsymbol{k}^{(1,A)}_{DOX,ci,cf}$ [a]	$\boldsymbol{\Gamma}^{(1,B)}_{DOX,ci,cf}$ [b]	$\boldsymbol{A}^{(1)}_{DOX,ci,cf}$	$\boldsymbol{B}^{(1)}_{DOX,ci,cf}$	$V_{d,DOX}$ [c]	S_a [d]
1,2	0.0476 (16)	0.0004 (11)	2.7957 (37)	2.2966 (12)	4.7097 (21)	0.0281
2,0	1.4336 (56)	0.3946 (16)	1.4489 (13)	1.1124 (20)		
2,1	1.0463 (16)	0.00 (50)	2.3406 (73)	N/A**		
1,3	0.00000074 (21)	0.00 (28)	2.7956 (12)	N/A**		
3,1	0.0000011 (18)	0.00 (54)	2.3399 (32)	N/A**		

units of:
[a] $\left[\frac{\mu\text{mol}}{\text{m}^2}\right]^{1-A^{(1)}_{DOX,ci,cf}}\text{min}^{-1}$ [b] $\left[\frac{\mu\text{mol}}{\text{m}^2}\right]^{-B^{(1)}_{DOX,ci,cf}}$ [c] $\left[\text{L}\cdot\text{m}^{-2}\right]$ [d] $\left[\mu\text{mol}\cdot\text{l}^{-1}\right]^2$
** The parameter is indeterminate because the saturation parameter is zero.

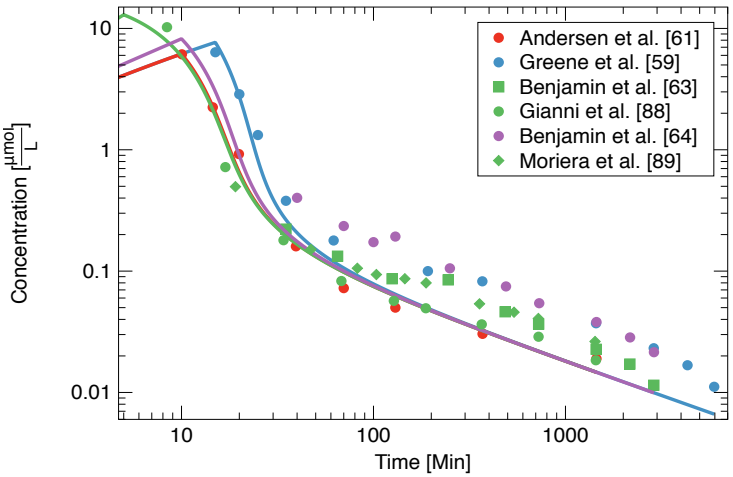

Figure B.7: Comparison of theoretical and experimental concentrations of DOX using the parameters from Table B.7. The clinical data and curves are for an infusion of 9.19 $\mu\text{mol}\cdot\text{m}^{-2}\cdot\text{min}^{-1}$ (red and blue), 22.08 $\mu\text{mol}\cdot\text{m}^{-2}\cdot\text{min}^{-1}$ (green) and 11.04 $\mu\text{mol}\cdot\text{m}^{-2}\cdot\text{min}^{-1}$ (purple).

B.1.8 Multi-Process Model for the Three-Compartment Model

In this model, like the one and two-compartment single molecule case, the influence of the other process on the three-compartment case 2 model parameters were investigated. The new model included multiple processes which interacts with the dominant process to describe the kinetics of DOX in the compartments. Table B.8 shows the PK parameters of the three-compartment case 2.2 model. According to the parameters, there is an additional process in the distribution of the molecule from comapartment one, which corresponds to the terminal distribution of the DOX from compartment one to two. This process is approximately zeroth-order at very high concentration, and second order at low concentration. In compartment two, three processes describe the elimination of DOX. Along with the primary process with exponent $A = 1.4685$, there are additional first and second order processes to describe the elimination. This behavior is also noticeable during the redistribution kinetics, where extra first and second order terms influence the dominant process. When accounting for the presence of these extra processess the variance reduces by 13.17% from the model

in Table B.7.

Table B.8: Three-compartment model case 2.2 parameters of DOX with S_a minimized.

ci, cf	$\boldsymbol{k}^{(1,A)}_{DOX,ci,cf}$ [a]	$\boldsymbol{\Gamma}^{(1,B)}_{DOX,ci,cf}$ [b]	$\boldsymbol{A}^{(1)}_{DOX,ci,cf}$	$\boldsymbol{B}^{(1)}_{DOX,ci,cf}$	$V_{d,DOX}$ [c]	S_a [d]
1,2	0.0429 (55)	0.032 (18)	0.9905 (34)	1.0021 (11)	5.11 (22)	0.0244
1,2	0.0337 (62)	0.0039 (59)	2.0007 (22)	2.001 (35)		
2,0	1.0180 (76)	0.00 (17)	1.4785 (28)	N/A**		
2,0	0.0093 (10)	0.0080 (65)	0.9939 (87)	0.9986 (12)		
2,0	0.0007 (54)	0.0034 (15)	2.0011 (13)	1.991 (69)		
2,1	1.063 (42)	0.1295 (36)	1.4963 (57)	1.1399 (53)		
2,1	0.0034 (64)	0.0006 (54)	1.000 (14)	1.0041 (29)		
2,1	0.005 (50)	0.0014 (76)	1.99 (70)	2.003 (94)		
1,3	0.0253 (53)	0.0078 (39)	2.004 (31)	1.998 (50)		
3,1	0.000064 (15)	0.00 (22)	1.4839 (16)	N/A**		

units of:
[a] $\left[\frac{\mu\text{mol}}{\text{m}^2}\right]^{1-A^{(1)}_{DOX,ci,cf}}\text{min}^{-1}$ [b] $\left[\frac{\mu\text{mol}}{\text{m}^2}\right]^{-B^{(1)}_{DOX,ci,cf}}$ [c] $\left[\text{L}\cdot\text{m}^{-2}\right]$ [d] $\left[\mu\text{mol}\cdot\text{l}^{-1}\right]^2$
** The parameter is indeterminate because the saturation parameter is zero.

Figure B.8 shows the concentration profile of DOX using the three-compartment case 2.2 parameters. The extra first order phase results in a rapid elimination of the drug from compartment one at high concentrations. The short distribution and initial elimination phase of DOX can also be observed.

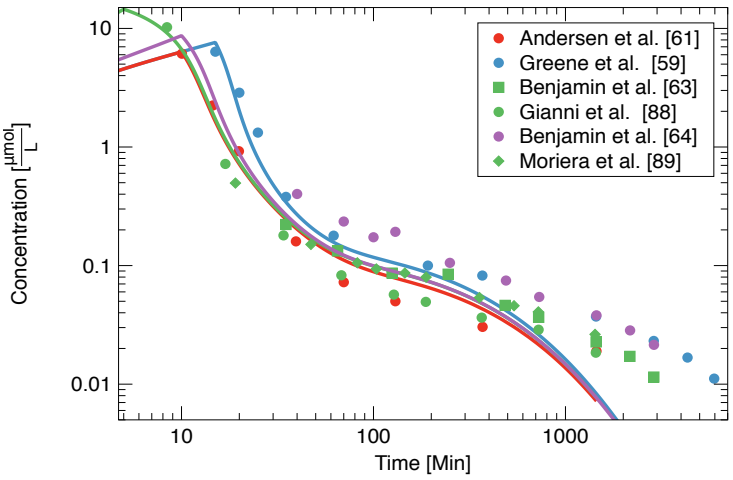

Figure B.8: Comparison of theoretical and experimental concentrations of DOX using data from Table B.8. The clinical data and curves are for an infusion of 9.19 $\mu\text{mol}\cdot\text{m}^{-2}\cdot\text{min}^{-1}$ (red and blue), 22.08 $\mu\text{mol}\cdot\text{m}^{-2}\cdot\text{min}^{-1}$ (green) and 11.04 $\mu\text{mol}\cdot\text{m}^{-2}\cdot\text{min}^{-1}$ (purple).

B.1.9 Drug Interaction Effects for the Three-Compartment Model

The model was also used to test the effect of the presence of a drug in a compartment on the flow into the compartment, specifically how the presence of drug *di* in compartment *cj* affects the rate of flow of the same drug from compartment *ck* to *cj* and vice versa. The α term was allowed to have a negative value and the β, *C* and *D* terms only positive values. Table B.9 shows the three-compartment model case 2.2 parameters. According to the parameters, the distribution of DOX from compartment one to compartment two is inhibited by the drug in compartment two, which is also noticeable in the reverse process where the redistribution is inhibited by the presence of DOX in compartment one. Conversely, there was no inhibition of the flow from compartment one to three, which is expected since the amount of DOX in compartment three is small relative to compartment two. Using this model, we observed a 12% decrease in the vairance from the model in Table B.7. Figure B.9 shows the simulation of DOX concentrations using the three-compartment model 3.1 parameters. The curves show an improved high and low concentration fits compared to the three-compartment model in figure B.7. The drug is distributed less rapidly from compartment one.

Table B.9: Three-compartment model case 3.1 parameters of DOX with S_a minimized.

ci,cf	$\boldsymbol{k}^{(1,A)}_{DOX,ci,cf}$ [a]	$\boldsymbol{\Gamma}^{(1,B)}_{DOX,ci,cf}$ [b]	$\boldsymbol{A}^{(1)}_{DOX,ci,cf}$	$\boldsymbol{B}^{(1)}_{DOX,ci,cf}$	$V_{d,DOX}$ [e]
1,2	0.0942 (76)	0.0538 (64)	3.2646 (35)	2.5222 (17)	5.1666 (96)
2,0	1.0229 (19)	0.0151 (30)	1.46405 (55)	1.11564 (17)	
2,1	1.0552 (40)	0.1469 (25)	1.5114 (64)	1.1524 (55)	
1,3	0.00174 (26)	0.0303 (63)	3.26461 (18)	2.53877 (77)	
3,1	0.1049 (27)	0.00 (14)	1.49597 (74)	N/A**	
ci,cf	$\boldsymbol{\alpha}^{(1,C)}_{DOX,ci,cf\|DOX,cf}$ [c]	$\boldsymbol{\beta}^{(1,D)}_{DOX,ci,cf\|DOX,cf}$ [d]	$\boldsymbol{C}^{(1)}_{DOX,ci,cf\|DOX,cf}$	$\boldsymbol{D}^{(1)}_{DOX,ci,cf\|DOX,cf}$	S_a [f]
1,2	0.0559 (12)	0.000 (33)	0.9985 (13)	N/A**	0.0248
1,2	-0.01457 (20)	0.0188 (27)	0.03687 (77)	0.0067 (53)	
2,1	0.08485 (15)	0.00 (21)	1.07595 (68)	N/A**	
2,1	-0.0010 (25)	0.0065 (14)	0.00489 (17)	0.00238 (66)	
1,3	0.0216 (89)	0.00496 (17)	1.00046 (99)	1.0220 (68)	
1,3	0.00110 (85)	0.02093 (77)	0.01312 (37)	0.00120 (85)	
3,1	-0.07301 (15)	0.04194 (43)	1.0039 (53)	1.006 (15)	
3,1	0.0134 (15)	0.0046 (26)	0.00365 (24)	0.0022 (15)	

units of:
[a] $\left[\frac{\mu\text{mol}}{\text{m}^2}\right]^{1-A^{(1)}_{DOX,ci,cf}}\text{min}^{-1}$ [b] $\left[\frac{\mu\text{mol}}{\text{m}^2}\right]^{-B^{(1)}_{DOX,ci,cf}}$
[c] $\left[\frac{\mu\text{mol}}{\text{m}^2}\right]^{-C^{(1)}_{DOX,ci,cf\|DOX,cf}}$ [d] $\left[\frac{\mu\text{mol}}{\text{m}^2}\right]^{-D^{(1)}_{DOX,ci,cf\|DOX,cf}}$
[e] $\left[\text{L}\cdot\text{m}^{-2}\right]$ [f] $\left[\mu\text{mol}\cdot\text{l}^{-1}\right]^2$
** The parameter is indeterminate because the saturation parameter is zero.

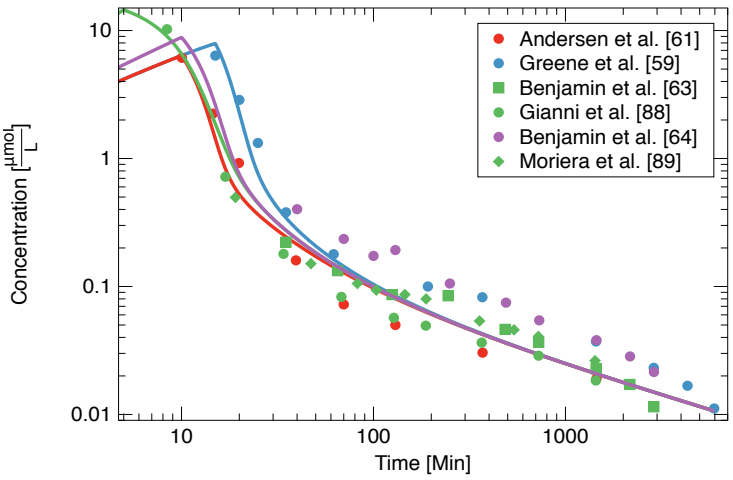

Figure B.9: Comparison of theoretical and experimental concentrations of DOX using data from Table B.9. The clinical data and curves are for an infusion of 9.19 $\mu\text{mol}\cdot\text{m}^{-2}\cdot\text{min}^{-1}$ (red and blue), 22.08 $\mu\text{mol}\cdot\text{m}^{-2}\cdot\text{min}^{-1}$ (green) and 11.04 $\mu\text{mol}\cdot\text{m}^{-2}\cdot\text{min}^{-1}$ (purple).

B.2 Four-Molecule Models

B.2.1 Four-Molecule, One-Compartment Model

Table B.10 shows the parameters of the four-molecule, one-compartment model when S_a was minimized. The parameters are for the case where the one-compartment model parameters of DOX from Table B.1 were left fixed and the DOL parameters alone varied. According to the parameters, the PK process of DOL in the body is concentration dependent and is $A - B \approx 1.05$ at high concentrations, and exponent $A \approx 2.61$ at low concentrations. The rate of dissociation of the enzyme is slower than the rate of formation, which implies that the metabolite is being produced at a rate that is slower than the parent drug is binding.

Table B.10: One-compartment model PK parameters for DOL with S_a minimized.

Type	$\boldsymbol{k}^{(1,p1)}_{Type,2,0}$ [a]	$\boldsymbol{\Gamma}^{(1,p1)}_{Type,2,0}$ [b]	$\boldsymbol{A}^{(1,p1)}_{Type,2,0}$	$\boldsymbol{B}^{(1,p1)}_{Type,2,0}$	$V_{d,Type}$ [g]
DOX	0.0056 (31)*	0.0029 (11)*	2.725 (21)*	2.598 (58)*	6.58 (19)*
DOXOL	0.520 (15)	0.0422 (21)	2.606 (74)	1.558 (31)	10.008 (41)
Type	$\boldsymbol{k}^{(3,p1)}_{Type,2\|\|d3,2,d2,2}$ [c]	$\boldsymbol{\Gamma}^{(3,p1)}_{Type,2\|\|d3,2,d2,2}$ [d]	$\boldsymbol{A}^{(3,p1)}_{Type,2\|\|d3,2,d2,2}$	$\boldsymbol{B}^{(3,p1)}_{Type,2\|\|d3,2,d2,2}$	S_a [h]
DOXCBR1	0.0002 (15)	0.9962 (42)	2.8601 (32)	1.3228 (22)	0.0403
$\boldsymbol{k}^{(4)}_{DOX,2,CBR1,2\|d4,2}$ [e]	$\boldsymbol{\Gamma}^{(4)}_{DOX,2,CBR1,2\|d4,2}$ [f]	$\boldsymbol{A}^{(4,DOX)}_{DOX,2,CBR1,2\|d4,2}$	$\boldsymbol{B}^{(4,DOX)}_{DOX,2,CBR1,2\|d4,2}$	$\boldsymbol{A}^{(5,CBR1)}_{DOX,2,CBR1,2\|d4,2}$	$\boldsymbol{B}^{(5,CBR1)}_{DOX,2,CBR1,2\|d4,2}$
0.0069 (28)	0.0029 (16)	2.725 (49)	2.598 (22)	0.00254 (96)	0.0000 (31)

units of:

[a] $\left[\frac{\mu\text{mol}}{\text{m}^2}\right]^{1-A^{(1)}_{DOX,ci,cf}}\text{min}^{-1}$ [b] $\left[\frac{\mu\text{mol}}{\text{m}^2}\right]^{-B^{(1)}_{DOX,ci,cf}}$

[c] $\left[\frac{\mu\text{mol}}{\text{m}^2}\right]^{1-A^{(3,p1)}_{Type,ci\|d3,cf,d2,cf}}\text{min}^{-1}$ [d] $\left[\frac{\mu\text{mol}}{\text{m}^2}\right]^{-B^{(3,p1)}_{Type,ci\|d3,cf,d2,cf}}$

[e] $\left[\frac{\mu\text{mol}}{\text{m}^2}\right]^{1-(A^{(4,DOX)}_{DOX,ci,Type,cf\|d4,cf}+A^{(5,CBR1)}_{DOX,ci,Type,ci\|d4,cf})}\text{min}^{-1}$ [f] $\left[\frac{\mu\text{mol}}{\text{m}^2}\right]^{-(B^{(4,DOX)}_{DOX,ci,Type,cf\|d4,cf}+B^{(5,CBR1)}_{DOX,ci,Type,ci\|d4,cf})}$ [g] $\left[\text{L}\cdot\text{m}^{-2}\right]$ [h] $\left[\mu\text{mol}\cdot\text{l}^{-1}\right]^2$

where:

$d2 = DOL$ $d3 = CBR1$ $d4 = DOXCBR1$

*These parameters are from Table B.1

Figure B.10 shows the concentration curves of DOX and DOL using the parameters in Table B.10. The figure shows a slightly increased DOL concentration over the range of time considered.

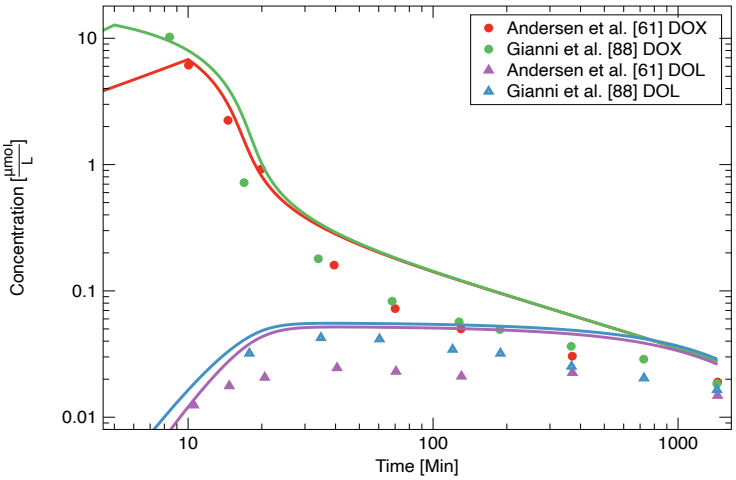

Figure B.10: Comparison of theoretical and experimental concentrations of DOX and DOL using the parameters from Table B.10. The curves represent the infusion data from Andersen *et al.* [61](red and purple) and Gianni *et al.* [88](green and blue).

To test the possibility of a better fit of both DOX and DOL data, the parameters describing the PK of both drugs were varied. The result from the new model was a smaller variance, however, the parameters from this model were roughly similar to the model from Table B.10. The slower DOL elimination rate observed was accompanied by a faster rate of binding of DOX to CBR1. Again, the rate of formation of the metabolite is slower than the rate of parent molecule binding to the enzymes. The noticeable changes to the parameters is the elimination process of DOL, which is approximately zeroth-order at high concentrations and exponent $A \approx 1.50$ at low concentrations.

Table B.11: One-compartment model PK parameters for DOX and DOL with S_a minimized.

Type	$\boldsymbol{k}^{(1,p1)}_{Type,2,0}$ [a]	$\boldsymbol{\Gamma}^{(1,p1)}_{Type,2,0}$ [b]	$\boldsymbol{A}^{(1,p1)}_{Type,2,0}$	$\boldsymbol{B}^{(1,p1)}_{Type,2,0}$	$V_{d,Type}$ [g]
DOX	0.0056 (61)	0.0062 (91)	2.725 (13)	2.5996 (99)	6.59 (87)
DOXOL	0.5204 (17)	0.0417 (33)	1.5005 (33)	1.5007 (15)	10.00 (63)
Type	$\boldsymbol{k}^{(3,p1)}_{Type,2\|\|d3,2,d2,2}$ [c]	$\boldsymbol{\Gamma}^{(3,p1)}_{Type,2\|\|d3,2,d2,2}$ [d]	$\boldsymbol{A}^{(3,p1)}_{Type,2\|\|d3,2,d2,2}$	$\boldsymbol{B}^{(3,p1)}_{Type,2\|\|d3,2,d2,2}$	S_a [h]
DOXCBR1	0.0001 (22)	0.9967 (16)	2.863 (82)	1.322 (40)	0.0389
$k^{(4)}_{DOX,2,CBR1,2\|d4,2}$ [e]	$\Gamma^{(4)}_{DOX,2,CBR1,2\|d4,2}$ [f]	$A^{(4,DOX)}_{DOX,2,CBR1,2\|d4,2}$	$B^{(4,DOX)}_{DOX,2,CBR1,2\|d4,2}$	$A^{(5,CBR1)}_{DOX,2,CBR1,2\|d4,2}$	$B^{(5,CBR1)}_{DOX,2,CBR1,2\|d4,2}$
0.0078 (60)	0.0062 (28)	2.725 (33)	2.600 (76)	0.0000 (29)	0.0043 (61)

units of:

[a] $\left[\frac{\mu\text{mol}}{\text{m}^2}\right]^{1-A^{(1)}_{DOX,ci,cf}}\text{min}^{-1}$ [b] $\left[\frac{\mu\text{mol}}{\text{m}^2}\right]^{-B^{(1)}_{DOX,ci,cf}}$

[c] $\left[\frac{\mu\text{mol}}{\text{m}^2}\right]^{1-A^{(3,p1)}_{Type,ci\|d3,cf,d2,cf}}\text{min}^{-1}$ [d] $\left[\frac{\mu\text{mol}}{\text{m}^2}\right]^{-B^{(3,p1)}_{Type,ci\|d3,cf,d2,cf}}$

[e] $\left[\frac{\mu\text{mol}}{\text{m}^2}\right]^{1-(A^{(4,DOX)}_{DOX,ci,Type,cf\|d4,cf}+A^{(5,CBR1)}_{DOX,ci,Type,ci\|d4,cf})}\text{min}^{-1}$ [f] $\left[\frac{\mu\text{mol}}{\text{m}^2}\right]^{-(B^{(4,DOX)}_{DOX,ci,Type,cf\|d4,cf}+B^{(5,CBR1)}_{DOX,ci,Type,ci\|d4,cf})}$ [g] $\left[\text{L}\cdot\text{m}^{-2}\right]$ [h] $\left[\mu\text{mol}\cdot\text{l}^{-1}\right]^2$

where:

$d2 = DOL$ $d3 = CBR1$ $d4 = DOXCBR1$

Figure B.11 shows the concentration curves of DOX and DOL using the parameters in Table B.11. The figure shows that the parameters model both molecule concentrations well.

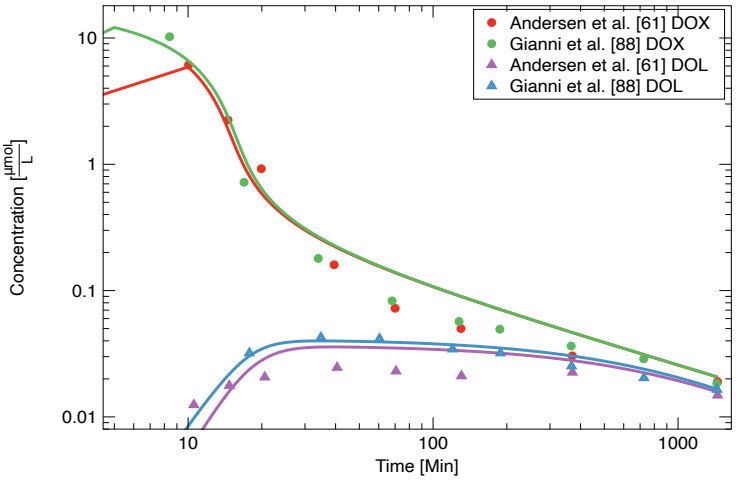

Figure B.11: Comparison of theoretical and experimental concentrations of DOX and DOL using the parameters from Table B.11. The curves represent the infusion data from Andersen *et al.* [61](red and purple) and Gianni *et al.* [88](green and blue).

B.2.2 Four-Molecule, Two-Compartment Model

Table B.12 shows the parameters developed from the four-molecule, two-compartment model. DOX model parameters shown in Table B.4 were left fixed, and the total number of DOL parameters varied. The parameters suggest that the distribution of DOL in compartment one to compartment two is a process of exponent $A - B \approx 1.18$ at high concentrations. The redistribution and elimination of DOL metabolized in compartment two are two distinct processes. The elimination is approximately zeroth-order at very high DOL concentrations in compartment two. The terminal PK of the drug in the compartment is dominated by elimination, which may mean greater absorption into the cells or elimination from the body. The parameters show an increased contribution of the enzymes to the catalysis of DOX, suggesting an increased binding of DOX to the enzyme.

Figure B.12 shows the concentration curves of DOX and DOL using the parameters in Table B.12. The figure shows that the concentrations of DOL is increased an approaches DOX concentration at long times.

Table B.12: Two-compartment PK parameters for DOX and DOL with S_a minimized.

Type	ci,cf	$\boldsymbol{k}^{(1,p1)}_{Type,ci,cf}$ [a]	$\boldsymbol{\Gamma}^{(1,p1)}_{Type,ci,cf}$ [b]	$\boldsymbol{A}^{(1,p1)}_{Type,ci,cf}$	$\boldsymbol{B}^{(1,p1)}_{Type,ci,cf}$	$V_{d,Type}$ [g]
DOX	1,2	0.0401 (98)*	0.0016 (90)*	3.0093 (61)*	2.964 (13)*	5.41 (12)*
DOX	2,0	0.465 (24)*	0.7452 (29)*	2.055 (35)*	1.2153 (42)*	
DOX	2,1	1.3489 (15)*	0.0058 (44)*	1.679 (38)*	2.465 (57)*	
DOXOL	1,2	0.0127 (60)	0.015 (38)	2.750 (34)	1.5753 (24)	4.51 (60)
DOXOL	2,0	0.0034 (19)	0.0014 (40)	1.091 (82)	0.9963 (85)	
DOXOL	2,1	0.001 (22)	0.134 (72)	2.6697 (56)	1.6147 (27)	
Type	ci,cf	$\boldsymbol{k}^{(3,p1)}_{Type,ci\|\|d3,cf,d2,cf}$ [c]	$\boldsymbol{\Gamma}^{(3,p1)}_{Type,ci\|\|d3,cf,d2,cf}$ [d]	$\boldsymbol{A}^{(3,p1)}_{Type,ci\|\|d3,cf,d2,cf}$	$\boldsymbol{B}^{(3,p1)}_{Type,ci\|\|d3,cf,d2,cf}$	S_a [h]
DOXCBR1	2,2	0.131 (31)	0.9527 (92)	2.85 (71)	1.4709 (41)	0.0365
$\boldsymbol{k}^{(4)}_{DOX,2,CBR1,2\|d4,2}$ [e]	$\boldsymbol{\Gamma}^{(4)}_{DOX,2,CBR1,2\|d4,2}$ [f]	$\boldsymbol{A}^{(4,DOX)}_{DOX,2,CBR1,2\|d4,2}$	$\boldsymbol{B}^{(4,DOX)}_{DOX,2,CBR1,2\|d4,2}$	$\boldsymbol{A}^{(5,CBR1)}_{DOX,2,CBR1,2\|d4,2}$	$\boldsymbol{B}^{(5,CBR1)}_{DOX,2,CBR1,2\|d4,2}$	
0.57 (11)	0.7452 (33)	2.0557 (49)	1.2153 (50)	0.238 (46)	0.2587 (19)	

units of:

a $\left[\frac{\mu\text{mol}}{\text{m}^2}\right]^{1-A^{(1)}_{DOX,ci,cf}}\text{min}^{-1}$ b $\left[\frac{\mu\text{mol}}{\text{m}^2}\right]^{-B^{(1)}_{DOX,ci,cf}}$ c $\left[\frac{\mu\text{mol}}{\text{m}^2}\right]^{1-A^{(3,p1)}_{mol,ci\|\|d3,cf,d2,cf}}\text{min}^{-1}$ d $\left[\frac{\mu\text{mol}}{\text{m}^2}\right]^{-B^{(3,p1)}_{mol,ci\|\|d3,cf,d2,cf}}$

e $\left[\frac{\mu\text{mol}}{\text{m}^2}\right]^{1-(A^{(4,DOX)}_{DOX,ci,Type,cf\|d4,cf}+A^{(5,CBR1)}_{DOX,ci,Type,ci\|d4,cf})}\text{min}^{-1}$ f $\left[\frac{\mu\text{mol}}{\text{m}^2}\right]^{-(B^{(4,DOX)}_{DOX,ci,Type,cf\|d4,cf}+B^{(5,CBR1)}_{DOX,ci,Type,ci\|d4,cf})}$ g $\left[\text{L}\cdot\text{m}^{-2}\right]$ h $\left[\mu\text{mol}\cdot\text{l}^{-1}\right]^2$

where:

$d2 = DOL$ $d3 = CBR1$ $d4 = DOXCBR1$

*These parameters are from Table B.4

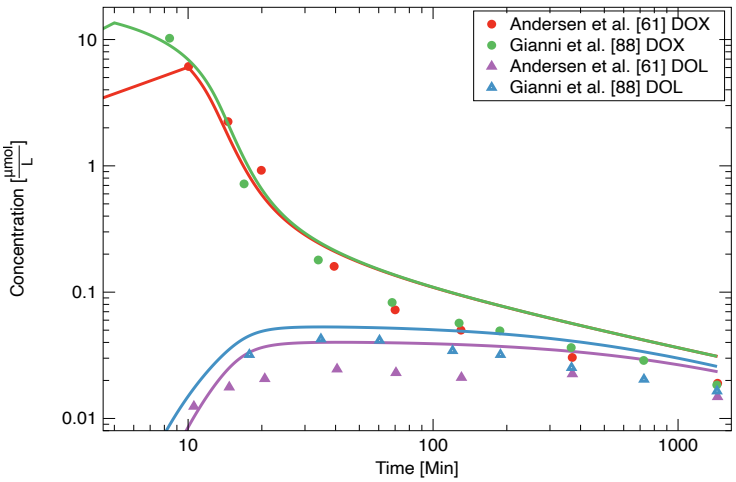

Figure B.12: Comparison of theoretical and experimental concentrations of DOX and DOL using data from Table B.12. The curves represent the infusion data from Andersen *et al.* [61](red and purple) and Gianni *et al.* [88](green and blue).

Appendix C

Comparison of Theoretical and Clinical Concentrations

The plasma concentration curves of the drugs modelled in this work plotted against the digitized data from published studies are shown here. The graphs of DOX are plotted using the one-molecule three-compartment model case 2.2 parameters in Table 3.24. The curves of pegylated DOX in Asian patients are plotted using the parameters from Table 4.12, and the curves of liposomal DOX are plotted using parameters from Table 3.29.

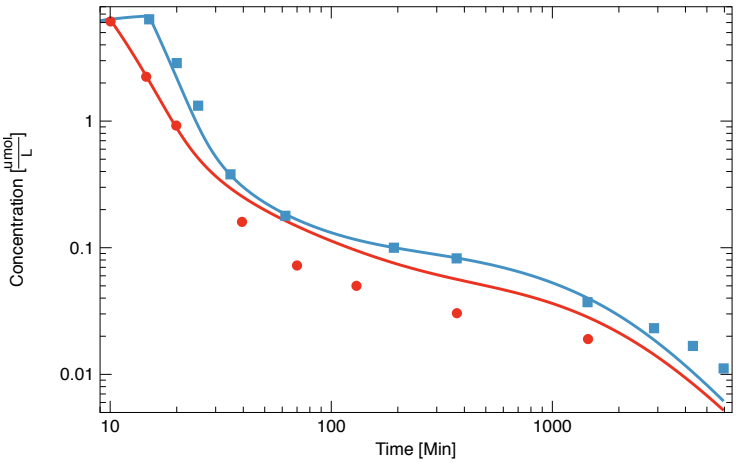

Figure C.1: Comparison of theoretical and clinical concentrations of DOX. The curves and data represent DOX infusion of 9.19 $\mu mol \cdot m^{-2} \cdot min^{-1}$ from Andersen *et al.* [61] (red) and Greene *et al.* [59] (blue).

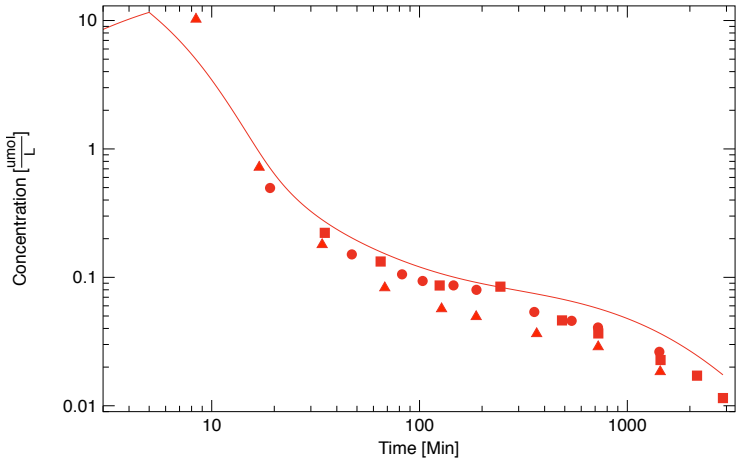

Figure C.2: Comparison of theoretical and clinical concentrations of DOX. The curve and data represent DOX infusion of 22.08 $\mu mol \cdot m^{-2} \cdot min^{-1}$ from Moriera *et al.* [89] (circles), Gianni *et al.* [88] (triangles), and Benjamin *et al.* [63] (squares).

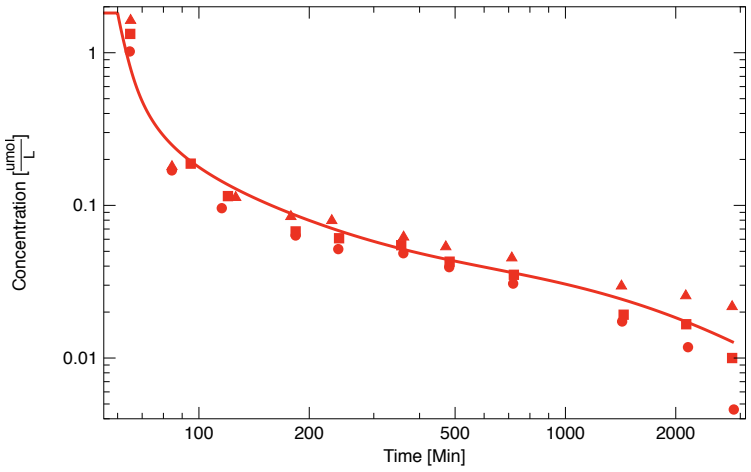

Figure C.3: Comparison of theoretical and clinical concentrations of DOX. The curve and data represent DOX infusion of 2.05 $\mu mol \cdot m^{-2} \cdot min^{-1}$ from normal weight (circles), mildly obese (squares) and obese patients (triangles) from Rodvold *et al.* [92]

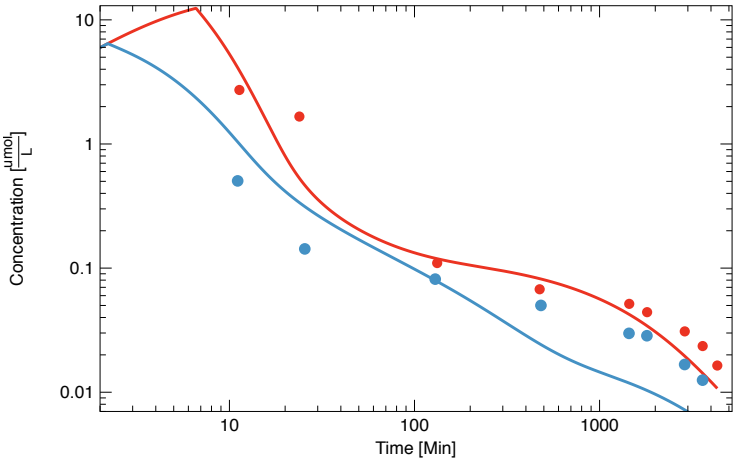

Figure C.4: Comparison of theoretical and clinical concentrations of DOX. The curves and data represent DOX infusion of 20.91 $\mu mol \cdot m^{-2} \cdot min^{-1}$ for 2.2 (blue) and 6.6 (red) minutes from Twelves *et al.* [93].

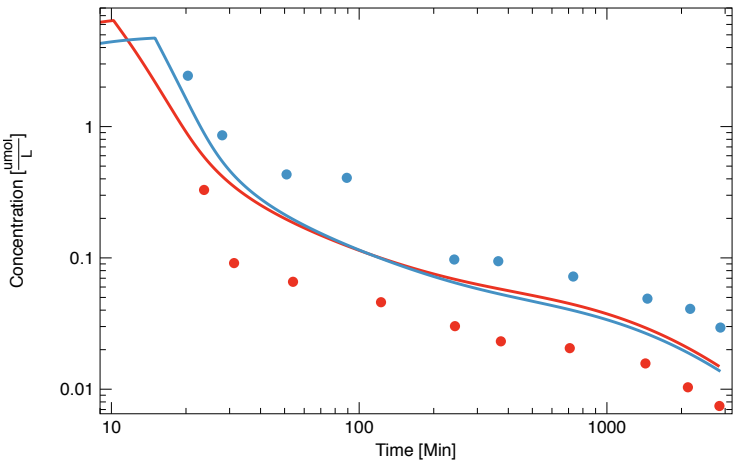

Figure C.5: Comparison of theoretical and clinical concentrations of DOX. The curves and data represent DOX infusion of 9.27 $\mu mol \cdot m^{-2} \cdot min^{-1}$ and 6.27 $\mu mol \cdot m^{-2} \cdot min^{-1}$ to patients GON (red) and BOU (blue) from Jacquet *et al.* [97].

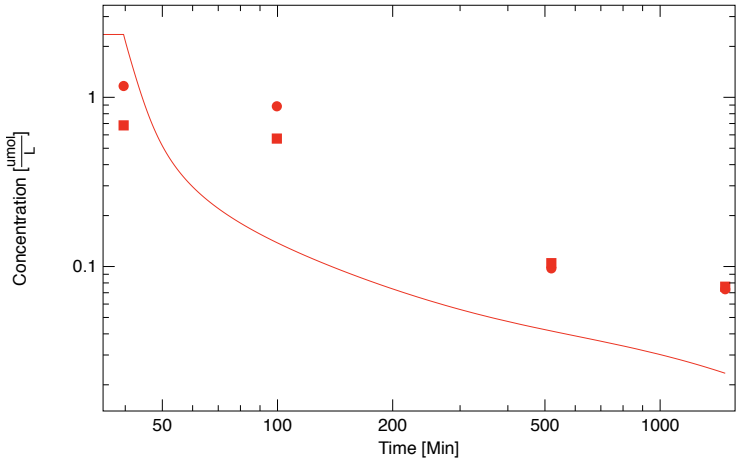

Figure C.6: Comparison of theoretical and clinical concentrations of DOX. The curve and data represent DOX infusion of 2.79 $\mu mol \cdot m^{-2} \cdot min^{-1}$ from normal weight (circles), overweight patients (squares) from Barpe *et al.* [96].

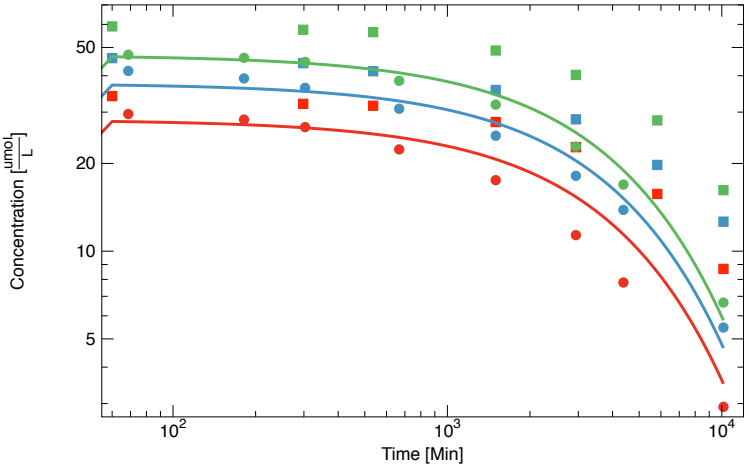

Figure C.7: Comparison of theoretical and clinical concentrations of PLD in Asian patients. The curves and data represent PLD infusion of 0.86 $\mu mol \cdot m^{-2} \cdot min^{-1}$ (red), 1.15 $\mu mol \cdot m^{-2} \cdot min^{-1}$ (blue) and 1.44 $\mu mol \cdot m^{-2} \cdot min^{-1}$ (green) from Hong *et al.* [84] (circles) and Fujusaka *et al.* [127](squares).

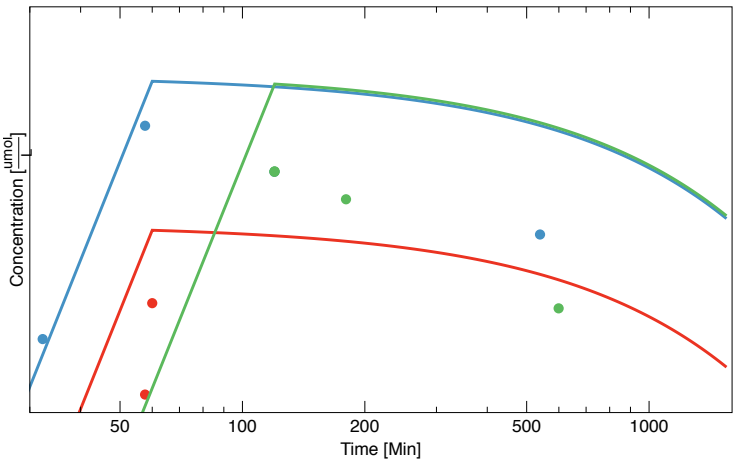

Figure C.8: Comparison of theoretical and clinical concentrations of PLD in Asian patients. The curves and data represent PLD infusion of 0.93 $\mu mol \cdot m^{-2} \cdot min^{-1}$ (red), 1.22 $\mu mol \cdot m^{-2} \cdot min^{-1}$ (blue) and 0.61 $\mu mol \cdot m^{-2} \cdot min^{-1}$ (green) from Matsmura *et al.* [128].

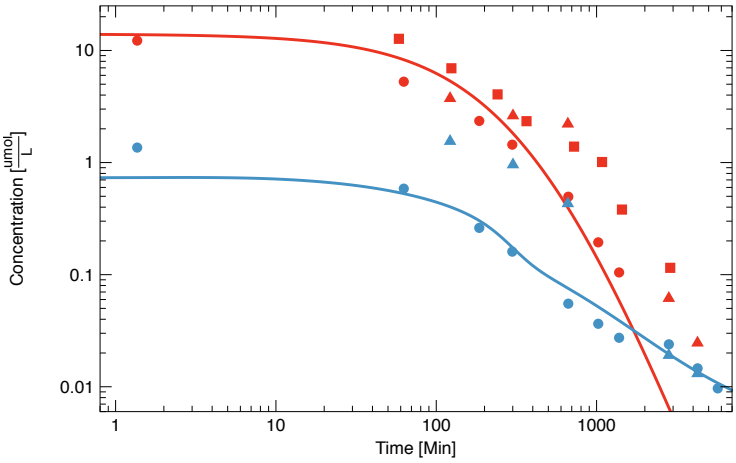

Figure C.9: Comparison of theoretical and clinical concentrations of liposomal and free DOX. The curves and data represent the concentrations of MYO (red) and DOX (blue) following the infusion of 2.16 $\mu mol \cdot m^{-2} \cdot min^{-1}$ MYO. The theoretical curves are compared with clinical measurements from the Mross *et al.* [101] (circles), Chastager *et al.* [129] (triangles) and Svenson *et al.* [130] (squares) studies.

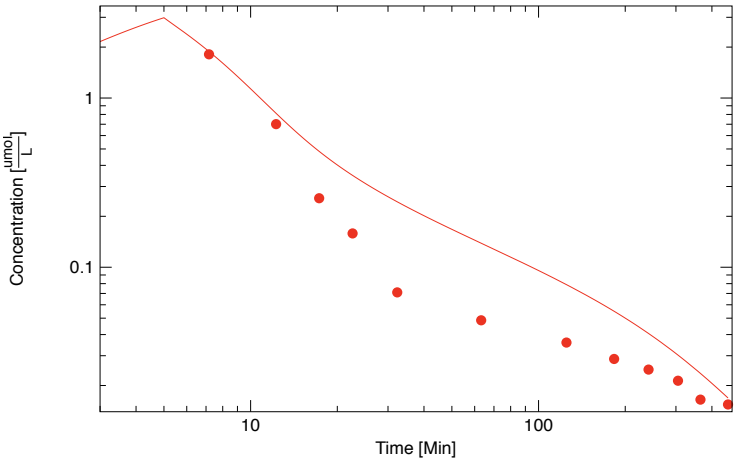

Figure C.10: Comparison of theoretical and clinical concentrations of DOX. The curve and data represent DOX infusion of 5.52 $\mu mol \cdot m^{-2} \cdot min^{-1}$ from Erttmann *et al.* [95].

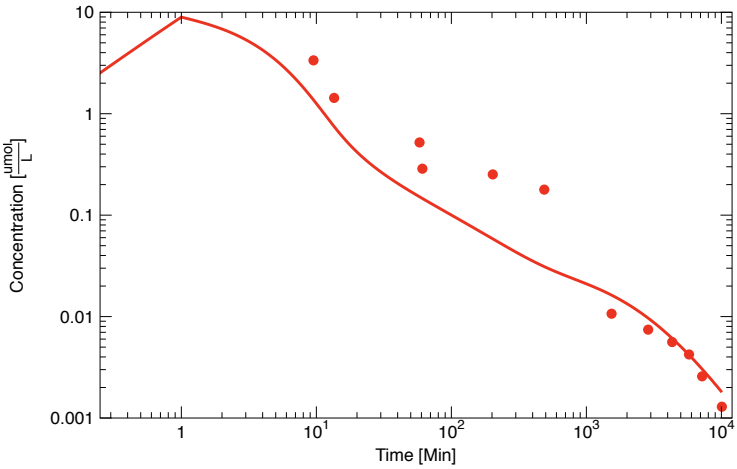

Figure C.11: Comparison of theoretical and clinical concentrations of DOX. The curve and data represent DOX infusion of 55.19 $\mu mol \cdot m^{-2} \cdot min^{-1}$ from Speth *et al.* [91].

Appendix D

Clinical Data Information

Table D.1: Concentration-time values of DOX and DOL digitized from clinical data.

	DOX		DOL	
Data set	Time [min]	Conc [$\mu mol \cdot l^{-1}$]	Time [min]	Conc [$\mu mol \cdot l^{-1}$]
Andersen *et al.* [61]	15.01	6.3641	15.01	0.0062
	20.00	2.87041	14.73	0.0176
	19.90	0.922	20.56	0.0206
	39.46	0.1600	40.56	0.0245
	70.00	0.0724	70.56	0.0230
	130.00	0.0500	130.56	0.0210
	370.00	0.0304	370.56	0.0225
	1450.00	0.019	1450.00	0.0148
Greene *et al.* [59]	10.04	6.12	10.56	0.0125
	20.00	2.8704	N/A**	N/A**
	25.00	1.3228	26.80	0.0231
	35.00	0.3796	38.60	0.0502
	62.00	0.1788	62.21	0.0451
	192.00	0.1000	192.05	0.0396
	369.00	0.0823	369.10	0.0396
	1443.00	0.0371	1455.00	0.0274
	2883.00	0.0231	2895.00	0.0179
	4324.00	0.0168	4323.19	0.0132
	5952.00	0.0111	5952.00	0.0066
Gianni *et al.* [88]	8.40	10.2377	N/A**	N/A**
	16.92	0.7196	17.79	0.0320
	33.99	0.1796	34.85	0.0425
	68.05	0.0828	60.44	0.0415
	127.69	0.0568	120.16	0.0343
	187.34	0.0494	188.40	0.0320
	366.26	0.0364	367.54	0.0252
	724.13	0.0287	725.83	0.0203
	1439.86	0.0184	1442.42	0.0165
Rodvold *et al.* [92][a]	64.76	1.0193	62.66	0.1163

Continued on next page

Table D.1 – continued from previous page

Data set	DOX		DOL	
	Time [min]	Conc [$\mu mol \cdot l^{-1}$]	Time [min]	Conc [$\mu mol \cdot l^{-1}$]
	84.36	0.1695	91.88	0.0377
	115.44	0.0959	121.11	0.0292
	183.60	0.0635	182.21	0.0243
	240.00	0.0517	240.66	0.0256
	361.20	0.0486	360.22	0.0294
	481.80	0.0394	482.44	0.0256
	720.00	0.0307	721.55	0.0220
	1428.00	0.0174	1439.31	0.0149
	2160.00	0.0118	2160.23	0.0106
	2880.00	0.0046	2881.15	0.0044
Rodvold *et al.* [92][b]	64.94	1.3284	62.66	0.1093
	94.98	0.1877	91.88	0.0433
	120.00	0.1150	121.11	0.0320
	183.60	0.0675	182.21	0.0279
	241.20	0.0609	240.66	0.0243
	356.40	0.0548	360.22	0.0206
	483.08	0.0428	482.44	0.0206
	723.26	0.0351	721.55	0.0182
	1441.61	0.0192	1439.31	0.0122
	2136.00	0.0167	2160.23	0.0106
	2850.00	0.0100	2881.15	0.0068
Rodvold *et al.* [92][c]	65.10	1.6283	62.66	0.0946
	84.42	0.1794	91.88	0.0946
	126.00	0.1126	121.11	0.0375
	178.20	0.0845	182.21	0.0299
	230.40	0.0795	240.66	0.0255
	361.80	0.0620	360.22	0.0228
	471.60	0.0535	482.44	0.0220
	714.00	0.0453	721.55	0.0199
	1422.00	0.0296	1439.31	0.0138
	2130.00	0.0256	2160.23	0.0106
	2850.00	0.0217	2881.15	0.0046
Moriera *et al.* [89]	19.09	0.4964	14.09	0.0829
	47.23	0.1509	42.23	0.0736
	82.40	0.1055	77.40	0.0679
	103.50	0.0937	98.50	0.0628
	145.70	0.0865	140.70	0.0580
	187.91	0.0799	182.91	0.0557
	356.72	0.0537	351.72	0.0495
	539.60	0.0458	534.60	0.0439
	722.49	0.0407	717.49	0.0406

Continued on next page

Table D.1 – continued from previous page

	DOX		DOL	
Data set	Time [min]	Conc [$\mu mol \cdot l^{-1}$]	Time [min]	Conc [$\mu mol \cdot l^{-1}$]
	1425.88	0.0263	1420.88	0.0284
Benjamin *et al.* [64]	N/A**	N/A**	25.00	0.1034
	40.00	0.4017	40.00	0.0835
	70.00	0.2353	55.00	0.0722
	100.00	0.1733	70.00	0.0606
	130.00	0.1926	N/A**	N/A**
	250.00	0.1055	250.00	0.0675
	490.00	0.0748	490.00	0.0722
	730.00	0.0544	730.00	0.0535
	1450.00	0.0381	1450.00	0.0370
	2170.00	0.0284	2170.00	0.0258
	2890.00	0.0215	2890.00	0.0191
Wurz *et al.* [90]	19.02	2.833400	19.02	N/A**
	23.66	0.329300	23.66	N/A**
	74.46	0.217110	74.46	N/A**
	145.20	0.149000	145.20	N/A**
	255.60	0.121000	255.60	N/A**
	486.60	0.058800	486.60	N/A**
	1455.00	0.035000	1455.00	N/A**
	1935.00	0.030900	1935.00	N/A**
	2895.00	0.028500	2895.00	N/A**
	3375.00	0.024200	3375.00	N/A**
	4323.00	0.022000	4323.00	N/A**
Speth *et al.* [91]	9.52	3.356667	9.52	N/A**
	13.54	1.431463	13.54	N/A**
	58.12	0.520699	58.12	N/A**
	61.00	0.287029	61.00	N/A**
	202.60	0.252070	202.60	N/A**
	487.60	0.178473	487.60	N/A**
	1537.00	0.010672	1537.00	N/A**
	2869.00	0.007433	2869.00	N/A**
	4320.10	0.005612	4320.10	N/A**
	5761.00	0.004232	5761.00	N/A**
	7201.00	0.002576	7201.00	N/A**
	10081.00	0.001293	10081.00	N/A**
Twelves *et al.* [93][a]	11.32	2.7231	11.32	N/A**
	23.88	1.6633	23.88	N/A**
	132.60	0.1098	132.60	N/A**
	474.60	0.0675	474.60	N/A**
	1446.60	0.0515	1446.60	N/A**
	1806.80	0.0442	1806.80	N/A**

Continued on next page

Table D.1 – continued from previous page

Data set	DOX		DOL	
	Time [min]	Conc [$\mu mol \cdot l^{-1}$]	Time [min]	Conc [$\mu mol \cdot l^{-1}$]
	2886.60	0.0309	2886.60	N/A**
	3606.60	0.0236	3606.60	N/A**
	4326.60	0.0164	4326.60	N/A**
Twelves *et al.* [93][b]	11.08	0.504139	11.08	N/A**
	25.54	0.142778	25.54	N/A**
	129.40	0.081509	129.40	N/A**
	482.20	0.050046	482.20	N/A**
	1442.20	0.029807	1442.20	N/A**
	1802.20	0.028519	1802.20	N/A**
	2882.20	0.016725	2882.20	N/A**
	3602.20	0.012512	3602.20	N/A**
Wilhm *et al.* [94]	358.20	0.0865	358.20	N/A**
	370.80	0.0440	370.80	N/A**
	386.40	0.0283	386.40	N/A**
	423.00	0.0217	423.00	N/A**
	480.00	0.0159	480.00	N/A**
	606.00	0.0131	606.00	N/A**
	840.00	0.0105	840.00	N/A**
	1068.00	0.0081	1068.00	N/A**
	1788.00	0.0052	1788.00	N/A**
	2514.00	0.0041	2514.00	N/A**
	3240.00	0.0026	3240.00	N/A**
Erttmann *et al.* [95]	7.17	1.8123	7.17	N/A**
	12.26	0.7010	12.26	N/A**
	17.30	0.2557	17.30	N/A**
	22.60	0.1584	22.60	N/A**
	32.30	0.0710	32.30	N/A**
	63.20	0.0486	63.20	N/A**
	125.00	0.0359	125.00	N/A**
	183.00	0.0287	183.00	N/A**
	241.00	0.0248	241.00	N/A**
	305.00	0.0213	305.00	N/A**
	365.00	0.0165	365.00	N/A**
	455.00	0.0154	455.00	N/A**
Barpe *et al.* [96][a]	39.61	1.166513	39.61	N/A**
	99.60	0.885005	99.60	N/A**
	519.60	0.097516	519.60	N/A**
	1479.60	0.073413	1479.60	N/A**
Barpe *et al.* [96][b]	39.61	0.682612	39.61	N/A**
	99.60	0.570377	99.60	N/A**
	519.60	0.104692	519.60	N/A**

Continued on next page

Table D.1 – continued from previous page

Data set	DOX		DOL	
	Time [min]	Conc [$\mu mol \cdot l^{-1}$]	Time [min]	Conc [$\mu mol \cdot l^{-1}$]
	1479.60	0.075989	1479.60	N/A**
Benjamin *et al.* [63]	35.00	0.2221	35.00	N/A**
	65.00	0.1328	65.00	N/A**
	125.00	0.0864	125.00	N/A**
	245.00	0.0846	245.00	N/A**
	485.00	0.0462	485.00	N/A**
	725.00	0.0366	725.00	N/A**
	1445.00	0.0227	1445.00	N/A**
	2165.00	0.0172	2165.00	N/A**
	2885.00	0.0115	2885.00	N/A**
Jacquet *et al.* [97][a]	23.66	0.3292	23.66	N/A**
	31.27	0.0913	31.27	N/A**
	54.08	0.0658	54.08	N/A**
	122.52	0.0460	122.52	N/A**
	243.60	0.0302	243.60	N/A**
	373.20	0.0232	373.20	N/A**
	708.04	0.0205	708.04	N/A**
	1430.43	0.0157	1430.43	N/A**
	2122.42	0.0103	2122.42	N/A**
	2844.81	0.0075	2844.81	N/A**
Jacquet *et al.* [97][b]	20.352	2.43946	20.352	N/A**
	28.0026	0.85848	28.0026	N/A**
	50.9322	0.43219	50.9322	N/A**
	89.1486	0.40715	89.1486	N/A**
	242.0142	0.09721	242.0142	N/A**
	364.3063	0.09436	364.3063	N/A**
	731.1834	0.07213	731.1834	N/A**
	1457.201	0.04894	1457.201	N/A**
	2168.1192	0.04092	2168.1192	N/A**
	2871.3	0.02947	2871.3	N/A**

**Concentration not given at this time.
[92]a,b,c corresponds to the normal weight, mildly obese and obese patients data respectively.

[93]a,b corresponds to the 75 $mg \cdot m^{-2}$ and 25 $mg \cdot m^{-2}$ dose respectively.

[96]a,b corresponds to normal and overweight patient data.

[97]a,b corresponds to data from patients GON and BOU respectively.

Table D.2: Concentration-time values of pegylated and free DOX digitized from clinical data.

	Encapsulated DOX		Free DOX	
Data set	Time [min]	Conc [$\mu mol \cdot l^{-1}$]	Time [min]	Conc [$\mu mol \cdot l^{-1}$]
Gabizon *et al.* [86][a]	39.81	39.0955	N/A**	N/A**
	72.11	35.2937	N/A**	N/A**
	120.58	31.8592	N/A**	N/A**
	233.65	28.7608	233.65	0.3691
	605.19	23.4383	605.19	0.4417
	1445.22	19.1003	1445.22	0.5551
	2882.88	12.2062	2882.88	0.8140
	4320.60	7.3174	4320.60	0.1638
	10087.50	2.4045	10087.50	0.0569
Gabizon *et al.* [86][b]	39.81	23.2642	N/A**	N/A**
	72.11	20.9935	N/A**	N/A**
	120.58	18.9434	N/A**	N/A**
	233.65	16.8767	N/A**	N/A**
	605.19	13.3942	605.19	0.3364
	1445.22	10.4947	1445.22	0.4883
	2882.88	6.9587	2882.88	0.6517
	4320.60	4.1106	4320.60	0.1378
	10087.50	1.1531	10087.50	0.0431
Matsmura *et al.* [128][a]	32.27	10.2204	32.27	0.4527
	57.62	20.8300	45.00	0.5980
	60.00	25.6049	57.62	0.2684
	119.85	17.6309	119.85	0.0483
	539.31	11.9033	539.31	0.0428
	1502.69	3.6505	1502.69	0.0316
Matsmura *et al.* [128][b]	32.27	23.6105	30.00	0.6226
	57.62	38.2230	32.27	0.5582
	60.00	51.7250	57.62	0.4079
	119.85	34.4496	119.85	0.0749
	539.31	29.8997	539.31	0.0623
	1502.69	13.0887	1502.69	0.0828
Matsmura *et al.* [128][c]	57.62	14.9016	57.62	0.2132
	119.85	34.4496	119.85	0.2319
	120.00	34.4834	120.00	0.2677
	179.77	32.3754	179.77	0.0525
	599.23	25.3071	599.23	0.0785
	1560.31	6.1647	1558.00	0.0451
Fujisaka *et al.* [127][a]	25.98	31.7918	25.98	N/A**
	60.00	34.0541	60.00	N/A**
	298.11	32.0299	298.11	N/A**

Continued on next page

Table D.2 – continued from previous page

Data set	Encapsulated DOX		Free DOX	
	Time [min]	Conc [$\mu mol \cdot l^{-1}$]	Time [min]	Conc [$\mu mol \cdot l^{-1}$]
	536.22	31.5536	536.22	N/A**
	1500.00	27.7434	1500.00	N/A**
	2940.00	22.7424	2940.00	N/A**
	5820.00	15.7173	5820.00	N/A**
	10140.00	8.6921	10140.00	N/A**
Fujisaka *et al.* [127][b]	25.98	41.7937	25.98	N/A**
	60.00	45.9611	60.00	N/A**
	298.11	44.1751	298.11	N/A**
	536.22	41.4365	536.22	N/A**
	1500.00	35.7211	1500.00	N/A**
	2940.00	28.3387	2940.00	N/A**
	5820.00	19.7657	5820.00	N/A**
	10140.00	12.6214	10140.00	N/A**
Fujisaka *et al.* [127][c]	25.98	56.0821	25.98	N/A**
	60.00	59.0589	60.00	N/A**
	298.11	57.5109	298.11	N/A**
	536.22	56.4393	536.22	N/A**
	1500.00	48.8188	1500.00	N/A**
	2940.00	40.2458	2940.00	N/A**
	5820.00	28.1006	5820.00	N/A**
	10140.00	16.1936	10140.00	N/A**

**Concentration not given at this time.
[86]a,b corresponds to 25 $mg \cdot m^{-2}$ and 50 $mg \cdot m^{-2}$ infusions respectively.
[128]a,b,c corresponds to doses of 32.5 $mg \cdot m^{-2}$ over 1 h , 45.5 $mg \cdot m^{-2}$ over 1 h and 45.5 $mg \cdot m^{-2}$ over 2 hs respectively.
[127]a,b,c corresponds to doses of 30 $mg \cdot m^{-2}$ over 1 h , 40 $mg \cdot m^{-2}$, and 50 $mg \cdot m^{-2}$ over 1 h respectively.

Table D.3: Concentration-time values of non-pegylated and free DOX digitized from clinical data.

Data set	Encapsulated DOX		Free DOX	
	Time [min]	Conc [$\mu mol \cdot l^{-1}$]	Time [min]	Conc [$\mu mol \cdot l^{-1}$]
Mross *et al.* [101]	30.68	8.4155	30.68	0.9351
	61.36	12.2447	61.36	1.3605
	122.73	5.2662	122.73	0.5851
	245.45	2.3515	245.45	0.2613
	357.95	1.4441	357.95	0.1605
	726.14	0.4960	726.14	0.0551
	1084.09	0.1942	1084.09	0.0365
	1442.05	0.1046	1442.05	0.0273
	2884.09	0.0027	2884.09	0.0239
	4326.14	0.0000	4326.14	0.0146
	5757.95	0.0000	5757.95	0.0097

Continued on next page

Table D.3 – continued from previous page

Data set	Encapsulated DOX		Free DOX	
	Time [min]	Conc [$\mu mol \cdot l^{-1}$]	Time [min]	Conc [$\mu mol \cdot l^{-1}$]
	7200.00	0.0000	7200.00	0.0079
Svenson *et al.* [130]	78.59	20.0904	78.59	1.2537
	126.95	11.1670	126.95	0.6238
	151.13	9.1478	151.13	0.5110
	241.81	5.8725	241.81	0.3665
	362.72	3.9407	362.72	0.2904
	725.44	2.2395	725.44	0.1561
	1082.12	1.6604	1082.12	0.1071
	1444.84	0.6767	1444.84	0.0658
	2883.63	0.3257	2883.63	0.0117
	4322.42	0.0852	4322.42	0.0027
	5761.21	0.0297	5761.21	0.0013
	7200.00	0.0163	7200.00	0.0007
Chastagner *et al.* [129][a]	0.65	8.4830	2.60	4.0397
	121.95	3.7370	301.35	0.7410
	301.01	2.6200	309.89	0.7267
	662.02	2.2121	662.70	0.3971
	2822.31	0.0615	2819.43	0.0286
	4260.58	0.0246	4261.99	0.0074
Chastagner *et al.* [129][b]	0.65	3.7916	2.60	2.0420
	121.95	1.5489	301.35	0.6218
	301.01	0.9575	309.89	0.2301
	662.02	0.4309	662.70	0.1499
	2822.31	0.0191	2819.43	0.0119
	4260.58	0.0131	4261.99	0.0050

**Concentration not given at this time.
[129]a,b corresponds to 75 and 60 $mg \cdot m^{-2}$ infusions respectively.

Appendix E

Code for the computation of the drug

Listing E.1: C++ Code of the model

```
#include <dlib/optimization.h>
#include <dlib/global_optimization.h>
#include <iostream>
#include <valarray>
#include <fstream>
#include <iomanip>
#include <cmath>
#include <string>
#include <complex>
#include <sstream>

using namespace std;
using namespace dlib;


const int drug = 5;
const int comp = 5;
const int order = 3;
const int dataset = 3;

double ton, toff;

double K[375] = {0.0};
double R[375] = {0.0};
double A[375] = {0.0};
double B[375] = {0.0};

double K1[75] = {0.0};
double R1[75] = {0.0};
double A1[75] = {0.0};
double B1[75] = {0.0};

double K2[375] = {0.0};
double R2[375] = {0.0};
double A2[375] = {0.0};
double B2[375] = {0.0};

double K3[1125] = {0.0};
double R3[1125] = {0.0};
```

```
double A3[1125] = {0.0};
double B3[1125] = {0.0};
double A4[1125] = {0.0};
double B4[1125] = {0.0};



// Define the vector quatities
using Array = std::valarray<double>;
using vec = std::vector<double>;
using vec2 = std::vector<vec>;
using v_int = std::vector<int>;

Array X(drug * comp);                          // Declare the variables
Array I(drug * comp);

// Vectors
vec ton_A, t_off_A;
vec2 inf_set, conc_set,
time_set, Xclin;

v_int n_patients_Xclin;

// Runge Kutta Solvers
double RK4_main(std::vector<double>(&P));
void Rk4(double& t, Array &X, const Array&,
         void (*rhs_eval)(double, const Array&, Array&),
         Array (*f)(const Array& , double),  double h);
Array f(const Array& , double);
void derivs(double t, const Array (&X), Array&);
void dxdt1(const Array &X, Array(&dydx));
void dxdt2(const Array &X, Array(&dydx));
void dxdt3(const Array &X, Array(&dydx));
void dxdt4(const Array &X, Array(&dydx));


void writeToFile( std::ofstream &outfile, double t,
        Array X, bool header );
void lim( Array &Y, double value );
int index(int, int, int, int);
int ij(int i, int j, int k);
           // Function for drug casting
int ij(int i, int j, int k, int l);
           // Overload for 3D
int ijkl(int i, int j, int k, int l, int m);
           // 3D 2P casting to 1D
double rate( double x, double p ) ;
double comp_pow(double x, double y);

// Rate Constants
void flowRates(std::ifstream &ifs, double (&K)[375],
               double (&R)[375], double (&A)[375], double (&B)[375],
               double (&K1)[75], double (&R1)[75], double (&A1)[75],
               double (&B1)[75]);
```

```
void meta_Decay(std::ifstream &infile, double (&K2)[375], double (&R2)
    [375],
                double (&A2)[375], double (&B2)[375], double (&K3)
    [1125],
                double (&R3)[1125], double (&A3)[1125], double (&B3)
    [1125],
                double (&A4)[1125], double (&B4)[1125]);

// Time and Concentration Files
void readConc(std::ifstream &infile, vec(&ton), vec(&toff),
              vec2(&conc_set), vec2(&inf_set));
void readTime(std::ifstream &infile,  v_int (&n_patients_Xclin),
              vec2 (&time_set), vec2 (&Xclin_set));


typedef matrix<double,0,1> column_vector;

int main() try
{
     std::ifstream infile("/Users/CodeFiles/Downloads/input.txt");
     std::ifstream infile2("/Users/CodeFiles/Downloads/Meta_Decay.txt");
     std::ifstream infile3("/Users/CodeFiles/Downloads/
    Conc_Infusion_Input.txt");
     std::ifstream infile4("/Users/CodeFiles/Downloads/Time_Xclin.txt");


      // Update the rate constants; starting values and the clinical
    values
     if (infile.is_open() && infile2.is_open() &&  infile3.is_open() &&
    infile4.is_open()){
          flowRates(infile, K, R, A, B,
                    K1, R1, A1, B1);
          meta_Decay(infile2, K2, R2, A2, B2,
                     K3, R3, A3, B3, A4, B4);
          readConc(infile3, ton_A, t_off_A,
                   conc_set, inf_set);
          readTime(infile4, n_patients_Xclin,
                   time_set, Xclin);
     }

     else std::cerr << "One of the file(s) is not open. Try again!" <<
    std::endl;

          //Update the starting points of the search vector
          column_vector starting_point = {X0, X1, X2, X3, X4, X5, X6, X7,
    ....., XN-1};

          auto RK4main = [&](const column_vector& x) {

              double var;
              double var_solve = 0.0;

              double hmax = 0.1;
              int sum_np = 0;
```

```
            for (int a = 0; a != dataset; ++a)
            {
                Array X (conc_set[a].data(), conc_set[a].size());

                 // Update the infusion
                Array I (inf_set[a].data(), inf_set[a].size());


                K[index(0,2,0,1)] = x(0);   R[index(0,2,0,1)] = x(1);
                K[index(0,1,2,1)] = x(2);   R[index(0,1,2,1)] = x(3);
                K[index(0,1,3,1)] = x(4);   R[index(0,1,3,1)] = x(5);
                K[index(0,1,4,1)] = x(6);   R[index(0,1,4,1)] = x(7);
                K[index(0,2,1,1)] = x(8);   R[index(0,2,1,1)] = x(9);
                K[index(0,3,1,1)] = x(10);  R[index(0,3,1,1)] = x(11);
                K[index(0,4,1,1)] = x(12);  R[index(0,4,1,1)] = x(13);

                K3[ijkl(0,2,3,2,0)] = x(15); R3[ijkl(0,2,3,2,0)] = x(16)
;
                A3[ijkl(0,2,3,2,0)] = x(17); B3[ijkl(0,2,3,2,0)] = x(18)
;
                K3[ijkl(0,2,3,1,0)] = x(19); R3[ijkl(0,2,3,1,0)] = x(20)
;

                K[index(0,2,0,2)] = x(21);   R[index(0,2,0,2)] = x(22);
                K[index(0,2,1,2)] = x(23);   R[index(0,2,1,2)] = x(24);
                K[index(0,3,1,2)] = x(25);   R[index(0,3,1,2)] = x(25);
                K[index(0,1,2,2)] = x(26);   R[index(0,1,2,2)] = x(27);
                K[index(0,1,3,2)] = x(28);

                // Implicit miror-imaging

                K3[ijkl(2,0,3,2,0)] = K3[ijkl(0,2,3,2,0)];
                R3[ijkl(2,0,3,2,0)] = R3[ijkl(0,2,3,2,0)];
                A3[ijkl(2,0,3,2,0)] = A3[ijkl(0,2,3,2,0)];
                B3[ijkl(2,0,3,2,0)] = B3[ijkl(0,2,3,2,0)];
                K3[ijkl(2,0,3,1,0)] = K3[ijkl(0,2,3,1,0)];
                R3[ijkl(2,0,3,1,0)] = R3[ijkl(0,2,3,1,0)];


               /*****
                T_start = Starting time of the data set.
                n_data = Number of data points from the clinical CT
graph.
                T_on = Start-time of infusion of the data set.
                T_off = Stop-time of infusion of the data set
                n_patients = Number of patients
               *****/


                int ti = time_set[a][0];
                int n_data = static_cast<int>(time_set[a].size());
                ton = ton_A[a];
                toff = t_off_A[a];
```

```
                int n_patients = n_patients_Xclin[a];


                for (int i = 0; i < n_data - 1; ++i){
                    double npoints = (time_set[a][i+1] - time_set[a][i])
/hmax;
                    int stepSize = (int) npoints + 1;
                    double h = (time_set[a][i+1] - time_set[a][i])/
stepSize;
                    int priorRun ( 0 ), c, d;
                    c = priorRun - i;
                    d = stepSize +  c - 1;
                    priorRun += stepSize;

                    // Store Starting value of X
                    std::valarray<double> X0(X.size()),

                    X1(X.size()),
                    X_conv(X.size());
                    double t0 = time_set[a][i];

                    for ( int j = c; j <= d; ++j ) {
                        X0 = X;
                        double t_j ( t0 );

                        // Do RK4 method and solve for X
                        Rk4(t0, X, I, derivs, f, h);

                        // Store the new valus of X
                        X1 = X;
                        double h_conv ( h );
                        int count = 1; double conv = 100;
                        int n;

                        // Begin the while loop for the convergence
                        while (count < 20 && conv > 1e-7){
                            double t_conv = t_j;
                            n = (int) pow (2, count);
                            h_conv *= 0.5;
                            X_conv = X0;

                            for ( int l = 0; l != n; ++l )
                                // Do RK4 with X_conv and tconv +
lh_conv;
                                Rk4(t_conv, X_conv, I, derivs, f, h_conv
);

                            // Test the min/max of the set of vectors
                             X_conv.min() < -1e-7 ? conv = 100 :
                                conv = abs(X1 - X_conv).max();
                             ++count;
                        }

                        // Return new values for X
```

```
                    X = X_conv;

                    // Clip X's for negative values
                    lim(X, 1e-7);

                }

                // Var_Solve = Mean Difference of the Concentrations
 from datapoints.
                var_solve += n_patients * pow((X[1] - x(14) * Xclin[
a][i])
                                                /(X[1] + x(14) * Xclin
[a][i]), 2);

            }

        }
        var =  (4.0/423.0) * var_solve;


        infile.close(); infile2.close();
        infile3.close(); infile4.close();

        return var;

    };

    find_min_bobyqa(RK4main,
                    starting_point,
                    50,    // number of interpolation points
                    uniform_matrix<double>(29,1, 0),  // lower bound
 constraint
                    uniform_matrix<double>(29,1, 30),   // upper
bound constraint
                    0.07,   // initial trust region radius
                    1e-6,  // stopping trust region radius
                    10000    // max number of objective function
evaluations
                    );
    std::cout << "Powells Solution:\n" << starting_point << std::
endl;

  }

    catch (std::exception& e){
        cout << e.what() << endl;
 }

    void Rk4(double& t, Array &X, const Array(&I),
             void (*rhs_eval)(double, const Array&, Array&),
             Array (*f)(const Array& , double),  double h){

        // Number of Coupled ODEs
        int nX = X.size();
```

```
        // Local arrays
        Array k1(nX), k2(nX), k3(nX), k4(nX),
        Inf(nX), f1(nX), dydx(nX);

        // Zeroth intermediate step
        (*rhs_eval) (t, X, dydx);                    // Solves the
unique equation for each X
        Inf = (*f)( I, t);                           // Adds the
infusion
        k1 = h * ( Inf + dydx);                      // Soves the
First midpoint
        f1 = X + k1 / 2.;                            // Takes the
first increment


        // First intermediate step
        (*rhs_eval) (t + h / 2., f1, dydx);          // Solves the
unique equation for each X
        Inf = (*f)( I, t + h/2 );                    // Adds the
infusion
        k2 = h * ( Inf + dydx );                     // Soves the
First midpoint
        f1 = X + k2 / 2.;                            // Takes the
first increment

        // Second intermediate step
        (*rhs_eval) (t + h / 2., f1, dydx);
        Inf = (*f)( I, t + h/2 );
        k3 = h * ( Inf + dydx );
        f1 = X + k3;


        // Third intermediate step
        (*rhs_eval) (t + h, f1, dydx);
        Inf = (*f)( I, t + h );
        k4 = h * ( Inf + dydx );

        // Full Step
        X += k1 / 6. + k2 / 3. + k3 / 3. + k4 / 6.;

        t += h;

        return;
    }

    Array f(const Array(&I), double t0){

        Array f1 (I.size());

        (t0 >= ton && t0 < toff) ? f1 = I : f1 = 0.0;

        return f1;
    }
```

```
    void derivs(double t, const Array(&X), Array(&dydx)){

        int N  =  X.size();

        Array dX1(N), dX2(N), dX3(N), dX4(N);

        dxdt1(X, dX1);
        dxdt2(X, dX2);
        dxdt3(X, dX3);
        dxdt4(X, dX4);

        dydx = dX1 + dX2 + dX3 + dX4;
        //(dX1 + dX2 + dX3 + dX4);
    }


    // Flow Kinetics
    void dxdt1(const Array &X, Array(&dydx)){
       dydx = 0.0; int ijk, ikj;

        for(int i = 0; i != drug; ++i)
            for(int j = 0; j!= comp; ++j)
                for(int l = 0; l!= comp; ++l)
                    for(int m = 0; m!= order; ++m){
                        ijk = index(i, j, l, m);
                        ikj = index(i, l, j, m);
                        dydx[i*comp + j] += -K[ijk] * rate(X[i*comp
+ j], A[ijk])
                        /(1. + R[ijk] * rate(X[i*comp + j], B[ijk]))
                        + K[ikj] * rate(X[i*comp + l], A[ikj])
                        /(1. + R[ikj] * rate(X[i*comp + l], B[ikj]))
;
                    }
      }


      /* Reaction: Drug Release
         DoxCRel/LipoDox ====> Dox
         Drug list:
         4 ==> DoxCRel/LipoDox
         0 ==> Dox
         */
      void dxdt2(const Array &X, Array(&dydx)){

        dydx = 0.0; int ijk;

        for(int l = 0; l != order; ++l){
            ijk = ij(4, 0, l);
            dydx[4*5 + 2] -= K1[ijk] * rate(X[4*5 + 2], A1[ijk])/(1.
 + R1[ijk] * rate(X[4*5 + 2], B1[ijk]));
            dydx[0*5 + 2] += K1[ijk] * rate(X[4*5 + 2], A1[ijk])/(1.
 + R1[ijk] * rate(X[4*5 + 2], B1[ijk]));
        }
```

```
    }


  /* Reaction: Complex dissociation
       DoxCBR1 ====> Doxol + CBR1
       Drug list:
       1 ==> Doxol
       2 ==> CBR1
       3 ==> DoxCBR1
       */
  void dxdt3(const Array &X, Array(&dydx)){

      dydx = 0.0; int ijk;


      for(int m =0; m!=order; ++m){
          ijk = ij(3, 2, 1, m);
          dydx[3*5 + 2]  -= K2[ijk] * rate(X[3*5 + 2], A2[ijk])
/(1. + R2[ijk] * rate(X[3*5 + 2], B2[ijk]));
          dydx[2*5 + 2]  += 0.5*K2[ijk] * rate(X[3*5 + 2], A2[ijk
])/(1. + R2[ijk] * rate(X[3*5 + 2], B2[ijk]));
          dydx[1*5 + 2]  += 0.5*K2[ijk] * rate(X[3*5 + 2], A2[ijk
])/(1. + R2[ijk] * rate(X[3*5 + 2], B2[ijk]));
        }
    }

  /* Reaction: Complex Formation
       Dox + CBR1 ====> DoxCBR1
       Drug list:
       1 ==> Dox
       2 ==> CBR1
       3 ==> DoxCBR1
       */

  void dxdt4(const Array &X, Array(&dydx)){


      dydx = 0.0;

      for(int m = 0; m!=order; ++m)
          for(int p = 0; p!=order; ++p){
              dydx[0*5 + 2] -= K3[ijkl(0, 2, 3, m, p)] * comp_pow(
X[0*5 + 2], A3[ijkl(0, 2, 3, m, p)]) * rate(X[2*5 + 2], A4[ijkl(0, 2,
 3, m, p)])
              /(1. + R3[ijkl(0, 2, 3, m, p)] * comp_pow(X[0*5 +
2], B3[ijkl(0, 2, 3, m, p)]) * rate(X[2*5 + 2], B4[ijkl(0, 2, 3, m, p
)]));

              dydx[2*5 + 2] -= K3[ijkl(0, 2, 3, m, p)] * comp_pow(
X[0*5 + 2], A3[ijkl(0, 2, 3, m, p)]) * rate(X[2*5 + 2], A4[ijkl(0, 2,
 3, m, p)])
              /(1. + R3[ijkl(0, 2, 3, m, p)] * comp_pow(X[0*5 +
2], B3[ijkl(0, 2, 3, m, p)]) * rate(X[2*5 + 2], B4[ijkl(0, 2, 3, m, p
)]));
```

```
                dydx[3*5 + 2] += K3[ijkl(0, 2, 3, m, p)] * comp_pow(
X[0*5 + 2], A3[ijkl(0, 2, 3, m, p)]) * rate(X[2*5 + 2], A4[ijkl(0, 2,
 3, m, p)])
                /(1. + R3[ijkl(0, 2, 3, m, p)] * comp_pow(X[0*5 +
2], B3[ijkl(0, 2, 3, m, p)]) * rate(X[2*5 + 2], B4[ijkl(0, 2, 3, m, p
)]));
            }
    }

    void writeToFile( std::ofstream &outfile, double t, Array X,
bool header ){
        if ( header )
        {
            outfile SPH " " << " t";
            for ( int i = 0; i != drug; ++i )
                for ( int j = 0; j != comp; ++j)
                    outfile SPH 'C' << i << j;
            outfile << '\n';
        }

        outfile SPD t;
        for ( int i = 0; i != drug; ++i)
            for ( int j = 0; j != comp; ++j )
                outfile SPD X[ i * comp + j ];
        outfile << '\n';
    }

   // Limiting Condition
    void lim( Array &X, double value ){
        int N = X.size();
        for ( int i = 0; i < N; i++ ) if ( X[i] < value ) X[i] =
0.00;
    }

    int index(int i, int j, int k, int l){
        int nij = (i * comp + j) * comp + k;
        return nij * order  + l;
    }

    // Converts 2D * 10 to [ij]
    int ij(int i, int j, int k){
        return (i * drug * order) + j * order + k;
    }

    // Converts 3D * 10 to [ijk]
    int ij(int i, int j, int k, int l){
        int ijk = (((i * drug) + j) * drug);
        return (ijk + k) * order + l;
    }
    // Coverts 3D * 20 ro [ijkl]
    int ijkl(int i, int j, int k, int l, int m){
        int nij = ((( i * drug + j) * drug + k) * order) + l;
        return (nij * order) + m;
```

```
    }
    // QUASI-rate law
    double rate( double x, double p ){
        double Hx, val;
        double ex = 1e10 * (0.5 * 1e-7 - x);
        Hx = 1.0 / (1.0 + exp (ex) );
        p == 0 ? val = pow(x,p) * Hx : val = pow(x, p);
        return val;
    }

    double comp_pow(double x, double y){
        double Hx;
        std::complex<double> sol = x;
        std::complex<double> ex_a = y;
        double ex = 1e10 * (0.5 * 1e-7 - x);
        Hx = 1.0 / (1.0 + exp (ex) );
        return pow(sol,ex_a).real() * Hx;
    }

    void flowRates(std::ifstream &ifs, double (&K)[375],
                   double (&R)[375], double (&A)[375], double (&B)
[375],
                   double (&K1)[75], double (&R1)[75], double (&A1)
[75],
                   double (&B1)[75]){
        std::string line, line1;
        int flag, ijk;
        double Rij, Kij, Aij, Bij;

        int count = 0;

        while(count != 45 && std::getline(ifs, line)){

            std::istringstream ss(line);
            ss >> flag >> ijk >> Aij >> Bij >> Kij >> Rij;
            K[ijk] = Kij; R[ijk] = Rij;
            A[ijk] = Aij; B[ijk] = Bij;

            ++count;
        }

        while(count != 49 && std::getline(ifs, line1)){

            std::istringstream ss(line1);
            ss >> flag >> ijk >> Aij >> Bij >> Kij >> Rij;
            K1[ijk] = Kij; R1[ijk] = Rij;
            A1[ijk] = Aij; B1[ijk] = Bij;

            ++count;
        }

    }

    // A <---> B + C  Rate terms
```

```
    void meta_Decay(std::ifstream &infile, double (&K2)[375], double
 (&R2)[375],
                    double (&A2)[375], double (&B2)[375], double (&
K3)[1125],
                    double (&R3)[1125], double (&A3)[1125], double
(&B3)[1125],
                    double (&A4)[1125], double (&B4)[1125]){

        std::string line, line1;
        int flag, ijk;
        double Rij, Kij, Aij, Bij, Cij, Dij;

        int count = 0;

        while(count != 6 && getline(infile, line)){
            std::istringstream ss (line);
            ss >> flag >> ijk >> Aij >> Bij >> Kij >> Rij;
            K2[ijk] = Kij; R2[ijk] = Rij;
            A2[ijk] = Aij; B2[ijk] = Bij;

            ++count;
        }



        while(count != 24 && getline(infile, line1)){
            std::istringstream ss(line1);
            ss >> flag >> ijk >> Aij >> Bij >> Cij
            >> Dij >> Kij >> Rij;
            K3[ijk] = Kij;  R3[ijk] = Rij;
            A3[ijk] = Aij;  B3[ijk] = Bij;
            A4[ijk] = Cij;  B4[ijk] = Dij;

            ++count;
        }
    }

    void readConc(std::ifstream &infile, vec(&ton), vec(&toff),
                  vec2(&conc_set), vec2(&inf_set)){
        int f1;
        double x0, iff, ton1, toff1;
        for (int i = 0; i != dataset; ++i){
            vec X_row, I_row;
            infile >> f1 >> ton1 >> toff1;

            ton.push_back(ton1); toff.push_back(toff1);
            for(int j = 0; j!=25; ++j){
                infile >> x0;
                X_row.push_back(x0);
            }
            for(int j = 0; j!=25; ++j){
                infile >> iff;
                I_row.push_back(iff*1e6/(543.500 * (toff1 - ton1)));
            }
```

```
            conc_set.push_back(X_row);
            inf_set.push_back(I_row);
        }
    }

    void readTime(std::ifstream &infile,  v_int (&n_patients_Xclin),
                  vec2 (&time_set), vec2 (&Xclin_set)){

        // f1 = flag, n = number of timepoints
        int f1, n, np1, np2; double t, xi;
        for (int i = 0; i != dataset; ++i){
            // row by row time set
            vec t_row, Xi_row;
            infile >> f1 >> np1;
            for(int j = 0; j != np1; ++j){
                infile >> t;
                t_row.push_back(t);
            }
            infile >> n >> np2;
            //std::cout << " n = " << n << std::endl;
            n_patients_Xclin.push_back(n);
            for(int j = 0; j != np2; ++j){
                infile >> xi;
                Xi_row.push_back(xi);
            }

            time_set.push_back(t_row);
            Xclin_set.push_back(Xi_row);
        }
    }
```